UNIVERSITÀ
DEGLI STUDI
DI BRESCIA

DIPARTIMENTO DI INGEGNERIA MECCANICA E INDUSTRIALE

DOTTORATO DI RICERCA IN INGEGNERIA MECCANICA E INDUSTRIALE

settore scientifico disciplinare ING-IND/13

CICLO XXXVII

Handcycling Dynamics: An Integrated Analysis of Biomechanics, Vibrations, and Performance using IMUs and Modeling

DOTTORANDO
Michele Sanguinetta

PRIMO SUPERVISORE
Giovanni Legnani

Anno Accademico 2025/26

Abstract

Handcycling has emerged as a vital solution for independent mobility and physical activity, bridging the domains of rehabilitation, assistive technology, and competitive sport. For individuals with spinal cord injury or lower-limb impairments, the handbike offers biomechanical advantages over traditional wheelchair propulsion; however, the rigid coupling between the athlete and the frame exposes the upper bodya system inherently more vulnerable to repetitive strain than the lower limbsto significant mechanical stress. Despite the known risks associated with long-term exposure to road irregularities, the propagation of vibrations and accelerations through the handbike and rider system in real-world conditions remains incompletely understood. This thesis addresses this gap by developing and validating a methodological and analytical framework to quantify such dynamics, linking mechanical design and propulsion patterns to performance and comfort.

The research is structured into four phases. First, a structured literature review maps the scientific landscape on handbikes up to 2022, classifying documents by clinical focus, device characteristics, forces, geometry, sensors, and actuation. This synthesis highlights a strong emphasis on physiology and laboratory-based testing, contrasted with limited and non-standardized assessments of vibrations, surface effects, and in-field measurement.

Second, an Artificial Upper Limb Mechanism (AULM) is presented. The device was developed to replicate planar handcycling kinematics under motor-driven, repeatable conditions. Using this bench simulator, multiple inertial measurement unit (IMU) locations are compared in terms of the cycle-to-cycle stability of total acceleration. The results show that sensors placed on mechanically constrained links near the actuated joint or handle produce markedly more repeatable profiles than distal or more compliant sites, providing practical criteria for sensor placement in field studies.

Third, a compact three-degree-of-freedom vibrational model was formulated to represent the coupled response of the front wheel, frame and seat, and rider trunk. Preliminary outdoor measurements on a commercial handbike were used to support a nominal parameterization and plausibility check of the model, and to interpret how low-frequency cadence-related content and roughness-related vibration components may propagate through the handbike–rider system.

Finally, the validated IMU configuration and the dual analytical framework were applied to an outdoor handcycling study on a mixed-surface circuit comprising straights, curves, a climb, and a gravel segment. Eight IMUs distributed over mechanical and anatomical sites provided segment-specific descriptors of total acceleration and jerk in the

time domain. Comparing two laps performed by two different participants revealed an overall reduction in variability, peak amplitude, and impulsive events in Ride 2 relative to Ride 1, especially at the main mechanical interfaces. These findings are consistent with smoother propulsion, reduced vibrational harshness, and more stable control under the tested conditions. The combined percent-cycle and time-aligned views help separate differences in cycle morphology and control strategy from differences in pacing.

Overall, this thesis delivers an integrated framework that combines taxonomy, bench validation, lumped-parameter modeling, and real-world sensing. The proposed methods and findings support the more informed design of handbikes, vibration-aware coaching strategies, and targeted rehabilitation protocols for users who rely on handcycling for daily mobility and sport.

Abstract in italiano

L'handcycling rappresenta oggi una soluzione rilevante per la mobilità autonoma, la riabilitazione e la pratica sportiva. Per persone con lesione midollare o limitazioni agli arti inferiori, l'handbike offre vantaggi biomeccanici rispetto alla carrozzina tradizionale; tuttavia, il collegamento rigido tra atleta e telaio espone il tronco e gli arti superiori a sollecitazioni meccaniche ripetute. In condizioni reali, la propagazione di vibrazioni e accelerazioni attraverso il sistema handbike–rider è ancora poco caratterizzata. Questa tesi affronta tale problema sviluppando un framework metodologico e analitico per collegare progettazione meccanica, strategia propulsiva, comfort e prestazione.

Il lavoro è articolato in quattro fasi. La prima consiste in una revisione strutturata della letteratura sulle handbike fino al 2022, con classificazione dei contributi in base ad aspetti clinici, caratteristiche del dispositivo, forze, geometria, sensori e attuazione. L'analisi evidenzia una forte attenzione a fisiologia e prove di laboratorio, ma anche una limitata standardizzazione delle misure outdoor, degli effetti della superficie e delle vibrazioni.

La seconda fase introduce un Artificial Upper Limb Mechanism (AULM), progettato per riprodurre la cinematica planare dell'handcycling in condizioni controllate e ripetibili. Il banco ha permesso di confrontare diverse posizioni di sensori inerziali (IMU), valutando la stabilità ciclo-per-ciclo dell'accelerazione totale. I risultati indicano che i sensori montati su elementi più vincolati, in prossimità del giunto attuato o dell'interfaccia mano–manubrio, producono profili più ripetibili rispetto a siti distali o più cedevoli, fornendo criteri pratici per il posizionamento nelle prove sul campo.

La terza fase propone un modello vibrazionale compatto a tre gradi di libertà per rappresentare la risposta accoppiata di ruota anteriore, telaio–sedile e tronco del rider. Misure preliminari outdoor su una handbike commerciale sono state utilizzate per una parametrizzazione nominale e per una verifica di plausibilità, con l'obiettivo di interpretare la possibile propagazione di contenuti legati alla cadenza e alle irregolarità del terreno nel sistema handbike–rider.

Infine, la configurazione IMU validata è stata applicata a uno studio outdoor su un circuito misto composto da rettilinei, curve, salita e ghiaia. Otto sensori, distribuiti tra siti meccanici e anatomici, hanno fornito descrittori segment-specific dell'accelerazione totale e del jerk nel dominio del tempo. Il confronto tra due giri, eseguiti da due partecipanti diversi, mostra nel Ride 2 una riduzione complessiva di variabilità, ampiezza dei picchi ed eventi impulsivi rispetto al Ride 1, soprattutto alle principali interfacce meccaniche. Tali risultati sono coerenti con una propulsione più regolare, una minore severità vibrazionale

e un controllo più stabile nelle condizioni testate, pur richiedendo cautela interpretativa per la numerosità limitata del campione e per le variabili non rigidamente controllate.

Nel complesso, la tesi propone un approccio integrato che combina tassonomia, validazione su banco, modellazione a parametri concentrati e misure in ambiente reale. I metodi e i risultati ottenuti possono supportare la progettazione di handbike più confortevoli, strategie di coaching sensibili alle vibrazioni e protocolli riabilitativi mirati per utenti che utilizzano l'handcycling nella mobilità quotidiana o nello sport.

Contents

1 Introduction **1**

2 Handbike for Daily Use, Sport, and Rehabilitation Purposes: A Literature Review of Actuation and Technical Characteristics **5**

3 The Ideal Handcycling: Simulation and Analysis of the Task through an Artificial Upper Limb Mechanism (AULM) **51**

3.1 Introduction 51
3.2 Materials and Methods 52
3.2.1 Artificial Upper Limb Mechanism 52
3.2.2 Instrumentation and Sensor Positions 54
3.2.3 Experimental Protocol 55
3.2.4 Data Processing 55
3.2.5 Outcome Metrics and Statistical Analysis 55
3.3 Results 56
3.3.1 Repeatability of the AULM Motion 56
3.3.2 Impact of interpolation on synchronization quality 56
3.3.3 Effect of Sensor Position on Signal Variability 57
3.3.4 Quantitative summary of sensor variability 58
3.4 Conclusions 60

4 Vibrational Model of Handbike and Handcyclist **62**

4.1 Introduction 62
4.2 Model Description 63
4.2.1 System Representation and Degrees of Freedom 63
4.2.2 Equations of Motion 64
4.2.3 Natural Frequencies and Mode Shapes 66
4.3 Preliminary Outdoor Measurements 66
4.3.1 Experimental Setup 66
4.3.2 Data Acquisition and Signal Processing 68
4.4 Model–Data Comparison 68
4.4.1 Model Parameterization 68
4.5 Results 69
4.5.1 Dominant frequency content 69

4.5.2 Cycle-based acceleration descriptors . . . 69
4.6 Conclusions . . . 70

5 Handcycling in the Real Context: Experimental Evaluation on the Field 71
5.1 Introduction . . . 71
5.2 Study Context and Objectives . . . 71
5.2.1 Objectives . . . 72
5.2.2 Scope and interpretability of the comparison . . . 73
5.3 Materials and Methods . . . 73
5.3.1 Participants . . . 73
5.3.2 Experimental setup . . . 73
5.3.3 Protocol . . . 74
5.3.4 Sensors and placement . . . 75
5.3.5 Data acquisition protocol . . . 75
5.3.6 Signal processing . . . 76
5.3.7 Synchronization and preprocessing . . . 76
5.3.8 Segmentation . . . 77
5.3.9 Descriptor selection and rationale . . . 77
5.3.10 Inter-lap comparison . . . 78
5.4 Results . . . 78
5.4.1 Framework for cross-lap comparison . . . 78
5.4.2 Percent-cycle analysis . . . 79
5.4.3 Time domain . . . 86
5.4.4 Interpretation caveats: speed, gearing, and riding style . . . 93

6 Discussion 113
6.1 Synthesis across the thesis . . . 113
6.2 Design guidelines for handbike comfort, stability, and usability . . . 114
6.3 Model-based interpretation of frequency-domain content . . . 115
6.4 Interpretation of field results (Chapter 5) . . . 116
6.4.1 Interpretation of percent-cycle results . . . 116
6.4.2 Interpretation of time-domain results . . . 118
6.4.3 Linking vibrational modeling and experimental findings . . . 120
6.4.4 Limitations and future perspectives . . . 121

7 Conclusions 125

Chapter 1

Introduction

Handcycling sits at the crossroad of biomechanics, rehabilitation engineering, and sports performance. Unlike push-rim wheelchair propulsion, the closed-chain mechanics of the handbike allow force to be applied throughout the entire 360ř crank cycle. This fundamental change in how the upper body interacts with a vehicle has far-reaching consequences: smoother transmission of effort, lower peak joint loads at the shoulder, and, in many contexts, higher mechanical efficiency [1, 2, 3]. Over time, what began as an assistive technology for daily mobility has also become a performance platform and a training tool, inviting clinicians, engineers, and coaches to ask, often with different emphases, the same question: how can we measure, interpret, and ultimately improve what happens when a person handcycles in the real world [4, 5, 6]?

For people with spinal cord injury and other mobility impairments, the handbike is first an enabler of participation. It allows users to cover greater distances and more steadily than push-rim propulsion in many everyday settings, and it creates a viable pathway to meet physical-activity guidelines with equipment and routines that are acceptable and often enjoyable [7, 8]. Yet the same device also exposes the user to stresses that require careful attention. Outside the laboratory, routes are not uniform. Surfaces change from smooth asphalt to broken pavement or gravel; curves come at different radii and with different entries; gradients rise and fall. These features inject variability into the system in the form of terrain-induced excitation and steering demands. In a handbike, variability is not noise in the statistical sense; it is the lived context of the task.

This tension between control and variability calls for a research perspective that extends beyond the boundaries of any single discipline. Physiology explains how internal load responds to external demands, but on its own it can't fully account for why hand or backrest vibration intensify on specific surfaces or during certain manoeuvres. Mechanics clarifies transmission pathways from wheel to frame to rider, but it needs data to remain anchored in reality. Wearable sensing offers the possibility of measuring performance in realistic settings, but it must be validated and interpreted carefully if it is to withstand the complexities of outdoor use. For these reasons, the present thesis moves gradually from conceptual synthesis, to modeling, to measurement, and finally to applied field analysis, with the aim of linking mechanical configuration and propulsion strategy to the patterns

of vibration observed during outdoor handcycling.

The starting point is a structured review of the handbike literature up to 2022, organized in a taxonomy that gives the field a clear and common way to describe handcycling research [9]. In that analysis, documents were not only counted and clustered; they were evaluated by categoriesclinical tests, device, forces, geometry, sensors, and actuationthat highlight areas where knowledge is well established and others where understanding can still be strengthened. This evaluation highlights distinct trends. Clinical and physiological aspects are comparatively well represented, often in controlled environments with ergometers and treadmills. Technical details that matter on the road backrest angle, handle geometry, crank mode appear, but unevenly. Actuation itself is treated both as a mechanical choice (synchronous versus asynchronous) and as a control problem with consequences for stability and steering [10, 11]. The review thus serves a double function: it situates handcycling among allied domains and it makes clear that progress will require methods that bridge laboratory insight and field validity.

From there, the thesis turns to measurement, because without repeatable sensing there is no reliable story to tell. Before evaluating the sensors in outdoor human trials, we analyzed their behaviour by testing them on a motor-driven Artificial Upper Limb Mechanism (AULM). This platform replicates handcycling kinematics with high repeatability, enabling controlled assessment of sensor linearity, drift, bandwidth, and noise characteristics [12]. The study addressed the practical need to identify sensor locations capable of yielding cycle-wise acceleration signatures that are as stable and informative as possible. By comparing locations on rigid links and around joints, and by looking at dispersion across many cycles under controlled cadence, the study shows that some sites, especially those close to the actuated joint or the hand interface, yield more repeatable profiles, whereas others accentuate local corrections and inflate variance. The conclusion is not a rigid prescription but a principle: if field analysis is to discriminate between genuine control changes and mere sensor noise, site selection should be guided by repeatability benchmarks rather than convenience alone.

With a dependable way to look at signals, the next step is to develop a language to reason about comfort and vibration. Here the long-standing literature on seated human exposure provides both examples and cautions. Lumped-parameter modelsrigid bodies connected by effective springs and dampersare not full-body simulators, but they capture the dominant pathways of transmission and are simple enough to be fitted and validated against experimental data [13, 14, 15]. Following that tradition, this thesis proposes a compact three-degree-of-freedom model of the handbikerider system that couples front and rear wheel contact to the frame and to the seatrider interface [16]. The intent is conceptual clarity rather than exhaustive detail. When the road injects energy at specific frequencies, when posture shifts the effective seat stiffness, when geometry moves mass relative to support points, the model predicts how amplitudes and phases will reallocate along the chain from input to trunk to hands. Outdoor measurements will later support and contextualize these predictions, without being detailed here.

Equipped with synthesis, validated sensing, and a working model, the analysis moves

outdoors, where handcycling actually happens. On a mixed-surface loop including straights, tight turns, a climb, and a gravel segment, multiple IMUs are distributed across mechanical and anatomical sites: wheel to read terrain input, backrest to index transmission to the trunk, handle and wrists to index distal control. In such a setting, a single way of looking at data is not enough. If one collapses everything to cycles and averages them, changes in timing and pace disappear and transients are washed out. If one preserves time and overlays signals as they occurred, morphology and regularity of the cycle are harder to read. The thesis therefore adopts two complementary lenses on exactly the same signals: a percent-cycle representation that highlights the geometry and regularity of the propulsion pattern, and a time-aligned view that keeps absolute timing and entry conditions intact. Read together, they allow one to say whether a quieter profile is the result of steadier execution at the same pace or the byproduct of slower approaches, and to localize where and when improvements are realized on the wheel because of better line choice, at the backrest because of posture, or at the hands because steering corrections are restrained.

Across this arc, a methodological thread ties the studies together. Taxonomy comes first so that measurement can be purposeful: the sensors behavior is evaluated in controlled environment before their use in the real-world, ensuring that what happens outdoors is not misinterpreted as a sensor artefact. Moreover, dual-domain analysis prevents conflating shape with time. The technical content of the chapters reflects this logic. The review offers the vocabulary and the roadmap [9]. The AULM study turns that vocabulary into a protocol for sensor placement that trades sensitivity for reliability in a transparent way [12]. The vibrational model translates outdoor signatures into a compact set of parameters that can be interrogated and, in principle, tuned through design or coaching [16]. Finally, the outdoor analysis shows, in a real-world setting, how variability and jerk vary between the two rides (two participants) and across circuit segments when terrain and control demands change, and how these evolutions align with the models transmission pathways.

Handcycling research will continue to benefit from work that progresses through cross-disciplinary contributions. Physiological studies refine how training is dosed and recovered; classification-aware ergonomics clarifies how geometry should be assigned or adapted; sensor engineering makes real-world data acquisition more reliable. But what the community most needs are integrative frameworks that treat the riderbike system as distributed, that separate input, transmission, and control, and that speak clearly to practice. This thesis is offered in that spirit. It aims to show that when measurement is validated, modeling is honest about its scope, and outdoor analysis respects the realities of terrain and timing, the handbike can be understood as a systemand once it is legible, it can be improved for comfort, sustainability, and performance alike [9, 12, 16, 10, 11, 13, 14, 15, 7, 8, 5, 4, 6].

This chapter has outlined the overall aims, structure, and methodological rationale of the research, framing handcycling within its multidisciplinary intersection of biomechanics, engineering, and rehabilitation. With the scope of the work defined, the following chapter provides the necessary theoretical foundation by mapping the current state of the art.

Specifically, Chapter 2 reviews the scientific literature on handbike architectures, propulsion strategies, and technical characteristics, establishing the baseline upon which the subsequent methodological validation and modeling phases are built.

Chapter 2

Handbike for Daily Use, Sport, and Rehabilitation Purposes: A Literature Review of Actuation and Technical Characteristics

In this chapter, the following peer-reviewed journal article is reproduced in its original published layout, including the journal formatting, logos, and pagination. The paper was conceived as a structured literature review on handbikes and their technical characteristics and, within this thesis, it provides a comprehensive and systematic overview of the state of the art, serving as an embedded annex that frames the experimental work presented in the subsequent chapters.

Bibliographic reference
Michele Sanguinetta, Giovanni Incerti, Cinzia Amici, and Giovanni Legnani.
Handbike for Daily Use, Sport, and Rehabilitation Purposes: A Literature Review of Actuation and Technical Characteristics. *Actuators*, 2024, 13(2), 50.
doi: 10.3390/act13020050.

actuators

IMPACT FACTOR 2.2

CITESCORE 3.9

Review

Handbike for Daily Use, Sport, and Rehabilitation Purposes: A Literature Review of Actuation and Technical Characteristics

Michele Sanguinetta, Giovanni Incerti, Cinzia Amici and Giovanni Legnani

Special Issue
Actuators in Assistive and Rehabilitation Robotics

Edited by
Prof. Dr. Xiangrong Shen and Dr. Vishesh Vikas

actuators

MDPI

Review

Handbike for Daily Use, Sport, and Rehabilitation Purposes: A Literature Review of Actuation and Technical Characteristics

Michele Sanguinetta, Giovanni Incerti, Cinzia Amici * and Giovanni Legnani

Department of Mechanical and Industrial Engineering, University of Brescia, Via Branze 38, 25123 Brescia, Italy; m.sanguinetta@unibs.it (M.S.); giovanni.incerti@unibs.it (G.I.); giovanni.legnani@unibs.it (G.L.)
* Correspondence: cinzia.amici@unibs.it

Abstract: With respect to alternative devices like traditional wheelchairs, handbikes can offer advantages from biomechanical and physiological perspectives, to several kinds of users. Assuring high mechanical efficiency and homogeneous force distributions along cycles, and being suitable for indoor and outdoor activities, these systems are used for rehabilitation, sports, and daily applications. From a technical perspective, their main characteristics can vary with the device final purpose and operational context. This review aims to provide an overall outline of handbikes in the literature from a general and comprehensive point of view, up until 2022. The analysis is performed (i) with a systematic approach, without a priori limitations on document type and content focus, and (ii) to identify the areas of interest for the scientific development of these systems. A systematic evaluation method for the identification and analysis of the documents was designed and implemented and the selection criteria, as well as the rationale for the procedure, are described. A specific taxonomy was defined and applied for the subsequent analysis, and each category is specifically evaluated and described, detailing the main outcomes of the literature analysis and relative discussion. Particular attention is paid to actuation strategies and propulsion efficiency. Finally, the main results of the work and future developments for handbikes are briefly synthesized.

Keywords: handbike; wheelchair; handcycling; actuation; propulsion; biomechanics; rehabilitation review

Citation: Sanguinetta, M.; Incerti, G.; Amici, C.; Legnani, G. Handbike for Daily Use, Sport, and Rehabilitation Purposes: A Literature Review of Actuation and Technical Characteristics. *Actuators* **2024**, *13*, 50. https://doi.org/10.3390/act13020050

Academic Editors: Xiangrong Shen and Vishesh Vikas

Received: 7 December 2023
Revised: 15 January 2024
Accepted: 22 January 2024
Published: 26 January 2024

1. Introduction

Handbikes are vehicles composed of two-rear wheels and one front wheel. The latter is connected to a handle through a roller chain, which is able to increase the mechanical efficiency, with respect to traditional wheelchairs, up to 15 [1]. Handbikes may present various architectures to adapt to the needs of different users. Figure 1 collects the most common kinds of handbikes. Besides the most traditional solutions, nowadays hybrid devices are also available, which functionally transform wheelchairs into handbikes by adding custom or off-the-shelf attachments to traditional wheelchairs. In the present work, only integrated devices, realized as a whole to enable handcycling, and often referred to as fixed-frame devices, will be properly considered as handbikes; hybrid solutions will be also partially described, but an analysis of these systems is outside the main purpose of the present work. Figure 2 presents an example of the considered handbikes, depicting the main components of this kind of devices and synthesizing the basic applied nomenclature.

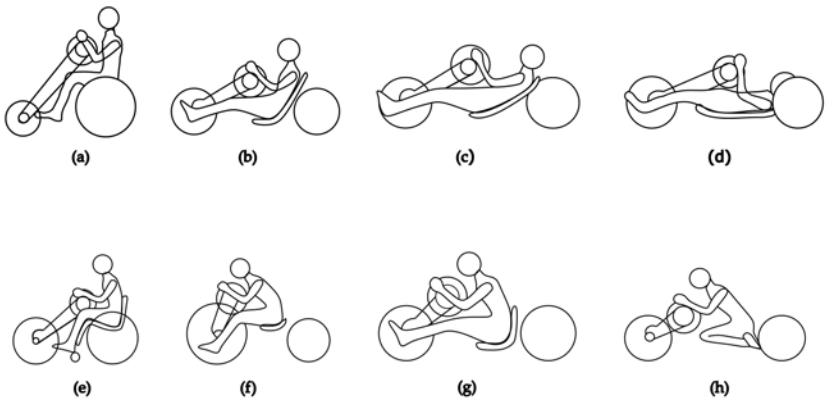

Figure 1. Schematic of the most common kinds of handbike architectures, divided into arm propulsion on the upper row, and arm trunk propulsion on the lower row, with: (**a**) attach unit handbike, (**b**) recumbent 60° rigid frame, (**c**) recumbent 30° rigid frame, (**d**) recumbent 0° rigid frame, (**e**) attach unit handbike, (**f**) car-seat, (**g**) long-seat, and (**h**) knee-seat.

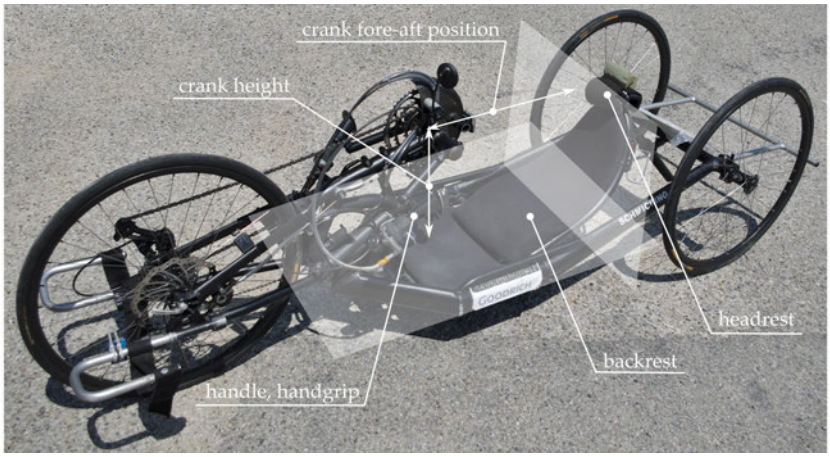

Figure 2. Example of handbike: main components and basic applied nomenclature. Modified version of the image by C. Bucco-Lechat, 2014 [2].

According to literature, using a handbike for daily life confers advantages from a biomechanical and physiological point of view with respect to traditional wheelchairs for several kinds of patients, like subjects affected by spinal cord injury (SCI) [3,4].

For instance, as observed in the work by Dallmeijer et al. of 2004 [5], the propulsion of a handbike depends on a closed-chain motion, and the force applied to the handle contributes to movement during all the 360° of the motion cycle. Furthermore, in a work of 2012, Arnet et al. [6] shows that the force distribution is more homogeneous during an entire handle rotation of the handbike, also referred to as the hand-cycle, than during an analogous wheelchair cycle. This is due to the fact that, for the handbike, an individual's hands are always in contact with the handle during the propulsion act; for the wheelchair instead, the hands have to transmit sufficient force on the wheel generating movement in a short amount of time. As a result, the force during a wheelchair cycle presents peaks three times higher than a handbike, and generates significant torques at the shoulder joints. Over time, this condition could lead to overuse injuries called repetitive strain injuries (RSI).

Another advantage of the handbike is its versatility. Handbikes can be used outdoors and indoors and for different purposes, such as for training, also attached to a traditional ergometer, or to follow rehabilitation programs. In this latter case, handbikes can be equipped with specific components, like additional gears assuring different gear ratios, as

shown in the study by Van Der Woude et al. [7], to confer fluidity to the movement and enhance mechanical efficiency.

Focusing on technical solutions, the backrest deserves particular attention. Indeed, the backrest can be reclining as well as not even present, according to the needs of the user and the severity of their impairment, or depending on the UCI (Union Cycliste Internationale) rules in the case of racing. In the first case, with backrest, according to Nevin et al. [3] we have an Arm power Propulsion (AP), propelled by paraplegic patients, and the backrest angle can range from 0° to 60°(see Figure 1a–d). In this scenario, propulsion is only given by upper limbs movements. The second case, without backrest, is called Arm Trunk Propulsion (ATP), and in these devices the trunk's flexion/extension contributes to propelling the handbike (as depicted in Figure 1e–h).

The kind of propulsion can also be classified into two types: synchronous and asynchronous. According to the works conducted by Kraaijenbrink et al. [8,9], the synchronous mode with the extra use of trunk is the more efficient way to propel a handbike in terms of power production and vehicle conduction.

Furthermore, handbikes also play an important role in rehabilitation. As exposed in the work of Nooijen et al. [10], wider physical benefits like greater power production and maximal oxygen consumption have been detected in the SCI subject when handbike training was added to the traditional rehabilitation program. In addition, a cross-sectional study by Van Der Woude et al. [11] reveals that handcycling is an effective intervention, which is able to maintain an active lifestyle and enables preventing secondary health conditions like pressure sores, urinary tract infections, osteoporosis, upper-extremity pain and cardiovascular diseases.

According to the Scopus database, the interest of the scientific community in handbikes and their features has remarkably increased since 2008, reaching a peak in 2021 and 2022 with 20 published documents every year, as Figure 3 depicts. Within all the published documents, only seven were classified as reviews according to Scopus.

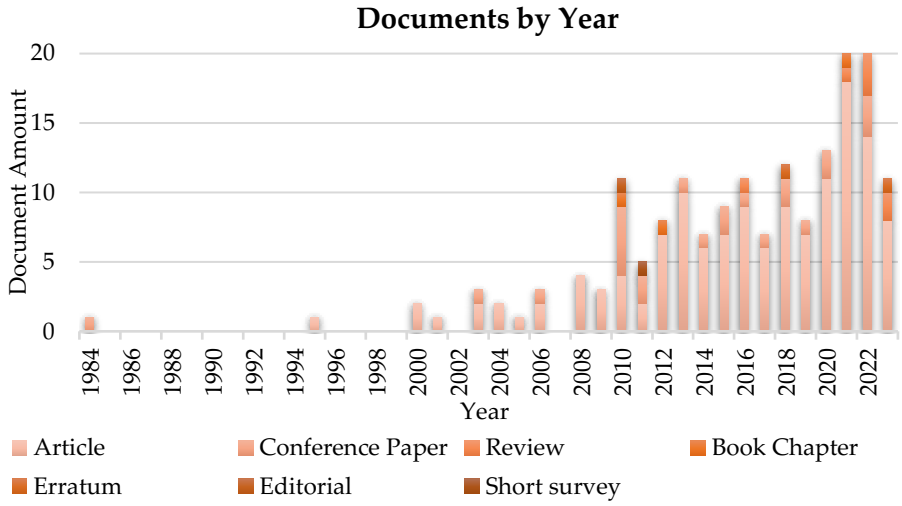

Figure 3. Documents referring to the "Handbike" topic in the Scopus database, by year.

Among the first literature reviews, there is the work published in 2016 by Rice et al. [4]. However, more than outlining an overview of the overall scientific literature from a broad perspective, the paper mainly focuses on the specific topic of the technology used in sports where a wheelchair is needed. In 2021, Flueck et al. [12] present a narrative review, but centered it on nutritional considerations for para-cycling athletes. Finally, Nevin et al. [3], Goodlin et al. [13], and Rayes et al. [14] published three additional review works in 2022. In the first one, Nevin et al. proposed a narrative review of the handbike analyzing 49 documents, focusing on biomechanics and physiology characteristics of competitive handcycling, such as seat positioning, crank height, and fore-aft position, as well as peak

aerobic power output, and relative upper body strength, suggesting practical training of the human upper body for competitive performance. The work by Goodlin et al. [13] instead depicts an overview of para-cycling, including evaluations on technological solutions from tandem cycling, to handcycling, to tricycles. Similarly, Rayes et al. [14] describe adaptive sports for the SCI subject, including the handbike, among several others, without a dedicated focus.

Since none of the previous works seem to provide an overall technical outline of handbike in literature from a general and comprehensive point of view, this review analyzes scientific literature until 2022 (i) with a systematic approach, without a priori limitations to document type or content focus, and (ii) with the main aim of depicting an overview of the areas of interest for scientific developments of these systems, giving particular attention to the actuation field.

To reach this goal, a systematic evaluation method for identification and analysis of the documents was designed and implemented. The following Section 2 describes selection criteria and rationale of this procedure, introducing the taxonomy applied for the subsequent analysis. Each category is then specifically evaluated and described in Section 3, detailing main outcomes of the literature analysis and relative evaluations. Finally, Section 4 briefly summarizes the main results and possible limitations of the work.

2. Materials and Methods

This section describes the procedure applied to select the analyzed research products, the identified taxonomy for the data evaluation, and the implemented data processing.

2.1. Data Selection

The research was performed querying the Scopus database with the string *TITLE-ABS-KEY (hand*bik* OR hand*cycl*)*. The last query was run on the 30 November 2023, providing 174 results, classified according to the Scopus database as follows: 136 articles, 24 conference papers, 7 reviews, 3 book chapters, 2 errata, 1 editorial, and 1 short survey.

Two exclusion criteria were imposed on the results of the string search: (i) documents must have been published within 2022, and (ii) the document language of the full text was required to be English. The final dataset was therefore composed of 160 documents.

Figure 4 presents a schematic of the applied data selection process, whereas Figure 5a,b depict the distribution of the results as total number of documents by type and their evolution in time, respectively.

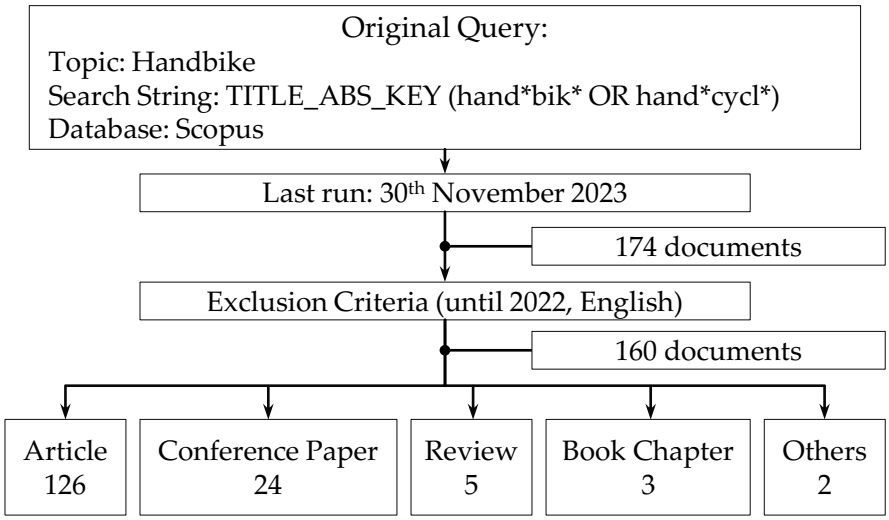

Figure 4. Flow chart of the applied documents selection process ('Others' includes editorials, short surveys, and errata).

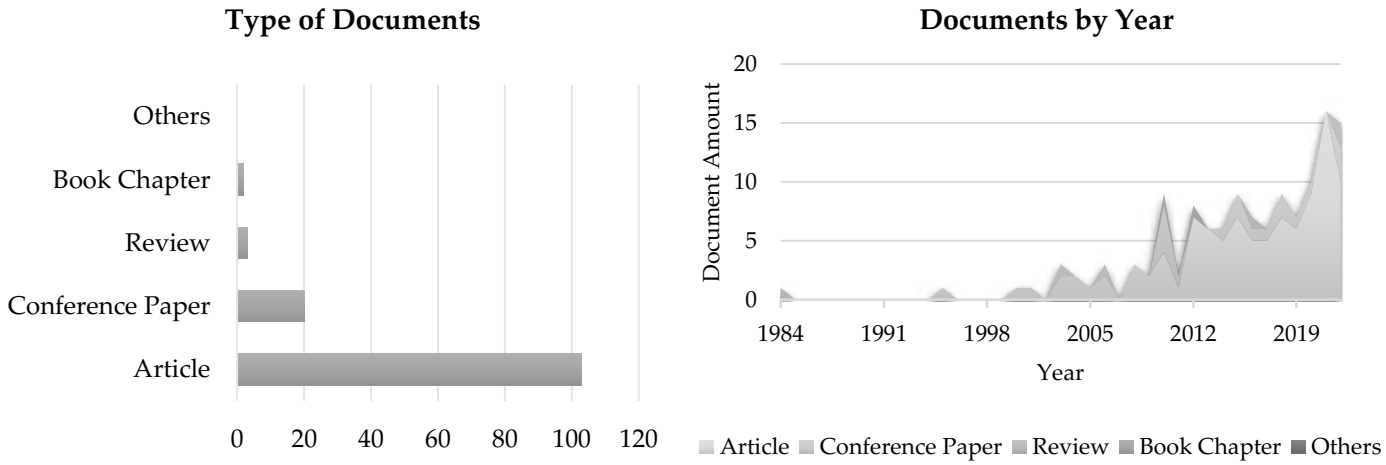

(**a**) (**b**)

Figure 5. Literature overview. (**a**) Total number of documents divided by type; the category 'Others' includes errata, short surveys, and editorials. (**b**) Evolution in time of the total number of documents by type.

2.2. Taxonomy

To investigate and classify the main topic of the documents, a set of categories and sub-categories was initially defined based on preliminary analysis of previous works and authors' experience. The list was interactively integrated during the analysis, and the following categories were finally identified:

Clinical tests. To be included in this class, documents shall include results regarding main physiological parameters in handcycling (e.g., maximal oxygen uptake VO2, Blood lactate BLa, energy expenditure EE, and power output PO), or involve patients to produce results. Papers in this category can therefore be clinical studies, but this characteristic is not mandatory.

Device. This category collects documents focusing on the analysis of the devices for the experimental setup of handbike testing. For instance, papers describing the use of ergometers or treadmills during data acquisition, as well as focusing on the design process of the whole handbike, or the study of parts of it, are included in this class.

Forces. This section includes documents investigating the forces exerted by the user during a handcycle. The analysis can include the assessment of forces generated in the subject at different anatomical areas (like the shoulder or all the upper limb), as well as at the interface with the device (i.e., handle).

Geometry. This category collects the documents that study mechanical adjustments of the handbike that alter the biomechanics of athletes or patients. For instance, works referring to modifications at crank inclination, height, and length, as well as distance between cranks, or backrest inclination, and wheels dimensions or pressure, are classified within this class.

Sensors. This class gathers the works dealing with sensors and measurement systems used to access the performance of the subject and/or the handbike, both in laboratory and outdoor environments, for tests, sport practice, and race conditions. No distinction in the inclusion was made between papers presenting custom-made systems and works using commercial sensors.

Actuation. This category collects the documents which study the propulsion of the handbike, both in terms of biomechanical models of the handcycling and technical solutions, like different crank modes.

Other. This class gathers the studies focusing on topics not expressly falling into one or more of the previous categories, such as literature reviews.

Each document in the subset of the 160 selected products was in particular classified according to a set of sub-classes for each category. Figure 6 collects the applied taxonomy. The classification was performed assigning each paper to one or more sub-classes.

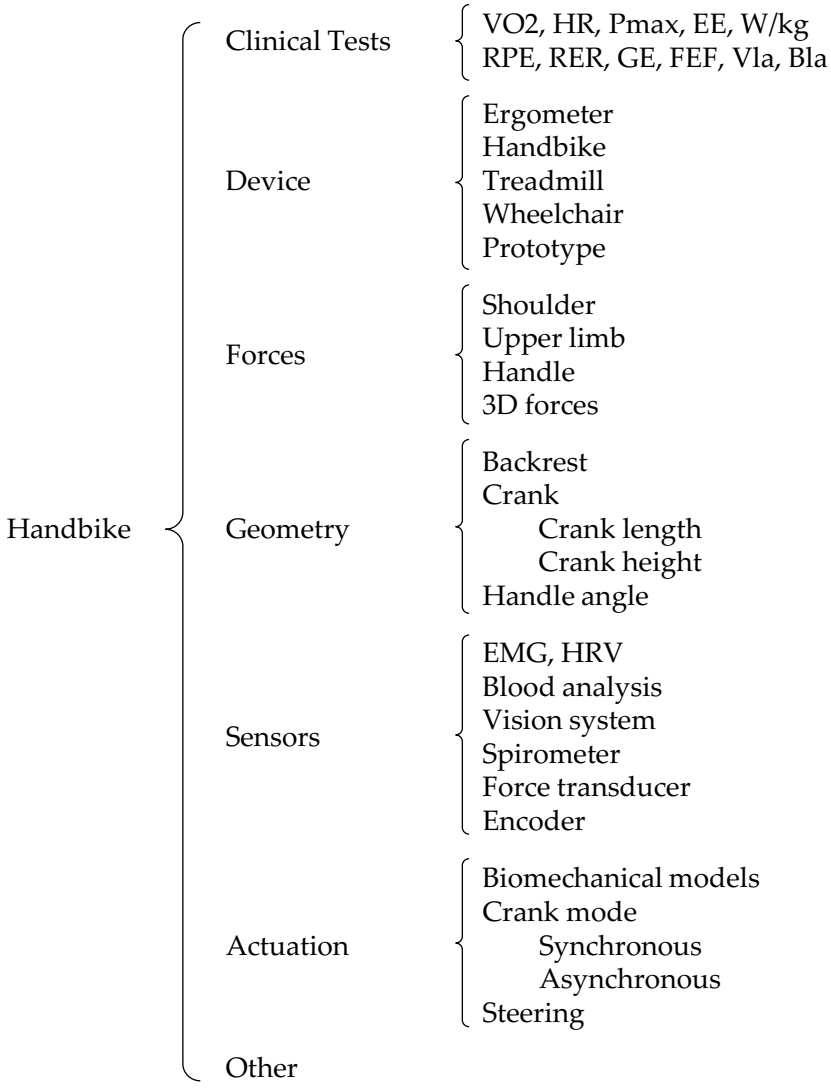

Figure 6. Applied taxonomy: classes and sub-classes adopted for the classification of the analyzed documents.

For the category Clinical Tests, a set of sub-classes was identified, corresponding to the most common measurable quantities associated with the assessment of performance, such as biosignals, functional quantities, and performance indexes. The following sub-classes were therefore identified:

VO2, Maximal Oxygen Uptake [mL/min]: this quantity corresponds to the maximum rate of oxygen consumption measured during incremental exercise;

HR, Heart Rate [Bpm]: this parameter represents the frequency of the heartbeat measured by the number of beats of the heart per minute;

$\mathbf{P_{max}}$, Power Peak [W]: this index describes the maximal power exerted during specific tasks, like incremental, exhaustion, or sprint tests;

EE, Energy Expenditure [kcal/h]: this parameter evaluates the mean energy consumption. This value is typically evaluated according to the definition used by Abel et al. in 2006 [1,15];

W/kg, Power per Kilogram [W/kg]: this index computes the power produced by the subject, per kilogram;

RPE, Rating of Perceived Exertion: this quantity is evaluated according to the RPE Borg Scale, i.e., a clinical scale used to assess an individual's perception of their own exertion or effort during physical activity or exercise [16].

RER, Respiratory Exchange Ratio: this index measures the ratio between the produced volumes of carbon dioxide (VCO2) and oxygen (VO2);

GE, Gross Efficiency: this parameter computes the ratio between the power measured on the handbike, and the estimation of the power generated by the user;

FEF, Fraction Effective Force: this quantity accesses the component of force that actively contributes to the motion of the crank;

Vla, Lactate Production [mmol/(L·s)]: this index estimates the maximal lactate accumulation rate produced by the subject;

Bla, Blood Lactate Concentration [mmol/L]: this index assesses the lactate concentration in the subject's blood.

For the Device category, the sub-classes presented in the following were considered:

Ergometer. This sub-class gathers papers including the use of ergometers for handbike-related applications;

Handbike. This sub-category collects the works providing some technical details of the used handbike, for instance describing the device model;

Treadmill. This sub-class includes papers presenting treadmills in the experimental setup of the handbike;

Wheelchair. This sub-category collects the works that include comparisons between handbike and wheelchair perfomances;

Prototypes. This sub-class includes papers describing prototypes of innovative solutions, such as new methods of propulsion with respect to handcycling, or re-designs of classic devices.

For the Forces category, a set of sub-classes corresponding to relevant anatomical districts were identified. An additional field was considered to capture those works investigating handcycling as a three-dimensional movement. The final set of sub-classes was therefore composed of the following:

Shoulder. The shoulder sub-category includes all the papers that are related to the study of the forces and torques acting on the whole shoulder complex in general, or on parts of it, like the glenohumeral joint, when using a handbike or a wheelchair.

Upper Limb. This sub-class collects all the documents involving the investigation of forces exerted during handbike activities by muscles of the upper body.

Handle. The Handle sub-category collects all the papers that study the force exchanged between the subject and the handle grip when handcycling.

3D Forces. This sub-class includes the papers in which force is analyzed in space, therefore evaluating the three components of the force vector.

For the Geometry class, four sub-classes were investigated:

Backrest. This sub-class gathers the works dealing with the investigation of the backrest of handbikes, analyzing its effects on the handbike performance.

Crank. This sub-class includes the documents proposing and comparing different settings regarding the handbike crank, with particular attention to crank length and height.

Handle Angle. The Handle Angle sub-category collects the papers focusing on the analysis of the handle grip's angle, for instance evaluating the effect of modifications in its value.

For the Sensors category, the followings sub-classes were considered, depicting the most spread measurement systems integrated or applied to handbikes, as well as the most commonly measured quantities for both the handbike and the user:

Electromyography. This sub-class collects all the papers describing the use of electromyographic (EMG) sensors during tests performed with a handbike.

Heart Rate Variability [HRV]: This sub-category gathers the works presenting sensors of different kinds, that record heartbeats fluctuations.

Blood Analysis. This sub-class gathers the works that include sensors for the analysis of the user's blood, i.e., sensors that enable the assessment of chemical or physical properties of blood samples taken during or after a test.

Vision System. The vision system sub-class collects all the documents related to the acquisition of real-time movements of the subjects, through vision capture systems.

Spirometer. This sub-category collects the papers involving the use of systems to measure the volume of air expired or inspired by the subject's lungs, for instance to identify ventilation patterns.

Force Transducer. The force transducer sub-class collects the documents related to instruments placed on the handle that provide information about the forces exerted by subjects, for instance, in terms of amplitude and direction.

Encoder. This sub-category gathers documents in which encoders are used or investigated.

Finally, the following sub-classes were identified for the Actuation category:

Biomechanical models. This sub-class gathers all the works describing the handcycling task with biomechanical models, for instance presenting the design of new models, investigating solutions for the identification of related parameters, or optimization strategies for handbike propulsion.

Crank mode. This sub-category collects all the documents that investigate the propulsion of the device from a mechanical perspective. This includes for instance the analysis of the different crank modes, as well as the comparison of the two main types of possible propulsion, namely synchronous and asynchronous, which depict the conditions of shift-phase between left and right handles at 0° or 180°, respectively.

Steering. The steering sub-class collects those papers presenting studies in which the handbike used for tests or outdoor activities has the capacity to turn the crank around an axis in the sagittal plane of the subject in order to change the direction of motion.

Each category was then independently analyzed with respect to the following aspects:

- The distribution of the documents in time, by type;
- An analysis of the documents by sub-class;
- A discussion of main characteristics and results of the category, with particular attention to sub-classes.

In particular, the first two levels of analysis were performed through an observational approach, aiming to outline a quantitative description of the literature, whereas the final level of investigation was performed through a detailed study of the documents that aimed to provide the reader with a descriptive analysis of the most relevant findings currently available in the scientific literature.

According to these considerations, the following Section 3 presents for each subsection a first part, reporting the quantitative aspects of the analysis, and a second part, depicting

the descriptive analysis, as the main results of the defined categories with specific attention to the identified sub-classes.

3. Results and Discussion

The set of 160 documents was analyzed by applying the proposed taxonomy, and 32 products were classified as out of topic. The final set of documents, analyzed by categories and sub-classes, was therefore composed of 128 products.

The list of the evaluated documents is reported in Table A1, with the synthesis of the classification among categories and an extract of the sub-classes. More detailed investigations by category are presented in the following.

3.1. Clinical Tests

There were 107 documents classified in the clinical test category, and these were distributed among 95 articles, 11 conference papers, and 1 book chapter, as Figure 7a shows. The number of published documents, and number of articles in particular, has especially increased in the last twenty years, with a peak of 14 articles reached in 2021.

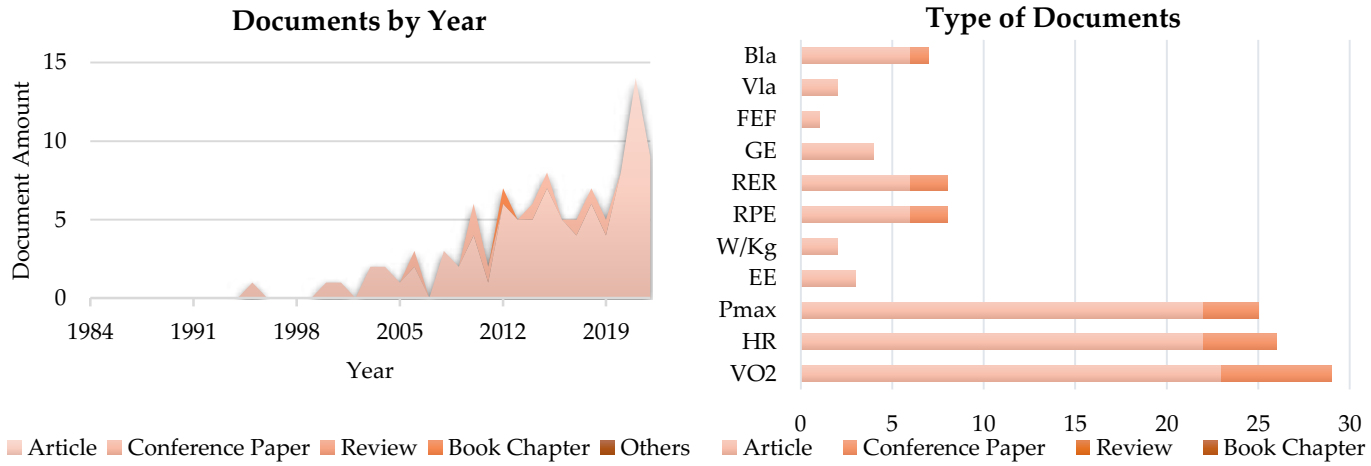

(**a**) (**b**)

Figure 7. Clinical test category: (**a**) evolution of documents in time, and (**b**) number of documents in each sub-class for the clinical test category, divided by document type.

Clinical Test Sub-Classes

Figure 7b presents the distribution of identified documents among the sub-fields of the clinical test category: the most studied quantities are the maximal oxygen uptake (VO2), with 29 documents, then heart rate (HR) and maximum pressure (P_{max}), with 26 and 25 documents, respectively. The graph also allows capturing the distribution by type of document. In more detail, most of the products are classified as articles, followed distantly by conference papers.

While investigating the documents in this category, the opportunity of evaluating additional elements in more detail, for better understanding and comparison purposes, emerged. In particular, the documents revealed interesting analogies and differences when investigating the applied experimental setups and protocols. Table 1 presents an example of those characteristics for an illustrative subset of relevant documents.

The data reveal that 41 documents enrolled subjects without disabilities, 64 involved subjects with disabilities, such as SCI, tetraplegia, and paraplegia, and 12 documents enrolled both subjects with and without disabilities. Referring to the exploited instrumentation, 43 documents used handbikes and 3 documents used both handbike and wheelchair. In some cases, hybrid handbikes are also used for the acquisitions, especially where the use of a treadmill is required, as in the experimental setups described in Figure 8.

Table 1. Example of characteristics describing applied experimental setups and protocols for the documents classified into the clinical test category.

Document ID	Subject		Instrumentation		Experimental Conditions					Environment			
	with Disability	without Disability	HB	Wheelchair	RPE	%HRR	Fixed Power	Fixed Lactate	Exhaustion	Indoor	Race	Train	Therapy
Abel_2003 [17]	x		x						x				
Dallmeijer_2004 [5]	x	x	x				x [1]						
Lovell_2012 [18]	x		x				x [2]		x				
Verellen_2012*a* [19]		x	x			x	x [3]						
Hettinga_2013 [20]	x	x	x						x				
Abel_2015 [21]		x	x				x [4]						
Bakkum_2015 [22]													
Fischer_2015 [23]	x									x			
Hettinga_2016 [24]		x				x			x				
Schoenmakers_2016 [25]		x				x							
Hutchinson_2017 [26]	x				x					x			
Kraaijenbrink_2017 [27]		x					x [5]						
Quittmann_2018 [28]		x	x						x				
Rappelt_2022 [29]		x	x				x				x		
Kouwijzer_2022 [30]	x		x							x			
Abonie_2021 [31]		x	x			x							
Hutchinson_2021 [32]	x	x	x	x					x				
Kouwijzer_2021 [33]	x						x [6]						
Hall_2022 [34]	x		x						x				
Muchaxo_2022 [35]	x		x						x				

[1] (25–35) W. [2] (50–80) W. [3] 130 W. [4] 20 W. [5] (0–10–20) W. [6] (0–5–10–15–20) W.

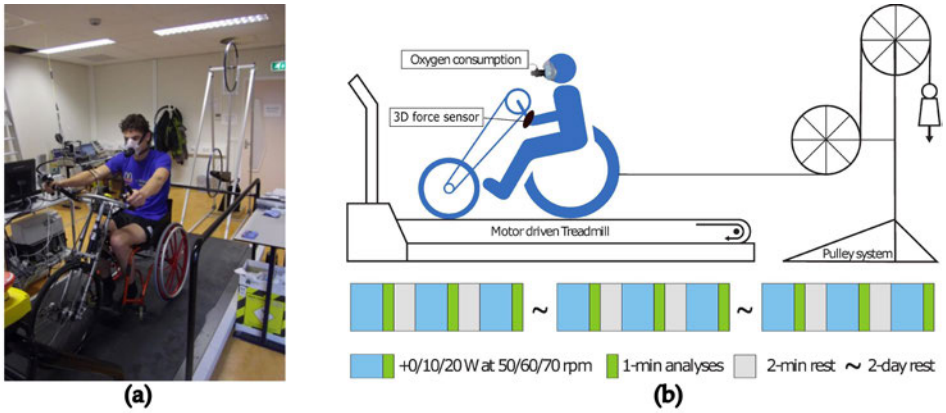

Figure 8. Examples of experimental setups for the assessment of relevant quantities in the Clinical Test category: (**a**) a spirometer is used to evalute VO2 while the subject is handcycling on a treadmill with a hybrid handbike (source: Schoenmakers et al., 2016 [25]) and (**b**) a 3D force sensor is used to compute the power production (source: Kraaijenbrink et al., 2017 [27]).

Focusing on the experimental conditions, in two cases the evaluations were performed at fixed RPE condition, and in four cases at fixed %HRR. In 12 documents, fixed power conditions were imposed, and in two cases a fixed lactate threshold was applied. In 16 cases, the test was conducted until the subject's exhaustion. Finally, considering the environment of the data acquisition, in 25 works, the tests were performed in a laboratory, in 5 documents during races, in 12 cases during training, and in 3 works during rehabilitation training sessions.

Evaluating in more detail the content of the investigated documents, several interesting aspects emerge. The assessment of oxygen uptake VO2 and peak oxygen uptake $VO2_{max}$ holds vital significance for a wide spectrum of professionals, including clinicians and athletes. Particularly in SCI individuals engaged in upper-body exercises, it not only stands out as a predictor of all-cause mortality, but also the percentage of $VO2_{max}$ is advocated for as a fundamental metric for customizing exercise intensity based on an individual's fitness level. In the work conducted by Hutchinson et al. [26], a method of evaluating $VO2_{max}$ is presented. Participants have to complete five two-minute stages at clamped RPE of respectively 11 (light), 13 (somewhat hard), 15 (hard), 17 (very hard), and 20 (maximal exertion) on Borg's RPE scale. Gas exchange variables were collected throughout the test. The authors explain that this test is a valid protocol to assess $VO2_{max}$ in novice, recreationally active, and young handbike users. According to Dallmeijer et al. [5], handcycling is less strenuous and produces a higher exercise response than the traditional wheelchair at a moderate power output level. In fact, the authors' data reveal that tests conducted at a constant power of 35 W present lower values of VO2 and HR, both for paraplegic and subjects without disabilities. Accordingly, the authors suggest handbikes as a means of transportation in daily life. Abonie et al. [31] also highlight how low-intensity upper-body handbike training (training conducted at 30% of maximal subject's heart rate) on a powered treadmill reduces VO2 and improves physical capacity and prevents premature fatigue and overuse in untrained subjects. On the other hand, Hall et al. [34] evaluate how SCI subjects reach high values of $VO2_{max}$ when they regularly use handbikes for at least 1 hour per day. According to Hall et al., handbike-trained SCI subjects have the higher aerobic capacity and, as a consequence, more tolerance to high-intensity exercise. Similarly to Hall et al., the study conducted by Lovell et al. [18] reveals, through a peak aerobic test carried out on an electromagnetically braked cycle ergometer, that handbike-trained SCI subjects had higher $VO2_{max}$ with respect to their age-matched non-trained counterparts. According to the authors, handbike training can therefore prevent cardiovascular disease, and $VO2_{max}$ can serve as a predictor for 20 km time trial performance. Rappelt et al. [29] find that lower-body low-frequency electromyostimulation (EMS) significantly increases acute oxygen uptake. In their work, 26 healthy participants completed a task of sitting,

sitting with concurrent EMS of the legs, handcycling, and handcycling with concurrent EMS of the legs. The protocol consists of four 10 min intervals interspersed with 5 min of passive rest. EMS was applied for 2–3 min. Electrodes were positioned at buttocks, with intensity 80.0 ± 22.7 mA, at thighs, with intensity 94.5 ± 20.5 mA, and at calves, with intensity 77.5 ± 19.1 mA. The average power output during handcycling was 35.9 ± 8.4 W. Participants were given instructions to maintain a target cranking cadence of 60 rpm. According to the authors, the simultaneous use of EMS on the participants' legs led to an acute increase in oxygen demand, amounting to a 39.7% rise (from 0.97 ± 0.21 L/min to 1.36 ± 0.44 L/min) when compared to handcycling without additional EMS stimulation.

Concerning heart rate, Hettinga et al. [24] find that local exercise for the upper body using a handbike could significantly improve heart rate peak (4%), peak $VO2_{peak}$ (+18.1%), and PO_{peak} (+31.9%) in females. In the works carried out by Abonie et al., Verellen et al., and Hettinga et al. [19,20,31], heart rate was used as a fixed parameter to conduct tests, and heart rate reserve (HRR) was especially considered, meant as the ratio between instant heart rate and heart rate peak (HR_{peak}). In particular, the subjects involved in the study of Abonie et al. performed tests at a fixed heart rate reserve of 30%, while participants engaged by Verellen et al. and by Hettinga et al. performed at 80% to 90% HRR.

Focusing on P_{max}, the same work of 2021 by Abonie et al. [31] also evaluated the effect of 7-week low-intensity upper-body handbike training in untrained individuals without disabilities. This kind of training increases the P_{max} by 20% with respect to the control group who receives no training. In the work by Lovell et al. [18], P_{max} for trained handcyclists would appear to be the best predictor of 20 km time trial performance. The authors clarify that the greater P_{max} is due to improved central and peripheral aerobic factors rather than muscular size.

Considering the energy expenditure, EE, the work by Abel et al. [17] reveals that using a handbike at moderate intensity allows an EE high enough to maintain a good health state in the person with disability, and to prevent cardiovascular disease. Specifically, a 60 min training session each day allows achieving the value of 350 kcal consumed which is described by Abel et al. as the greatest value to reduce the risk of myocardial infarction.

An additional parameter investigated in the literature is the relative peak functional performance (W/kg), which expresses the amount of power generated by an individual in relation to their body weight. In the study carried out by Abel et al. in 2015 [21], relative peak functional performance was adopted to study the effect on the subjects of three different handbike grip angles. No significant differences emerged among the three hand grip angles for W/kg.

Focusing then on the rating of perceived exertion, RPE, Hutchinson et al. [32] monitored exercise intensity in the patient with tetraplegia and paraplegia, comparing the values of a clinical scale, namely the Borg exertion scale, obtained from the two populations samples. In their study, 134 competitive subjects were split in three groups depending on the severity of illness: tetraplegic, paraplegic, and non-SCI. Subjects completed a first sub-maximal step test, then a graded exercise test, to exhaustion; during the second test, the intensity was gradually increased by 10–20 W/min or 0.1 $m \cdot s^{-1}$/min, until the participants reached a point of volitional exhaustion. According to the analysis performed by the authors, the data collected throughout the test were not affected by age or sex. In another study, Hutchinson et al. [26] conducted tests at specific RPE values to assess the oxygen uptake during handcycling.

As an alternative approach to the assessment of the intensity level of training, Dallmejer et al. [5] investigate the respiratory exchange ratio (RER), calculated as the ratio between the volume of produced carbon dioxide VCO2 and the maximal oxygen uptake VO2. In fact, Dallmeijer et al. use RER as the value to determine whether the subject's exercise is conducted at a submaximal level, that is, with an RER value of less than 1.0.

Among the papers in literature, gross-efficiency (GE) is also investigated. According to Hettinga et al. [20] and Dallmeijer et al. [5], this quantity is computed as the percentage ratio between power output (PO) and the power value associated with a basal metabolism

condition P_{met}. This value P_{met} was in particular calculated from the previously identified quantities VO2 and RER, as Pmet = VO2 · [(4940 · RER + 16,040)/60)]. In this work by Hettinga et al. [20], seven physically able male participants underwent an incremental peak exercise handcycling test on a treadmill. Furthermore, two indoor treadmill sessions were conducted at speeds of 1.3 m/s with a slope of 0.7%, and 1.0 m/s with a slope of 4.8%. Additionally, three outdoor over-ground exercise sessions were completed at speeds of 1.7, 3.3, and 5.0 m/s. One of the participants also engaged in an 8-kilometer handcycling session outdoors, representing a typically covered distance. The results indicate that GE increases as the intensity of the test arises, probably because the relative fraction of basal metabolism contributing to energy expenditure decreases with intensity.

The fraction effective force parameter, FEF, expresses a force effective index, as it evaluates the contribution of the tangential force component F_{tan} to the forward propulsion, and is calculated as the ratio between F_{tan} and the total force F_{tot} acting on the handle during handcycling. In the study conducted by Kraaijenbrink et al. [27], twelve capable men used an instrumented add-on handcycle on a motorized level treadmill, riding at a speed of 1.94 m/s. They underwent three sessions, each comprising three four-minute blocks of steady-state exercise. Between the blocks, they changed gears (70, 60, and 52 rpm) and adjusted resistance levels (+0 W, +10 W, +20 W) in a counterbalanced order across sessions. FEF was used as the main outcome to evaluate that a cadence of 52 rpm against a higher resistance of about 35 W leads to a more optimal direction of forces.

Finally, Vla and Bla evaluate lactate production and its concentration in the subject's blood, respectively. In the study by Quittmann et al. [28], Vla is evaluated for twelve able-bodied nationally competitive triathletes that underwent a series of tests, including a familiarization session, a sprint test, an incremental step test, and a continuous load trial at a fixed lactate concentration of 4 mmol/L. These trials were performed on a racing handcycle, which was mounted on an ergometer. The 15 s All-Out sprint test was performed to assess the participants' anaerobic performance and lactic power, and Vla_{max} was calculated as the difference between maximal post-exercise lactate and resting lactate. To evaluate this quantity, a normalization was performed, dividing the maximal post-exercise lactate by the difference between the test's duration, and the initial exercise phase during which no lactate formation was assumed. The participants' mean values for la_{max} and Vla_{max} were 6.64 ± 1.32 mmol/L, and 0.45 ± 0.11 mmol/(L·s), respectively. The incremental step tests started with an initial load of 20 W and increased every 5 min by 20 W until volitional exhaustion. In this case, la and HR were collected within the last 30 s of every power level, and the mean la at volitional exhaustion was 9.64 ± 2.24 mmol/L. For the continuous load trial, the mean Vla at the end of the tests was 5.36 ± 1.85 mmol/L. In their work, Quittmann et al. reveal that Vla_{max} can be considered a promising parameter for exercise testing in handcycling, since it shows a positive correlation with anaerobic performance and a negative correlation with aerobic performance measures, and moreover, parameters related to post-exercise lactate kinetics and Vla_{max} are interconnected and provide valuable insights into the athlete's physiology. Therefore, it is advisable to utilize both approaches in tandem for a comprehensive assessment.

Focusing on Bla, Hall et al. [34] found that individuals with spinal cord injury who were trained in handcycling had higher Bla (9.9 ± 3.7) than able-bodied males who were trained in power lifting (9.2 ± 1.7) and than the control group of fourteen subjects (9.8 ± 1.2 mmlol/L). According to the authors' findings, this suggests that these athletes likely have a higher aerobic capacity, which is most likely a result of more extensive training.

Besides the set of works described so far, which mainly emphasize specific details primarily on individual parameters that identify sub-classes, several papers also investigate more parameters or cross-cutting aspects. For instance, in the work by Fischer et al. [23] an additional division between tetraplegic and paraplegic patients is made. In tests conducted at sub-maximal speed, the authors find that the tetraplegic patient has a lower aerobic speed (4.7 ± 0.6 m/s vs. 7.1 ± 0.9 m/s) and mechanical power (54 ± 15 W vs. 111 ± 25 W) with respect to the paraplegic patient at equal metabolic cost. Schoenmakers et al. [25]

studied the difference between moderate-intensity continuous training (MICT) and high-intensity interval training (HIIT). Despite training 22% less time for HITT than MICT, a higher improvement is obtained in the patient trained with HIIT. Power output peak values represent a 47.1 $\pm$ 20.7% increase for HIIT and 32.2 $\pm$ 8.1% increase for MICT.

Instead, Kouwijzer et al. [33] analyzed the physical capacity of 33 subjects comparing at 1-year follow-up with the physical capacity assessed before and after the training period for the HandbikeBattle event. Data showed an increase in the capacity during the training period, which remained stable after the follow-up. The authors therefore suggest that keeping committed to a challenge may ease long-term exercise maintenance.

Finally, additional considerations, at a more general level, can be retrieved by the works of de Groot et al. [36] and Nooijen et al. [37]; in the former, data revealed that the SCI level of the subject is not significantly associated with racing performance, assessed as race time. In the latter, the authors compared the performance of 168 athletes racing in elite para-cycling events with different devices, i.e., bicycles, tricycles, recumbent handbikes, and kneeling handbikes. According to the data, bike type and impairment type were not effect modifiers in the studied relation between road time trial performance and sprint power.

Table 2 synthesizes the main highlights that emerged from the analysis of the Clinical Tests category and its sub-classes.

Table 2. Clinical Tests: highlights for the category and sub-classes.

Clinical Tests: Highlights
General remarks
• Handbikes could be used as means of transportation in everyday life: handcycling is less strenuous and produces higher exercise response than the traditional wheelchair at a moderate power output level [5].
• Low-intensity upper-body handbike training reduces VO2, improves physical capacity, and prevents premature fatigue and overuse in untrained subjects [31]. Handbike training can prevent cardiovascular disease [18].
• The SCI level of a subject is not significantly associated with racing performance, as racing time [36].
• Bike type and impairment type may not be effect modifiers in the relation between road time trial performance and sprint power [37].
VO2
• $VO2_{max}$ can be used as predictor of all-cause mortality in SCI patients engaged in upper-body exercises, and as a basis for customizing exercise intensity [26].
• Lower-body low-frequency EMS significantly increases the acute oxygen uptake [29].
Peak functional performance (W/kg)
• Different hand grip angles on the handbike do not significantly affect the amount of power generated by the subject in relation to their body weight [21].
RER
• RER can be used as parameter to discriminate whether an exercise is performed at a submaximal level [5].
FEF
• Lower velocity at a higher resistance level offers better direction forces [27].
Vla
• Vla is a promising parameter for exercise testing in handcycling: it presents positive and negative correlation with anaerobic and aerobic performance measures, respectively [28].

3.2. Device

The documents for the Device category were distributed as follows: 85 articles, 15 conference papers, and 1 book chapter, as shown in Figure 9a. The increase in publications became relevant from 2012, although a peak in 2010 with four articles and four conference papers emerged.

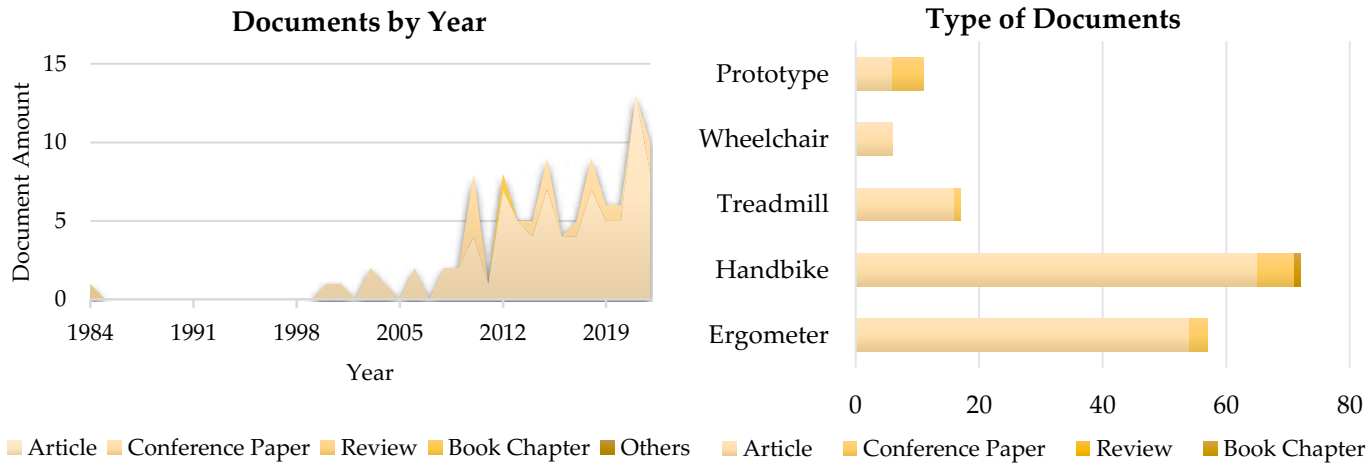

Figure 9. Device category: (**a**) evolution of documents in time, and (**b**) number of documents in each sub-class for the device category, divided by document type.

Device Sub-Classes

The device category was subdivided into sub-classes, each related to different methods for analyzing hand propulsion in subjects, as indicated in Figure 9b. In the same figure, the distribution of documents reveals that articles are the predominant form of publication in each sub-class.

Focusing on the content of the documents, different aspects that affect the device are collected in this class; Figure 10 presents some examples of these elements, whereas Figure 11 collects illustrative examples of handbike prototypes at a glance.

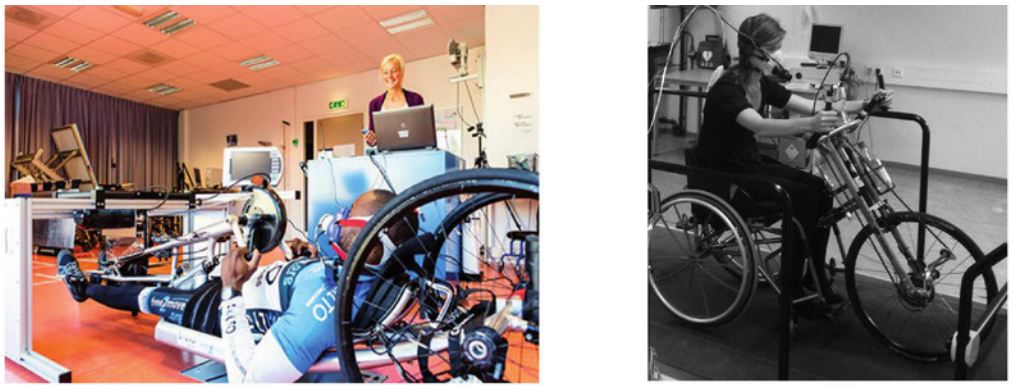

Figure 10. Examples of elements considered in the Devices category: from the left, (**a**) an ergometer used for indoor activities (source: de Groot et al., 2018 [38]), and (**b**) a handbike attach-unit mounted on a treadmill (source: Hettinga et al., 2013 [20]).

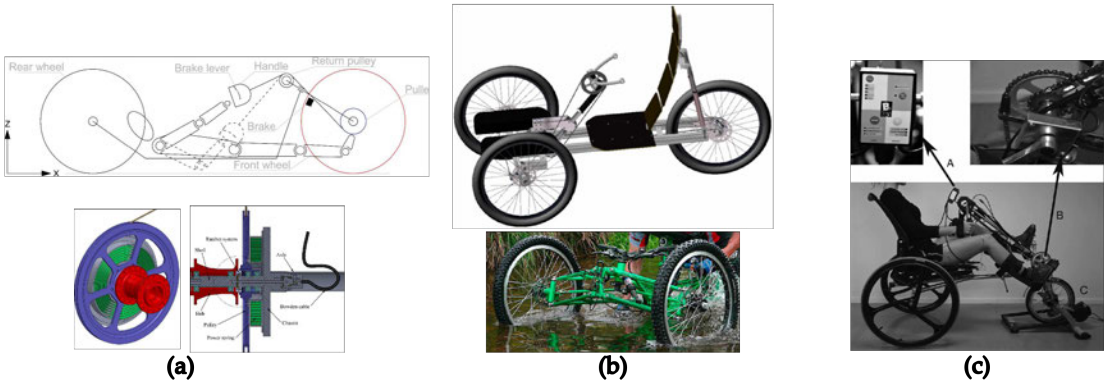

Figure 11. Examples of prototypes: from the left, (**a**) an innovative propulsion system applied to a recumbent handbike (source: Quaglia et al., 2019 [39]), (**b**) a multi-adjustable handbike chassis for off-road use (source: Siebert, 2010 [40]), and (**c**) a hybrid cycle showing the detail of the mounted stimulator (source: Bakkum et al., 2014 [41]).

Ergometer

In 57 cases, an ergometer was used to perform handbike tests. The most used ergometer is the Cyclus II (RBM elektronik-automation GmbH, Leipzig, Germany), which was utilized 29 times, followed by Tacx Flow (Technische Industries, Waibstadt, Germany) in 6 studies, and CycleOps Fluid 2 (Saris, Medison, WI, USA), which was used once.

Handbike

According to data, handbikes were utilized 72 times; 5 of those instances involved outdoor activities or races, and in 17 studies the handbike was mounted on a treadmill, to simulate road conditions or control handle velocity in comparative studies with wheelchair users. Among the most frequently used handbikes Shark RS, Spirit 468, Spirit 469, and Spirit 470 (Sopur, Sunrise Medical, Malsch, Germany) have been identified. These devices were used in experiments 16 times. The Tracker Tour (Double Performance, Gouda, The Netherlands), a wheelchair attach-unit, was mentioned seven times. Finally, the BerkelBike Pro (BerkelBike B.V., St Michielsgestel, The Netherlands) was used in three experiments; this device is defined as a hybrid-bike, as it combines synchronous handcycling with asynchronous Functional Electrical Stimulation-induced leg cycling.

Treadmill

In the study conducted by Abel et al. [1], a motor-driven treadmill was employed to elicit the subject's physiological responses at maximum load one week before the race. The treadmill velocity was set at 12 km/h, with a progressive increase of 2 km/h every 3 min. Abonie et al. [31], on the other hand, utilized a motor-driven treadmill with a constant power output to achieve 30% of the participant's Heart Rate Reserve (HRR).

Arnet et al. and Hettinga et al. [20,42] employed a motor-driven treadmill to simulate different velocities and slopes. The treadmills used in these studies were the Mill (Forcelink, Culemborg, The Netherlands) and the Mill-track (Enraf Nonius, The Netherlands).

Arnet et al., Kraaijenbrink et al., and Schoenmakers et al. [25,27,42] incorporated a pulley system in conjunction with a motor-driven treadmill to maintain an external power output. For Kraaijenbrink and Schoenmakers, the treadmills used were the Motek force Link b.v. (Motek Medical B.V., Houten, The Netherlands) and Mill-track (Enraf Nonius, The Netherlands), respectively.

Wheelchair

The documents classified in the Wheelchair sub-category allow the investigation of analogies and differences between handbike and wheelchair use. Wheelchair propulsion is used in some cases as a baseline for comparison, given the higher popularity of this topic in the scientific literature, which makes it a de facto gold standard [5,32,43].

In other cases, like in the work by Nooien et al. of 2015 [10], the handbike is used as an experimental setup tool, to enable the acquisition of the relevant data in the defined protocol. In fact, unlike what happens in wheelchair propulsion, during handcycling, user and device create a closed kinematic chain: this makes subsequent cycles and repetitions more standardized and comparable, reducing the potential variability of the task across sessions and across subjects [44].

Prototype

Regarding prototypes, several of the analyzed papers focus on wheelchairs more than handbikes mockups. For instance, Chong et al. [45] introduce a new type of wheelchair, aiming to catalyze the development of such devices for children with cerebral palsy. This wheelchair meets the 3As criteria, focusing on availability, accessibility, and affordability. It is equipped with a heartbeat monitoring system, training programs, and a user interface, making it a promising tool in this domain.

In the work conducted by Quaglia et al. [39], an innovative propulsion system is proposed, named Handwheelchair. In this case, the mechanism works as an attachment that functionally transforms a wheelchair into a handbike.

Instead, Siebert et al. [40] addressed two primary challenges associated with handbikes: traction optimization, as most of the weight rests on the two non-driven rear wheels, and the inability to simultaneously pedal and steer in off-road handbiking. To address these issues, a new prototype was developed featuring two steerable front wheels, one of which is powered, allowing users to pedal and control the device with both arms simultaneously. Additionally, a multi-adjustable backrest was incorporated to accommodate the specific requirements of individual users.

The main highlights that emerged from the analysis of the Device category and its sub-classes are collected in Table 3.

Table 3. Device: highlights for the category and sub-classes.

Device: Highlights
General remarks
• Ergometers are often used in handbike tests, as well as treadmills, to simulate different velocities and slopes. • Wheelchair propulsion can be used as a baseline for comparison [5,32,43]. • Handbikes can be also used as experimental setup tool [10].
Prototype
• Wheelchair prototypes are more common in the literature than handbike prototypes. • Prototypes often focus on the optimization or the design of innovative solutions for components [39], and more rarely of devices [40].

3.3. Forces

The Forces category collects a total of 25 articles, 4 conference papers, and 1 book chapter, as indicated in Figure 12a. The distribution of documents dealing with the forces exerted during handcycling reveals a first peak of interest in 2012, with the publication of five documents, and another peak in 2021, with four published articles.

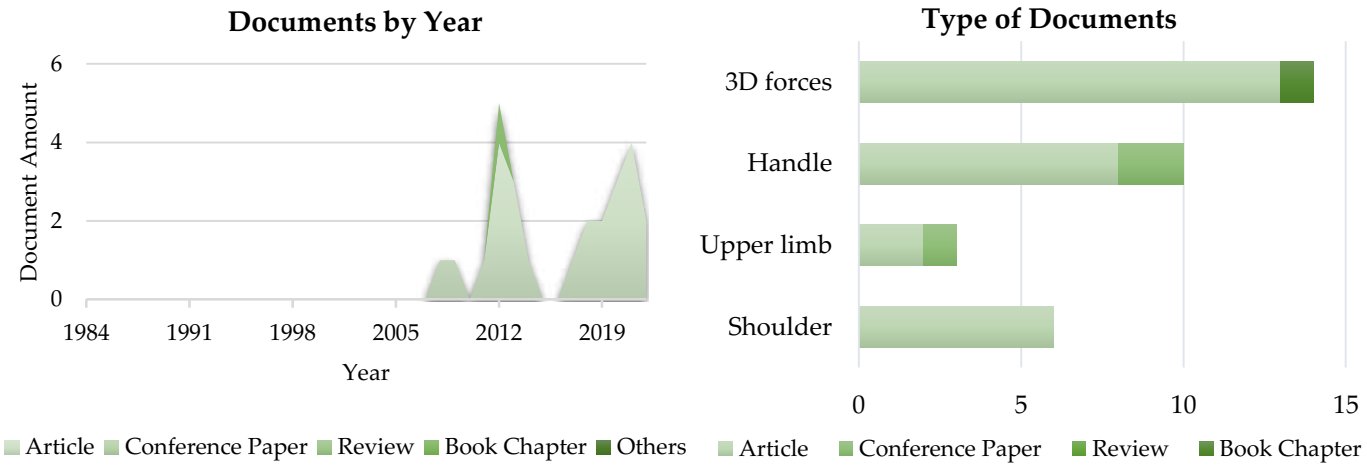

(**a**) (**b**)

Figure 12. Forces category: (**a**) evolution of documents in time, and (**b**) number of documents in each sub-class for the forces category, divided by document type.

Forces Sub-Classes

Within the sub-classes, 10 documents investigated the forces at the handle, 6 at the shoulder, and 3 performed the analysis considering the whole upper limb. Notably, 14 papers explored forces in a 3D context, moving beyond the sagittal plane to offer a comprehensive view of the results (see Figure 12b). Articles represent the predominant type of publication in the Forces class. Most of the documents address the study of 3D forces, with 13 articles and 1 book chapter, representing 56% of the overall production. The peak of works on this aspect was in 2012.

Figure 13 presents some examples of schematics for the evaluation of 3D forces on the handle depicted in the analyzed literature.

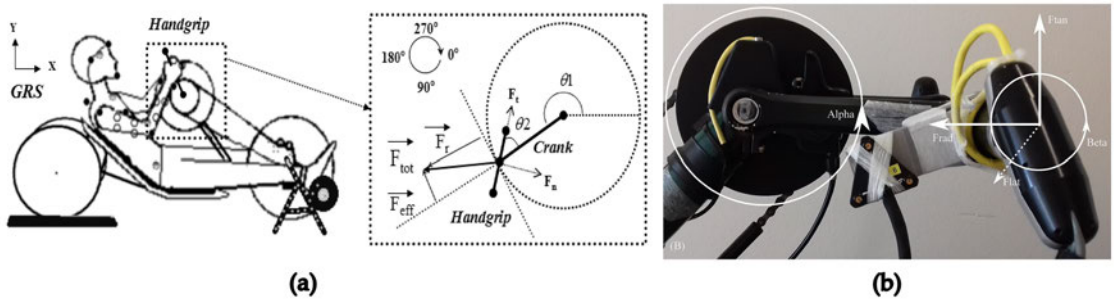

(**a**) (**b**)

Figure 13. Examples of schematics for the evaluation of the forces exchanged between subject and handbike at the handle level: from the left, an example of (**a**) model (source: Faupin et al., 2010 [46]) and (**b**) real setup (source: Kraaijenbrink et al., 2017 [27]) of 3D force measurement on the handle during handcycling.

Shoulder

The shoulder is among the anatomical areas that are more involved in handcycling. Among the six documents classified within this category, Arnet et al. proposed a comparison between handbike and wheelchair performance [6,43]. In the first study conducted by Arnet et al. [6], eight subjects with paraplegia underwent testing while propelling both a handbike and a wheelchair at different power output levels (25, 35, 45, and 55 W). The treadmill speed was adjusted to 1.6 m/s for the handbike and 1.11 m/s for the wheelchair, aiming to simulate everyday propulsion conditions. The estimated force exerted on the rotator cuff during handbiking was approximately 268 N, marking a 29% reduction compared

to the force generated when using a wheelchair at a constant power output of 25 W. This discrepancy grew at a constant power output of 55 W, with the handbike recording a force of 345 N, representing a 70% decrease compared to the wheelchair. During handcycling, glenohumeral contact forces were distributed across the entire cycle, reaching their peak at the end of the cycle. In contrast, wheelchair propulsion exhibited a force peak in the middle of the push phase, with smaller peaks at the beginning and end of the recovery phase. Regarding muscle activation, the supraspinatus and infraspinatus muscles were most engaged during handcycling. Arnet et al. [6] reported that their percentage of activation during handcycling was less than 5%, reducing the risk of overuse injuries compared to traditional wheelchair use and making the handbike a suitable device for daily use.

In the second study, Arnet et al. [43] focused on the impact on the shoulder joint caused by external force production during an entire handbike cycle or in the push phase of the wheelchair on different slopes. Across all slope variations, the force acting on the handle (Total Force and Mean Force calculated over the last 30 s of each repetition) was approximately three times lower during handcycling compared to wheelchair propulsion. Additionally, F_{peak} was about 60 N for the handbike and 160 N for the wheelchair during the push phase, resulting in lower torque on the glenohumeral joint and reducing the risk of shoulder injuries.

The position of the backrest and the crank position were also found to influence shoulder load. Arnet et al. [47] demonstrated that an upright backrest position led to lower shoulder load and reduced muscle activation (specifically the supraspinatus and infraspinatus), while mechanical efficiency, calculated, according to the definition proposed by Kraaijenbrink in 2017 [27], as the percentage of Power Output PO over Energy Expenditure EE, remained constant. However, no significant differences were observed when changing the crank position.

Upper Limb

For the analyzed data, three documents were classified in the Upper Limb category [48–50]. Among their findings, Nevin et al., in a work of 2021 [48], state that there is a strong correlation between strength tests and handcycling performance. The authors conducted tests on 13 UCI male handcyclists belonging to H3/H4 categories, which included a graded exercise test, a 15 s all-out sprint, and a 15 km Individual Time Trial, and the study revealed a significant relationship between upper body strength and handcycling performance. Specifically, improvements in maximal upper body strength led to enhanced gross mechanical efficiency in handbiking. This allowed cyclists to generate the same power output while minimizing the workload required to produce it. Higher mechanical efficiency can also extend the endurance of type I muscle fibers, delaying the activation of less efficient type II fibers. Additionally, there was an observed improvement in strength stiffness, resulting in a better mechanical transmission of force to the handle.

Handle

In works dealing with the handbike handles, particular attention is paid to the interaction with the user in terms of force exchange and propulsion optimization. For instance, in the case of van Drongelen et al. [51], force measurements were taken by replacing the handle's stud with a force transducer, providing three voltage outputs related to the three force components. Encoders were positioned between the handgrip and the handle, and between the handle and the crank, to express forces in the global coordinate system of the bike. According to the authors, the force characteristics can be influenced by several parameters, including crank speed, crank height, and power output.

Arnet et al. [42] studied the correlation between handle speed and force characteristics. They found that, at a constant power output (PO) and gear setting, an increase in crank speed led to a decrease in both total force (F_{tot}) and tangential force (F_{tan}), from 24.2 N to 18.2 N and 20.0 N to 13.5 N, respectively. However, at higher speeds, F_{tot} and F_{tan} did not decrease uniformly across all sectors of the cycling motion, resulting in the Force

Effectiveness Fraction (FEF) not decreasing in every sector. FEF decreased in the sector where gravity acted against the crank's movement but increased in other sectors. Due to the complex nature of the upper limb joint framework, applying force becomes less efficient at higher velocities. Therefore, selecting a lower gear ratio is advisable to maintain a sufficient FEF. The analysis of the relative work produced in each sector revealed that, in sectors where less work was generated (e.g., "lift up" against gravity), work decreased with greater speed, possibly due to inertia. However, in areas where the highest amount of relative work was produced (e.g., "pull down" and "press down", following gravity), the relative work increased with increasing speed. This was because, due to inertia, the crank rotated evenly without the need for high force application.

Kramer et al. [52] also demonstrated an increment in work production during the pull-down phase, suggesting an improved efficiency. Modifying handle angles, particularly a pronated 30° angle, has been shown to enhance the work generation and increase the efficiency of handcycling.

Jacquier-Bret et al. [53] introduced a new index called the Postural Force Production Index (PFPI) to evaluate force production in handcycling. This index considers both the rotation of the handgrips and the patient's ability to generate force from their current posture. The fore-aft position, i.e., the longitudinal position of the crank with respect to the subject's shoulder, also affects the force application and the distribution of relative work.

Vegter et al. [54] tested participants without disabilities on a recumbent handbike at different crank-fore-aft positions (103%, 100%, 97%, 94% of arm length), at two different power outputs (30 W and 60 W). Increasing the crank distance correlated with a decrease in elbow flexion and an increase in shoulder protraction, shifting work production to the pull phase, where the highest torque was recorded. For a more consistent power output, which is useful in daily life, a shorter crank-fore-aft position is recommended to evenly distribute work production throughout the entire cycle, maintaining handle velocity as consistently as possible.

Table 4 depicts the main highlights that emerged from the analysis of the Forces category and its sub-classes.

Table 4. Forces: highlights for the category and sub-classes.

Forces: Highlights
General remarks
• The force characteristics can be affected by several parameters, such as crank speed, crank height, and power output [51].
Shoulder
• Handcycling reduces the risk of overuse injuries compared to the wheelchair: glenohumeral contact forces are distributed across the cycle [6] and lower torques act on the glenohumeral joint [43]. • The backrest position influences the shoulder load: an upright backrest position produces a lower shoulder load and muscle activation [47]. Mechanical efficiency remains constant [27].
Upper Limb
• Improvements in upper body strength enhance gross mechanical efficiency in handbiking [48]. An improved strength stiffness provides better mechanical transmission of forces to the handle [48].
Handle
• At high velocity, selecting a lower gear ratio is advisable to maintain a sufficient force effectiveness fraction: applying force becomes less efficient at high velocities [42]. • A pronated 30° handle angle enhances work generation and increases the efficiency of handcycling [52]. • A short crank-fore-aft position is recommended in daily life: it maintains handle velocity as constant as possible and allows for an even distribution of the work production throughout the cycle [54].

3.4. Geometry

According to the literature, 22 documents have been published for the Geometry category: in particular, 16 articles, 5 conference papers, and 1 book chapter. Figure 14a

describes the evolution of scientific production over time, identifying three peaks, in 2015, 2019, and 2021, with three documents each.

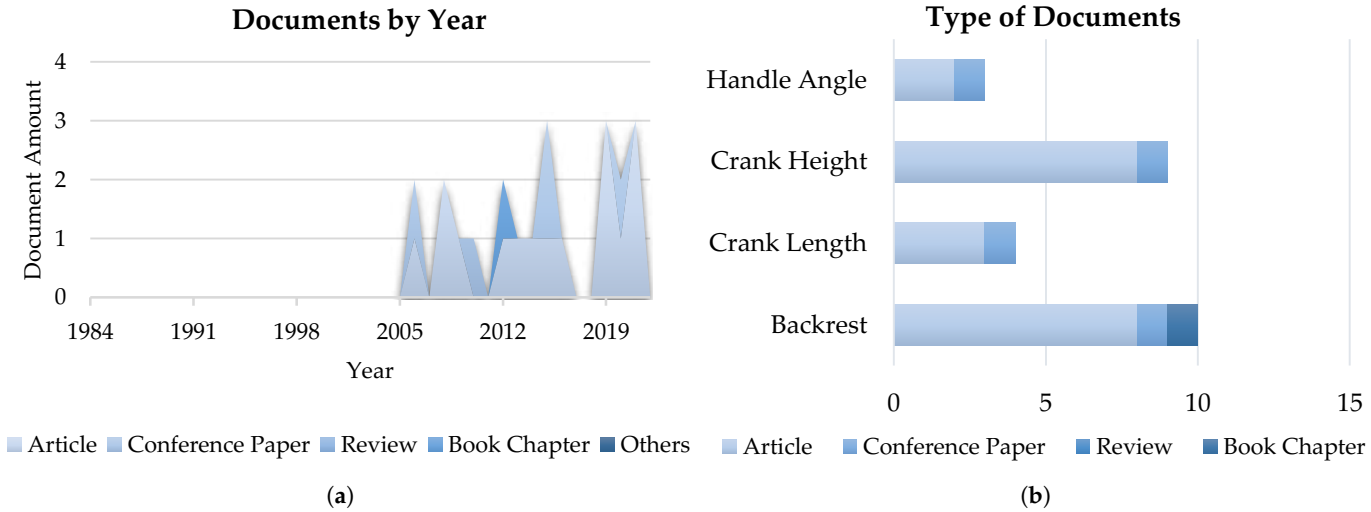

Figure 14. Geometry category: (**a**) evolution of documents in time, and (**b**) number of documents in each sub-class for the geometry category, divided by document type.

Geometry Sub-Classes

Regarding the sub-classes, most of the studies investigate changes in the crank height and backrest. Backrest has been analyzed in 10 documents, of which 8 are articles, 1 is a conference paper, and 1 a book chapter, whereas crank height has been studied in 8 articles and 1 conference paper. The distribution of sub-classes publications is represented in Figure 14b. Paper production is concentrated in three specific time windows: between 2006 and 2010, 2012 and 2017, and from 2018 to 2022. A higher level of production was reached in the second period, with a focus on crank and backrest. Most of the production is represented by articles for all sub-classes.

Some examples of the different aspects that could be evaluated in the documents included in the Geometry class are illustrated in Figure 15.

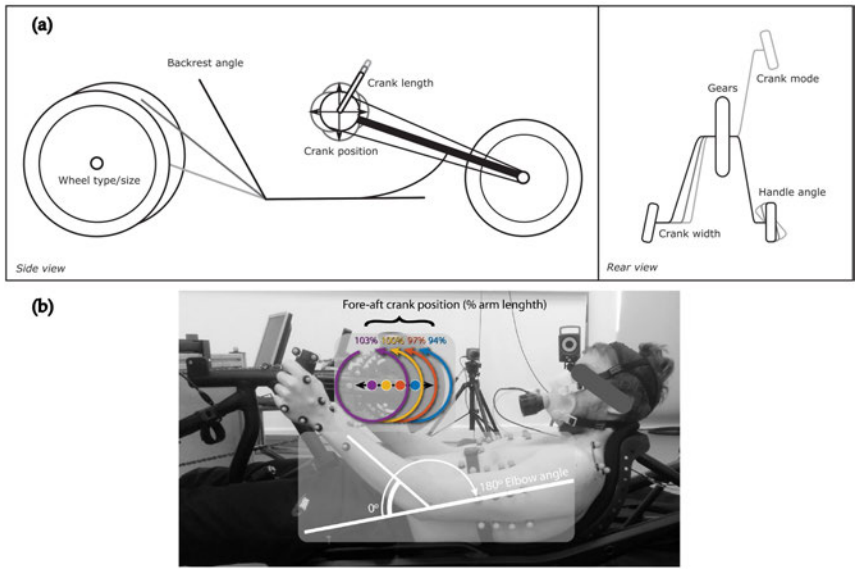

Figure 15. Examples of variabilities evaluated in the documents of the Geometry class: (**a**) different types of handbike settings (source: Kraaijenbrink et al., 2021 [55]), and (**b**) models of different configurations for the crank-fore aft position (source: Vegter et al., 2019 [54]).

Backrest

Among the analyzed data, the first document exploring the effect of backrests on handcycling performance is a work of 2008 by Faupin et al. [56]. In this paper, the authors investigated the impact of backrest position on subjects without disabilities during an 8-second sprint test at different gear ratios. They found that the absence of a backrest improved movement efficiency, especially at higher gear ratios. These results hold significance for patients with trunk mobility issues, suggesting potential benefits and considerations for optimizing backrest positions to enhance performance and reduce risks of injury.

In 2014, Arnet et al. [47] demonstrated that altering the backrest inclination affects the glenohumeral contact force and the forces exerted by the supraspinatus and infraspinatus muscles but does not affect mechanical efficiency. Decreasing the backrest inclination led to an increase in mean and high peak glenohumeral contact force; this phenomenon is particularly noticeable in the lying position, which is common in handbike cycling. Consequently, the lying configuration presents a higher risk of overuse injuries compared to other backrest conditions. Their findings suggest that the most optimal inclination stands at 60°, resulting in the lowest shoulder load. Litzenberger et al. [57] corroborate this outcome by testing a world-class male handbiker across various parameters. They found that a lower backrest position increased the elbow range of motion (ROM), while the opposite was true for higher backrest positions.

The effect of backrest inclination on handcycling performance is so relevant that handbikes can be classified as Arm-Powered or Arm Trunk-Powered depending on this value. The inclination can assume a fixed value, as 90° in the attach-unit handbike, which often presents a motor drive system, or may range from 0° to 60°, depending on factors such as: kind of use (e.g., race or mobility), severity of impairment, or UCI categories (e.g., H1, H2, H3, H4, and H5). In fact, backrest inclination affects several biomechanical factors, such as the trunk flexion/extension, the power production, the crank velocity, and the muscles recruitment.

Crank

Crank position and crank length are fundamental parameters for what concernes handbike daily use. In fact, crank geometry is strongly related to ROM of the upper limb, muscle activation, and force expressed on the crank itself or in shoulder joints. Faupin et al. [58] described a kinematic model with seven degrees of freedom, presenting as input quantities the lengths of the patient's arm segments, the shoulder position, and the size of the crank; the output of the model was the joints kinematics. To achieve an optimal position, i.e., one that reduces the risk of repetitive strain injuries (RSI), by moving the crank axis or modifying the distance between cranks, the following indications were identified:

1. The distance between left and right extremes of the crank is to be set equal to the distance between the shoulders;
2. The crank height should remain below the axis passing through the acromions;
3. The crank should be positioned so as to avoid complete elbow extension.

In the study conducted by Vegter et al. [54], untrained subjects with disabilities were examined on a recumbent handbike at a consistent power output of 60 W. They found that increasing the distance between the acromial angle and the handle's center, specifically at 94%, 97%, 100%, and 103% of the arm's length, resulted in decreased elbow flexion (from 42° to 29°) and a more pronounced shoulder protraction (from 29° to 36°). This alteration shifted the distribution of work during the pull phase, with 69% of the work being produced at the 103% arm length position. However, since handbike races and daily activities benefit from a more equal distribution of work and fatigue among muscle groups, a shorter crank-fore-aft position is favored. This not only aids in reducing speed fluctuations but also helps evenly distribute fatigue. Interestingly, there were no observed effects on VO2, mechanical efficiency, or heart rate when choosing the most extended crank fore-aft position.

The work by Stone et al. [59] was conducted under similar conditions, with a horizontal crank positioned at 97% of the arm length, and with this configuration the authors found more favorable handcycling conditions. This positioning improved the musculature surrounding the joints, enabling more economical force production. Stone et al. discovered that, at 70% of athletes' peak power output, the 97% position was 4% more economical than the 94% and 103% positions. Such data hold significance in endurance competitions or longer activities, where energy-saving measures can influence final results. While the crank length in normal handbikes during professional competitions can vary from 150 mm to 180 mm, the physiological economy remains unaffected by changes in crank length. However, shorter crank lengths are favored during races due to the reduced frontal areas that they offer, which become especially smaller when the crank is at the top dead center, subsequently decreasing air resistance and creating more advantageous conditions. Litzenberger et al. [60] reported that shorter cranks led to higher electromyography (EMG) values for the upper limb muscles throughout the cycle. Moreover, the crank length is related to the number of revolutions per minute (rpm) that the subject can comfortably express. A 190 mm crank length suits a cadence of 180 rpm, while a length of 139 mm is favorable for 125 rpm. Thus, depending on the conditions, crank length can remarkably influence handbike performance.

Handle angle

During handcycling, force is transmitted to the crank through the handle grip. Abel et al. [21] tested participants without disabilities, with incremental tests to exhaustion performed with the three different hand grip angles presented in Figure 16: 0° for a horizontal configuration, 90° for a vertical configuration, and 10° for a diagonal configuration. For each angle, four parameters were evaluated, i.e., peak functional performance (W/kg), peak heart rate (bpm), associated lactate concentrations (mmol/l), and peak oxygen uptake per kilogram of body weight (Ml/min·kg). No significant differences emerged among the three hand grip angles for any parameter, but the vertical position seems to be less efficient than the horizontal and diagonal in the analysis of the lactate concentration. Kramer et al. [52] focus on the correlation between handle angle and work distribution. The effect of the angle on the work distribution is relevant in the pull-down and lift-up phase. In these phases, a higher work production was achieved with angles of −15° and 30°, but the phenomenon of premature fatigue related to these configurations should be further studied, since these results were obtained with a 30 s test.

Figure 16. Handle angle configurations analyzed by Abel et al. [21]: from the left, (**a**) horizontal (0°), (**b**) vertical (90°), and (**c**) diagonal (10°) configuration. Source: Abel et al., 2015 [21].

The main highlights that emerged from the analysis of the Geometry category and its sub-classes are synthesized in Table 5.

Table 5. Geometry: highlights for the category and sub-classes.

Geometry: Highlights
Backrest
• The backrest inclination affects several biomechanical factors, such as trunk flexion/extension, power production, crank velocity, and muscles recruitment.
• The absence of a backrest improves movement efficiency in individuals without disabilities, especially at high gear ratios [56].
• The backrest inclination affects glenohumeral contact forces and forces generated by supra/infraspinatus muscles; it does not affect mechanical efficiency [47]. The lying configuration presents a higher risk of overuse injuries [47]. The optimal backrest inclination for the lowest shoulder load is at 60° [47].
• A lower backrest position increases the elbow ROM [57].
Crank
• To minimize the risk of repetitive strain injuries, (i) the distance between cranks must be equal to the distance between shoulders, (ii) the crank height must be below the axis of acromions, and (iii) the crank should avoid complete elbow extension [58].
• Increasing the crank-fore-aft decreases the elbow flexion and increases the shoulder protraction [54]. A short crank-fore-aft is favored for handbike races and daily use: it aids in evenly distributing fatigue and reducing velocity fluctuations [54]. Shorter crank lengths are favored during races, as they offer reduced frontal areas and resistance [59].
• A horizontal crank at 97% of the arm length offers optimal economical force production [59].
Handle
• Modifications to the alignment of the handles do not seem to generate significant differences in W/kg (peak functional performance), HR_{peak}, Bla, and VO2 [21]. Vertical alignment seems to be less efficient than the others for Bla [21].
• The angle of the handles affects the work distribution in the pull-down and lift-up phases [52].

3.5. Sensors

The Sensor category comprises 94 documents, divided into 83 articles and 11 conference papers. The presence of sensors within the set of analyzed documents has almost constantly increased since the beginning of the millennium, reaching a peak in 2021 with 15 published papers (see Figure 17a).

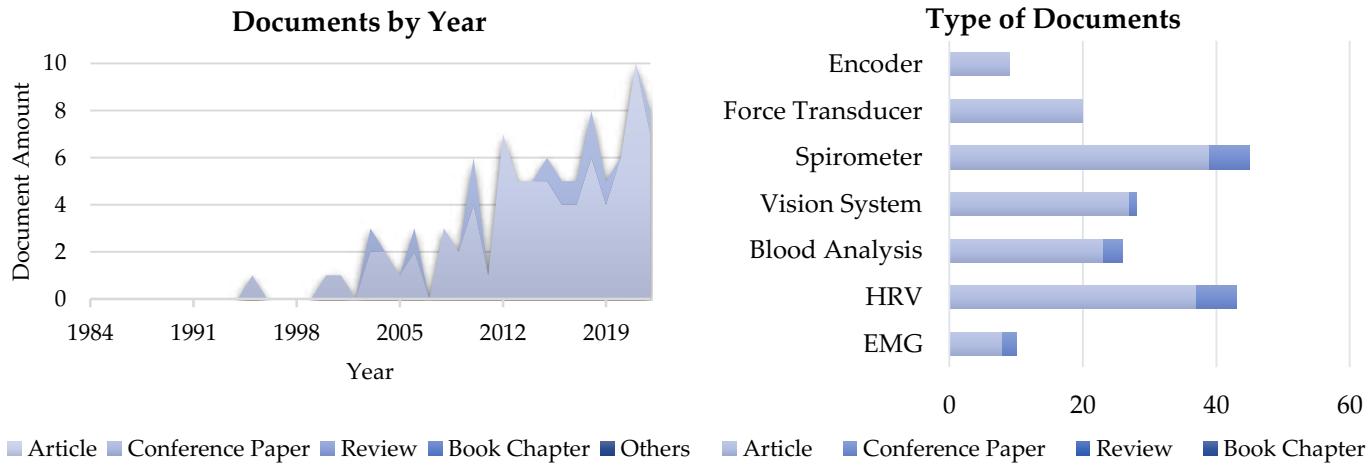

Figure 17. Sensors category: (**a**) evolution of documents in time, and (**b**) number of documents in each sub-class for the sensors category, divided by document type.

Sensors Sub-Classes

The sensors most commonly used for handbike measurements are synthesized in Figure 17b. The most applied devices are spirometers, with 45 publications. HRV sensors are also remarkably present, with 43 documents.

The analysis of the used sensors in time reveals a globally increasing trend in the last years. Often, documents state names and models of commercial devices, revealing that in scientific literature the most used sensors are generally produced by few companies, that are often key players in their market. Regardless of the various brands, the works involving EMG and optical cameras often provide the gathered data to biomechanical models, like in the cases of Litzenberger et al. [60], Quittmann et al. [61], or Mason et al. [62]. Similarly, the use of sensors for the assessment of physiological parameters is particularly common in the case of studies with a clinical focus, as in the works by Antunes et al. [63] or Stone et al. [64].

The analysis of Table A1 also allows appreciating the almost complete overlapping between documents classified in the Sensors category and in the Clinical Tests class, highlighting the strong relation between these aspects. Some examples of the sensors and devices described in the documents included in the sensors class are presented in Figure 18.

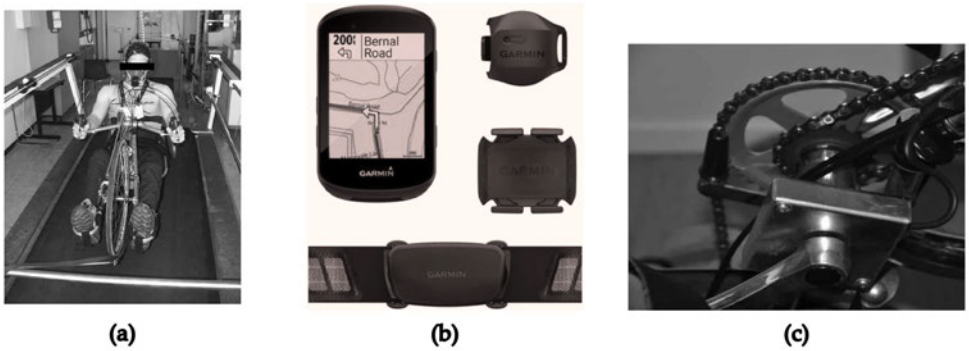

Figure 18. Examples of sensors used in the experimental setup of documents in the sensors category: from the left, (**a**) a spirometer used in V02 measurements (source: Abel et al., 2006 [1]), (**b**) a bike computer, a cadence sensor, and an HR sensor (source: Koontz et al., 2021 [65]), and (**c**) an encoder mounted on a handbike (source: Bakkum et al., 2014 [41]).

Table 6 presents the main highlights that emerged from the analysis of the Sensors category and its sub-classes.

Table 6. Sensors: highlights for the category and sub-classes.

Sensors: Highlights
General remarks
• The number of sensors used by experimental setup seems to follow an increasing trend. • The data for biomechanical models are often collected with EMG sensors and optical cameras. In documents with a clinical focus, sensors for the assessment of physiological parameters are typically used.

3.6. Actuation

According to the data, for the Actuation category 61 documents have been published; 46 works are classified as articles in the Scopus database, 14 as conference papers, and 1 as a book chapter (see Figure 19a). Also for this class, the analysis of the number of papers published in time reveals an increasing trend, with a peak in 2021 of eight documents.

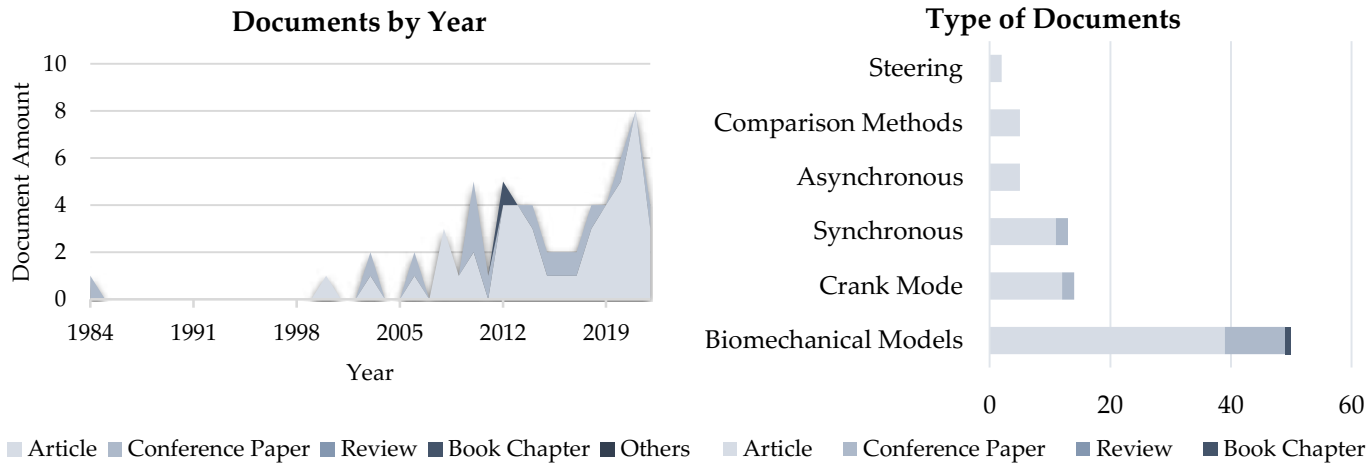

(**a**) (**b**)

Figure 19. From the left: (**a**) evolution of documents in time, and (**b**) number of documents in each sub-class for the Actuation category, divided by document type.

Actuation Sub-Classes

The distribution of documents by sub-class presented in Figure 19b reveals that most of the documents focus on biomechanical models, particularly articles (39 articles, making up 78% of the documents in the sub-class). The crank mode is investigated in 15 documents, mainly devoted to the study of the synchronous configuration (14 documents). Steering is especially evaluated in only three documents.

Figure 20 collects some illustrative examples of models applied to the investigation of the actuation propulsion included in the Actuation class.

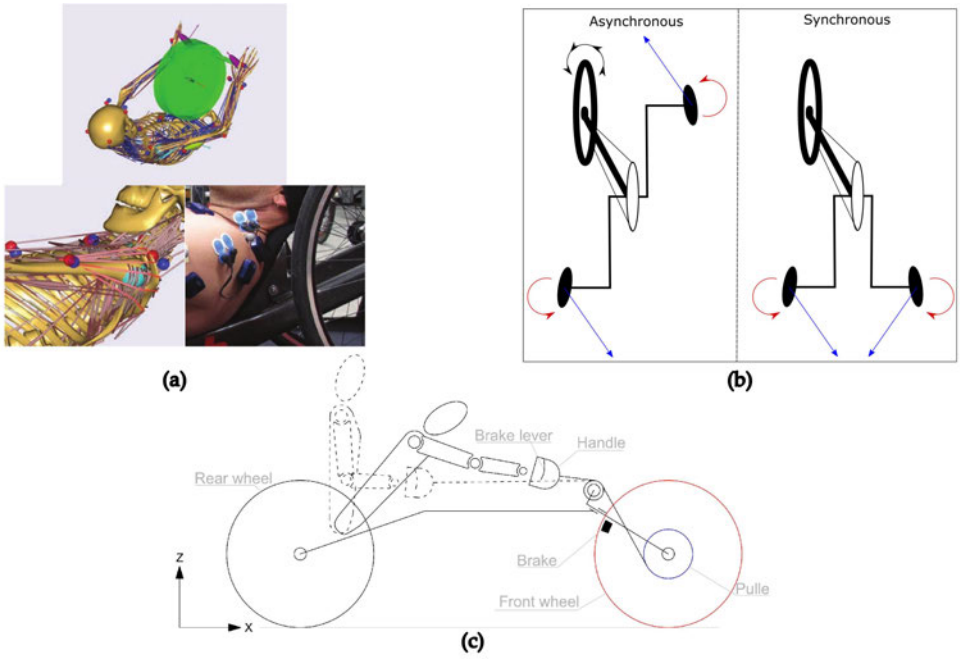

Figure 20. Examples of actuation propulsion models: (**a**) details of a biomechanical model of the handcycling (source: Felsner et al., 2016 [66]), (**b**) schematic of synchronous and asynchronous handbike propulsion (source: Kraaijenbrink et al., 2020 [8]), and (**c**) a new type of handbike propulsion (source: Quaglia et al., 2019 [39]).

Biomechanical Models

Among the analyzed data, 51 documents investigated the propulsion task with biomechanical models. For instance, in the study conducted by Felsner et al. [66], a musculoskeletal model of a handcyclist was developed. The model was realized using the software AnyBody 6.0.5 (AnyBody Technology, Aalborg, DE). To validate the model, the muscle activity of the pectoralis major, deltoid, biceps brachii, and triceps brachii (TRIC), on both sides, was examined and compared to the recorded activity from a previous study, in which one male elite handbiker was tested. For the validation, different settings were considered (power level, crank height, crank length, and height of the backrest) and different muscles thresholds were applied, i.e., 10%, 20%, 25%, and 30% of the maximum muscular activity. To quantitatively assess the results, the mean overlap duration between the simulated and measured muscle activation phases was calculated. The overlap of muscle activation times ranged between 64% and 75%, satisfying the model validation. The most promising results were achieved using thresholds of 10% and 20% of the maximum muscular activity.

In the work by Mazzola et al. [67], a model was developed to describe the ergonomic behavior of a handbike to be assessed for elite competition. Information about the aerodynamic performance of the device was collected through an experimental campaign in wind tunnel. In the study, the results of ergonomic and aerodynamic tests are conflicting. The ergonomic analysis showed two key findings: increasing the length of the handlebar levers negatively affects ergonomic scores in all riding positions, and a more upright riding position is associated with lower perceived ergonomic discomfort. On the other hand, the vertical position of the torso has a negative impact on the aerodynamic drag coefficient, consistent with the observation that increasing the wind-exposed surface area leads to higher drag values. The results on handlebar lever length are also in contrast with the ergonomic analysis: longer levers seem to be more aerodynamically efficient.

Several papers then focus on specific aspects of the propulsion, like muscular activity [57,60] and activation patterns [61,68], techniques for the EMG signal processing [66,69], or shoulder loads, also assessed applying dedicated models such as Delft Shoulder or Elbow Model [70,71]. In 2010, Groen et al. [72,73] proposed a power balance model to describe the handcycling task, that enables the estimation of realistic values for power losses and power output, evaluating the physiological responses of subjects under given conditions (e.g., a range of regular velocities, on a treadmill or track). The model is expected to be a useful tool in the study of elite performance.

A different kind of approach is proposed in works with clinical purposes: in these cases, more than depicting new models that describe the handcycling task, models that combine physiological parameters are evaluated. In these works, predictive models are implemented, and ANOVA tests [8,27] or regression models, from linear, to hyperbolic and multilevel models [35,37,64,74–76], are generally applied to elaborate the data.

Finally, two additional works make use of models to evaluate the performance predictors: by Hettinga et al. [20] and de Groot et al. [36]. In particular, the first paper evaluates the physical stress and strain of handcycling by applying a set of training guidelines proposed by the American College of Sports Medicine; the latter analyzes a mountain time trial in handcycling in terms of exercise intensity in order to determine predictors of race time.

Crank mode

Since the handbike originally derives from traditional bikes, the handcycling crank was initially asynchronous, i.e., the cranks were mounted with a phase shift of 180 degrees. Over the years, handcycling has become more popular, and the crank mode has changed from asynchronous to synchronous, setting the cranks parallel.

In the work conducted by Kraaijenbrink et al. [8], twelve men without disabilities performed tests on handbikes, in both asynchronous and synchronous modes. The tests were performed by placing the handbike on a treadmill, which was set at a speed of 1.94 m/s; the resistance during the analysis was 15 W, and the crank length was 0.17 m. According to the authors' data, in the synchronous mode the tangential force is maximum

in the lift-push up phase, when the crank moves from the horizontal position towards the subject, with a module of 10 N. In the asynchronous configuration, the force is the highest during press-down phase (∼16 N). The radial force, i.e., the force that produces a torque around the steering axle, had a significant excursion in the asynchronous mode, ranging between its higher peak (20 N) and lower peak (−10 N). This variation causes high levels of muscles activation in order to stabilize the crank. An excursion is also seen in the synchronous mode, but presenting lower values (from 10 N to −10 N); nonetheless, the average radial force in this propulsion mode is equal to zero. The Force Effectiveness Fraction, FEF, was significantly higher during synchronous propulsion (50%) than asynchronous (25%); however, the synchronous mode was less efficient in the lift-pull up phases (from 0° to 90°), where the FEF is almost zero. The power production was more constant during asynchronous cycling throughout the cycle (∼12 W); in the synchronous mode, a lower power production is generated in the push phases (almost 0 W), and a higher power production (40 W) in the pull phases. The difference between push and pull phases during the synchronous cranking causes an acceleration and subsequent deceleration of the angular crank velocity. From a metabolic point of view, the same energy expenditure (EE) was consumed in the performed tests for both methods (3.5 W/kg); therefore, the synchronous mode was revealed to be more efficient, generating more power at the same cost. The mechanical efficiency (ME) was higher in the synchronous mode (6.5%) than in the asynchronous configuration (5%), while the heart rate (HR) was the same for both the modes (86 bpm). Table 7 synthesizes the described data in a schematic form.

Table 7. Synchronous and asynchronous handcycling: schematic comparison by parameter according to the data described by Kraaijenbrink et al. [8].

Parameter	Synchronous		Asynchronous	
Tangential forces	↑	(10 N)	↑↑	(16 N)
	max in lift-push up phase		max in press-down phase	
Radial forces	↑	([−10 N; 10 N])	↑↑	([−10 N; 20 N])
FEF	↑↑	(50%)	↑	(25%)
	less efficient in lift-pull up phase			
Power Production	variable	([∼0 W; 40 W])	∼constant	(12 W)
	push phase–pull phase			
EE	=		=	
ME	↑↑	(6.5%)	↑	(5%)
HR	=		=	

Oviedo et al. [77] focused on physiological differences in SCI patients and subjects without disabilities, comparing asynchronous cranking on an ergometer versus the recumbent synchronous handcycling. For the initial set-up, the ergometer was set at 10 W. This value was incremented by 10 W each minute, until reaching the maximum value of 90 W. Significant differences were found by the authors, and the main numerical values detected during the tests are synthesized in graphical format in Figure 21. For the peak of the volume of oxygen uptake VO2 (see Figure 21a), significant differences were found between subjects without disabilities and SCI patients at all the workloads. In particular, ranging from 30 W to 90 W, the handbike seems to be more efficient than the ergometer for SCI subjects. The maximum difference is reached at 60 W. As Figure 21b depicts, the respiratory exchange ratio RER was lower for the SCI patients, in both the conditions of handcycling with handbike and ergometer, and a maximal difference of 0.28 was found at the workload of 80 W. Analyzing the heart rates synthesized in Figure 21c, SCI patients with asynchronous cranking depicted high values of HR for each workload, reaching a peak of 140 bpm at 90 W, and confirming that handcycling in the configuration of asynchronous crank ergometer is a mode of propulsion that requires a high activation of muscles.

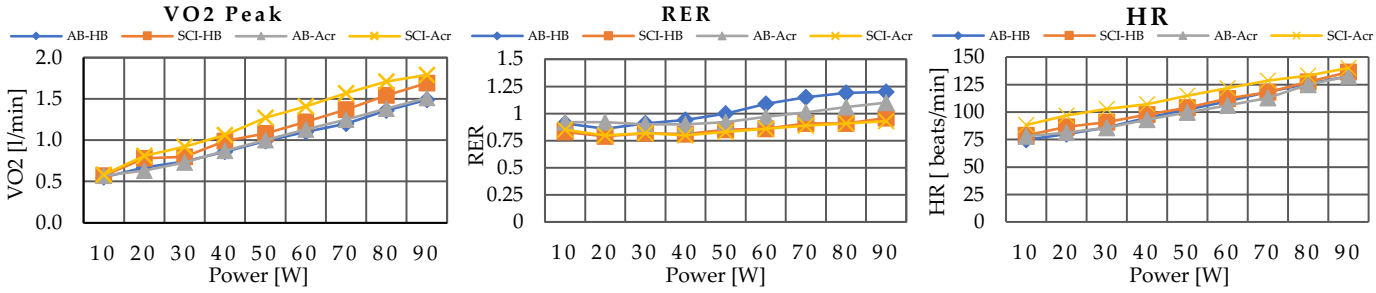

(**a**) (**b**) (**c**)

Figure 21. From the left: (**a**) peaks of volume of oxygen uptake (VO2), (**b**) respiratory exchange ratio (RER), and (**c**) heart rate (HR), as detected by Oviedo et al. [77] with respect to power output. Data are compared for the different combinations of SCI patients (SCI) and subjects without disabilities (AB), and with traditional handbike (HB) and asynchronous crank ergometer (Acr).

Steering

Steering is the capacity to rotate the crank in order to change direction. In the work conducted by Kraaijenbrink et al. [9], sixteen subjects without disabilities were tested with both synchronous and asynchronous crank modes, with an ergometer also able to simulate steering effects. The resistance of the ergometer was set at 35 W, while the crank velocity was set at 3.3 m/s (60 rpm). In the study, the steering was revealed to have a significant effect on both the crank modes from a physiological point of view. From a kinetic point of view, the synchronous crank mode was more efficient than the asynchronous mode. In fact, in synchronous configuration, the FEF increased from 56%, when the fork axle is fixed, to 59% in steering condition. In asynchronous mode, the FEF decreased from 22% to 19%. The reason, as explained by Kraaijenbrink et al. [8], is that in synchronous handcycling the moments produced with respect to the steering axle are opposite, so the total moment is almost null throughout the cycle. In asynchronous handcycling, the moments produced are the same, causing a rotation of the front wheel, so more control and consequently more muscle activation is needed.

The main highlights that emerged from the analysis of the Actuation category and its sub-classes are depicted in Table 8.

Table 8. Actuation: highlights for the category and sub-classes.

Actuation: Highlights
Biomechanical Models
• Biomechanical models of the propulsion task have been developed, which analyze the subject (e.g., musculoskeletal model of the handcyclist [66]) and the device (ergonomic behavior of a handbike [67]).
• Models often focus on specific aspects of the propulsion, such as muscular activity or shoulder loads.
• Biomechanical models for clinical purposes often combine physiological parameters: predictive and regression models are often used.
Crank mode
• The handcycling crank was originally asynchronous and has changed to synchronous over time.
• Handcycling in the configuration of asynchronous crank ergometer requires a high activation of muscles [77].
Steering
• Steering requires more control and muscle activation in asynchronous handcycling: steering produces moments, that are internally balanced in the case of synchronous cycling, but cause a rotation of the front wheel in the case of an asynchronous configuration [8].

3.7. Final Remarks

In the analysis, a set of categories and sub-classes was identified and examined. Besides the information extracted by the application of the proposed taxonomy, additional

interesting aspects emerged. For instance, a hint of the historical evolution of the handbike can be outlined, as synthesized in graphical form in Figure 22.

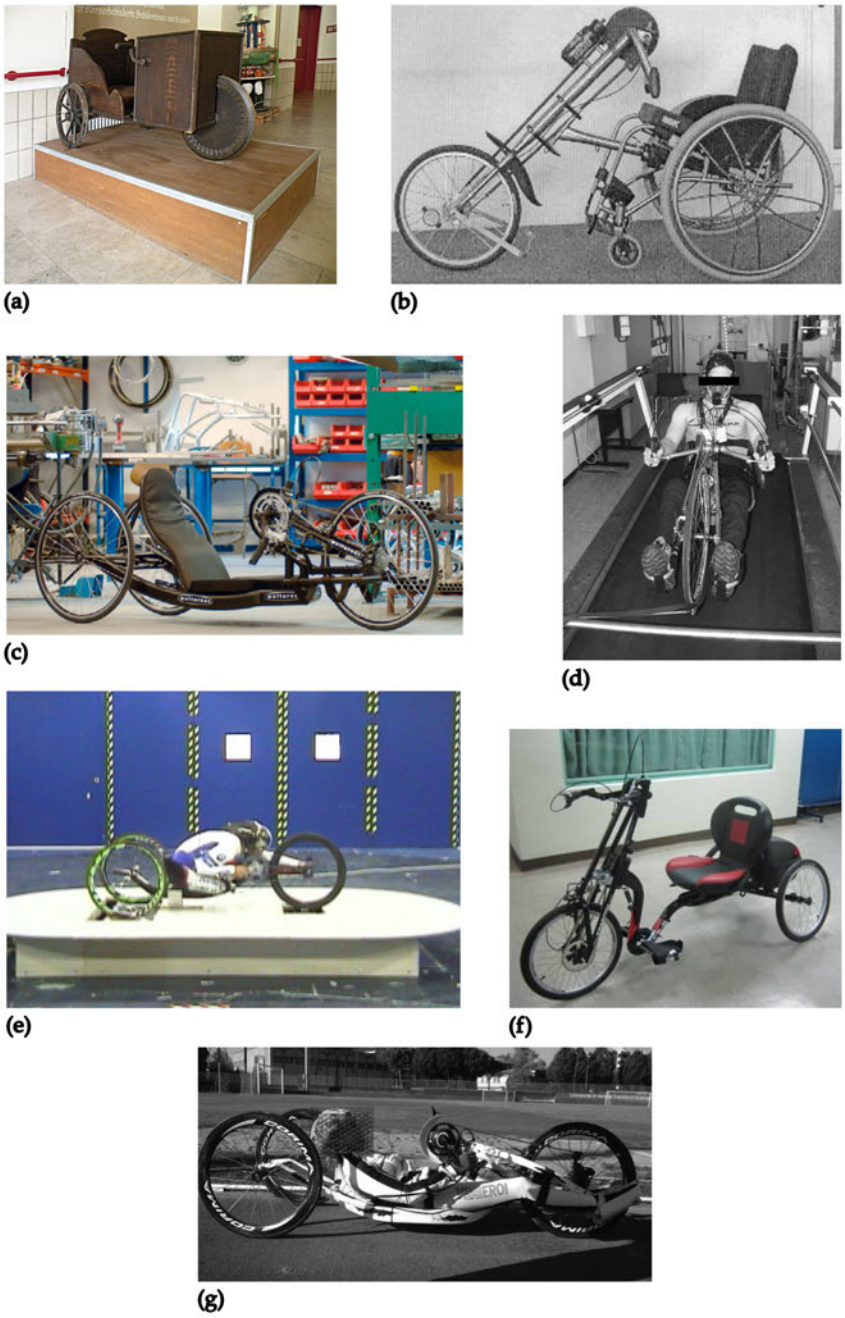

Figure 22. Handbike evolution: (**a**) the first handbike prototype made by Stephan Farffler in 1655 (image by V. Muratov, 2011 [78]), (**b**) a handbike with attach-unit (source: Dellmeijer et al., 2004 [5]), (**c**) a recumbent arm-powered road handbike (source: Siebert, 2010 [40]), (**d**) a touring handbike (source: Abel et al., 2006 [1]), (**e**) a race kneeling handbike (source: Belloli et al., 2014 [79]), (**f**) the "electric-assisted handcycle" by Jeang et al. (source: Jeang et al., 2015 [80]), and (**g**) a race recumbent handbike (source: Fischer et al., 2020 [81]).

An additional element is the relevance given in the scientific literature to the topics of comfort and discomfort of the handbike for the user. Attention is often afforded to the optimization of device configuration for performance improvement [58,73], but the sensibility of researchers is also towards ergonomics and usability of the system for the subject [59,67].

Literature also describes comparisons between handcycling and other tasks, especially hybrid-cycling [11,22,41,82–84]: these works generally present a clinical approach, and evaluate the comparison in terms of physiological parameters for the analyzed conditions.

Focusing on the design of new devices, besides the description of new handbike prototypes, some works depict innovative solutions for parts of the handbike: examples of these studies are the new transmission presented by Cavallone et al. [85], the new ergometer proposed by Verellen et al. [86], the new wheel rotation monitor by Hiremath et al. [87], or the new fork by Solazzi et al. [88]. These kinds of innovations may be difficult to capture with focused reviews, since the proposed systems can often be applied to different types of devices, like handbikes and wheelchairs. In this sense, interesting hints for the design of handbikes could also be extracted from the analysis of papers focusing on collateral topics. For instance, Florio et al. [89] investigated the unmet needs, use, and provision of assistive devices: handbikes are listed among the less frequently used devices, but are considered together with adapted cars and manual wheelchairs.

Interdisciplinary contamination among application fields is also at the basis of additional solutions, like the tandem bicycle proposed by Schwandt et al. [90], or the watercraft designed by Fuglsang et al. [91] by combining parts of a handbike and a waterbike.

As the relation between wheelchair and handbike is particularly close, literature also presents examples of attachments that enable the functional transformation of a wheelchair into a handbike. This is for instance the case for the studies proposed by Janssen et al. [92] and Dallmeijer et al. [5]. Moreno et al. identify an alternative solution, presenting the adaptation of an electric scooter to propel a conventional wheelchair [93], whereas Quaglia et al. design an innovative system of manual propulsion, defined as Handwheelchair.q [39].

Finally, few works deal with assistive or externally provided propulsion in handbikes. Siebert et al. [40] propose a powered rear wheel that can be mounted on the device instead of the traditional wheel, and nowadays some examples of analogous systems are also currently available on the market. The only case of an electric-assisted handcycle is presented by Jeang et al. [80]: the paper describes the design and development process of the device, from the concept definition to the release and testing of the first-generation prototype. For the actuation, few details are provided, but that the system incorporates a hub brushless motor which was tested for applicability and functionality by the various manufacturers that provided it. The lack of works on power-assisted solutions for handbikes in literature may be partially expected considering that handbikes are mostly used as a tool to improve mobility or to exercise in subjects with disabilities. Nonetheless, since the comfort of the user seems to be a particularly relevant element in the scientific literature on this topic, such a limited number of works still seems partially surprising. This is especially true when considering that few examples of power-assisted handbikes seem to be already available on the market (see Table 9). Given these considerations, a research focus also on this topic and on the development of handbikes equipped with external motors can be reasonably expected in the next future.

Finally, the world of handbikes represents a peculiar market sector, characterized by relatively small market shares and many professionals as final users. Perhaps also for this reason, commercial devices are rapidly evolving and developers keep implementing innovative technological solutions. According to this consideration, a market analysis investigating the main technical characteristics of off-the-shelf devices, as well as a thorough patent review, could provide valuable hints about possible trends and evolutions in the design of handbikes. Integrating the current work with this kind of analyses may de facto provide a comprehensive overview of the state of the technique on handbikes.

Table 9. Technical characteristics of three examples of electric handbike: Scrambler RS (by Handbike Garage, I), #Elba4All (by CGDE, I), and E-Handbike (by Custom Regeneration and G5Mobility, I).

Parameter	Scrambler RS	#Elba4All	E-Handbike *
Motor & Transmission			
Motor	OliEds Sport 85 Nm 250 W	Polini E-P3 70 Nm 250 W	by G5Mobility
Max Velocity	25 km/h		
Battery	single (540 W), double (2· 540 W)	single (500 W), double (2·500 W)	
Roundtrip (km)		220 (single battery)	>100
Wheels & Brakes			
Front wheel	27.5″ boost 148″	27.5″	
Rear wheel	27.5″ boost 110/15″	27.5″	
Brakes	anterior hydraulic 203 mm, posterior hydraulic 180 mm mono-pump		
Frame & Measures			
Frame	alluminium		
Width (cm)	80	80	
Length With wheels (cm)	220	220	
Length without wheels (cm)	180		
Span from the ground (cm)	20		
Maximum high with wheels (cm)	60	80	
Maximum load (kg)	100	110	
Pilot height (cm)	160–210		

* The company produces handbikes by reconditioning sports products.

4. Conclusions

In this work, a study of the scientific literature on handbikes was proposed, organizing the results with both a quantitative and a qualitative analyses. The analysis was performed with a systematic approach, and with the main purpose of depicting a comprehensive overview of the topic, with particular attention paid to actuation solutions and propulsion strategies.

Although the current literature review provides a general overview of technical characteristics of handbikes, the applied method may represent a limitation, as the proposed categories and sub-classes were identified and optimized in order to capture at best the peculiarities of the current dataset of documents. In this sense, analyzing the same dataset with different purposes may suggest modifications to the taxonomy, in order to elicit different characteristics of the works in literature.

Author Contributions: Conceptualization, C.A., G.I. and G.L.; methodology, C.A.; software, M.S.; validation, C.A., G.I. and G.L.; formal analysis, M.S. and C.A.; data curation, M.S., C.A., G.I. and G.L.; writing—original draft preparation, M.S. and C.A.; writing—review and editing, G.I., C.A. and G.L.; supervision, G.L. All authors have read and agreed to the published version of the manuscript.

Funding: This research received no external funding.

Institutional Review Board Statement: Not applicable.

Informed Consent Statement: Not applicable.

Data Availability Statement: The data presented in this study are available on request from the corresponding author.

Conflicts of Interest: The authors declare no conflict of interest.

Abbreviations

The following abbreviations are used in this manuscript:

AP	Arm propulsion
ATP	Arm trunk propulsion
Bla	Blood lactate concentration
EE	Energy expenditure
EMG	Electromyography
EMS	Electromyostimulation
FEF	Fraction effective force
FES	Functional electrical stimulation
GE	Gross efficiency
HITT	High intensity interval training
HR	Heart rate
HRR	Heart rate reserve
HRV	Heart rate variability
ME	Mechanical efficiency
MICT	Moderate intensity continuous training
P_{max}	Power peak
PO	Power output
RER	Respiratory exchange ratio
ROM	Range of motion
RPE	Rating of perceived exertion
RSI	Repetitive strain injuries
SCI	Spinal cord injury
UCI	Union Cycliste Internationale
VCO2	Volume of produced carbon dioxide
Vla	Lactate production
VO2	Maximal oxygen uptake
W/kg	Power per kilogram

Appendix A

In the following, an extract of the tables obtained from the classification procedure applied to the data is presented as Table A1.

Table A1. Main categories and some example of sub-classes classifications. Marks between brackets describe the absence of data required to populate technical details in sub-classes. From the left, document identification code, document type (Ar = article, CP = conference paper, Re = review, BC = book chapter), and if the publication is open access. For each category, the first column collects the general classification and possible additional sub-columns describe additional details. For the Actuation category, BioM describes the Biomechanical Models sub-class, Sync and Async are the crank modes synchronous and asynchronous, respectively, and CM is the presence of comparison methods.

Document ID	Type	OA	Clinical Tests	Subjects	Device	Prototype	Forces	3D	Sensors	Geometry	Actuation	BioM	Crank Mode	Sync	Async	CM	Steering	Other
Schwandt 1984 * [90]	CP				x	x					x						(x)	
Maki 1995 [94]	Ar		x	x					x									x
Van Der Woude 2000 [7]	Ar		x	x	x				x		x		x	x	x	x		
Janssen 2001 [92]	Ar		x	x	x				x									
Abel 2003 [17]	Ar		x	x	x				x		x		x	x	x	x		
Abel 2003a [95]	Ar		x	x	x				x									
Faupin 2003 [96]	CP								x		x	x						
Dallmeijer 2004 [5]	Ar	x	x		x				x									
Knechtle 2004 [97]	Ar	x	x	x					x									
Postma 2005 [98]	Ar	x	x	x					(x)									x
Abel 2006 [1]	Ar	x	x	x	x				x									
Faupin 2006 [99]	Ar		x	x	x				x	(x)	x	x						
Faupin 2006a [100]	CP		x	x					(x)	x	x	x						
Faupin 2008 [58]	Ar	x	x	x	x				x	x	x	x						
Faupin 2008a [56]	Ar		x	x	x		x	x	x	x	x	x	x	x				
Verellen 2008 [101]	Ar		x	x					x		x	x						x
Krämer 2009 [52]	Ar		x	x	x		x	x	x	x	x	x						
Meyer 2009 [102]	Ar		x	x	x				(x)									x
Abel 2010 [103]	Ar	x	x	x	x				x									x
Bollini 2010 [104]	CP				x	x					x							
Faupin 2010 [46]	Ar	x	x	x	x				x		x	x						
Goosey-Tolfrey 2010 [105]	Ar	x	x	x	x				x									
Groen 2010 * [72]	Ar		x	x	x				x		x	x						
Groen 2010a [73]	CP		x	x	x				x		x	x						
Rice 2010 [106]	BC																	x
Siebert 2010 [40]	CP	x			x	x				(x)								
Van Drongelen 2010 [107]	CP		x	x	x		x		x		x		x	x				

Table A1. *Cont.*

Document ID	Type	OA	Clinical Tests		Device		Forces		Sensors	Geometry	Actuation		Crank Mode				Steering	Other
			Subjects		Prototype		3D				BioM		Sync		Async	CM		
Hettinga 2011 [108]	CP		x	x							x	x						
Van Drongelen 2011 [51]	Ar		x	x	x	(x)	x	x	x									
Allgrove 2012 [109]	Ar	x	x	x	x				x									
Arnet 2012 [6]	Ar		x	x	x		x		x	(x)	x	x	x	x				
Arnet 2012a [42]	Ar	x	x	x	x		x	x	x		x	x	x	x				
Arnet 2012b [70]	Ar	x	x	x	x		x		x		x	x						
Lovell 2012 [18]	Ar	x	x	x	x				x									
Mazzola 2012 [67]	BC		x	x	x		x	x		x	x	x						x
Verellen 2012 [86]	Ar				x	x	x	x	x		x	x						
Verellen 2012a [19]	Ar		x	x	x				x									
Arnet 2013 [43]	Ar		x	x	x		x	x	x		x	x						
Hettinga 2013 [20]	Ar	x	x	x	x				x		x	x						x
Jacquier-Bret 2013 [53]	Ar				x		x		x	x	x	x						
Koopman 2013 [110]	Ar	x	x	x	x				x									
Van Der Woude 2013 [11]	Ar		x	x														x
Van Drongelen 2013 [71]	Ar		x	x	x		x	x	x		x	x	x	x				x
Arnet 2014 [47]	Ar	x	x	x	x		x		x	x	x	x						
Bakkum 2014 [41]	Ar	x	x	x	x	x			x									
Belloli 2014 [79]	CP	x	x	x	x						x	x						x
de Groot 2014 [36]	Ar	x	x	x	x				x		x	x						
Fischer 2014 [111]	Ar		x	x					x									x
Meyns 2014 [82]	Ar	x	x	x	x				x		x		(x)					x
Abel 2015 [21]	Ar	x	x	x	x				x	x	x	x						
Bakkum 2015 [22]	Ar	x	x		x	x			x									
Bakkum 2015a * [83]	Ar	x	x		x	x												
Fischer 2015 [23]	Ar		x	x	x				x									x
Jeang 2015 [80]	CP				x	(x)				(x)								x
Litzenberger 2015 [60]	CP	x	x	x	x				x	x	x	x						
Nooijen 2015 [10]	Ar	x	x	x	x				x									x
Nooijen 2015a [112]	Ar		x	x	x													
Simmelink 2015 [113]	Ar	x	x	x	x				x									

Table A1. *Cont.*

Document ID	Type	OA	Clinical Tests		Device		Forces		Sensors	Geometry	Actuation		Crank Mode			Steering	Other
				Subjects		Prototype		3D				BioM		Sync	Async	CM	
Abreu 2016 [114]	Ar	x	x	x					x								x
Arnet 2016 [115]	Ar		x	x	x												x
Felsner 2016 [66]	CP	x		x					(x)		x	x					
Hettinga 2016 [24]	Ar	x	x	x	x				x								
Litzenberger 2016 [57]	Ar		x	x	x				x	x	x	x					
Rice 2016 [4]	Re																x
Schoenmakers 2016 [25]	Ar	x	x	x	x				x								
Azizpour 2017 [116]	CP		x	x	x		(x)		x		x	x					
Fuglsang 2017 [91]	Ar	x															x
Hoekstra 2017 * [117]	Ar		x	x	x				x								
Hutchinson 2017 [26]	Ar	x	x	x	x				x								
Kraaijenbrink 2017 [27]	Ar	x	x		x		x	x	x		x	x	x	x			x
Zeller 2017 [118]	Ar		x		x				x								
Azizpour 2018 [119]	Ar		(x)	x	x	x	x		x		x	x					
Chong 2018 [45]	CP				x	x			(x)								x
de Groot 2018 [38]	Ar	x	x	x	x												x
de Groot 2018a [38]	Ar	x	x	x	x				x								
Kouwijzer 2018 [120]	Ar	x	x	x	x				x		x	x					
Legnani 2018 [121]	CP		x	x	x		x		x		x	x					
Morse 2018 [122]	Ar	x	x	x	x				x								x
Quittmann 2018 [28]	Ar		x	x	x		(x)	(x)	x		x	x					
Quittmann 2018a [123]	Ar		x	x	x				x								
Cudicio 2019 [124]	CP		x	x	x				x								x
Quaglia 2019 [39]	Ar	x			x	x					x	x					
Stangier 2019 [125]	Ar	x	x		x				x								
Stone 2019 [126]	Ar	x	x	x	x		(x)		x	x	x	x					
Stone 2019a [59]	Ar	x								x							x
Stone 2019b [127]	Ar	x	x	x	x				x		x	x					x
Vegter 2019 [54]	Ar	x	x	x	x		x		x	x	x	x	x	x			
Chaikhot 2020 [128]	Ar	x	x	x													
Fischer 2020 [81]	Ar	x	x	x					x								x

Table A1. *Cont.*

Document ID	Type	OA	Clinical Tests		Device		Forces		Sensors	Geometry	Actuation		Crank Mode				Steering	Other
			Subjects		Prototype		3D				BioM		Sync		Async	CM		
Himarosa 2020 [129]	CP	x			x	x				(x)	x		x	x				
Kouwijzer 2020 [130]	Ar	x	x	x														
Kouwijzer 2020a [74]	Ar	x	x	x	x				x		x	x						
Kraaijenbrink 2020 [8]	Ar	x	x	x	x		x	x	x	(x)	x	x	x	x	x	x	x	
Quittmann 2020 [61]	Ar		x	x	x		x	x	x		x	x						
Quittmann 2020a [69]	Ar		x	x	x		(x)		x		x	x						x
Stone 2020 [64]	Ar	x	x	x	x				x		x	x						x
Turoń-Skrzypińska 2020 [131]	Ar	x																x
Abonie 2021 [31]	Ar	x	x	x	x				x		x		x	x				
Hutchinson 2021 [32]	Ar	x	x	x	x				x							(x)		
Koontz 2021 [65]	Ar	x	x	x	x				x									
Kouwijzer 2021 [33]	Ar	x	x	x														
Kraaijenbrink 2021 [55]	Ar	x	x	x	x		x	x	x		x	x	x	x	x	x	x	
Kraaijenbrink 2021a [9]	Ar	x																x
Mason 2021 [62]	Ar	x	x	x	x				x	x	x	x						
Muchaxo 2021 [76]	Ar	x	x	x	x				x	x	x	x						
Nevin 2021 [132]	Ar	x	x	x	x		(x)		x									
Nevin 2021a [48]	Ar		x	x	x		x											
Nevin 2021b [49]	Ar	x	x	x	x		x		x									
Nooijen 2021 [37]	Ar	x	x	x	x						x	x						
Oviedo 2021 [77]	Ar		x	x	x				x	x	x		x	x	x	x		
Quittmann 2021 [133]	Ar		x	x	x													
Quittmann 2021a [68]	Ar		x	x	x				x		x	x						x
Stephenson 2021 [134]	Ar	x																x
Abonie 2022 [135]	Ar	x	x	x	x				x									
Antunes 2022 [63]	Ar		x	x	x				x									
Antunes 2022a [75]	Ar		(x)	(x)	(x)						x	(x)						
Digo 2022 [50]	CP		x	(x)	(x)		x		x		x	x						
Hall 2022 [34]	Ar	x	x	x	x				x									
Hutchinson 2022 [136]	Ar	x	x	x	x				x									
Kouwijzer 2022 [30]	Ar	x	x	x	x													

Table A1. *Cont.*

Document ID	Type	OA	Clinical Tests		Device		Forces		Sensors	Geometry	Actuation		Crank Mode			Steering	Other
				Subjects		Prototype		3D				BioM	Sync	Async	CM		
Muchaxo 2022 [35]	Ar	x	x	x	x		x	x	x		x	x					x
Nevin 2022 [3]	Re	x															x
Pasko 2022 [137]	CP		(x)	(x)													x
Quittmann 2022 [138]	Ar		x	x	x		x	x	x		x	x					
Rappelt 2022 [29]	Ar	x	x	x					x								
Rayes 2022 [14]	Re	x															x
Solazzi 2022 [88]	CP	x			x	(x)											
Soo Hoo 2022 [139]	Ar	x	x	x													x

* Full text not available. Data were retrieved from title and abstract only.

References

1. Abel, T.; Schneider, S.; Platen, P.; Strüder, H. Performance diagnostics in handbiking during competition. *Spinal Cord* **2006**, *44*, 211–216. [CrossRef] [PubMed]
2. Bucco-Lechat, C. Wikimedia Commons. 2014. Available online: https://commons.wikimedia.org/wiki/File:Salon_de_l%27auto_de_Gen%C3%A8ve_2014_-_20140305_-_Skoda_Vision_C.jpg (accessed on 15 January 2024)
3. Nevin, J.; Kouwijzer, I.; Stone, B.; Quittmann, O.; Hettinga, F.; Abel, T.; Smith, P. The Science of Handcycling: A Narrative Review. *Int. J. Sport. Physiol. Perform.* **2022**, *17*, 335–342. [CrossRef] [PubMed]
4. Rice, I. Recent Salient Literature Pertaining to the Use of Technology in Wheelchair Sports. *Curr. Phys. Med. Rehabil. Rep.* **2016**, *4*, 329–335. [CrossRef]
5. Dallmeijer, A.; Zentgraaff, I.; Zijp, N.; Van Der Woude, L. Submaximal physical strain and peak performance in handcycling versus handrim wheelchair propulsion. *Spinal Cord* **2004**, *42*, 91–98. [CrossRef]
6. Arnet, U.; Van Drongelen, S.; Scheel-Sailer, A.; Van Der Woude, L.; Veeger, D. Shoulder load during synchronous handcycling and handrim wheelchair propulsion in persons with paraplegia. *J. Rehabil. Med.* **2012**, *44*, 222–228. [CrossRef] [PubMed]
7. Van Der Woude, L.; Bosmans, I.; Bervoets, B.; Veeger, H. Handcycling: Different modes and gear ratios. *J. Med. Eng. Technol.* **2000**, *24*, 242–249. [CrossRef] [PubMed]
8. Kraaijenbrink, C.; Vegter, R.; Hensen, A.; Wagner, H.; Van Der Woude, L. Biomechanical and physiological differences between synchronous and asynchronous low intensity handcycling during practice-based learning in able-bodied men. *J. NeuroEng. Rehabil.* **2020**, *17*, 29 . [CrossRef]
9. Kraaijenbrink, C.; Vegter, R.; Ostertag, N.; Janssens, L.; Vanlandewijck, Y.; van der Woude, L.; Wagner, H. Steering Does Affect Biophysical Responses in Asynchronous, but Not Synchronous Submaximal Handcycle Ergometry in Able-Bodied Men. *Front. Sport. Act. Living* **2021**, *3*, 741258. [CrossRef]
10. Nooijen, C.; Van Den Brand, I.; Ter Horst, P.; Wynants, M.; Valent, L.; Stam, H.; Van Den Berg-Emons, R. Feasibility of Handcycle Training during Inpatient Rehabilitation in Persons with Spinal Cord Injury. *Arch. Phys. Med. Rehabil.* **2015**, *96*, 1654–1657. [CrossRef]
11. Van Der Woude, L.; de Groot, S.; Postema, K.; Bussmann, J.; Janssen, T.; Post, M. Active LifestyLe Rehabilitation Interventions in aging Spinal Cord injury (ALLRISC): A multicentre research program. *Disabil. Rehabil.* **2013**, *35*, 1097–1103. [CrossRef]
12. Flueck, J. Nutritional considerations for para-cycling athletes: A narrative review. *Sports* **2021**, *9*, 154. [CrossRef] [PubMed]
13. Goodlin, G.; Steinbeck, L.; Bergfeld, D.; Haselhorst, A. Adaptive Cycling: Classification, Adaptations, and Biomechanics. *Phys. Med. Rehabil. Clin. N. Am.* **2022**, *33*, 31–43. [CrossRef] [PubMed]
14. Rayes, R.; Ball, C.; Lee, K.; White, C. Adaptive Sports in Spinal Cord Injury: A Systematic Review. *Curr. Phys. Med. Rehabil. Rep.* **2022**, *10*, 145–153. [CrossRef] [PubMed]
15. Heymsfield, S. *Human Body Composition*; Human kinetics: Champaign, IL, USA, 2005; Volume 918.
16. Borg, G. *Borg's Perceived Exertion and Pain Scales*; Human Kinetics: Champaign, IL, USA, 1998.
17. Abel, T.; Kröner, M.; Rojas, V.; Peters, C.; Klose, C.; Platen, P. Energy expenditure in wheelchair racing and handbiking —A basis for prevention of cardiovascular diseases in those with disabilities. *Eur. J. Prev. Cardiol.* **2003**, *10*, 371–376. [CrossRef] [PubMed]
18. Lovell, D.; Shields, D.; Beck, B.; Cuneo, R.; McLellan, C. The aerobic performance of trained and untrained handcyclists with spinal cord injury. *Eur. J. Appl. Physiol.* **2012**, *112*, 3431–3437. [CrossRef] [PubMed]
19. Verellen, J.; Meyer, C.; Janssens, L.; Vanlandewijck, Y.; Lacour, J.R. Peak and submaximal steady-state metabolic and cardiorespiratory responses during arm-powered and arm-trunk-powered handbike ergometry in able-bodied participants. *Eur. J. Appl. Physiol.* **2012**, *112*, 983–989. [CrossRef] [PubMed]
20. Hettinga, F.; de Groot, S.; Van Dijk, F.; Kerkhof, F.; Woldring, F.; Van Der Woude, L. Physical strain of handcycling: An evaluation using training guidelines for a healthy lifestyle as defined by the American College of Sports Medicine. *J. Spinal Cord Med.* **2013**, *36*, 376–382. [CrossRef]
21. Abel, T.; Burkett, B.; Thees, B.; Schneider, S.; Askew, C.; Strüder, H. Effect of three different grip angles on physiological parameters during laboratory handcycling test in able-bodied participants. *Front. Physiol.* **2015**, *6*, 331. [CrossRef]
22. Bakkum, A.; de Groot, S.; Stolwijk-Swüste, J.; Van Kuppevelt, D.; Van Der Woude, L.; Janssen, T. Effects of hybrid cycling versus handcycling on wheelchair-specific fitness and physical activity in people with long-term spinal cord injury: A 16-week randomized controlled trial. *Spinal Cord* **2015**, *53*, 395–401. [CrossRef]
23. Fischer, G.; Figueiredo, P.; Ardigò, L. Physiological performance determinants of a 22-km handbiking time trial. *Int. J. Sport. Physiol. Perform.* **2015**, *10*, 965–971. [CrossRef]
24. Hettinga, F.; Hoogwerf, M.; van der Woude, L. Handcycling: Training effects of a specific dose of upper body endurance training in females. *Eur. J. Appl. Physiol.* **2016**, *116*, 1387–1394. [CrossRef] [PubMed]
25. Schoenmakers, P.; Reed, K.; Woude, V.; Hettinga, F. High intensity interval training in handcycling: The effects of a 7 week training intervention in able-bodied men. *Front. Physiol.* **2016**, *7*, 638. [CrossRef] [PubMed]
26. Hutchinson, M.; Paulson, T.; Eston, R.; Tolfrey, V. Assessment of peak oxygen uptake during handcycling: Test-retest reliability and comparison of a ramp-incremented and perceptually-regulated exercise test. *PLoS ONE* **2017**, *12*, e0181008. [CrossRef] [PubMed]

27. Kraaijenbrink, C.; Vegter, R.; Hensen, A.; Wagner, H.; Van Der Woude, L. Different cadences and resistances in submaximal synchronous handcycling in able-bodied men: Effects on efficiency and force application. *PLoS ONE* **2017**, *12*, e0183502. [CrossRef] [PubMed]
28. Quittmann, O.; Abel, T.; Zeller, S.; Foitschik, T.; Strüder, H. Lactate kinetics in handcycling under various exercise modalities and their relationship to performance measures in able-bodied participants. *Eur. J. Appl. Physiol.* **2018**, *118*, 1493–1505. [CrossRef] [PubMed]
29. Rappelt, L.; Held, S.; Donath, L. Handcycling with concurrent lower body low-frequency electromyostimulation significantly increases acute oxygen uptake: Implications for rehabilitation and prevention. *PeerJ* **2022**, *10*, e13333. [CrossRef] [PubMed]
30. Kouwijzer, I.; Valent, L.; van Bennekom, C.; Post, M.; van der Woude, L.; de Groot, S. Training for the HandbikeBattle: An explorative analysis of training load and handcycling physical capacity in recreationally active wheelchair users. *Disabil. Rehabil.* **2022**, *44*, 2723–2732. [CrossRef]
31. Abonie, U.; Monden, P.; van der Woude, L.; Hettinga, F. Effect of a 7-week low intensity synchronous handcycling training programme on physical capacity in abled-bodied women. *J. Sport. Sci.* **2021**, *39*, 1472–1480. [CrossRef]
32. Hutchinson, M.; Kouwijzer, I.; de Groot, S.; Goosey-Tolfrey, V. Comparison of two Borg exertion scales for monitoring exercise intensity in able-bodied participants, and those with paraplegia and tetraplegia. *Spinal Cord* **2021**, *59*, 1162–1169. [CrossRef]
33. Kouwijzer, I.; Valent, L.; Post, M.; Wilders, L.; Grootoonk, A.; Van Der Woude, L.; de Groot, S. The Course of Physical Capacity in Wheelchair Users during Training for the HandbikeBattle and at 1-Yr Follow-up. *Am. J. Phys. Med. Rehabil.* **2021**, *100*, 858–865. [CrossRef]
34. Hall, B.; Sikora, M.; Jonas, D.; Matthews, E.; Zebrowska, A. Handcycling Training in Men with Spinal Cord Injury Increases Tolerance to High Intensity Exercise. *J. Hum. Kinet.* **2022**, *82*, 233–241. [CrossRef] [PubMed]
35. Muchaxo, R.; de Groot, S.; Kouwijzer, I.; van der Woude, L.; Nooijen, C.; Janssen, T. Association between upper-limb isometric strength and handcycling performance in elite athletes. *Sport. Biomech.* 2022, *Online ahead of print*. [CrossRef] [PubMed]
36. de Groot, S.; Postma, K.; Van Vliet, L.; Timmermans, R.; Valent, L. Mountain time trial in handcycling: Exercise intensity and predictors of race time in people with spinal cord injury. *Spinal Cord* **2014**, *52*, 455–461. [CrossRef] [PubMed]
37. Nooijen, C.; Muchaxo, R.; Liljedahl, J.; Bjerkefors, A.; Janssen, T.; van der Woude, L.; Arndt, A.; de Groot, S. The relation between sprint power and road time trial performance in elite para-cyclists. *J. Sci. Med. Sport* **2021**, *24*, 1193–1198. [CrossRef]
38. de Groot, S.; Kouwijzer, I.; Baauw, M.; Broeksteeg, R.; Valent, L. Effect of self-guided training for the HandbikeBattle on body composition in people with spinal cord injury. *Spinal Cord Ser. Cases* **2018**, *4*, 79. [CrossRef] [PubMed]
39. Quaglia, G.; Bonisoli, E.; Cavallone, P. The design of a new manual wheelchair for sport. *Machines* **2019**, *7*, 31. [CrossRef]
40. Siebert, M. Adjustable handbike-chassis for offroad-use ("mountain handbike"). *Procedia Eng.* **2010**, *2*, 3157–3162. [CrossRef]
41. Bakkum, A.; de Groot, S.; Onderwater, M.; De Jong, J.; Janssen, T. Metabolic rate and cardiorespiratory response during hybrid cycling versus handcycling at equal subjective exercise intensity levels in people with spinal cord injury. *J. Spinal Cord Med.* **2014**, *37*, 758–764. [CrossRef]
42. Arnet, U.; Van Drongelen, S.; Van Der Woude, L.; Veeger, D. Shoulder load during handcycling at different incline and speed conditions. *Clin. Biomech.* **2012**, *27*, 1–6. [CrossRef]
43. Arnet, U.; Van Drongelen, S.; Veeger, D.; Van Der Woude, L. Force application during handcycling and handrim wheelchair propulsion: An initial comparison. *J. Appl. Biomech.* **2013**, *29*, 687–695. [CrossRef]
44. Amici, C.; Ragni, F.; Ghidoni, M.; Fausti, D.; Bissolotti, L.; Tiboni, M. Multi-Sensor Validation Approach of an End-Effector-Based Robot for the Rehabilitation of the Upper and Lower Limb. *Electronics* **2020**, *9*, 1751. [CrossRef]
45. Chong, Y.; Yang, T. Development of portable hand cycle for children with cerebral palsy—The Malaysian scenario: Wheelchair propulsion motion. In Proceedings of the 5th IEEE Region 10 Humanitarian Technology Conference 2017, R10-HTC, Dhaka, Bangladesh, 21–23 December 2017; Volume 2018, pp. 873–877. [CrossRef]
46. Faupin, A.; Gorce, P.; Watelain, E.; Meyer, C.; Thevenon, A. A biomechanical analysis of handcycling: A case study. *J. Appl. Biomech.* **2010**, *26*, 240–245. [CrossRef]
47. Arnet, U.; van Drongelen, S.; Schlüssel, M.; Lay, V.; van der Woude, L.; Veeger, H. The effect of crank position and backrest inclination on shoulder load and mechanical efficiency during handcycling. *Scand. J. Med. Sci. Sport.* **2014**, *24*, 386–394. [CrossRef] [PubMed]
48. Nevin, J.; Smith, P. The Relationship between Absolute and Relative Upper-Body Strength and Handcycling Performance Capabilities. *Int. J. Sport. Physiol. Perform.* **2021**, *16*, 1311–1318. [CrossRef] [PubMed]
49. Nevin, J.; Smith, P. The anthropometric, physiological, and strength-related determinants of handcycling 15-km time-trial performance. *Int. J. Sport. Physiol. Perform.* **2021**, *16*, 259–266. [CrossRef] [PubMed]
50. Digo, E.; Gastaldi, L.; Antonelli, M.; Cornagliotto, V.; Pastorelli, S. Estimation of Force Effectiveness and Symmetry During Kranking Training. In *Proceedings of the I4SDG Workshop 2021. I4SDG 2021. Mechanisms and Machine Science, Online, 25–26 November 2021*; Quaglia, G., Gasparetto, A., Petuya, V., Carbone, G., Eds.; Springer: Berlin, Germany, 2022; Volume 108, pp. 201–208. [CrossRef]
51. Van Drongelen, S.; van den Berg, J.; Arnet, U.; Veeger, D.; van der Woude, L. Development and validity of an instrumented handbike: Initial results of propulsion kinetics. *Med. Eng. Phys.* **2011**, *33*, 1167–1173. [CrossRef] [PubMed]
52. Krämer, C.; Schneider, G.; Böhm, H.; Klöpfer-Krämer, I.; Senner, V. Effect of different handgrip angles on work distribution during hand cycling at submaximal power levels. *Ergonomics* **2009**, *52*, 1276–1286. [CrossRef] [PubMed]

53. Jacquier-Bret, J.; Faupin, A.; Rezzoug, N.; Gorce, P. A new postural force production index to assess propulsion effectiveness during handcycling. *J. Appl. Biomech.* **2013**, *29*, 798–803. [CrossRef] [PubMed]
54. Vegter, R.; Mason, B.; Sporrel, B.; Stone, B.; van der Woude, L.; Goosey-Tolfrey, V. Crank fore-aft position alters the distribution of work over the push and pull phase during synchronous recumbent handcycling of able-bodied participants. *PLoS ONE* **2019**, *14*, e0220943. [CrossRef] [PubMed]
55. Kraaijenbrink, C.; Vegter, R.; de Groot, S.; Arnet, U.; Valent, L.; Verellen, J.; van Breukelen, K.; Hettinga, F.; Perret, C.; Abel, T.; et al. Biophysical aspects of handcycling performance in rehabilitation, daily life and recreational sports; a narrative review. *Disabil. Rehabil.* **2021**, *43*, 3461–3475. [CrossRef]
56. Faupin, A.; Gorce, P.; Meyer, C.; Thevenon, A. Effects of backrest positioning and gear ratio on nondisabled subjects' handcycling sprinting performance and kinematics. *J. Rehabil. Res. Dev.* **2008**, *45*, 109–116. [CrossRef] [PubMed]
57. Litzenberger, S.; Mally, F.; Sabo, A. Biomechanics of elite recumbent handcycling: A case study: Influence of backrest position, crank length and crank height on muscular activity and upper body kinematics. *Sport. Eng.* **2016**, *19*, 201–211. [CrossRef]
58. Faupin, A.; Gorce, P. The effects of crank adjustments on handbike propulsion: A kinematic model approach. *Int. J. Ind. Ergon.* **2008**, *38*, 577–583. [CrossRef]
59. Stone, B.; Mason, B.; Warner, M.; Goosey-Tolfrey, V. Horizontal Crank Position Affects Economy and Upper Limb Kinematics of Recumbent Handcyclists. *Med. Sci. Sport. Exerc.* **2019**, *51*, 2265–2273. [CrossRef]
60. Litzenberger, S.; Mally, F.; Sabo, A. Influence of different seating and crank positions on muscular activity in elite handcycling—A case study. *Procedia Eng.* **2015**, *112*, 355–360. [CrossRef]
61. Quittmann, O.; Abel, T.; Albracht, K.; Meskemper, J.; Foitschik, T.; Strüder, H. Biomechanics of handcycling propulsion in a 30-min continuous load test at lactate threshold: Kinetics, kinematics, and muscular activity in able-bodied participants. *Eur. J. Appl. Physiol.* **2020**, *120*, 1403–1415. [CrossRef] [PubMed]
62. Mason, B.; Stone, B.; Warner, M.; Goosey-Tolfrey, V. Crank length alters kinematics and kinetics, yet not the economy of recumbent handcyclists at constant handgrip speeds. *Scand. J. Med. Sci. Sport.* **2021**, *31*, 388–397. [CrossRef]
63. Antunes, D.; Borszcz, F.; Nascimento, E.; Cavalheiro, G.; Fischer, G.; Brickley, G.; De Lucas, R. Physiological and Perceptual Responses in Spinal Cord Injury Handcyclists during an Endurance Interval Training: The Role of Critical Speed. *Am. J. Phys. Med. Rehabil.* **2022**, *101*, 977–982. [CrossRef]
64. Stone, B.; Mason, B.; Stephenson, B.; Goosey-Tolfrey, V. Physiological responses during simulated 16 km recumbent handcycling time trial and determinants of performance in trained handcyclists. *Eur. J. Appl. Physiol.* **2020**, *120*, 1621–1628. [CrossRef]
65. Koontz, A.; Garfunkel, C.; Crytzer, T.; Anthony, S.; Nindl, B. Feasibility, acceptability, and preliminary efficacy of a handcycling high-intensity interval training program for individuals with spinal cord injury. *Spinal Cord* **2021**, *59*, 34–43. [CrossRef]
66. Felsner, E.M.; Litzenberger, S.; Mally, F.; Sabo, A. Musculoskeletal Modelling of Elite Handcycling Motion: Evaluation of Muscular On-and Offset. *Procedia Eng.* **2016**, *147*, 168–174. [CrossRef]
67. Mazzola, M.; Andreoni, G.; Campanardi, G.; Costa, F.; Gibertini, G.; Grassi, D.; Romero, M. *Effects of Seat and Handgrips Adjustments on a Hand Bike Vehicle. An Ergonomic and Aerodynamic Study for a Quantitative Assessment of Paralympics Athlete's Performance*; CRC Press: Boca Raton, FL, USA, 2012; pp. 569–576.
68. Quittmann, O.; Abel, T.; Vafa, R.; Mester, J.; Schwarz, Y.; Strüder, H. Maximal lactate accumulation rate and post-exercise lactate kinetics in handcycling and cycling. *Eur. J. Sport Sci.* **2021**, *21*, 539–551. [CrossRef] [PubMed]
69. Quittmann, O.; Meskemper, J.; Albracht, K.; Abel, T.; Foitschik, T.; Strüder, H. Normalising surface EMG of ten upper-extremity muscles in handcycling: Manual resistance vs. sport-specific MVICs. *J. Electromyogr. Kinesiol.* **2020**, *51*, 102402. [CrossRef] [PubMed]
70. Arnet, U.; van Drongelen, S.; Veeger, D.; van der Woude, L. Are the force characteristics of synchronous handcycling affected by speed and the method to impose power? *Med. Eng. Phys.* **2012**, *34*, 78–84. [CrossRef] [PubMed]
71. Van Drongelen, S.; Schlüssel, M.; Arnet, U.; Veeger, D. The influence of simulated rotator cuff tears on the risk for impingement in handbike and handrim wheelchair propulsion. *Clin. Biomech.* **2013**, *28*, 495–501. [CrossRef] [PubMed]
72. Groen, W.; Van Der Woude, L.; De Koning, J. A power balance model for handcycling. *Disabil. Rehabil.* **2010**, *32*, 2165–2171. [CrossRef]
73. Groen, W.; Van Der Woude, L.; De Koning, J. *The Power Balance Model: Useful in the Study of Elite Handcycling Performance*; IOS Press: Amsterdam, The Netherlands, 2010; Volume 26, pp. 85–87. [CrossRef]
74. Kouwijzer, I.; Valent, L.; Osterthun, R.; van der Woude, L.; de Groot, S. Peak power output in handcycling of individuals with a chronic spinal cord injury: Predictive modeling, validation and reference values. *Disabil. Rehabil.* **2020**, *42*, 400–409. [CrossRef]
75. Antunes, D.; Nascimento, E.; Brickley, G.; Fischer, G.; de Lucas, R. Determination of the speed-time relationship during handcycling in spinal cord injured athletes. *Res. Sport. Med.* **2022**, *30*, 256–263. [CrossRef]
76. Muchaxo, R.; de Groot, S.; Kouwijzer, I.; Van Der Woude, L.; Janssen, T.; Nooijen, C. A Role for Trunk Function in Elite Recumbent Handcycling Performance? *J. Sport. Sci.* **2021**, *39*, 2312–2321. [CrossRef]
77. Oviedo, G.; Alamo, J.; Niño-Mendez, O.; Travier, N.; Ventura, J.; Soto-Montañez, C.; Vidal, J.; Medina, J.; Javierre, C. Physiological responses in males with and without spinal cord injury to recumbent synchronous versus seated asynchronous arm crank stress tests | Respuestas fisiológicas en hombres con y sin lesión medular al realizar pruebas de esfuerzo con ergómetros de. *Retos* **2021**, 39, 565–571. [CrossRef]

78. Muratov, V. Wikimedia Commons. 2011. Available online: https://commons.wikimedia.org/wiki/File:Faffler_carriage.jpg (accessed on 15 January 2024).
79. Belloli, M.; Cheli, F.; Bayati, I.; Giappino, S.; Robustelli, F. Handbike aerodynamics: Wind tunnel versus track tests. *Procedia Eng.* **2014**, *72*, 750–755. [CrossRef]
80. Jeang, A.; Liang, F.; Huang, H. Handcycle design & development process for the disabled. In Proceedings of the 2015 IFToMM World Congress Proceedings, Taipei, Taiwan, 25–30 October 2015. [CrossRef]
81. Fischer, G.; Figueiredo, P.; Ardigò, L. Bioenergetics and Biomechanics of Handcycling at Submaximal Speeds in Athletes with a Spinal Cord Injury. *Sports* **2020**, *8*, 16. [CrossRef] [PubMed]
82. Meyns, P.; Van De Walle, P.; Hoogkamer, W.; Kiekens, C.; Desloovere, K.; Duysens, J. Coordinating arms and legs on a hybrid rehabilitation tricycle: The metabolic benefit of asymmetrical compared to symmetrical arm movements. *Eur. J. Appl. Physiol.* **2014**, *114*, 743–750. [CrossRef] [PubMed]
83. Bakkum, A.; Paulson, T.; Bishop, N.; Goosey-Tolfrey, V.; Stolwijk-Swüste, J.; Van Kuppevelt, D.; de Groot, S.; Janssen, T. Effects of hybrid cycle and handcycle exercise on cardiovascular disease risk factors in people with spinal cord injury: A randomized controlled trial. *J. Rehabil. Med.* **2015**, *47*, 523–530. [CrossRef] [PubMed]
84. Jansen, E.; de Groot, S.; Smit, C.; Thijssen, D.; TE Hopman, M.; Janssen, T. Vascular adaptations in nonstimulated areas during hybrid cycling or handcycling in people with a spinal cord injury: A pilot study of 10 cases. *Spinal Cord Ser. Cases* **2021**, *7*, 54. [CrossRef]
85. Cavallone, P.; Vieira, T.; Quaglia, G.; Gazzoni, M. Electomyographic activities of shoulder muscles during Handwheelchair.Q vs pushrim wheelchair propulsion. *Med. Eng. Phys.* **2022**, *106*, 103833. [CrossRef]
86. Verellen, J.; Janssens, L.; Meyer, C.; Vanlandewijck, Y. Development and application of a handbike ergometer to measure the 3D force generation pattern during arm crank propulsion in realistic handcycling conditions. *Sport. Technol.* **2012**, *5*, 65–73. [CrossRef]
87. Hiremath, S.; Ding, D.; Cooper, R. Development and evaluation of a gyroscopebased wheel rotation monitor for manual wheelchair users. *J. Spinal Cord Med.* **2013**, *36*, 347–356. [CrossRef]
88. Solazzi, L.; Schinetti, G.; Adamini, R. *Developed an Innovative Handbike Fork Made of Composite Material*; IOS Press: Amsterdam, The Netherlands , 2022; Volume 297, pp. 359–366. [CrossRef]
89. Florio, J.; Arnet, U.; Gemperli, A.; Hinrichs, T. Need and use of assistive devices for personal mobility by individuals with spinal cord injury. *J. Spinal Cord Med.* **2016**, *39*, 461–470. [CrossRef]
90. Schwandt, D. *Design Development of a Tandem Bicycle for Individuals with and without Lower Limb Disability*; SAE International: Troy, MI, USA, 1984; pp. 213–214.
91. Fuglsang, T.; Padulo, J.; Spoladore, M.; Dalla Piazza, M.; Ardigò, L. Development and testing of a novel arm cranking-powered watercraft. *Front. Physiol.* **2017**, *8*, 635. [CrossRef]
92. Janssen, T.; Dallmeijer, A.; Van Der Woude, L. Physical capacity and race performance of handcycle users. *J. Rehabil. Res. Dev.* **2001**, *38*, 33–40.
93. Moreno, B.; Peris-Fajarnés, G.; Lengua, I.; Moncho-Santonja, M. *Wheelchair Mobility Aid Through the Adaptation of Electric Scooters*; Springer: Berlin, Germany, 2020; pp. 184–190. [CrossRef]
94. Maki, K.; Langbein, W.; Reid-Lokos, C. Energy cost and locomotive economy of handbike and rowcycle propulsion by persons with spinal cord injury. *J. Rehabil. Res. Dev.* **1995**, *32*, 170–178. [PubMed]
95. Abel, T.; Vega, S.; Bleicher, I.; Platen, P. Handbiking: Physiological responses to synchronous and asynchronous crank montage. *Eur. J. Sport Sci.* **2003**, *3*, 1–9. [CrossRef]
96. Faupin, A.; Campillo, P.; Rémy-Néris, O.; Bouilland, S.; Thevenon, A.; Gorce, P. A kinematic study of the upper-limb motion of handcycle propulsion. *Arch. Physiol. Biochem.* **2003**, *111*, 38.
97. Knechtle, B.; Mülle, G.; Knech, H. Optimal exercise intensities for fat metabolism in handbike cycling and cycling. *Spinal Cord* **2004**, *42*, 564–572. [CrossRef] [PubMed]
98. Postma, K.; Berg-Emons Van Den, H.; Bussmann, J.; Sluis, T.; Bergen, M.; Stam, H. Validity of the detection of wheelchair propulsion as measured with an Activity Monitor in patients with spinal cord injury. *Spinal Cord* **2005**, *43*, 550–557. [CrossRef] [PubMed]
99. Faupin, A.; Gorce, P.; Campillo, P.; Thevenon, A.; Rémy-Néris, O. Kinematic analysis of handbike propulsion in various gear ratios: Implications for joint pain. *Clin. Biomech.* **2006**, *21*, 560–566. [CrossRef] [PubMed]
100. Faupin, A.; Gorce, P.; Rémy-Néris, O.; Thevenon, A. Ergonomie assessment of the handcycling propulsion. *Model. Meas. Control. C* **2006**, 146–155.
101. Verellen, J.; Meyer, C.; Reynders, S.; Van Biesen, D.; Vanlandewijck, Y. Consistency of within-cycle torque distribution pattern in hand cycling. *J. Rehabil. Res. Dev.* **2008**, *45*, 1295–1302. [CrossRef]
102. Meyer, C.; Weissland, T.; Watelain, E.; Ribadeau Dumas, S.; Baudinet, M.C.; Faupin, A. Physiological responses in handcycling. Preliminary study. *Ann. Phys. Rehabil. Med.* **2009**, *52*, 311–318. [CrossRef]
103. Abel, T.; Burkett, B.; Schneider, S.; Lindschulten, R.; Strüder, H. The exercise profile of an ultra-long handcycling race: The Styrkeprøven experience. *Spinal Cord* **2010**, *48*, 894–898. [CrossRef] [PubMed]
104. Bollini, M. *The Figure Eight Drive: A Two-Speed Drivetrain for Handcycles in the Developing World*; IOS Press: Amsterdam, The Netherlands, 2010; Volume 26, pp. 91–93. [CrossRef]

105. Goosey-Tolfrey, V.; Lenton, J.; Goddard, J.; Oldfield, V.; Tolfrey, K.; Eston, R. Regulating intensity using perceived exertion in spinal cord-injured participants. *Med. Sci. Sport. Exerc.* **2010**, *42*, 608–613. [CrossRef] [PubMed]
106. Rice, I.; Hettinga, F.; Laferrier, J.; Sporner, M.; Heiner, C.; Burkett, B.; Cooper, R. *Biomechanics*; Wiley: Hoboken, NJ, USA, 2010; pp. 31–50. [CrossRef]
107. Van Drongelen, S.; Arnet, U.; Van Der Woude, L.; Veeger, H. *Propulsion Effectiveness of Synchronous Handcycling* ; IOS Press: Amsterdam, The Netherlands, 2010; Volume 26, pp. 82–84. [CrossRef]
108. Hettinga, F.; Valent, L.; Van Der Woude, L. *Optimal Upper Body Exercise Training: Handcycling* ; IOS Press: Amsterdam, The Netherlands, 2011; Volume 29, pp. 751–757. [CrossRef]
109. Allgrove, J.; Chapman, M.; Christides, T.; Smith, P. Immunoendocrine responses of male spinal cord injured athletes to 1-h self-paced exercise: Pilot study. *J. Rehabil. Res. Dev.* **2012**, *49*, 925–934. [CrossRef] [PubMed]
110. Koopman, A.; Eken, M.; Van Bezeij, T.; Valent, L.; Houdijk, H. Does clinical rehabilitation impose sufficient cardiorespiratory strain to improve aerobic fitness. *J. Rehabil. Med.* **2013**, *45*, 92–98. [CrossRef] [PubMed]
111. Fischer, G.; Tarperi, C.; George, K.; Ardigò, L. An exploratory study of respiratory muscle endurance training in high lesion level paraplegic handbike athletes. *Clin. J. Sport Med.* **2014**, *24*, 69–75. [CrossRef] [PubMed]
112. Nooijen, C.; Vogels, S.; Bongers-Janssen, H.; Bergen, M.; Stam, H.; Van Den Berg-Emons, H. Fatigue in persons with subacute spinal cord injury who are dependent on a manual wheelchair. *Spinal Cord* **2015**, *53*, 758–762. [CrossRef]
113. Simmelink, E.; Borgesius, E.; Hettinga, F.; Geertzen, J.; Dekker, R.; Van Der Woude, L. Gross mechanical efficiency of the combined armleg (Cruiser) ergometer: A comparison with the bicycle ergometer and handbike. *Int. J. Rehabil. Res.* **2015**, *38*, 61–67. [CrossRef]
114. Abreu, E.; Alves, R.; Borges, A.; Lima, F.; de Paula Júnior, A.; Lima, M. Autonomic cardiovascular control recovery in quadriplegics after handcycle training. *J. Phys. Ther. Sci.* **2016**, *28*, 2063–2068. [CrossRef]
115. Arnet, U.; Hinrichs, T.; Lay, V.; Bertschy, S.; Frei, H.; Brinkhof, M. Determinants of handbike use in persons with spinal cord injury: Results of a community survey in Switzerland. *Disabil. Rehabil.* **2016**, *38*, 81–86. [CrossRef]
116. Azizpour, G.; Ousdad, A.; Legnani, G.; Incerti, G.; Lancini, M.; Gaffurini, P. *Dynamic Analysis of Handcycling: Mathematical Modelling and Experimental Tests*; Springer: Berlin, Germany, 2017; Volume 47, pp. 33–40. [CrossRef]
117. Hoekstra, S.; Valent, L.; Gobets, D.; van der Woude, L.; de Groot, S. Effects of four-month handbike training under free-living conditions on physical fitness and health in wheelchair users. *Disabil. Rehabil.* **2017**, *39*, 1581–1588. [CrossRef]
118. Zeller, S.; Abel, T.; Strueder, H. Monitoring training load in handcycling: A case study. *J. Strength Cond. Res.* **2017**, *31*, 3094–3100. [CrossRef] [PubMed]
119. Azizpour, G.; Lancini, M.; Incerti, G.; Gaffurini, P.; Legnani, G. An experimental method to estimate upper limbs inertial parameters during handcycling. *J. Appl. Biomech.* **2018**, *34*, 175–183. [CrossRef] [PubMed]
120. Kouwijzer, I.; Nooijen, C.; Van Breukelen, K.; Janssen, T.; de Groot, S. Effects of push-off ability and handcycle type on handcycling performance in able-bodied participants. *J. Rehabil. Med.* **2018**, *50*, 563–568. [CrossRef] [PubMed]
121. Legnani, G.; Incerti, G.; Lancini, M.; Azizpour, G. An identification procedure for evaluating the dynamic parameters of the upper limbs during handcycling. In Proceedings of the ASME Design Engineering Technical Conference, Quebec City, QU, Canada, 26–29 August 2018; Volume 5A. [CrossRef]
122. Morse, C.; Bostock, E.; Twiss, H.; Kapp, L.; Orme, P.; Jacques, M. The cardiorespiratory response and physiological determinants of the assisted 6-minute handbike cycle test in adult males with muscular dystrophy. *Muscle Nerve* **2018**, *58*, 427–433. [CrossRef] [PubMed]
123. Quittmann, O.; Meskemper, J.; Abel, T.; Albracht, K.; Foitschik, T.; Rojas-Vega, S.; Strüder, H. Kinematics and kinetics of handcycling propulsion at increasing workloads in able-bodied subjects. *Sport. Eng.* **2018**, *21*, 283–294. [CrossRef]
124. Cudicio, A.; Girardello, A.; Negro, F.; Orizio, C.; Arenghi, A.; Legnani, G.; Serpelloni, M. Topographical and physiological data collection for urban handbike tracks design. In Proceedings of the Pedestrians, Urban Spaces and Health—Proccedings of the 24th International Conference on Living and Walking in Cities, LWC 2019, Brescia, Italy, 12–13 September 2019; pp. 225–229.
125. Stangier, C.; Abel, T.; Zeller, S.; Quittmann, O.; Perret, C.; Strüder, H. Comparison of different blood lactate threshold concepts for constant load performance prediction in spinal cord injured handcyclists. *Front. Physiol.* **2019**, *10*, 1054. [CrossRef]
126. Stone, B.; Mason, B.; Bundon, A.; Goosey-Tolfrey, V. Elite handcycling: A qualitative analysis of recumbent handbike configuration for optimal sports performance. *Ergonomics* **2019**, *62*, 449–458. [CrossRef]
127. Stone, B.; Mason, B.; Warner, M.; Goosey-Tolfrey, V. Shoulder and thorax kinematics contribute to increased power output of competitive handcyclists. *Scand. J. Med. Sci. Sport.* **2019**, *29*, 843–853. [CrossRef]
128. Chaikhot, D.; Reed, K.; Petroongrad, W.; Athanasiou, F.; Van Kooten, D.; Hettinga, F. Effects of an Upper-Body Training Program Involving Resistance Exercise and High-Intensity Arm Cranking on Peak Handcycling Performance and Wheelchair Propulsion Efficiency in Able-Bodied Men. *J. Strength Cond. Res.* **2020**, *34*, 2267–2275. [CrossRef]
129. Himarosa, R.; Sunardi. Design, Frame Analysis and Manufacture of Handcycle Prototype. *J. Phys. Conf. Ser.* 2020, *1471*, 012058. [CrossRef]
130. Kouwijzer, I.; de Groot, S.; van Leeuwen, C.; Valent, L.; van Koppenhagen, C.; Grandjean Perrenod Comtesse, P.; Helmantel, E.; Dekker, M.; Zwinkels, M.; Metsaars, M.; et al. Changes in Quality of Life During Training for the HandbikeBattle and Associations With Cardiorespiratory Fitness. *Arch. Phys. Med. Rehabil.* **2020**, *101*, 1017–1024. [CrossRef]

131. Turoń-Skrzypińska, A.; Pawlukowska, W.; Szylińska, A.; Tomska, N.; Mikołajczyk-Kocięcka, A.; Ptak, M.; Dutkiewicz, G.; Rotter, I. Assessment of the relationship between selected factors and stress-coping strategies in handcyclists—A preliminary study. *Medicina* **2020**, *56*, 211. [CrossRef]
132. Nevin, J.; Smith, P. The Effectiveness of a 30-Week Concurrent Strength and Endurance Training Program in Preparation for an Ultra-Endurance Handcycling Challenge: A Case Study. *Int. J. Sport. Physiol. Perform.* **2021**, *16*, 1712–1718. [CrossRef] [PubMed]
133. Quittmann, O.; Abel, T.; Albracht, K.; Strüder, H. Reliability of muscular activation patterns and their alterations during incremental handcycling in able-bodied participants. *Sport. Biomech.* **2021**, *20*, 603–618. [CrossRef] [PubMed]
134. Stephenson, B.; Stone, B.; Mason, B.; Goosey-Tolfrey, V. Physiology of handcycling: A current sports perspective. *Scand. J. Med. Sci. Sport.* **2021**, *31*, 4–20. [CrossRef] [PubMed]
135. Abonie, U.; Albada, T.; Morrien, F.; Van Der Woude, L.; Hettinga, F. Effects of 7-week Resistance Training on Handcycle Performance in Able-bodied Males. *Int. J. Sport. Med.* **2022**, *43*, 46–54. [CrossRef] [PubMed]
136. Hutchinson, M.; Goosey-Tolfrey, V. Rethinking aerobic exercise intensity prescription in adults with spinal cord injury: Time to end the use of "moderate to vigorous" intensity? *Spinal Cord* **2022**, *60*, 484–490. [CrossRef] [PubMed]
137. Pasko, W.; Dydek, J.; Zielinski, J.; Hulewicz, T.; Sliz, M.; Dziadek, B.; Przednowek, K. Assessing Psychomotor Abilities in Handcyclists using Computerized Tests: An Initial Study. In Proceedings of the International Conference on Sport Sciences Research and Technology Support, icSPORTS—Proceedings, Valletta, Malta, 27–28 October 2022; Volume 2022, pp. 137–142.
138. Quittmann, O.; Abel, T.; Albracht, K.; Strüder, H. Biomechanics of all-out handcycling exercise: Kinetics, kinematics and muscular activity of a 15-s sprint test in able-bodied participants. *Sport. Biomech.* **2022**, *21*, 1200–1223. [CrossRef] [PubMed]
139. Soo Hoo, J.; Kim, H.; Fram, J.; Lin, Y.S.; Page, C.; Easthausen, I.; Jayabalan, P. Shoulder pain and ultrasound findings: A comparison study of wheelchair athletes, nonathletic wheelchair users, and nonwheelchair users. *PM R* **2022**, *14*, 551–560. [CrossRef]

Chapter 3

The Ideal Handcycling: Simulation and Analysis of the Task through an Artificial Upper Limb Mechanism (AULM)

3.1 Introduction

The literature review presented in Chapter 2 highlighted how most handcycling studies are still based on relatively small samples, heterogeneous experimental setups, and a limited control over measurement conditions. When data are collected directly on the road, the intrinsic variability of human execution and the unpredictable nature of the environment can easily mask the specific effect of design choices, such as sensor placement or frame configuration. As a consequence, it may be difficult to distinguish easily between differences that are genuinely due to the mechanical system and those that simply arise from fluctuations in the rider's performance or from changes in terrain. To address this issue, an intermediate step is required between purely theoretical modeling and fully outdoor tests. The idea is to reproduce the kinematics of handcycling in a controlled setting, where cadence, trajectory, and load can be imposed with high repeatability, while still preserving the essential features of the real task. In this context, bench simulators and artificial limb mechanisms represent a useful compromise: they allow studying the motion and the resulting signals under well-defined and repeatable conditions, without the noise introduced by fatigue, learning effects, or environmental disturbances.

The present chapter introduces an Artificial Upper Limb Mechanism (AULM) specifically designed to emulate the planar motion of the upper limb during handcycling. The AULM is driven by a motor according to prescribed crank trajectories and can host inertial sensors at different locations along the kinematic chain. By systematically comparing the signals acquired at these positions, it becomes possible to evaluate how sensor placement affects the stability of the measured acceleration profiles and, in turn, the reliability of the subsequent analysis.

The work pursues three main goals. First, to demonstrate that the bench-mounted AULM can reproduce a highly repeatable motion pattern over multiple cycles and conditions, so that it can be used as a reference tool for methodological studies. Second, to quantify how different candidate locations for inertial measurement units (IMUs) perform in terms of cycle-to-cycle variability, with particular attention to sites that are practically accessible in real handcycling. Third, to derive a set of recommendations for sensor placement that will guide the multi-IMU configuration adopted later in the outdoor study (Chapter 5).

In this perspective, the AULM represents the "ideal handcycling" scenario: the kinematics are prescribed and reproducible, thereby isolating sensor- and mounting-related effects from those linked to human variability. The findings of this chapter therefore play a key methodological role in the thesis, bridging the literature synthesis and modeling stages with the real-world application on a mixed-surface circuit.

3.2 Materials and Methods

3.2.1 Artificial Upper Limb Mechanism

The Artificial Upper Limb Mechanism (AULM) was conceived to replicate, in a simplified and controlled form, the main kinematic features of handcycling. The mechanism operates in a vertical plane and consists of a series of rigid segments connected by revolute joints, representing the shoulder, elbow, and wrist as shown in Figure 3.1. The distal link is rigidly connected to a handle that follows the trajectory imposed by a crank system, similar to that of a real handbike.

The geometry of the AULM was derived from anthropometric references and from typical handbike configurations documented in the literature, so that the range of motion and joint angles realistically approximate those of an adult rider. Link lengths and joint positions were selected to reproduce a closed kinematic chain between the handle and the simulated shoulder, while maintaining a structure that is robust and easy to instrument. The crank mechanism is driven by a motor unit with controllable angular velocity, allowing the benchmark cadence to be imposed under steady-state conditions. The AULM is mounted on a rigid support frame, which constrains the global motion and ensures that the only relevant degrees of freedom are those associated with the limb and crank system. This arrangement minimizes unwanted vibrations and structural deflections that could contaminate the signals, thereby emphasizing the contribution of the imposed kinematics and of the sensor placement.

Fig. 3.1: *The green circular arrow, denoted as $\theta(t)$, indicates the time-dependent rotational angle applied by the motor to the crank. The orange circular markers signify the location of the revolute joints representing shoulder, elbow, and wrist connecting arm and forearm.*

Kinematic constraints and degrees of freedom

To clarify the functional architecture of the AULM and the rationale behind IMU placement, the system can be interpreted in terms of constrained bodies and effective degrees of freedom (DoF). The supporting frame is assumed rigid with respect to the handcycle chassis, so that relative motion between frame and chassis is negligible within the investigated operating conditions. The motor imposes an approximately periodic rotation of the crank, which represents the dominant kinematic excitation for all mounted sensors.

In this representation, the effective DoF relevant to the present analysis can be summarized as follows:

- **Frame:** fully constrained reference body.
- **Crank:** one rotational DoF about its axis, driven by the motor ($\theta(t)$ in Fig. 3.1).
- **Handle:** rigidly connected to the crank.
- **Arm/forearm links:** connected by revolute joints (shoulder, elbow, wrist) and constrained by the closed kinematic chain; their motion is primarily dictated by the crank-driven handle trajectory.

Accordingly, IMUs mounted closer to the rigid drivetrain (e.g., crank/handle) are expected to provide more repeatable, phase-consistent acceleration profiles, whereas sensors placed on segments farther from the actuation point may be more sensitive to small mounting perturbations and local dynamics.

3.2.2 Instrumentation and Sensor Positions

To record the motion produced by the AULM, a commercial inertial measurement unit (IMU) was used, providing tri-axial acceleration, angular velocity, and orientation estimates at a fixed sampling rate. The sensor was housed in a small enclosure and could be mounted on different segments of the mechanism through dedicated clamps, designed to ensure firm contact and repeatable alignment across trials.

A set of candidate positions was defined to explore the effect of sensor placement along the kinematic chain. These locations were chosen to mimic sites that are practically accessible in real handcycling, such as near the handle, along the forearm, and in proximity to the elbow region (Figure 3.2). For each position, the local coordinate system of the IMU was aligned as consistently as possible with the corresponding segment axes, although small alignment errors were considered unavoidable and representative of realistic mounting conditions.

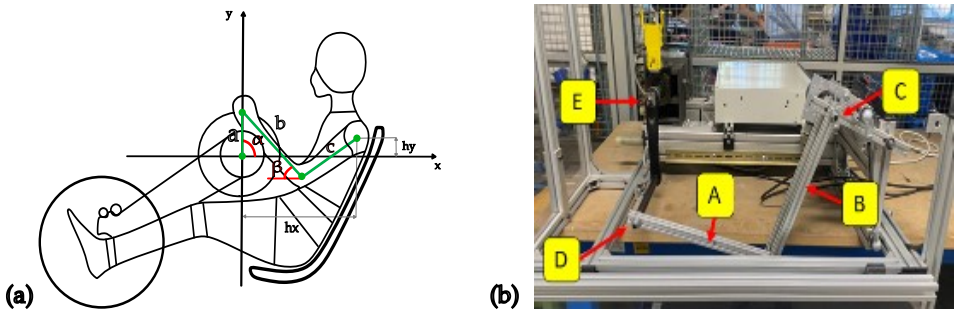

(**a**) *From the left: (a) kinematic planar model of the human upper arm during handcycling, and (b) positions A, B, C, D and E of the IMU system for the acquisitions in the experimental setup. Reproduced from [12] with permission from Springer Nature.*

(**b**) *Detail of sensors placement.*

Fig. 3.2

In addition to the IMU, a video camera was used to record each acquisition from a fixed viewpoint. The video footage was not processed quantitatively in this study, but served two complementary purposes: first, to verify that the mechanism operated as expected during all trials, and second, to provide a visual reference for interpreting the motion patterns and for documenting the experimental setup.

3.2.3 Experimental Protocol

The experimental protocol consisted of a series of acquisitions in which the motor drove the crank–handle system at a predefined angular velocity of 60 rpm for 60 s. For each sensor location, a block of nine consecutive cycles was recorded, preceded and followed by short transitional phases to ensure that the mechanism reached a stable regime before data were analyzed. Acceleration data were acquired at a constant sampling rate of 10 Hz.[1]

The order of the sensor positions was arranged so as to reduce any systematic influence of motor warm-up or minor mechanical drifts.

During each acquisition, the IMU logged acceleration and angular velocity samples, while the motor controller maintained the target crank velocity. The video camera was activated concurrently to capture the overall motion. All relevant metadata (sensor position, cadence, acquisition code) were annotated in a log file to allow consistent organization and post-processing of the dataset.

3.2.4 Data Processing

Data processing was performed in the MATLAB environment (The MathWorks Inc., Natick, MA, USA). Raw IMU streams were first imported and visually inspected to check for missing samples, saturation, or obvious artefacts. When necessary, leading and trailing segments corresponding to start-up and shut-down phases were trimmed, so that only steady-state cycles were retained for analysis.

The benchmark trial was performed at a constant cadence of 60 rpm for 60 s. Given the low acquisition frequency 10 Hz, the processing pipeline focused on robust time-domain synchronization and cycle segmentation rather than on high-frequency spectral characterization. First, the acceleration magnitude was computed from tri-axial accelerometer signals. Then, to improve peak localization during synchronization, signals were resampled from 10 Hz to 100 Hz using cubic-spline interpolation. Peaks were detected on the resampled acceleration-magnitude traces, and the relative shift among acquisitions was estimated from the first detected peak. The resulting time shift was then mapped back to the original sampling grid and applied to the original signals. Finally, cycles were segmented between consecutive peaks and phase-normalized for averaging and variability analysis. Resampling was used exclusively to improve peak localization and does not increase the physical bandwidth of the original acquisition.

3.2.5 Outcome Metrics and Statistical Analysis

To quantify the effect of sensor placement on signal stability, several complementary metrics were computed. At the single-cycle level, descriptive statistics such as mean, standard deviation, and peak values of the acceleration magnitude were calculated over

[1]The IMU family supports higher output rates (up to 200 Hz), while the default retrieval rate is 10 Hz; the rate used in this study refers to the configured output rate, not to the hardware limit.

each revolution. Across cycles, variability was summarized by coefficients of variation and by cycle-to-cycle dispersion of the phase-normalized profiles.

In addition, for each sensor position, an average cycle was obtained by aligning and averaging all phase-normalized traces. The residuals between individual cycles and this average shape were then used to compute cycle-wise error metrics with respect to the mean profile, namely the mean error and the maximum error. Lower error values correspond to more repeatable profiles and, by implication, to sensor positions that are more robust to small mounting perturbations or minor mechanical imperfections.

Finally, simple comparisons between positions were performed by ranking the candidate sites according to their variability metrics. This exploratory analysis was not intended to support formal hypothesis testing, but rather to identify trends and to highlight which locations merit priority when designing multi-IMU configurations for field studies.

3.3 Results

3.3.1 Repeatability of the AULM Motion

Across all acquisitions, the AULM produced highly regular motion patterns. The crank angular velocity quickly converged to the target value of 60 rpm after the onset of each trial and remained stable within narrow bounds for the duration of the recording. Visual inspection of the acceleration and angular velocity traces confirmed the absence of abrupt transients or drifts during the steady-state portions of the signal.

At the level of individual cycles, the phase-normalized acceleration magnitude exhibited smooth waveforms with well-defined peaks and troughs, reflecting the deterministic nature of the imposed kinematics. When cycles from the same condition and sensor position were overlaid, the envelopes were generally tight, indicating small cycle-to-cycle deviations. These observations support the use of the AULM as a reference platform for assessing sensor-related variability, in line with the methodological objectives of the study.

3.3.2 Impact of interpolation on synchronization quality

Figure 3.3 reports the mean phase-normalized cycle for each configuration, together with confidence bounds expressed as ±SD, obtained after the synchronization process applied to both original and interpolated signals. A consistent trend emerges from the comparison: the low acquisition frequency of the original data limits the temporal precision of peak localization, which propagates into suboptimal cycle alignment and inflated dispersion around the mean profile.

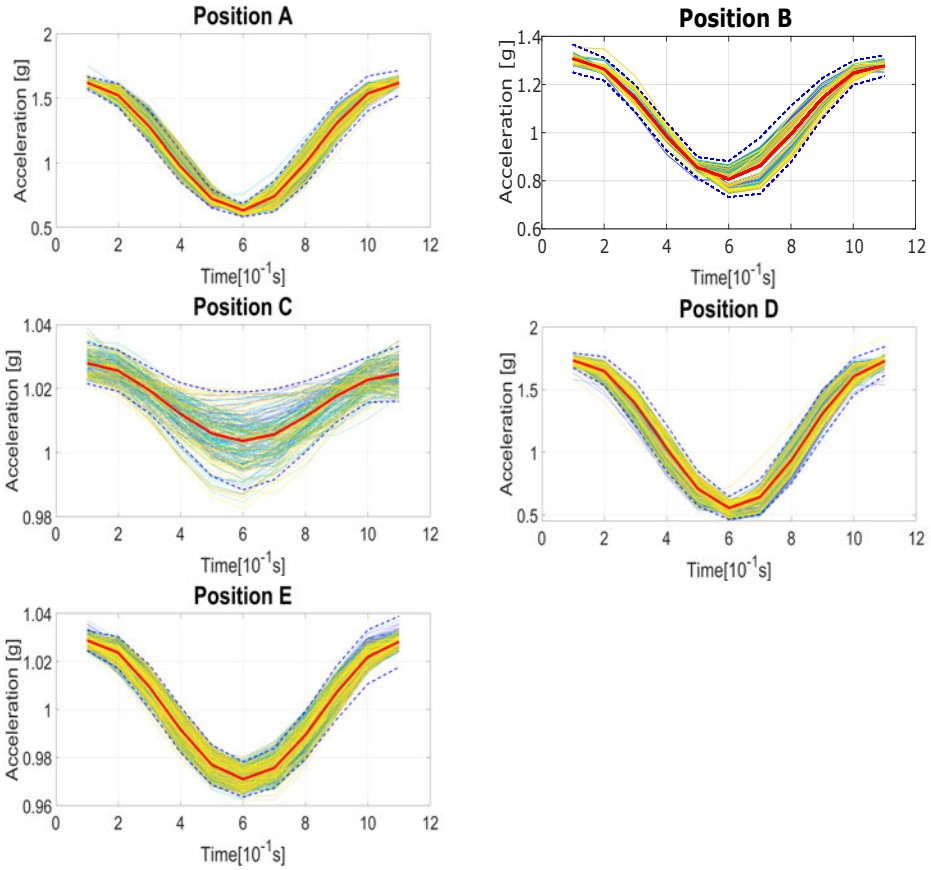

Fig. 3.3: *Acceleration profiles for each configuration. The individual cycles are depicted by a solid yellow line, the mean profile by a solid red line, and the ±1 SD boundaries by dashed blue lines. Reproduced from [12] with permission from Springer Nature.*

By contrast, the interpolated signals enable the identification of peak indices closer to the expected true maxima, producing a more accurate synchronization. This improvement is reflected by systematically narrower SD bounds in the phase-normalized profiles. The effect is particularly evident for configurations that exhibit sharper peaks, where sampling quantization in the original data can shift the detected maximum by one or more samples, thereby widening the cycle envelope after alignment.

Overall, these results indicate that the temporal resolution of the acquisition is a non-negligible contributor to apparent cycle-to-cycle variability. While interpolation mitigates this limitation, the observed differences support the practical recommendation that the acquisition frequency should be increased when the goal is to capture and align fast dynamics with higher fidelity, especially for the most sensitive configurations.

3.3.3 Effect of Sensor Position on Signal Variability

Although the overall motion was highly repeatable, clear differences emerged between the candidate sensor locations. Positions located on rigid elements directly driven by the crank mechanism, such as near the handle or on distal mechanical links, tended to exhibit the lowest variability. Their phase-normalized acceleration profiles closely overlapped

across cycles, indicating that the local motion was strongly constrained by the mechanism geometry.

By contrast, positions intended to emulate anatomical mounting sites, such as those in the vicinity of the elbow or along surrogate forearm segments, showed larger dispersion. In these locations, the combination of local flexibilities, small misalignment at mounting, and the distance from the primary actuation point made the measured acceleration more sensitive to minor differences in how the sensor was placed or tightened. Cycle envelopes were therefore wider, and variability metrics higher.

A functional interpretation can be drawn by comparing positions that represent analogous biomechanical roles. Positions E and C, for example, correspond to joints that are expected to remain stable during the artificial handcycling motion. This assumption is expected to remain reasonable for position E also in human arm-handcycling, whereas it may or may not be verified for position C, which models the rotation center of the pilots shoulder along the movement in the sagittal plane. Positions A and B, instead, represent sensors mounted on rigid segments (forearm and arm, respectively), placed as close as possible to their center of gravity. Finally, position D can be interpreted as an IMU located on the rotation joint of the handle, or equivalently on the pilots hand.

Across these functional groups, positions C and E exhibited the lowest numerical variability, with narrower dispersion and lower error metrics in both the original and interpolated analyses. Positions A and D, however, remained of particular methodological interest because they correspond to mechanically meaningful and practically transferable mounting sites for real handcycling applications. While position A remained among the most relevant practical candidates overall, it also showed occasional outliers, particularly in the interpolated analysis, suggesting that this placement may be more sensitive to small mounting perturbations or to local dynamics that are averaged out in other configurations. Importantly, the ranking of sensor positions remained qualitatively consistent between original and interpolated processing: locations that performed well under one processing approach also tended to remain among the most repeatable under the other.

3.3.4 Quantitative summary of sensor variability

The comparative analysis of variability metrics, including SD dispersion and cycle-wise mean/maximum error distributions (Fig. 3.4), revealed distinct differences across the tested locations. From a purely numerical standpoint, positions C and E showed the lowest cycle-to-cycle dispersion for the benchmark cadence (60 rpm), in both original and interpolated analyses. Positions A and D, while not minimizing all variability metrics, remained of specific methodological interest because they correspond to mechanically meaningful and practically transferable mounting sites for subsequent field studies.

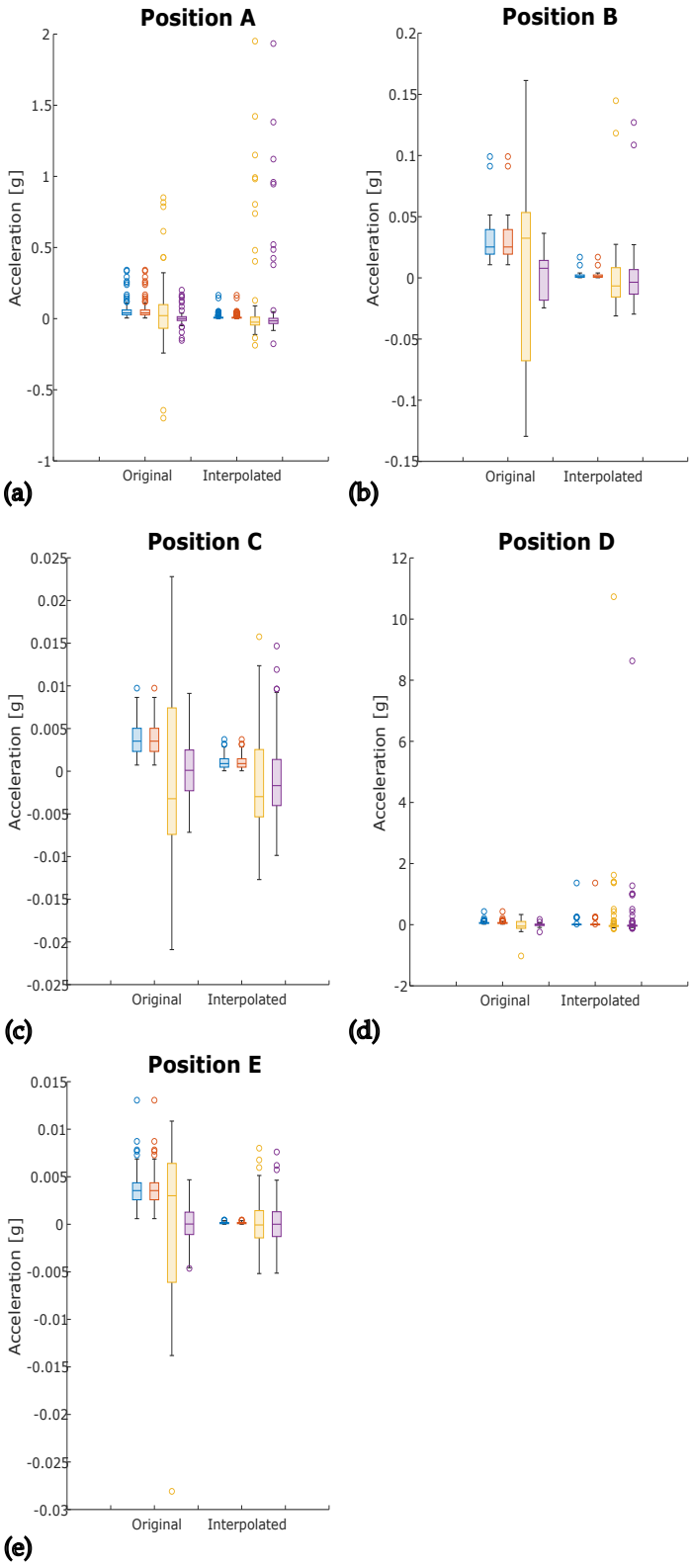

Fig. 3.4: *Comparison between original and interpolated signals. The mean and maximum standard deviation (SD) are shown in blue and red, respectively. The maximum and mean errors are plotted in yellow and purple. Reproduced from [12] with permission from Springer Nature.*

Tab. 3.1: *Repeatability metrics for each IMU location at 60 rpm, comparing original (10 Hz) and interpolated (100 Hz) processing. Values are reported as mean ± SD for the cycle-wise distributions.*

Pos.	Mean SD Orig. (m/s^2)	Mean SD Interp. (m/s^2)	Mean error Orig. (m/s^2)	Mean error Interp. (m/s^2)	Max error Orig. (m/s^2)	Max error Interp. (m/s^2)
A	0.04854 ± 0.03846	0.008525 ± 0.01164	0 ± 0.02802	0.0004446 ± 0.1443	0.01792 ± 0.1249	-0.002563 ± 0.1546
B	0.02994 ± 0.01566	0.001737 ± 0.00235	0 ± 0.01708	-0.0007275 ± 0.02363	0.002119 ± 0.06606	-0.001114 ± 0.02658
C	0.003936 ± 0.0024	0.001028 ± 0.000698	0 ± 0.003144	-0.001099 ± 0.003997	-0.0004081 ± 0.009635	-0.001767 ± 0.005144
D	0.07169 ± 0.1707	0.01096 ± 0.06955	0 ± 0.07897	0.000215 ± 0.4343	0.02761 ± 0.5511	0.001508 ± 0.542
E	0.003682 ± 0.001986	$0.0001305 \pm 8.742\times10^{-5}$	0 ± 0.002066	0 ± 0.001895	-0.000368 ± 0.008173	$-2.524\times10^{-6} \pm 0.002039$

Positions that mimicked more proximal anatomical placements, while still informative, showed greater dispersion and may require more careful installation procedures or additional averaging to reach comparable repeatability. These findings underscore the importance of using bench-based validation when designing sensor layouts for real-world studies, where individual differences and environmental factors will further challenge signal consistency.

Taken together, the results distinguish between numerical repeatability on the AULM and practical relevance for field deployment. While positions C and E provided the lowest variability under controlled bench conditions, positions D and A remain the most promising candidates for IMU placement when biomechanical relevance and transferability to real handcycling are also taken into account. The comparatively high dispersion in maximum error observed for position B will be investigated in future analyses to determine whether it reflects genuine sensitivity of that location or arises from instrumentation and mounting procedures.

Limitations. The AULM reproduces handcycling kinematics in a planar setting, whereas the real upper-limb motion is inherently three-dimensional, with out-of-plane components especially at the shoulder and wrist. Moreover, on the mechanism the IMU is rigidly fixed to a mechanical link, while on the human arm the sensor is coupled through deformable soft tissue. This compliant interface can introduce relative micro-motions between bone and sensor and additional vibration components. For these reasons, the results of this chapter should be interpreted as methodological indications on the relative robustness of candidate sensor sites, rather than as definitive predictions of in-vivo measurements.

3.4 Conclusions

This chapter presented the analysis of an Artificial Upper Limb Mechanism (AULM) applied as a bench-based tool to study handcycling kinematics and to validate candidate positions for inertial sensors. The mechanism reproduced a highly repeatable motion pattern, making it possible to isolate the effect of sensor placement on signal stability.

The analysis showed that the lowest numerical variability was observed at the most stable mechanical nodes, whereas positions emulating more proximal anatomical sites displayed higher variability. At the same time, the application-oriented selection of candidate sites for field studies should also account for biomechanical meaning and transferability of the mounting location, not numerical repeatability alone. These findings support the idea

that sensor layouts for field studies should be informed by prior repeatability benchmarks, rather than being chosen solely on the basis of convenience or intuition.

Methodologically, the AULM study establishes a robust foundation for the subsequent chapters of the thesis. Building on the validated sensor configurations identified here, the next step is to interpret how mechanical vibrations propagate through the handbikerider system. Chapter 4 therefore introduces a simplified vibrational model that links structural parameters to comfort and dynamic stability, forming the analytical core of the work before the transition to outdoor experimentation on a mixed-surface circuit in Chapter 5.

Chapter 4

Vibrational Model of Handbike and Handcyclist

4.1 Introduction

The experimental and methodological steps described in Chapters 2 and 3 emphasized two complementary needs in handcycling research. On the one hand, a systematic overview of existing devices and measurement approaches showed that many studies still focus on small samples, controlled ergometers, or descriptive field observations, often without an explicit representation of how mechanical vibrations propagate from the road to the rider. On the other hand, the bench-based validation performed with the Artificial Upper Limb Mechanism (AULM) demonstrated that, even when kinematics is perfectly repeatable, sensor placement and signal processing critically influence the stability of inertial measurements.

To transition from description to understanding, a compact analytical representation of the handbike-rider system is essential. While full multi-body simulations can capture detailed joint kinematics and contact interactions, they demand extensive modeling effort and parameter identification; moreover, this level of complexity is not strictly necessary for the questions addressed in this thesis. Instead, a lumped-parameter approach, in which the system is approximated by a small number of rigid bodies connected by springs and dampers, effectively captures the dominant vibrational transmission pathways while remaining transparent and tractable.

In this chapter, a simplified vibrational model of the handbike and rider ensemble is introduced and analyzed. The model is intentionally minimalistic: rather than attempting to describe every anatomical detail, it concentrates on the main interfaces through which vibrations are introduced, transmitted, and perceived. External perturbations from the road enter primarily at the wheels; the frame and the seat transmit these inputs to the rider; and the trunk and upper limbs respond according to posture and contact conditions. By relating these elements through a limited number of degrees of freedom, the model provides a conceptual map linking structural parameters, posture, and measured accelerations.

The specific objectives of this chapter are threefold. First, to formulate a three-

degree-of-freedom (3-DoF) linear model that represents the handbike frame dynamics and the rider response through a compact set of coordinates. Second, to extract from preliminary outdoor measurements a realistic range of dominant vibration frequencies and cycle-based descriptors, to support a plausibility check and nominal parameterization of the model (without formal identification). Third, to provide the methodological basis for the frequency-domain interpretation discussed in Chapter 6.3.

4.2 Model Description

4.2.1 System Representation and Degrees of Freedom

The handbike vibrational model can be described as a mechanical system made up of multiple rigid bodies coupled through elastic elements. It was introduced to analyze how vibrations generated by the road surface propagate through the structure and reach the rider, a key aspect when addressing comfort and performance in handbike design. Building on earlier contributions by Gunston et al. [17], who proposed simplified 2 DOF seat models including backrest and suspension systems, the present formulation adopts a comparable strategy. In particular, a main rigid body is used to represent the handbike frame, which is connected to the ground by two spring–damper pairs, indicated as k_1, c_1 and k_2, c_2. These elements model the front and rear wheel contact points, respectively, and account for the dynamic response of the system to road-induced excitations. A further rigid body is placed above the frame to approximate the riders body. This body is coupled to the handbike frame through a spring, denoted as k_s, which represents the seat compliance. In this way, the interaction between rider and handbike is captured, since the seat element attenuates part of the vibrations transmitted through the frame. The parameters a and b define the distances of the front and rear wheels, respectively, from the handbike center of gravity. These geometric quantities are required to assess stability and handling during operation. Moreover, h denotes the offset between the riders body and the handbike center of gravity.

- $y_1(t)$: vertical displacement at the front wheel contact point (road input);
- $y_2(t)$: vertical displacement at the rear wheel contact point (road input);
- x: vertical displacement of the riders upper body, lumped at the seat–trunk interface;
- x_G: vertical displacement of the handbike center of mass;
- ϑ: pitch rotation of the handbike about its center of mass.

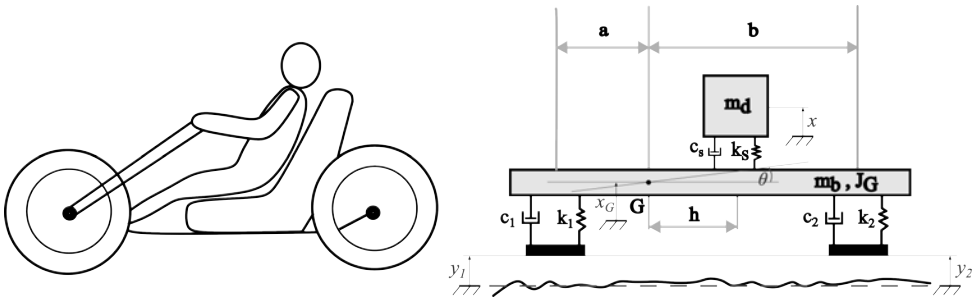

Fig. 4.1: *The system is represented as a 3-DOF model comprising the handbike chassis and the operator's body. The contact dynamics are governed by the front and rear tyre stiffnesses, k_1 and k_2, while the interface between the rider and the vehicle is defined by the seat stiffness k_s. The inertial properties include the drivers mass m_d, the handbike mass m_b, and its moment of inertia J_G. Correspondingly, the damping coefficients c_1, c_2, and c_s account for the energy dissipation within the tyres and the seat. Reproduced from [16] with permission from Springer Nature.*

Within this formulation, the selected coordinates are associated with equivalent masses m_b and m_d, as well as with effective stiffnesses k_1, k_2 and k_s and damping coefficients c_1, c_2 and c_s. These parameters capture the aggregated elastic and dissipative properties of the tyres, frame, seat, and soft tissues. The selection of a 3-DoF structure balances realism with simplicity. This configuration enables a clear distinction between: (i) the input entry points at the wheel contact patches; (ii) the mechanical transmission through the frame and rear supports (including the seat and backrest); and (iii) the response of the rider's trunk, which aligns with the location of the IMU sensors used in the outdoor experiments. While additional degrees of freedom could be introduced for greater detail (such as separating the backrest from the seat or including head motion), they would not necessarily enhance interpretability regarding the specific questions addressed here.

4.2.2 Equations of Motion

To investigate the 3DOF model in Figure. 4.1, the generalized coordinates x_G, ϑ and x are selected. The corresponding Lagrange equations are given in Eq. (4.1):

$$\begin{cases} \dfrac{d}{dt}\dfrac{\partial T}{\partial \dot{x}_G} - \dfrac{\partial T}{\partial x_G} + \dfrac{\partial R}{\partial \dot{x}_G} + \dfrac{\partial V}{\partial x_G} = 0 \\ \dfrac{d}{dt}\dfrac{\partial T}{\partial \dot{\vartheta}} - \dfrac{\partial T}{\partial \vartheta} + \dfrac{\partial R}{\partial \dot{\vartheta}} + \dfrac{\partial V}{\partial \vartheta} = 0 \\ \dfrac{d}{dt}\dfrac{\partial T}{\partial \dot{x}} - \dfrac{\partial T}{\partial x} + \dfrac{\partial R}{\partial \dot{x}} + \dfrac{\partial V}{\partial x} = 0 \end{cases} \tag{4.1}$$

The kinetic energy T, the elastic potential energy V and the Rayleighs dissipation function R assume the expressions in Eqs. (4.2), (4.3) and (4.4):

$$T = \frac{1}{2}\left(m_b \dot{x}_G^2 + J_G \dot{\vartheta}^2 + m_d \dot{x}^2\right) \tag{4.2}$$

$$V = \frac{1}{2}\Big[k_1(x_G - a\vartheta - y_1)^2 + k_2(x_G + b\vartheta - y_2)^2 + k_s(x - x_G - h\vartheta)^2\Big] \tag{4.3}$$

$$R = \frac{1}{2}\Big[c_1(\dot{x}_G - a\dot{\vartheta} - \dot{y}_1)^2 + c_2(\dot{x}_G + b\dot{\vartheta} - \dot{y}_2)^2 + c_s(\dot{x} - \dot{x}_G - h\dot{\vartheta})^2\Big] \tag{4.4}$$

By inserting these expressions into the Lagrange equations and adopting a matrix formulation, the equations of motion of the system can be derived as:

$$\mathbf{M}\ddot{\mathbf{x}} + \mathbf{C}\dot{\mathbf{x}} + \mathbf{K}\mathbf{x} = \mathbf{F} \tag{4.5}$$

in which the matrices $\mathbf{M}$, $\mathbf{C}$ and $\mathbf{K}$, as well as the vectors $\mathbf{x}$ and $\mathbf{F}$ are defined as:

$$\mathbf{M} = \begin{bmatrix} m_b & 0 & 0 \\ 0 & J_G & 0 \\ 0 & 0 & m_d \end{bmatrix} \quad \mathbf{C} = \begin{bmatrix} (c_1 + c_2 + c_s) & (-c_1a + c_2b + c_sh) & -c_s \\ (-c_1a + c_2b + c_sh) & (c_1a^2 + c_2b^2 + c_sh^2) & -c_sh \\ -c_s & -c_sh & c_s \end{bmatrix}, \tag{4.6}$$

$$\mathbf{K} = \begin{bmatrix} (k_1 + k_2 + k_s) & (-k_1a + k_2b + k_sh) & -k_s \\ (-k_1a + k_2b + k_sh) & (k_1a^2 + k_2b^2 + k_sh^2) & -k_sh \\ -k_s & -k_sh & k_s \end{bmatrix} \tag{4.7}$$

$$\mathbf{x} = \begin{Bmatrix} x_G \\ \vartheta \\ x \end{Bmatrix} \quad \mathbf{F} = \begin{Bmatrix} k_1 y_1(t) + k_2 y_2(t) \\ -k_1 a\, y_1(t) + k_2 b\, y_2(t) \\ 0 \end{Bmatrix} \tag{4.8}$$

This relationship can be reformulated by explicitly isolating the acceleration vector, yielding:

$$\ddot{\mathbf{x}} = \mathbf{M}^{-1}(\mathbf{F} - \mathbf{C}\dot{\mathbf{x}} - \mathbf{K}\mathbf{x}) \tag{4.9}$$

or, in its alternative version, as the three functions defined in:

$$\begin{cases} \ddot{x}_G = F_1(x_G, \vartheta, x, \dot{x}_G, \dot{\vartheta}, \dot{x}, t) \\ \ddot{\vartheta} = F_2(x_G, \vartheta, x, \dot{x}_G, \dot{\vartheta}, \dot{x}, t) \\ \ddot{x} = F_3(x_G, \vartheta, x, \dot{x}_G, \dot{\vartheta}, \dot{x}, t) \end{cases} \tag{4.10}$$

Introducing now the auxiliary functions:

$$u_1 = x_G, \quad u_2 = \vartheta, \quad u_3 = x, \quad u_4 = \dot{x}_G, \quad u_5 = \dot{\vartheta}, \quad u_6 = \dot{x} \tag{4.11}$$

the system of first-order differential equations assumes the final form:

$$\begin{cases} \dot{u}_1 = u_4 \\ \dot{u}_2 = u_5 \\ \dot{u}_3 = u_6 \\ \dot{u}_4 = F_1(u_1, u_2, u_3, u_4, u_5, u_6, t) \\ \dot{u}_5 = F_2(u_1, u_2, u_3, u_4, u_5, u_6, t) \\ \dot{u}_6 = F_3(u_1, u_2, u_3, u_4, u_5, u_6, t) \end{cases} \tag{4.12}$$

These differential equations can be efficiently integrated in the time domain using numerical methods with either fixed or adaptive time stepping.

4.2.3 Natural Frequencies and Mode Shapes

Solving the undamped eigenvalue problem associated with Eq. (4.5) (setting $\mathbf{C} = \mathbf{0}$) provides the natural frequencies and mode shapes of the coupled system. These modes represent fundamental patterns of motion in which masses oscillate in phase or out of phase with each other.

Typically, for realistic parameter values, the lowest-frequency mode is dominated by a rocking motion of the entire system, with the trunk and seat moving almost rigidly with the frame, while the wheel exhibits limited relative displacement. Intermediate modes may emphasize frame bending relative to the front wheel, whereas higher modes involve more pronounced relative motion of the trunk with respect to the seat–frame assembly.

These modal properties are useful for interpreting experimental observations. For instance, if significant spectral peaks are observed in accelerometer data at frequencies close to those of a particular mode, it suggests that the corresponding motion pattern is being excited by the road or by propulsion inputs. In the context of handcycling, this is particularly relevant for distinguishing low-frequency components associated with cadence and steering oscillations from higher-frequency content linked to road roughness and frame dynamics.

4.3 Preliminary Outdoor Measurements

4.3.1 Experimental Setup

To obtain realistic input signals and validate the model against a physical system, preliminary outdoor measurements were conducted on a commercial recumbent handbike (Race-X, Maddiline Cycle Snc, Verona, Italy) represented in Figure 4.2. The tests were performed in the parking area of the Medical Faculty at the University of Brescia, selected for its relatively flat asphalt surface and gentle curves, which provided a simple yet valid track (Figure 4.3).

Fig. 4.2: *a) The Race-X handbike employed in the experimental tests; b) IMU sensor mounted on the handbike handlebar. Reproduced from [16] with permission from Springer Nature.*

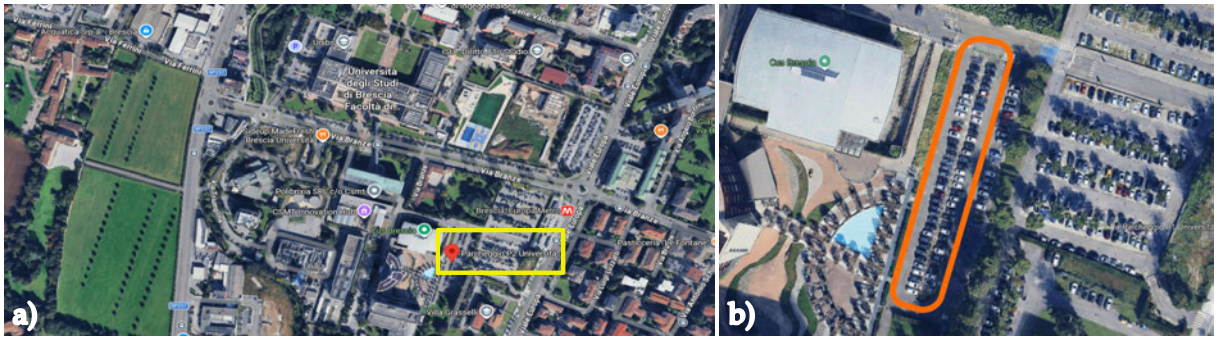

Fig. 4.3: *a) Parking area at the University of Brescia; b) Detailed view of the circuit.*

An inertial measurement unit (IMU), consistent with the hardware used in Chapter 5, was positioned at key locations. A total of eight trials were performed, each consisting of two laps around a closed circuit, and the trials were divided among three adults: the first two were performed by a male right-handed participant, the next two by a female right-handed subject, and the remaining four by a male left-handed young adult. The setup focused on two primary sites: (i) the handlebar region, serving as a distal control node for torque application and steering; and (ii) the rider's forearm, representing the proximal site where vibrations are perceived. For the first six trials, the sensor was mounted on the pilots left forearm, in a medial position, to capture the biomechanical response and vibration transmission through the participants body. In the final two trials, sensor was mounted on the handbike itself to characterize how signals are modulated at the steering interface, with placement on the left handlebar for one trial and on the right handlebar for the other.

During each trial, the rider completed two laps at self-selected, comparable speeds. The rider was instructed to maintain a steady pace on straight segments and to negotiate curves naturally. Although the protocol involved multiple trials with different participants, only the most continuous and artifact-free datasets were retained for the analysis presented in this chapter.

4.3.2 Data Acquisition and Signal Processing

Acceleration data were acquired at a constant sampling rate and transmitted wirelessly to a portable receiver, which was either worn by the rider or mounted on the frame.

The signal processing pipeline followed the methodology established in the field study of Chapter 5. Within the eight recorded trials, trials 6 and 8 were retained for the preliminary analysis because they provided the most continuous and reliable traces. Of these, trial 8 was considered the most informative, as it refers to the left handgrip acquisition and was performed by the left-handed participant, thus representing the most pertinent input at the steering interface. Initially, raw acceleration signals were inspected to remove artifacts, and intervals exhibiting signal loss or saturation were discarded. A Fourier-based inspection of the unfiltered signal was used to highlight the dominant frequency content, showing marked components close to 1 Hz, which can reasonably be associated with the cyclic motion of the handgrip. To enable a stable identification of these periodic events, a fourth-order zero-phase Butterworth low-pass filter with a 1 Hz cut-off was applied to the selected intervals. Peaks were subsequently detected as local maxima on the filtered waveform; their indices were then projected onto the original signal and used to partition the trace into individual cycles, each defined between two successive peaks. After segmentation, the extracted cycles were time-aligned to enforce temporal consistency across repetitions. Finally, the mean profile and its standard deviation (SD) were computed over the synchronized ensemble of cycles and adopted as compact descriptors for the subsequent analysis.

4.4 Model–Data Comparison

4.4.1 Model Parameterization

The preliminary outdoor measurements were not used to perform a formal parameter identification of the handbike–rider model. Instead, they served as a plausibility check to ensure that the simplified 3-DoF system exhibits response features in a frequency range consistent with the measured signals.

Accordingly, the model parameters were assigned on a nominal basis. Tyre-related properties (k_1, c_1, k_2, c_2) were set within typical ranges reported in the vibration and vehicle-dynamics literature and based on reasonable assumptions for the tested configuration. The seat–rider coupling (k_s, c_s) was then chosen to represent a realistic compliance at the interface, without applying an optimization procedure or a best-fit calibration to the experimental data. Under this approach, model simulations are intended to support qualitative interpretation rather than to provide identified physical parameters.

4.5 Results

4.5.1 Dominant frequency content

For the selected reference case (trial 8, left handgrip), the Fourier analysis of the original acceleration signal showed a dominant component around 1 Hz (Fig. 4.4), consistent with a periodic pattern in the handgrip action.

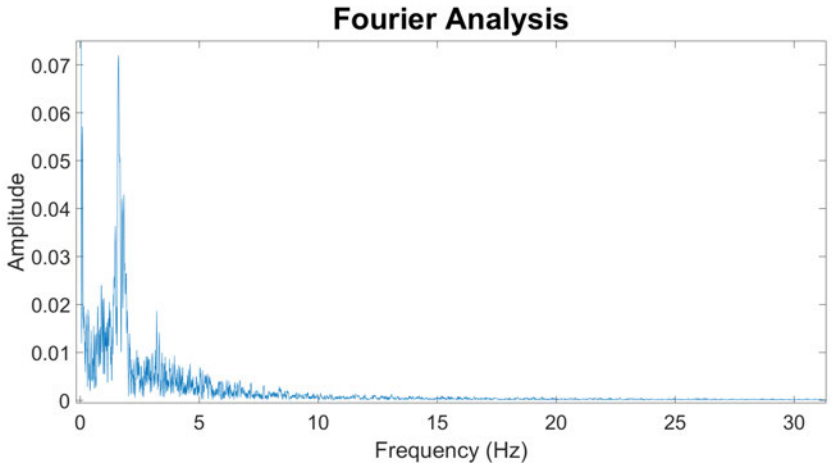

Fig. 4.4: *Fourier Analysis of acceleration on the left handlebar. Reproduced from [16] with permission from Springer Nature.*

4.5.2 Cycle-based acceleration descriptors

Using the cycle segmentation and synchronization procedure described in Section 4.3.2, the handlebar acceleration cycles were summarized through their mean profile and standard deviation (SD), as shown in Fig. 4.5.

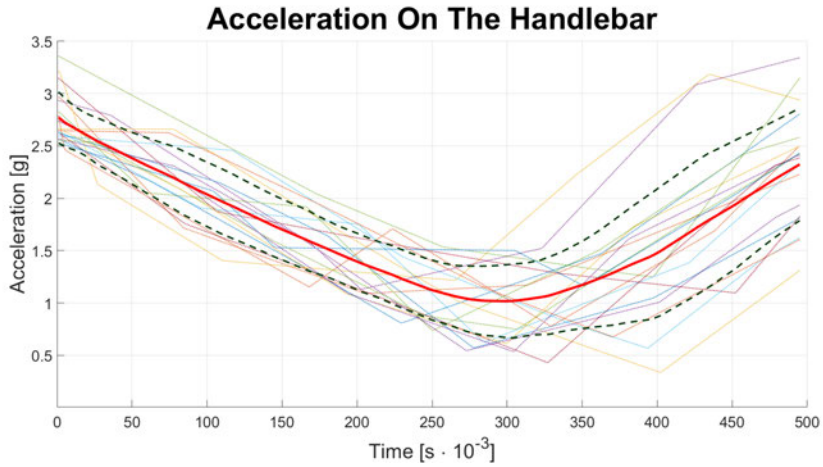

Fig. 4.5: *Total handlebar acceleration. The solid red line indicates the mean value, while the dashed dark green lines represent the standard deviation (SD) thresholds. Individual cycles recorded during acquisition are shown as thin colored lines. Reproduced from [16] with permission from Springer Nature.*

Tab. 4.1: *Summary of the main descriptors extracted from the handlebar acceleration signal (trial 8, left handgrip). Values are expressed in units of gravitational acceleration g.*

Descriptor	**Value**	**Notes**
Dominant frequency (FFT peak)	≈ 1 Hz	Peak from Fourier analysis of the raw signal.
Total acceleration range (min–max)	1.01–2.76 g	From cycle ensemble (synchronized cycles).
Cycle SD range (min–max)	0.20–0.64 g	Standard deviation computed across synchronized cycles.
Mean cycle SD	0.37 g	Average standard deviation over the cycle ensemble.

For the selected handlebar trial, the cycle analysis showed that the total acceleration ranged approximately from 1.01 g to 2.76 g, where g denotes the gravitational constant. Cycle-to-cycle variability, quantified by the SD of the synchronized ensemble, ranged from about 0.20 g to 0.64 g, with an average value close to 0.37 g. Data are summarized in Table 4.1.

4.6 Conclusions

This chapter has introduced a compact vibrational model of the handbike and rider system, based on three degrees of freedom and lumped mass, spring, and damper elements linking the wheel, the frame and seat, and the rider's trunk. The model is deliberately simple, yet sufficiently expressive to illuminate the main pathways through which road-induced vibrations are transmitted to the rider.

Preliminary outdoor measurements provided realistic acceleration traces and enabled the extraction of reference descriptors (dominant low-frequency content and cycle-based statistics) to support a plausibility check of the model response. Under nominal parameterization (without formal identification), the model offers a compact framework to relate wheel inputs, frame dynamics, and rider response, and to guide the interpretation discussed in Chapter 6.

Methodologically, the vibrational model complements the AULM-based validation and lays the groundwork for the field study presented in Chapter 5, where a distributed network of wearable IMUs is utilized to quantify segment-specific vibrations and stability during two laps (one per participant) on a mixed-surface circuit. Together, these elements form an integrated framework in which literature synthesis, controlled experiments, and analytical modeling jointly inform the interpretation of handcycling dynamics under real-world conditions.

Chapter 5

Handcycling in the Real Context: Experimental Evaluation on the Field

5.1 Introduction

Building upon the biomechanical and methodological background presented in Chapter 2, and following the sensor-validation and modeling phases developed in Chapters 3 and 4, this chapter applies the complete framework to *real-world handcycling*. The aim is to quantify how vibrations and stability vary between two outdoor laps (one per participant) on a mixed-surface circuit, using a distributed network of eight Inertial Measurement Units (IMUs) placed on both anatomical and mechanical sites of the handbike.

Previous literature on propulsion efficiency, posture, and vibration transmissionreviewed in Chapter 2has shown that smoother propulsion patterns are associated with reduced variability, lower high-frequency content, and improved comfort. Here, these principles are tested in real world conditions, linking quantitative IMU-based descriptors to rider performance and surface roughness.

Specifically, two complementary analytical lenses are implemented: (i) a *percent-cycle* normalization, which emphasizes signal morphology along a normalized segment progression, and (ii) a *time-aligned* comparison, which preserves absolute timing and transient events such as steering corrections or terrain impacts. This dual approach enables distinguishing between changes in propulsion geometry and changes in pacing or control, a crucial distinction when interpreting outdoor IMU data.

5.2 Study Context and Objectives

Within the integrated framework of this work, the present study constitutes the final experimental component, in which the validated sensor configuration and the dual analytical pipelines developed in the previous chapters are applied to real-world handcycling.

The experimental protocol involved two inexperienced handbike users (one male and one female), each completing a single lap of a 970 m mixed-surface outdoor circuit. The male participant performed Ride 1 and the female participant Ride 2. This design provides

a controlled yet realistic basis for quantifying differences in propulsion dynamics and vibration transmission between riders when the same course is covered under comparable conditions:

1. To quantify segment-specific exposure to acceleration and jerk across two laps, identifying whether one ride exhibits smoother and more stable propulsion dynamics than the other.

2. To separate the contributions of normalized signal morphology and temporal pacing, clarifying whether differences between rides are associated with steadier control or different pacing.

3. To interpret inter-lap differences through the lens of vibration transmission, relating them to the mechanical pathways previously modeled in Chapter 4.

These objectives are consistent with the methodological thread established throughout the thesis: measurement validation on the AULM bench, modeling of vibrational transmission, and field verification under mixed-surface conditions. The following sections detail the experimental setup, data acquisition, processing pipeline, and results of this outdoor study.

5.2.1 Objectives

The present study was designed with three main objectives, each grounded in recent work on handcycling biomechanics and vibration assessment.

The first objective is to describe how mechanical loading and movement stability change between the two laps, and how these changes vary across functionally different sections of the circuit (such as straights, curves, uphill segments, and rougher portions). Rather than treating the lap as a single, uniform unit, the study aims to identify where stability is actually gained or lost, in line with previous segment-based analyses of wheelchair and handcycling performance [18, 19, 20, 21, 22, 23]. This objective is qualitative in nature: it focuses on whether one ride shows smoother and more stable behavior, and where along the course such differences are most evident.

The second objective is to distinguish improvements that arise from more regular propulsion from those that simply reflect different pacing. In practice, a rider may appear smoother either because their propulsion pattern became steadier or because they chose a different speed profile. This objective therefore seeks to separate more regular propulsion patterns from timing-related changes (such as altered approach speed or recovery timing), building on recent recommendations to analyze both normalized signal shape and absolute time when interpreting inertial data in outdoor conditions [16, 24].

The third objective is to interpret the differences between Ride 1 and Ride 2 using the conceptual framework developed earlier in the thesis, in which the riderbike system is viewed as an inputtransmissioncontrol chain. From this perspective, terrain and course features act as inputs, the handbike structure and rider posture govern transmission, and

the steering and propulsion actions of the rider provide control [18, 19, 25]. The study aims to clarify whether observed changes between the two laps are more strongly associated with the way inputs are encountered, with how vibrations are transmitted through the system, or with how the rider manages steering and propulsion. This interpretation is intended to link the outdoor observations to the modeling and sensor-placement work presented in the previous chapters.

These three objectives provide a qualitative road map for the analyses that follow. The subsequent sections describe in detail the experimental protocol, the segmentation of the circuit, and the processing of the inertial signals used to quantify loading, variability, and transmission along the riderbike system.

5.2.2 Scope and interpretability of the comparison

The Ride 1 vs. Ride 2 comparison is used here to quantify, segment by segment and sensor by sensor, how the selected descriptors change between two laps over the same course. This pairwise comparison is intentionally *local*: it can highlight *where* differences occur and *how large* they are, but it does not allow the identification of an adaptation or learning trend (which would require repeated laps by the same participant) across repeated efforts.

Moreover, because the outdoor protocol did not rigidly constrain speed, cadence, or gear selection, the observed differences should be interpreted as the combined effect of mechanical excitation (surface and trajectory) and behavioural choices (pacing, gearing, steering and propulsion strategy). These potential confounders are discussed qualitatively at the end of the Results section.

5.3 Materials and Methods

5.3.1 Participants

Two handbike users participated in the study: one male competitive cyclist (naive to handcycling) and one female recreational cyclist naive to handcycling. Including both athletes allowed us to capture inter-individual variability in propulsion style, anthropometry, and upper-limb kinematicsfactors known to influence biomechanical efficiency and vibrational exposure [26, 27, 28, 29, 30]. Previous studies have shown that physiological responses, such as oxygen uptake and lactate accumulation, vary considerably across individuals depending on propulsion strategy and training background [23]. Table 5.1 reports the main anthropometric and background characteristics of the two participants.

Both participants completed at least one familiarization lap prior to the recorded trials.

5.3.2 Experimental setup

The experimental campaign took place at the Abba-Tartaglia Sports Center in Brescia, Italy, on a closed-loop circuit of 970 m (Figure 5.1). The route featured two straight segments of different length, two 90° turns, a short uphill section, and a gravel stretch.

Tab. 5.1: *Anthropometric and background information of the participants.*

Variable	Male	Female
Age [years]	32	25
Body mass [kg]	69	54
Stature [cm]	176	164
Experience [years]	0	0

This combination provided controlled conditions on straights and curves together with less predictable mechanical inputs from climbing and loose surfaces, which is suitable for studying vibration transmission and propulsion stability in outdoor handcycling. All trials were performed using a Maddiline handbike commonly adopted in both recreational and competitive contexts. No modifications were applied to the mechanical configuration of the bike.

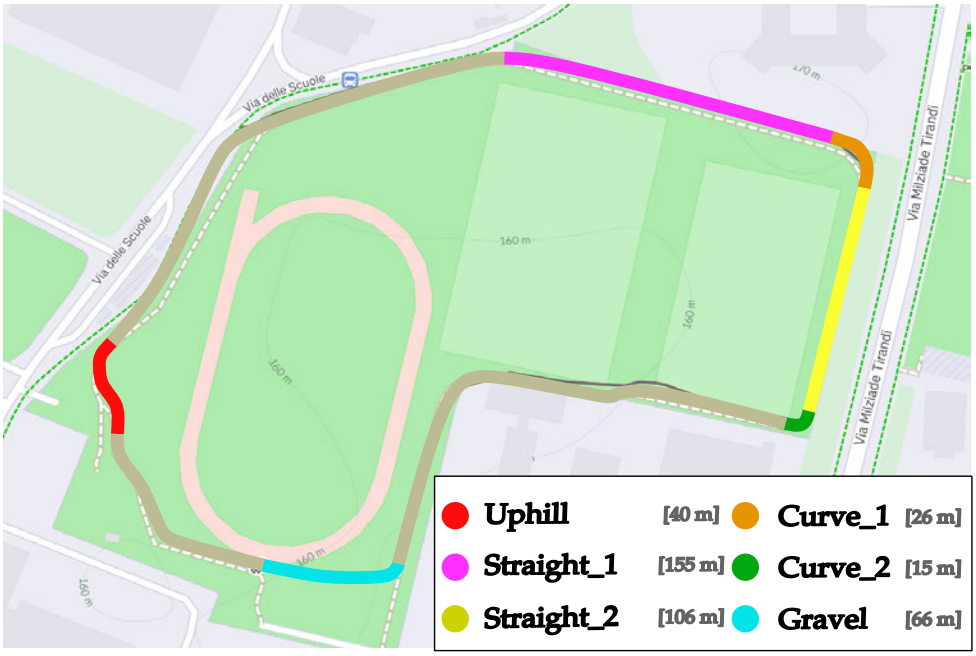

Fig. 5.1: *Layout of the 970 m mixed-surface circuit used for the outdoor handcycling trials.*

5.3.3 Protocol

Each participant performed one single lap of the 970 m circuit at self selected speed under stable environmental conditions. The two laps (Ride 1 and Ride 2) form the basis of all subsequent comparisons. Before data collection, participants familiarized themselves with the circuit and the instrumented handbike. During the recorded laps, the task consisted solely of completing the circuit without prescribed pacing, target cadence, or maneuvering constraints. The purpose was to capture natural propulsion and steering behaviour while maintaining consistency across laps and participants.

5.3.4 Sensors and placement

Eight WT9011DCL inertial measurement units (IMUs; WitMotion, Shenzhen, China) were used to record triaxial acceleration, angular velocity, and magnetic field at 100 Hz via Bluetooth transmission. Sensors were placed on both anatomical and mechanical locations to capture local inputs and global transmission patterns along the riderbike system. Their locations are shown in Figure 5.2:

- C7 vertebra (S1)
- Left wrist (S2)
- Right wrist (S3)
- Left knee (S4)
- Left front wheel (S5)
- Rear backrest (S6)
- Right leg (S7)
- Left handle (S8)

This configuration was chosen to capture both local vibrations at the propulsion interfaces and global transmission through the riderbike system. Wrist and handle sensors are highly sensitive to steering-induced loads and vibrational shocks, while trunk and backrest sensors provide information on whole-body transmissibility. Wheel-mounted sensors capture direct input from the terrain, whereas limb sensors allow observation of asymmetrical propagation patterns. Previous bench-based studies have demonstrated that IMU positioning strongly affects repeatability and accuracy, with distal placements providing more detailed information at the cost of greater variability [25, 31, 32]. The combination of multiple sites therefore increases the robustness and validity in outdoor experiments.

5.3.5 Data acquisition protocol

Before each recorded trial, all IMUs were connected through the Witmotion application, which established Bluetooth connections and enabled continuous acquisition of triaxial accelerations, angular velocities, and magnetic fields.

In parallel, a Garmin Edge 530 cycle computer was employed to record GPS coordinates and velocity profiles. The GPS stream was essential for segmenting the circuit into straights, curves, climb, and gravel, thereby adding a spatial reference frame to complement the IMU signals.

Each participant then performed one official lap at self-selected speed under stable environmental conditions. At the end of the trial, IMU data were exported in text format and converted into MATLAB-readable files, while the GPS log provided additional information for post-processing.

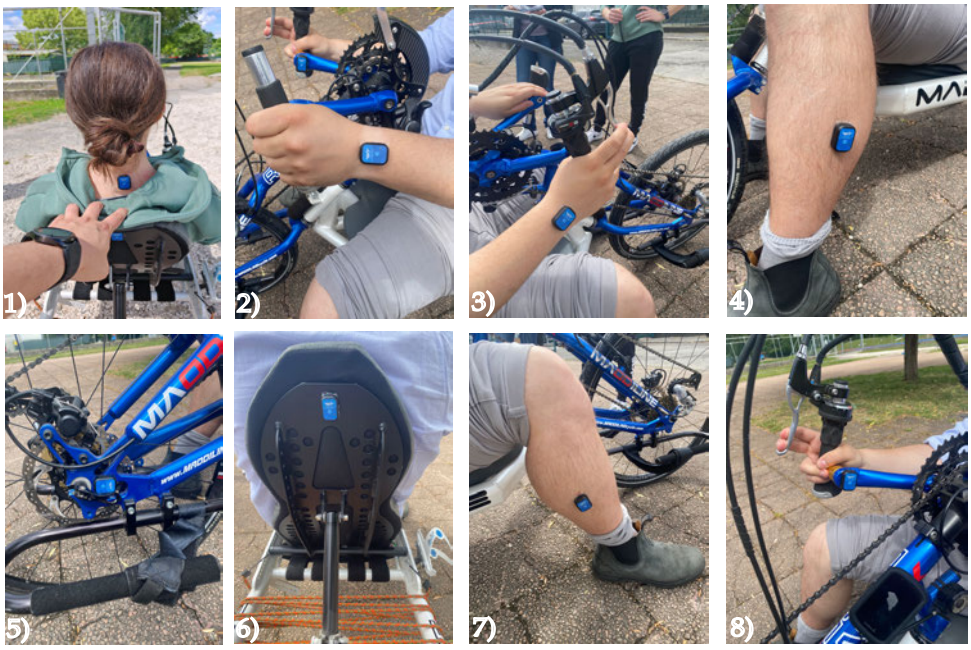

Fig. 5.2: *Placement of the eight WT9011DCL IMUs on the rider and the handbike. Sensors were located at C7 vertebra (S1), left wrist (S2), right wrist (S3), left knee (S4), left front wheel (S5), rear backrest (S6), right leg (S7), and left handle (S8). This configuration allowed capturing both local vibration inputs and global transmission patterns across the bikerider system.*

5.3.6 Signal processing

All processing steps were carried out offline. The detailed analysis pipeline is presented here because it forms the basis for all descriptors used in the Results section.

5.3.7 Synchronization and preprocessing

Sensor and GPS data were synchronized using a semi-automated alignment pipeline specifically developed for this study. For each lap, the corresponding GPX file and the full set of IMU recordings were loaded and inspected. Because each IMU stores an independent local timestamp and may exhibit clock drift or small packet-order irregularities, synchronization was performed by estimating and applying a global time offset between the IMU timeline and the GPS timeline.

The initial offset was derived from device timestamps, expressed as elapsed seconds from the beginning of each recording. To refine this estimate, two independent time markers were extracted: (i) the first significant increase in GPS-derived speed, computed via great-circle distances between consecutive latitudelongitude pairs; and (ii) the first high-magnitude acceleration peak measured from the IMU tri-axial acceleration norm. The temporal difference between these two events provided a data-driven correction term that compensated for initial misalignment and sensor triggering delays.

Following temporal alignment, GPS latitude, longitude, and elevation were interpolated onto the synchronized IMU time grid using linear interpolation. This allowed all

subsequent analyses to operate on a unified temporal reference frame. For quality control, each synchronization step generated a diagnostic plot overlaying GPS speed and IMU acceleration, enabling visual verification of alignment accuracy. All applied offsets and diagnostic information were logged automatically for each lap.

Finally, all synchronized data streams were saved preserving both raw and time-corrected variables for transparent downstream processing.

5.3.8 Segmentation

After synchronizing the IMU recordings with the GPS track for each lap, the circuit was segmented into its functional components (Uphill, two Straights, two Curves, and Gravel). Segmentation was performed using a custom MATLAB interface specifically developed for this study.

The interface displayed the GPS trace of the lap on a longitudelatitude map, shown in parallel with the corresponding altitude profile. Using the mouse, the operator could select the start and end point of each segment directly on the visualized track. Once the boundaries for each segment were defined during the first session, the same coordinates were automatically applied to all subsequent laps to ensure consistency and repeatability across participants and trials.

Table 5.2 reports the start and end coordinates used to define the segments across the circuit. These values were kept constant across laps and participants and served as reference markers for extracting the corresponding data windows.

Tab. 5.2: *Start and end coordinates for each segment of the circuit.*

Segment	Start (Lat / Lon)	End (Lat / Lon)
Uphill	45.561821 / 10.216010	45.561998 / 10.215863
Straight 1	45.563569 / 10.218084	45.563215 / 10.219958
Curve 1	45.563214 / 10.219958	45.563661 / 10.220085
Straight 2	45.563661 / 10.220085	45.562121 / 10.219782
Curve 2	45.562121 / 10.219782	45.562075 / 10.219628
Gravel	45.561504 / 10.217479	45.561510 / 10.216623

5.3.9 Descriptor selection and rationale

A limited set of descriptors was selected to balance interpretability, robustness, and relevance to comfort and control in outdoor handcycling.

Total acceleration magnitude (*AccTot*). The Euclidean norm of tri-axial acceleration provides an indicator of the overall acceleration level at each node of the rider–bike system. *AccTot* is robust in field conditions where small axis misalignments and local rotations are unavoidable.

Dispersion and peaks. Within each segment (time-aligned) and within each normalized segment progression (percent-cycle), dispersion was used as a proxy of stability: narrower distributions indicate more repeatable propulsion and fewer corrective actions. Peak values complement dispersion by capturing rare but potentially critical events (impacts, steering bursts). In the present chapter, dispersion is reported as standard deviation in the main tables to facilitate direct comparison across sensors and segments.

Jerk (time derivative of *AccTot*). Jerk emphasizes impulsive components and short transients that are weakly visible in mean acceleration alone. It is therefore used as a qualitative index of *harshness* and of rapid corrective actions, particularly at mechanical interfaces (wheel, backrest, handle) and distal anatomical sites (wrists).

5.3.10 Inter-lap comparison

Two complementary analysis modes were used. Percent-cycle normalization rescales the time axis of each segment to a common 0–100% progression, facilitating the visual comparison of waveform morphology and the identification of recurring features along the segment, whereas time-aligned analysis preserves the absolute time base of each ride to highlight pacing, entry-state conditions, and the temporal localization of transient events such as steering corrections or terrain impacts. Because both views are computed on the same per-ride sample sets—each segment having been acquired at uniform cadence and resampled to a common per-ride density before extracting the descriptors—the basic distribution statistics (mean, standard deviation, peak) are identical between the two representations by construction. The two analyses therefore differ in how the morphology is unfolded along the segment progression rather than in the summary numbers, and this is why corresponding entries in the percent-cycle and time-aligned tables coincide. The visual comparison provided by the percent-cycle and the time-aligned figures complements the tabular data by revealing differences in pacing, transient behavior, and signal morphology that are not captured by the summary statistics alone.

5.4 Results

5.4.1 Framework for cross-lap comparison

In this study, the comparison between Ride 1 and Ride 2 was conducted separately for each segment of the circuit (straights, curves, uphill, gravel). The segmentation procedure described in Section 5.3.8 provided, for every segment, the exact time windows and corresponding IMU streams to be analyzed.

Two distinct comparison strategies were applied:

- **Percent-cycle normalization**, where each segment was resampled onto a 0–100% normalized progression axis. This approach enabled a direct comparison of signal morphology between laps.

- **Time-aligned comparison**, where signals were analyzed on their original time base to preserve absolute pacing and entry conditions.

Both strategies were applied to the same synchronized IMU data after segmentation. For each segment and each sensor, we report:

- total acceleration magnitude (*AccTot*);
- dispersion (standard deviation);
- peak values;
- jerk metrics (when applicable).

All results are presented in the tables and figures of the following subsections, organized by segment and by comparison method (percent-cycle normalization and time-domain alignment).

5.4.2 Percent-cycle analysis

Curve 1

The first curve of the circuit provides a short segment in which the two rides can be compared under similar speed and steering demands. Figure 5.3 shows the location of Curve 1 within the circuit, with the analysed portion highlighted, while Table 5.3 reports the start and end GPS coordinates of the segment.

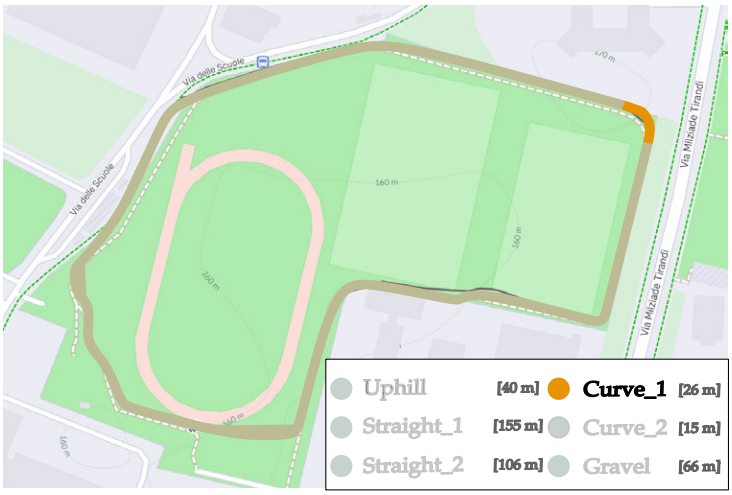

Fig. 5.3: *Top view of the circuit with the Curve 1 segment highlighted.*

Table 5.4 summarizes the percent-cycle statistics of total acceleration (*AccTot*) for all eight sensors in the two laps, while Figure 5.4 shows the corresponding percent-cycle traces.

Across sensors, the mean total acceleration is higher in Ride 1 than in Ride 2 for all sensors, with relative differences in mean ranging from +6.8% to +90.8% (Table 5.4).

Tab. 5.3: *Start and end GPS coordinates for the Curve 1 segment.*

Point	Latitude	Longitude
Start	45.563214	10.219958
End	45.563661	10.220085

Dispersion is also consistently higher in Ride 1, with the largest increases at the mechanical interfaces, especially at Sensor 5 and Sensor 6, while Sensor 7 also shows a marked increase. As shown in Figure 5.4, the two rides preserve a broadly similar normalized signal morphology, with peaks occurring at comparable normalized positions; the main difference therefore lies in amplitude and variability rather than in the overall phase pattern. These results suggest that, in this segment, Ride 2 maintained a more regular and less dispersed propulsion pattern under comparable cornering demands.

Sensor	Ride 1 Mean [g]	Ride 1 SD [g]	Ride 2 Mean [g]	Ride 2 SD [g]	ΔMean [%]	ΔSD [%]
Sensor 1	1.061	0.289	0.983	0.094	+7.8	+207.6
Sensor 2	1.444	0.796	1.109	0.394	+30.2	+102.0
Sensor 3	1.543	0.932	1.122	0.366	+37.5	+154.4
Sensor 4	1.046	0.375	0.979	0.204	+6.8	+84.0
Sensor 5	1.924	1.309	1.008	0.196	+90.8	+566.5
Sensor 6	3.102	1.370	2.335	0.206	+32.8	+565.5
Sensor 7	1.279	0.577	1.046	0.196	+22.2	+194.1
Sensor 8	1.760	0.774	1.153	0.460	+52.6	+68.4

Tab. 5.4: *Percent-cycle comparison of total acceleration (AccTot) in Curve 1 across all sensors. Relative differences are computed as* $(\text{Ride 1}/\text{Ride 2} - 1) \times 100$.

Curve 2

The second curve of the circuit provides a tighter, shorter bend in which the two rides can again be compared under similar cornering demands. Figure 5.5 shows the location of Curve 2 within the circuit, with the analysed portion highlighted, while Table 5.5 reports the start and end GPS coordinates of the segment.

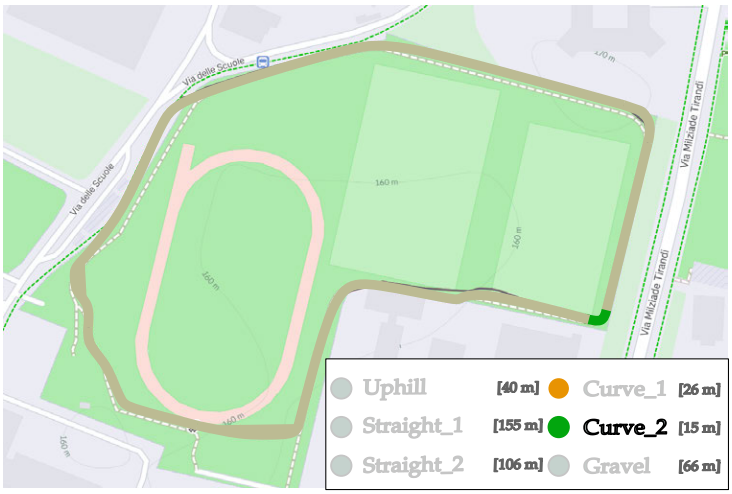

Fig. 5.5: *Top view of the circuit with the Curve 2 segment highlighted.*

Tab. 5.5: *Start and end GPS coordinates for the Curve 2 segment.*

Point	Latitude	Longitude
Start	45.562121	10.219782
End	45.562075	10.219628

Table 5.6 summarizes the percent-cycle statistics of total acceleration (*AccTot*) for all eight sensors in the two laps, while Figure 5.6 shows the corresponding percent-cycle traces.

Across sensors, mean total acceleration in Curve 2 is markedly higher in Ride 1 than in Ride 2 at the wrist sensors (Sensors 2–3, with relative differences of about +106% and +128%), while the trunk shows a more modest increase (+10% at Sensor 1) and the knee a slight decrease (−2% at Sensor 4); means are very similar or slightly lower in Ride 1 for Sensors 5–7 (within approximately ±3%) and only minimally higher at Sensor 8 (about +2%). Standard deviations are larger in Ride 1 at the proximal/anatomical sites (Sensors 1–4, with increases of about +60% to +274%), while they are close to zero in Ride 1 and substantially higher in Ride 2 at the mechanical and steering-related sites (Sensors 5–8, relative differences around −95% to −99%).

Straight 1

The first straight segment of the circuit offers a relatively undisturbed section in which the two rides can be compared under comparable propulsion demands. Figure 5.7 shows the location of Straight 1 within the circuit, with the analysed portion highlighted, while Table 5.7 reports the start and end GPS coordinates of the segment.

Sensor	Ride 1 Mean [g]	Ride 1 SD [g]	Ride 2 Mean [g]	Ride 2 SD [g]	ΔMean [%]	ΔSD [%]
Sensor 1	1.088	0.374	0.991	0.126	+9.8	+195.9
Sensor 2	2.279	1.266	1.107	0.423	+105.9	+198.8
Sensor 3	2.436	1.420	1.069	0.379	+127.9	+274.3
Sensor 4	0.940	0.350	0.962	0.219	−2.3	+59.8
Sensor 5	1.011	0.003	1.017	0.145	−0.6	−98.1
Sensor 6	2.315	0.002	2.328	0.170	−0.5	−98.9
Sensor 7	1.014	0.010	1.043	0.214	−2.8	−95.2
Sensor 8	1.085	0.004	1.064	0.514	+2.0	−99.3

Tab. 5.6: *Percent-cycle comparison of total acceleration (AccTot) in Curve 2 across all sensors. Relative differences are computed as* (Ride 1/Ride 2 − 1) × 100.

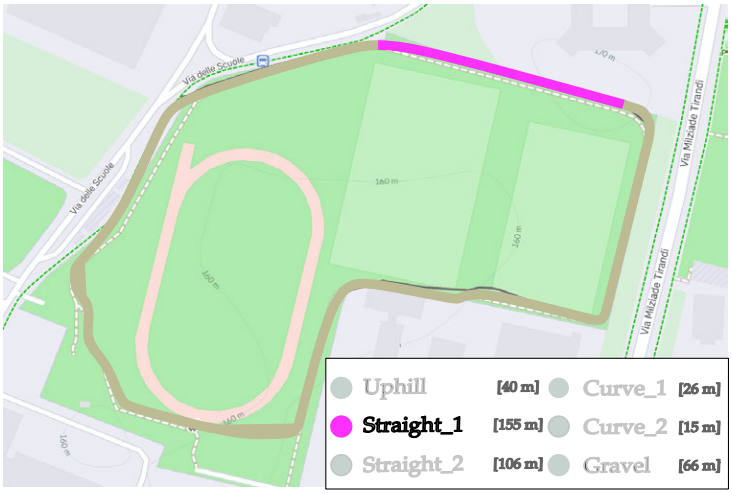

Fig. 5.7: *Top view of the circuit with the Straight 1 segment highlighted.*

Tab. 5.7: *Start and end GPS coordinates for the Straight 1 segment.*

Point	Latitude	Longitude
Start	45.563569	10.218084
End	45.563215	10.219958

Table 5.8 summarizes the percent-cycle statistics of total acceleration (*AccTot*) for all eight sensors in the two laps, while Figure 5.8 shows the corresponding percent-cycle traces.

Across sensors, the mean total acceleration is higher in Ride 1 than in Ride 2 for all sites, with relative differences in mean ranging from +2.2% to +77.7% (Table 5.8). Standard deviations are also higher in Ride 1, with relative differences between +42.3% and +1015.4%, and the largest increases at the wheel and backrest sensors (Sensors 5–6, where SD increases by approximately one order of magnitude).

Sensor	Ride 1 Mean [g]	Ride 1 SD [g]	Ride 2 Mean [g]	Ride 2 SD [g]	ΔMean [%]	ΔSD [%]
Sensor 1	1.015	0.264	0.993	0.104	+2.2	+154.4
Sensor 2	1.385	0.741	1.161	0.474	+19.2	+56.4
Sensor 3	1.353	0.664	1.143	0.445	+18.3	+49.3
Sensor 4	0.987	0.302	0.964	0.212	+2.4	+42.3
Sensor 5	1.813	1.628	1.021	0.146	+77.7	+1015.4
Sensor 6	2.067	1.500	1.332	0.158	+55.2	+850.3
Sensor 7	1.210	0.525	1.049	0.220	+15.3	+138.5
Sensor 8	1.788	1.024	1.193	0.562	+49.8	+82.2

Tab. 5.8: *Percent-cycle comparison of total acceleration (AccTot) in the Straight 1 segment across all sensors. Relative differences are computed as* (Ride 1/Ride 2 − 1) × 100.

Straight 2

The second straight segment of the circuit connects the exit of Curve 1 to the entry of Curve 2 and provides another section in which the two rides can be compared under relatively steady propulsion demands. Figure 5.9 shows the location of Straight 2 within the circuit, with the analysed portion highlighted, while Table 5.9 reports the start and end GPS coordinates of the segment.

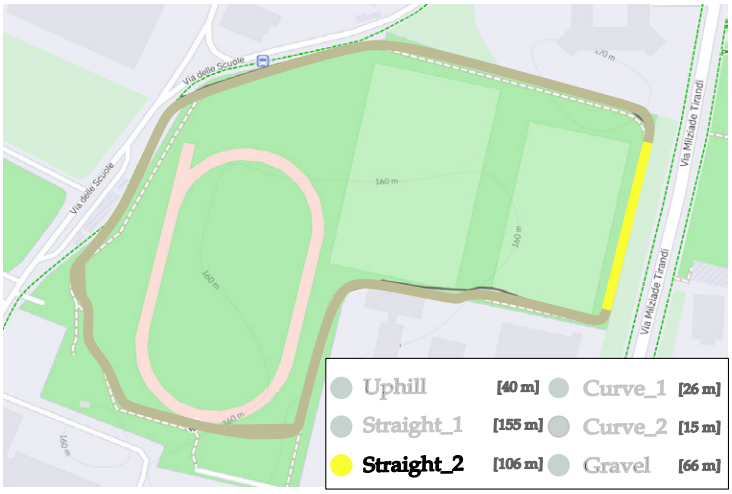

Fig. 5.9: *Top view of the circuit with the Straight 2 segment highlighted.*

Tab. 5.9: *Start and end GPS coordinates for the Straight 2 segment.*

Point	Latitude	Longitude
Start	45.563661	10.220085
End	45.562121	10.219782

Table 5.10 summarizes the percent-cycle statistics of total acceleration (*AccTot*) for all eight sensors in the two laps, while Figure 5.10 shows the corresponding percent-cycle traces.

Across sensors, the mean total acceleration is higher in Ride 1 than in Ride 2 at all sites, with relative differences in mean ranging from +0.7% (Sensor 4) to +14.5%

(Sensor 5) (Table 5.10). Standard deviations are consistently higher in Ride 1, with relative differences between +9.5% and +404.1%, and the largest increase at the rear backrest sensor (Sensor 6).

Sensor	Ride 1 Mean [g]	Ride 1 SD [g]	Ride 2 Mean [g]	Ride 2 SD [g]	ΔMean [%]	ΔSD [%]
Sensor 1	1.016	0.222	0.992	0.126	+2.4	+77.0
Sensor 2	1.280	0.659	1.165	0.484	+9.8	+36.3
Sensor 3	1.231	0.631	1.159	0.431	+6.2	+46.3
Sensor 4	0.983	0.324	0.977	0.241	+0.7	+34.8
Sensor 5	1.153	0.591	1.007	0.187	+14.5	+215.7
Sensor 6	2.489	0.799	2.315	0.158	+7.5	+404.1
Sensor 7	1.082	0.335	1.051	0.265	+2.9	+26.4
Sensor 8	1.334	0.600	1.241	0.548	+7.5	+9.5

Tab. 5.10: *Percent-cycle comparison of total acceleration (AccTot) in the Straight 2 segment across all sensors. Relative differences are computed as* $(\text{Ride 1}/\text{Ride 2} - 1) \times 100$.

Uphill

The uphill section of the circuit provides a continuous climbing segment in which the two rides can be compared under increased internal load and reduced forward speed. Figure 5.11 shows the location of the Uphill segment within the circuit, with the analysed portion highlighted, while Table 5.11 reports the start and end GPS coordinates of the segment.

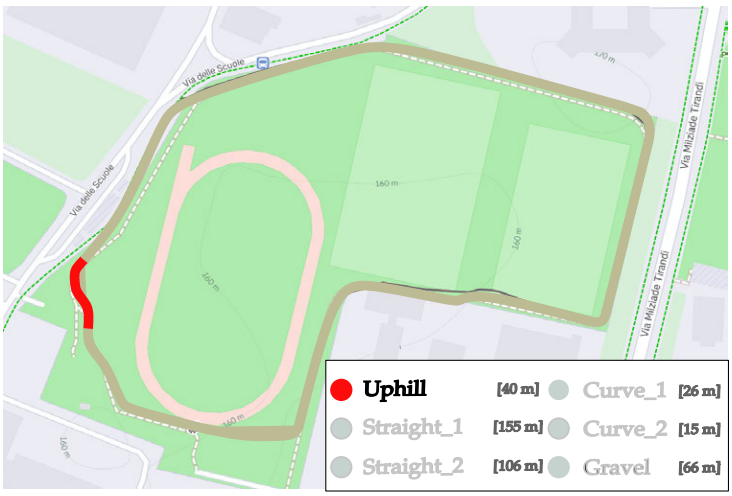

Fig. 5.11: *Top view of the circuit with the Uphill segment highlighted.*

Tab. 5.11: *Start and end GPS coordinates for the Uphill segment.*

Point	Latitude	Longitude
Start	45.561821	10.216010
End	45.561998	10.215863

Table 5.12 summarizes the percent-cycle statistics of total acceleration (*AccTot*) for all eight sensors in the two laps, while Figure 5.12 shows the corresponding percent-cycle traces.

Across sensors, the mean total acceleration is higher in Ride 1 than in Ride 2 at all sites, with relative differences in mean ranging from +0.9% to +21.1% (Table 5.12). Standard deviations are also higher in Ride 1, with relative differences between +35.4% and +333.5%, and the largest increases at the wheel and backrest sensors (Sensors 5–6).

Sensor	Ride 1 Mean [g]	Ride 1 SD [g]	Ride 2 Mean [g]	Ride 2 SD [g]	ΔMean [%]	ΔSD [%]
Sensor 1	1.000	0.159	0.990	0.095	+1.1	+66.7
Sensor 2	1.229	0.544	1.060	0.353	+16.0	+54.1
Sensor 3	1.212	0.474	1.047	0.344	+15.8	+37.8
Sensor 4	0.995	0.271	0.970	0.196	+2.6	+38.3
Sensor 5	1.023	0.525	1.014	0.122	+0.9	+331.8
Sensor 6	2.415	0.505	2.332	0.116	+3.6	+333.5
Sensor 7	1.062	0.349	1.043	0.188	+1.9	+85.4
Sensor 8	1.362	0.595	1.125	0.439	+21.1	+35.4

Tab. 5.12: *Percent-cycle comparison of total acceleration (AccTot) in the Uphill segment across all sensors. Relative differences are computed as* (Ride 1/Ride 2 − 1) × 100.

Gravel

The gravel section of the circuit provides the most irregular surface, introducing broadband stochastic excitation and making it a particularly sensitive segment for comparing the two rides. Figure 5.13 shows the location of the Gravel segment within the circuit, with the analysed portion highlighted, while Table 5.13 reports the start and end GPS coordinates of the segment.

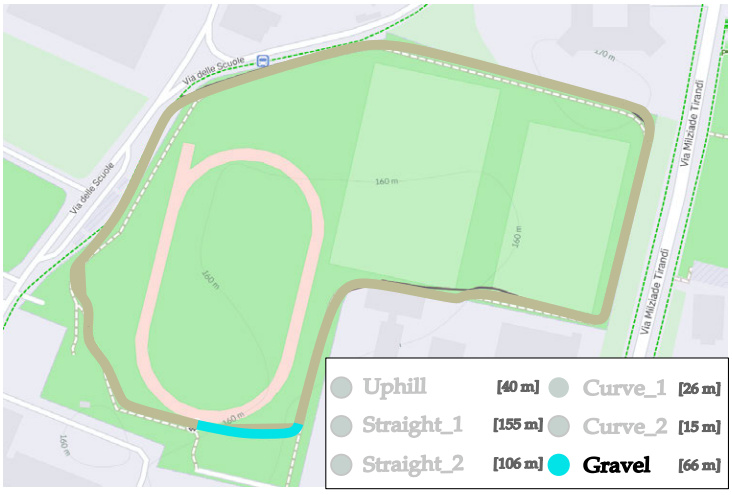

Fig. 5.13: *Top view of the circuit with the Gravel segment highlighted.*

Table 5.14 summarizes the percent-cycle statistics of total acceleration (*AccTot*) for all eight sensors in the two laps, while Figure 5.14 shows the corresponding percent-cycle traces.

Tab. 5.13: *Start and end GPS coordinates for the Gravel segment.*

Point	Latitude	Longitude
Start	45.561504	10.217479
End	45.561510	10.216623

Across sensors, mean total acceleration is higher in Ride 1 than in Ride 2 at all sites, with relative differences in mean ranging from +1.1% to +32.1% (Table 5.14). Standard deviations are also higher in Ride 1, with relative differences between +7.0% and +170.3%. As shown in Figure 5.14, both rides traverse the segment over comparable percent-cycle positions, with differences mainly reflected in the amplitude and dispersion of the traces.

Sensor	Ride 1 Mean [g]	Ride 1 SD [g]	Ride 2 Mean [g]	Ride 2 SD [g]	ΔMean [%]	ΔSD [%]
Sensor 1	1.042	0.243	0.998	0.120	+4.5	+103.1
Sensor 2	1.419	0.732	1.094	0.374	+29.8	+95.8
Sensor 3	1.426	0.800	1.079	0.336	+32.1	+138.1
Sensor 4	1.004	0.331	0.993	0.258	+1.1	+28.0
Sensor 5	1.141	0.533	1.029	0.248	+10.9	+114.4
Sensor 6	2.508	0.666	2.348	0.246	+6.8	+170.3
Sensor 7	1.074	0.300	1.047	0.280	+2.6	+7.0
Sensor 8	1.334	0.526	1.120	0.391	+19.1	+34.4

Tab. 5.14: *Percent-cycle comparison of total acceleration (AccTot) in the Gravel segment across all sensors. Relative differences are computed as* (Ride 1/Ride 2 − 1) × 100.

5.4.3 Time domain

In this section, we present the comparative analysis of the two laps (Ride 1 vs. Ride 2) maintaining the absolute time base. This approach allows for the observation of transient events, pacing strategies, and the settling behavior of the rider-bike system, which are critical for interpreting stability on mixed terrain.

Curve 1

The analysis for Curve 1 refers to the track portion highlighted in Figure 5.3. The comparison of total acceleration (*AccTot*) and Jerk reveals a distinct improvement in Ride 2.

Reading. As shown in Figure 5.15 and summarized in Table 5.15, the *AccTot* results indicate a substantial reduction in mechanical stress in Ride 2 across all sensor locations. At the mechanical interfaces (S5, S6, S8), Ride 2 reduced mean total acceleration by approximately 25% to 48%, with peak acceleration differences up to 6.04 g at the rear backrest (S6). The jerk analysis, shown in Figure 5.16 and summarized in Table 5.16, confirms the reduction in impulsivity: the standard deviation of the signal at the wheel (S5) dropped from 29.41 g/s in Ride 1 to 4.39 g/s in Ride 2. This reduction in high-frequency

		Ride 1			Ride 2			R1 vs R2		
Sensor	Site	μ	σ	Max	μ	σ	Max	$\Delta\mu$ [%]	$\Delta\sigma$ [%]	ΔMax [g]
S1	C7	1.061	0.289	3.030	0.983	0.094	1.264	+7.8	+207.6	+1.77
S2	Left wrist	1.444	0.796	6.370	1.109	0.394	2.148	+30.2	+102.0	+4.22
S3	Right wrist	1.543	0.932	9.149	1.122	0.366	2.117	+37.5	+154.4	+7.03
S4	Left knee	1.046	0.375	2.706	0.979	0.204	1.588	+6.8	+84.0	+1.12
S5	Left front wheel	1.924	1.309	6.750	1.008	0.196	2.004	+90.8	+566.5	+4.75
S6	Rear backrest	3.102	1.370	9.599	2.335	0.206	3.555	+32.8	+565.5	+6.04
S7	Right leg	1.279	0.577	3.213	1.046	0.196	1.639	+22.2	+194.1	+1.57
S8	Left handle	1.760	0.774	4.229	1.153	0.460	2.014	+52.6	+68.4	+2.21

Tab. 5.15: *Curve 1 (time-aligned):* AccTot *statistics. Ride 1 shows consistently higher loads across all metrics. Data for S3 are fully validated.*

		$\text{Jerk}_{\text{mean}}$ [g/s]		Jerk_{SD} [g/s]		Jerk_{max} [g/s]	
Sensor	Site	R1	R2	R1	R2	R1	R2
S1	C7	-0.01	0.03	6.72	2.22	26.40	6.75
S2	Left wrist	0.12	-0.12	19.06	6.86	94.13	49.75
S3	Right wrist	1.01	-5.11	15.27	5.24	56.86	25.74
S4	Left knee	-0.01	-0.08	9.78	5.20	42.16	25.31
S5	Left front wheel	-0.12	-0.03	29.41	4.39	123.88	32.31
S6	Rear backrest	-0.06	0.04	30.87	5.05	104.97	25.56
S7	Right leg	-0.23	-0.05	12.28	4.64	54.48	15.96
S8	Left handle	-0.06	0.00	18.41	5.95	55.91	25.81

Tab. 5.16: *Curve 1 (time-aligned): Jerk summary. Ride 1 exhibits extreme impulsivity (Max* $>$ *100 g/s on wheel and backrest).*

transients translates to the rider: peak jerk values at the hands (S2, S3) decreased by about 47% to 55% (e.g., S2 max jerk: 94.13 g/s vs 49.75 g/s), suggesting improved isolation from the rough tarmac during the cornering maneuver.

Curve 2

Curve 2 represents a tighter turn (see Figure 5.5). The comparison highlights how vibration transmission evolves under higher lateral loads.

Reading. As shown in Figure 5.17 and summarized in Table 5.17, the *AccTot* comparison highlights the upper-limb interface as the dominant bottleneck of Ride 1. At the wrists (S2, S3), Ride 1 shows markedly higher mean acceleration, variability, and peak loads than Ride 2. However, S5–S8 in Ride 1 show anomalously low dispersion in the *AccTot* traces, suggesting a transient logging issue for these channels.

The jerk analysis, shown in Figure 5.18 and summarized in Table 5.18, confirms the critical impulsivity at the hands. At the wrists (S2, S3), the standard deviation of jerk

		Ride 1			Ride 2			R1 vs R2		
Sensor	Site	μ	σ	Max	μ	σ	Max	$\Delta\mu$ [%]	$\Delta\sigma$ [%]	ΔMax [g]
S1	C7	1.088	0.374	2.927	0.991	0.126	1.501	+9.8	+195.9	+1.43
S2	Left wrist	2.279	1.266	8.009	1.107	0.423	2.129	+105.9	+198.8	+5.88
S3	Right wrist	2.436	1.420	9.593	1.069	0.379	2.108	+127.9	+274.3	+7.49
S4	Left knee	0.940	0.350	2.144	0.962	0.219	1.652	-2.3	+59.8	+0.49
S5	Left front wheel	1.011	0.003	1.018	1.017	0.145	1.600	-0.6	-98.1	-0.58
S6	Rear backrest	2.315	0.002	2.320	2.328	0.170	2.870	-0.5	-98.9	-0.55
S7	Right leg	1.014	0.010	1.042	1.043	0.214	1.598	-2.8	-95.2	-0.56
S8	Left handle	1.085	0.004	1.097	1.064	0.514	2.315	+2.0	-99.3	-1.22

Tab. 5.17: *Curve 2 (time-aligned): per-sensor totals of* AccTot*. Note: S5, S6, and S8 in Ride 1 show anomalous low dispersion ($\sigma < 0.01$), suggesting data logging issues for these channels in this lap.*

		$\text{Jerk}_{\text{mean}}$ [g/s]		Jerk_{SD} [g/s]		Jerk_{max} [g/s]	
Sensor	Site	R1	R2	R1	R2	R1	R2
S1	C7	0.00	−0.04	8.79	3.28	37.16	16.06
S2	Left wrist	−0.18	0.01	30.07	6.40	109.91	21.35
S3	Right wrist	−0.08	−0.15	29.49	6.11	168.31	18.67
S4	Left knee	−0.04	0.11	9.56	5.58	32.51	18.63
S5	Left front wheel	—	0.01	—	3.84	—	15.10
S6	Rear backrest	—	−0.09	—	4.87	—	18.93
S7	Right leg	—	0.01	—	5.08	—	13.59
S8	Left handle	—	0.01	—	7.04	—	28.52

Tab. 5.18: *Curve 2 (time-aligned): Jerk summary. Ride 1 shows critical impulsivity at the hands, while S5–S8 in Ride 1 are excluded because of anomalous low-dispersion behaviour in the corresponding* AccTot *traces.*

reaches approximately 30 g/s in Ride 1 against approximately 6 g/s in Ride 2, with peak values of 109.91 g/s at the left wrist and 168.31 g/s at the right wrist. The right wrist alone shows a peak ratio of approximately 9× between Ride 1 and Ride 2, indicating that a strong cornering impulse is transmitted almost unattenuated along the steering chain.

The trunk marker (S1) and the left knee (S4) show milder but coherent increases, with σ ratios of about 2.7× and 1.7×, respectively. For Ride 2, all eight sensors return values below 30 g/s in peak jerk and below 8 g/s in standard deviation, with the handle (S8) showing the largest dispersion ($\sigma = 7.04$ g/s, peak 28.52 g/s), consistent with the active steering correction pattern observed in other segments.

A transient sensor malfunction during Ride 1 prevented the acquisition of valid jerk data on S5–S8; the Ride 1/Ride 2 comparison is therefore based on the four functioning channels (S1–S4), while Ride 2 alone provides the baseline reference for the remaining sensors.

Straight 1

The analysis of the first straight segment (Straight 1) provides a baseline for steady-state propulsion performance.

		Ride 1			Ride 2			R1 vs R2		
Sensor	Site	μ	σ	Max	μ	σ	Max	$\Delta\mu$ [%]	$\Delta\sigma$ [%]	ΔMax [g]
S1	C7	1.015	0.264	2.739	0.993	0.104	1.814	+2.2	+154.4	+0.92
S2	Left wrist	1.385	0.741	5.207	1.161	0.474	3.502	+19.2	+56.4	+1.70
S3	Right wrist	1.353	0.664	5.485	1.143	0.445	4.212	+18.3	+49.3	+1.27
S4	Left knee	0.987	0.302	2.097	0.964	0.212	1.649	+2.4	+42.3	+0.45
S5	Left front wheel	1.813	1.628	14.029	1.021	0.146	1.906	+77.7	+1015.4	+12.12
S6	Rear backrest	2.067	1.500	9.433	1.332	0.158	2.280	+55.2	+850.3	+7.15
S7	Right leg	1.210	0.525	2.996	1.049	0.220	2.123	+15.3	+138.5	+0.87
S8	Left handle	1.788	1.024	7.058	1.193	0.562	3.487	+49.8	+82.2	+3.57

Tab. 5.19: *Straight 1 (time-aligned): per-sensor totals. Ride 1 shows extreme vibration levels at mechanical nodes (S5, S6).*

		$\text{Jerk}_{\text{mean}}$ [g/s]		Jerk_{SD} [g/s]		Jerk_{max} [g/s]	
Sensor	Site	R1	R2	R1	R2	R1	R2
S1	C7	0.01	-0.00	6.60	2.72	49.09	13.10
S2	Left wrist	0.03	-0.02	7.06	3.09	31.07	11.30
S3	Right wrist	-0.11	-0.10	13.93	7.80	71.03	47.76
S4	Left knee	-0.05	-0.17	9.29	7.05	38.74	74.78
S5	Left front wheel	0.04	0.00	30.14	4.85	232.34	93.12
S6	Rear backrest	-0.02	0.01	33.84	4.66	164.30	34.23
S7	Right leg	0.01	0.00	12.84	5.74	65.13	35.20
S8	Left handle	0.04	0.01	22.16	8.28	127.30	52.24

Tab. 5.20: *Straight 1 (time-aligned): Jerk summary. Ride 1 is characterized by extreme jerk peaks at the wheel ($>$ 230 g/s) and backrest ($>$ 160 g/s).*

Reading. As shown in Figure 5.19 and summarized in Table 5.19, Straight 1 offers clear evidence of the reduced vibration levels observed in Ride 2. Ride 1 reveals a harsh mechanical environment: the front wheel (S5) registers a mean acceleration of 1.81 g with impulsive peaks reaching 14.0 g, while the backrest (S6) shows a mean of 2.07 g and peaks near 9.4 g. In Ride 2, mean acceleration at the wheel drops to 1.02 g, while the standard deviation decreases from 1.628 g to 0.146 g, corresponding to a reduction of more than one order of magnitude.

The jerk analysis, shown in Figure 5.20 and summarized in Table 5.20, confirms the same trend in terms of impulsivity. Jerk peaks exceed 230 g/s at the wheel (S5) and 160 g/s at the rear backrest (S6) in Ride 1, indicating a lack of effective damping at the

main mechanical interfaces. Ride 2 suppresses much of this broadband impulsive content, reducing jerk variability at the wheel from 30.14 g/s to 4.85 g/s and at the backrest from 33.84 g/s to 4.66 g/s. This mechanical filtering also reduces stress transmission to the rider: mean acceleration at the wrists (S2, S3) is about 18–19% higher in Ride 1 than in Ride 2, while jerk variability decreases by approximately 44–56%.

Straight 2

The analysis of Straight 2 reinforces the findings from the first straight segment.

		Ride 1			Ride 2			R1 vs R2		
Sensor	Site	μ	σ	Max	μ	σ	Max	$\Delta\mu$ [%]	$\Delta\sigma$ [%]	ΔMax [g]
S1	C7	1.016	0.222	2.118	0.992	0.126	1.568	+2.4	+77.0	+0.55
S2	Left wrist	1.280	0.659	5.289	1.165	0.484	2.889	+9.8	+36.3	+2.40
S3	Right wrist	1.231	0.631	5.036	1.159	0.431	2.217	+6.2	+46.3	+2.82
S4	Left knee	0.983	0.324	2.016	0.977	0.241	1.692	+0.7	+34.8	+0.32
S5	Left front wheel	1.153	0.591	5.855	1.007	0.187	1.671	+14.5	+215.7	+4.18
S6	Rear backrest	2.489	0.799	7.949	2.315	0.158	3.139	+7.5	+404.1	+4.81
S7	Right leg	1.082	0.335	2.757	1.051	0.265	1.868	+2.9	+26.4	+0.89
S8	Left handle	1.334	0.600	4.645	1.241	0.548	2.266	+7.5	+9.5	+2.38

Tab. 5.21: *Straight 2 (time-aligned): per-sensor totals. Ride 1 shows consistently higher variability and peak loads.*

		$\text{Jerk}_{\text{mean}}$ [g/s]		Jerk_{SD} [g/s]		Jerk_{max} [g/s]	
Sensor	Site	R1	R2	R1	R2	R1	R2
S1	C7	-0.00	-0.05	5.74	3.20	22.78	12.29
S2	Left wrist	-0.17	-0.15	12.90	7.55	68.11	47.37
S3	Right wrist	-0.11	-0.10	13.93	7.80	71.03	47.76
S4	Left knee	-0.05	-0.17	9.29	7.05	38.74	74.78
S5	Left front wheel	+0.02	+0.01	12.40	4.83	79.75	28.23
S6	Rear backrest	+0.01	-0.00	18.28	4.56	104.97	22.92
S7	Right leg	-0.02	-0.00	7.75	6.23	41.34	24.67
S8	Left handle	-0.01	-0.06	10.29	7.61	71.57	46.77

Tab. 5.22: *Straight 2 (time-aligned): jerk summary. Jerk_{max} is reported as the maximum absolute jerk peak.*

Reading. As shown in Figure 5.21 and summarized in Table 5.21, mean acceleration values are closer between the two rides compared to Straight 1, but the dispersion metrics (σ) confirm a noisier environment in Ride 1. The standard deviation of acceleration at the rear backrest (S6) is over 400% higher in Ride 1, with the maximum acceleration

increasing from 3.139 g in Ride 2 to 7.949 g in Ride 1. This indicates that the trunk support is subjected to stronger vibration transmission during Ride 1.

The jerk analysis, shown in Figure 5.22 and summarized in Table 5.22, confirms a generally higher impulsive response in Ride 1, although with lower peak values than previously reported. The largest jerk peak is observed at the rear backrest (S6: 104.97 g/s), followed by the front wheel (S5: 79.75 g/s) and the left handle (S8: 71.57 g/s). Ride 2 markedly reduces jerk dispersion at the main mechanical interfaces, especially at S5 and S6: at the rear backrest, jerk variability decreases from 18.28 g/s in Ride 1 to 4.56 g/s in Ride 2, corresponding to an approximately fourfold reduction. At the front wheel, the peak jerk decreases from 79.75 g/s to 28.23 g/s, indicating a clear reduction of impulsive wheel–ground interactions.

Overall, the main Straight 2 pattern is driven by the mechanical interfaces, especially S5, S6, and S8, where Ride 1 shows higher jerk dispersion and larger impulsive events than Ride 2. Anatomical sensors S3 and S4 are interpreted cautiously because their extracted jerk summaries require verification. In the *AccTot* traces, this corresponds to attenuated transmission at the wrists, with peak accelerations decreasing from about 5.0 g in Ride 1 to approximately 2.2–2.9 g in Ride 2.

Uphill

The Uphill segment tests the system under sustained load at lower speeds.

		Ride 1			Ride 2			R1 vs R2		
Sensor	Site	μ	σ	Max	μ	σ	Max	$\Delta\mu$ [%]	$\Delta\sigma$ [%]	ΔMax [g]
S1	C7	1.000	0.159	1.671	0.990	0.095	1.534	+1.1	+66.7	+0.14
S2	Left wrist	1.229	0.544	4.834	1.060	0.353	2.233	+16.0	+54.1	+2.60
S3	Right wrist	1.212	0.474	2.516	1.047	0.344	2.570	+15.8	+37.8	-0.05
S4	Left knee	0.995	0.271	1.826	0.970	0.196	1.585	+2.6	+38.3	+0.24
S5	Left front wheel	1.023	0.525	4.933	1.014	0.122	1.736	+0.9	+331.8	+3.20
S6	Rear backrest	2.415	0.505	4.258	2.332	0.116	3.007	+3.6	+333.5	+1.25
S7	Right leg	1.062	0.349	2.120	1.043	0.188	1.739	+1.9	+85.4	+0.38
S8	Left handle	1.362	0.595	3.454	1.125	0.439	2.164	+21.1	+35.4	+1.29

Tab. 5.23: *Uphill (time-aligned): per-sensor totals of* AccTot*. Mechanical nodes (S5, S6) show a >300% increase in dispersion in Ride 1.*

Reading. As shown in Figure 5.23 and summarized in Table 5.23, the Uphill segment serves as a critical test of the system's behavior under sustained load. Although mean *AccTot* differences are less pronounced than dispersion changes, the variability metrics reveal a clear difference in ride quality. At the left front wheel (S5) and rear backrest (S6), the standard deviation of acceleration in Ride 1 is more than 300% higher than in Ride 2, indicating stronger vibration transmission along the wheel–frame–seat pathway.

The jerk analysis, shown in Figure 5.24 and summarized in Table 5.24, confirms this difference in impulsive behavior. Ride 1 exhibits sharp, high-frequency transients reaching

		$\text{Jerk}_{\text{mean}}$ [g/s]		Jerk_{SD} [g/s]		Jerk_{max} [g/s]	
Sensor	Site	R1	R2	R1	R2	R1	R2
S1	C7	0.02	0.00	18.98	4.06	78.48	13.25
S2	Left wrist	-0.01	0.03	8.55	5.88	30.06	26.88
S3	Right wrist	-0.01	0.03	8.55	5.88	31.54	28.91
S4	Left knee	-0.00	0.00	7.48	4.96	27.62	17.58
S5	Left front wheel	0.02	-0.01	12.88	2.68	88.48	27.65
S6	Rear backrest	0.02	0.00	13.61	2.89	75.51	12.76
S7	Right leg	0.07	-0.01	8.47	4.39	33.46	21.02
S8	Left handle	0.10	0.04	11.58	5.64	52.72	25.64

Tab. 5.24: *Uphill (time-aligned): Jerk summary. Ride 1 exhibits significantly higher peak jerk values at the wheel (88.5 g/s) and backrest (75.5 g/s).*

88.5 g/s at the wheel (S5) and 75.5 g/s at the backrest (S6). Ride 2 maintains a much smoother profile, with jerk peaks at the same locations contained below 28 g/s, suggesting a riding condition with reduced "micro-shocks" during the climbing effort.

Gravel

The Gravel section introduces broadband, stochastic excitation.

		Ride 1			Ride 2			R1 vs R2		
Sensor	Site	μ	σ	Max	μ	σ	Max	$\Delta\mu$ [%]	$\Delta\sigma$ [%]	ΔMax [g]
S1	C7	1.042	0.243	2.543	0.998	0.120	1.511	+4.5	+103.1	+1.03
S2	Left wrist	1.419	0.732	6.257	1.094	0.374	3.761	+29.8	+95.8	+2.50
S3	Right wrist	1.426	0.800	7.187	1.079	0.336	3.485	+32.1	+138.1	+3.70
S4	Left knee	1.004	0.331	2.705	0.993	0.258	2.345	+1.1	+28.0	+0.36
S5	Left front wheel	1.141	0.533	4.933	1.029	0.248	3.082	+10.9	+114.4	+1.85
S6	Rear backrest	2.508	0.666	8.647	2.348	0.246	3.397	+6.8	+170.3	+5.25
S7	Right leg	1.074	0.300	2.637	1.047	0.280	2.815	+2.6	+7.0	-0.18
S8	Left handle	1.334	0.526	2.871	1.120	0.391	3.672	+19.1	+34.4	-0.80

Tab. 5.25: *Gravel (time-aligned): per-sensor totals of* AccTot.

Reading. As shown in Figure 5.25 and summarized in Table 5.25, the Gravel segment confirms the stronger vibration exposure observed in Ride 1 on loose surfaces. Ride 1 is characterized by higher mean accelerations and increased dispersion across the main interfaces. At the wrist sensors (S2, S3), the mean acceleration is approximately 30% higher in Ride 1, with standard deviations more than doubling, indicating a rougher ride for the upper limbs. The mechanical nodes confirm this picture: the rear backrest (S6) shows a dispersion increase of 170% in Ride 1, with peak acceleration increasing from 3.397 g in Ride 2 to 8.647 g in Ride 1.

		$\text{Jerk}_{\text{mean}}$ [g/s]		Jerk_{SD} [g/s]		Jerk_{max} [g/s]	
Sensor	Site	R1	R2	R1	R2	R1	R2
S1	C7	−0.01	−0.02	5.69	3.90	34.22	16.74
S2	Left wrist	−0.44	−0.10	14.39	6.57	92.16	39.20
S3	Right wrist	−0.08	0.01	18.89	8.07	142.89	39.20
S4	Left knee	0.01	0.04	8.39	7.74	42.61	37.00
S5	Left front wheel	0.02	0.03	12.64	7.10	80.12	37.90
S6	Rear backrest	−0.03	0.01	15.49	7.30	127.58	31.43
S7	Right leg	−0.04	0.02	7.71	6.80	32.13	26.61
S8	Left handle	0.04	−0.09	10.59	8.00	44.52	64.27

Tab. 5.26: *Gravel (time-aligned): jerk summary. Ride 1 shows higher jerk variability and large impulsive peaks, especially at the right wrist (S3) and rear backrest (S6).*

The jerk analysis, shown in Figure 5.26 and summarized in Table 5.26, confirms the higher impulsive content in Ride 1. At the rear backrest (S6), jerk peaks reach 127.58 g/s in Ride 1 compared to 31.43 g/s in Ride 2. At the right wrist (S3), Ride 1 reaches the highest impulsivity of the segment, with a peak jerk of 142.89 g/s, more than three times the value recorded in Ride 2. Even at the trunk marker (S1), where mean acceleration is comparable between rides, jerk variability is approximately 45% higher in Ride 1 ($\sigma \approx 5.69$ vs. 3.90 g/s), with peak values about twice as large.

Overall, Ride 2 demonstrates better damping on loose surfaces, reducing both average vibrational load and most impulsive shocks. The only relevant exception is the left handle (S8), where Ride 2 shows a higher isolated jerk peak than Ride 1, suggesting that some local steering corrections may still occur even when the global vibration level is lower.

5.4.4 Interpretation caveats: speed, gearing, and riding style

Because this was a naturalistic outdoor protocol, several factors were not rigidly controlled and may partially confound the Ride 1 vs. Ride 2 comparison. First, speed and cadence can influence time-domain statistics: higher forward speed on rough surfaces increases input energy at the wheel, while cadence changes alter how percent-cycle normalization redistributes peaks and troughs along the normalized segment progression. Second, gear changes (and the timing of shifting) can introduce short transients in the upper-limb interfaces and modify the torque profile, with local effects particularly visible at the handle and wrist sensors. Third, riding style (line choice on gravel, cornering strategy, trunk bracing against the backrest) changes the effective coupling in the transmission chain.

The dual analysis adopted here partially mitigates these confounds. Percent-cycle normalization highlights repeatability and morphology, whereas time-aligned descriptors preserve entry conditions and pacing; reading both together reduces the risk of attributing differences to improved control when they simply reflect different speed profiles. Never-

theless, the present comparison should be interpreted as a segment-wise *snapshot* of two plausible strategies under real-world constraints.

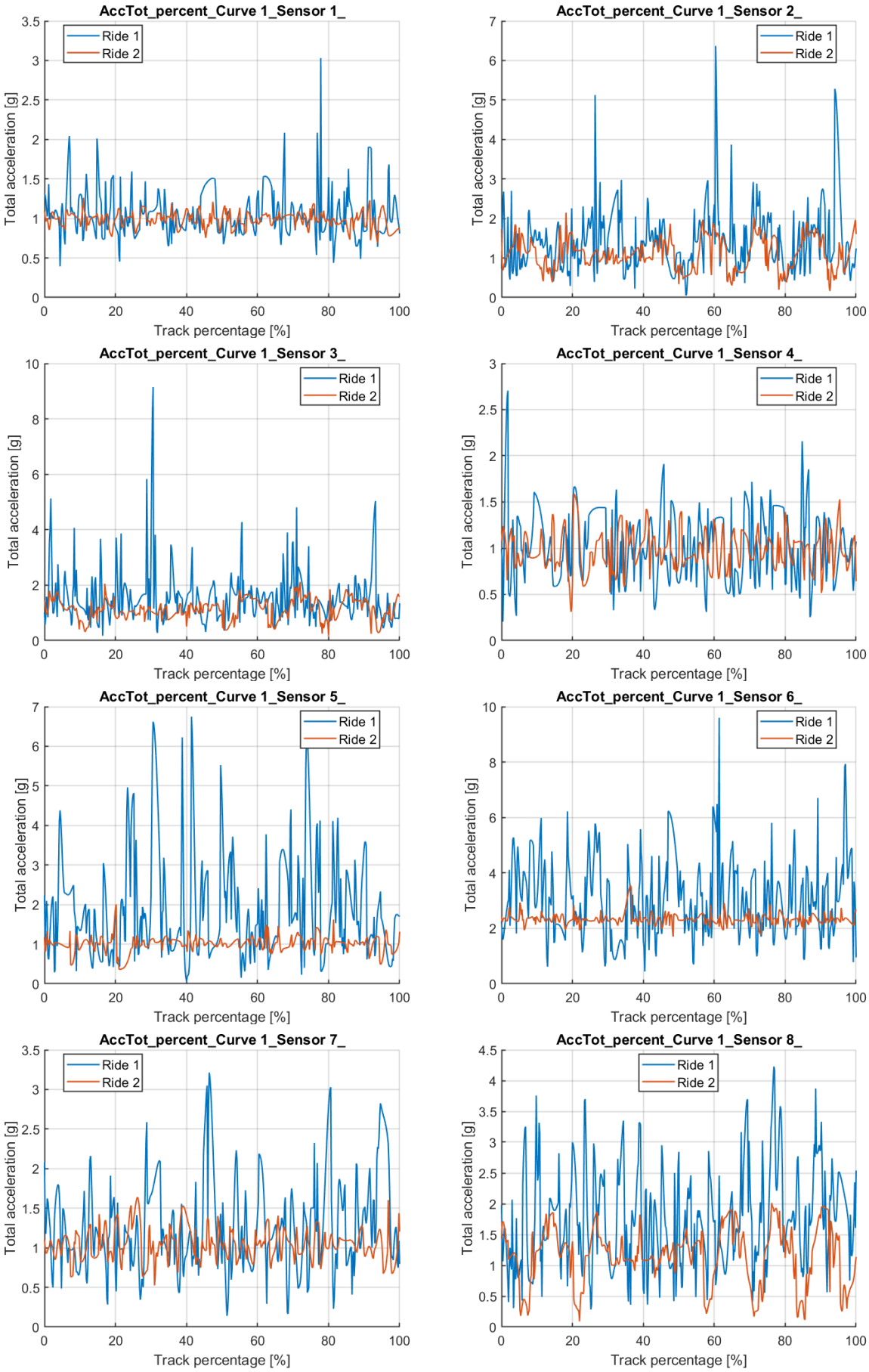

Fig. 5.4: *Percent-cycle traces of total acceleration (AccTot) for Curve 1 across all sensors. Ride 1 (male, 32 y) is shown in blue and Ride 2 (female, 25 y) in red.*

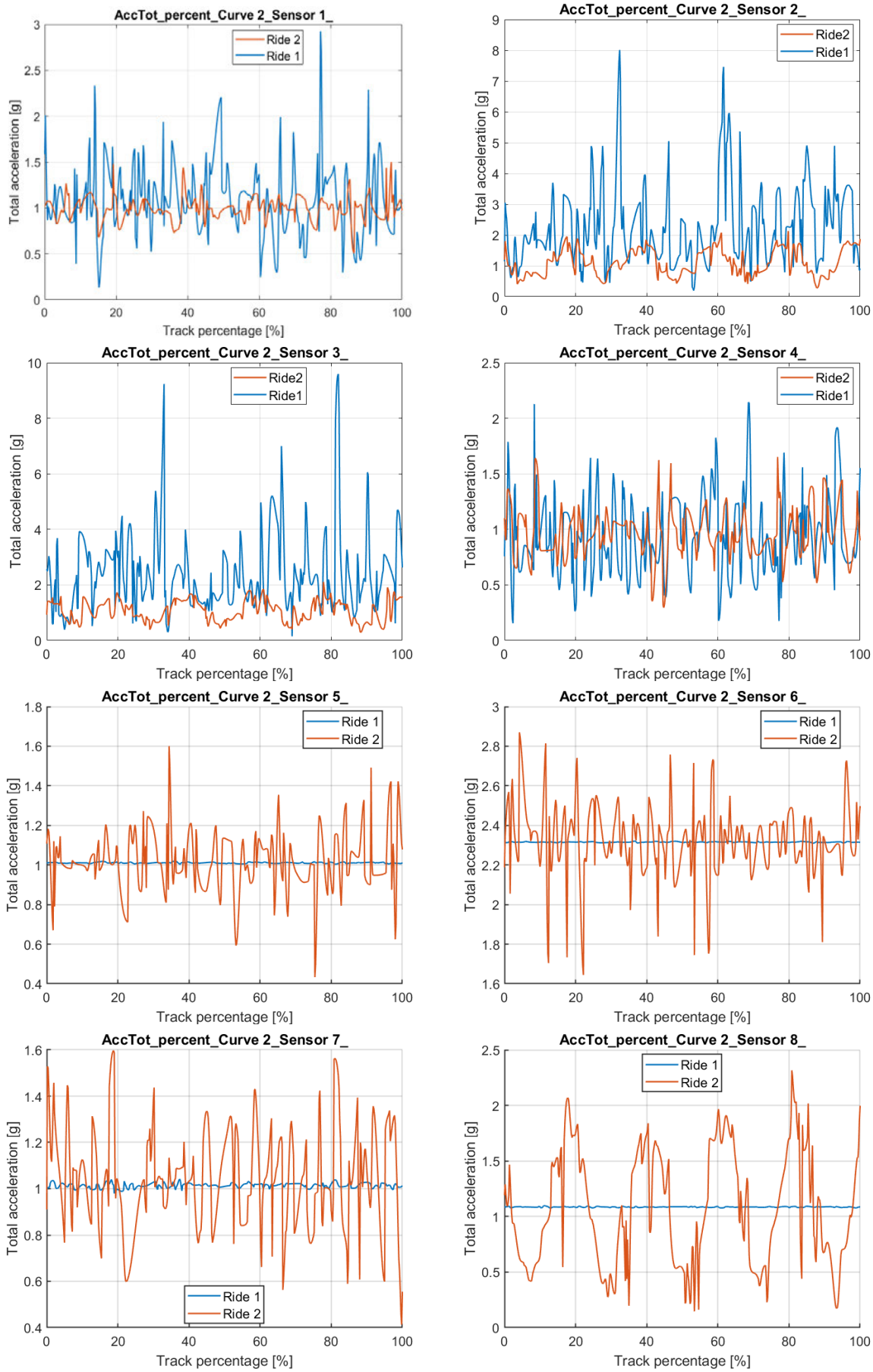

Fig. 5.6: *Percent-cycle traces of total acceleration (AccTot) for the Curve 2 segment across all sensors (Sensor 1–Sensor 8). Data are normalized to 0–100% of segment duration. Ride 1 (male, 32 y) is shown in blue; Ride 2 (female, 25 y) in red.*

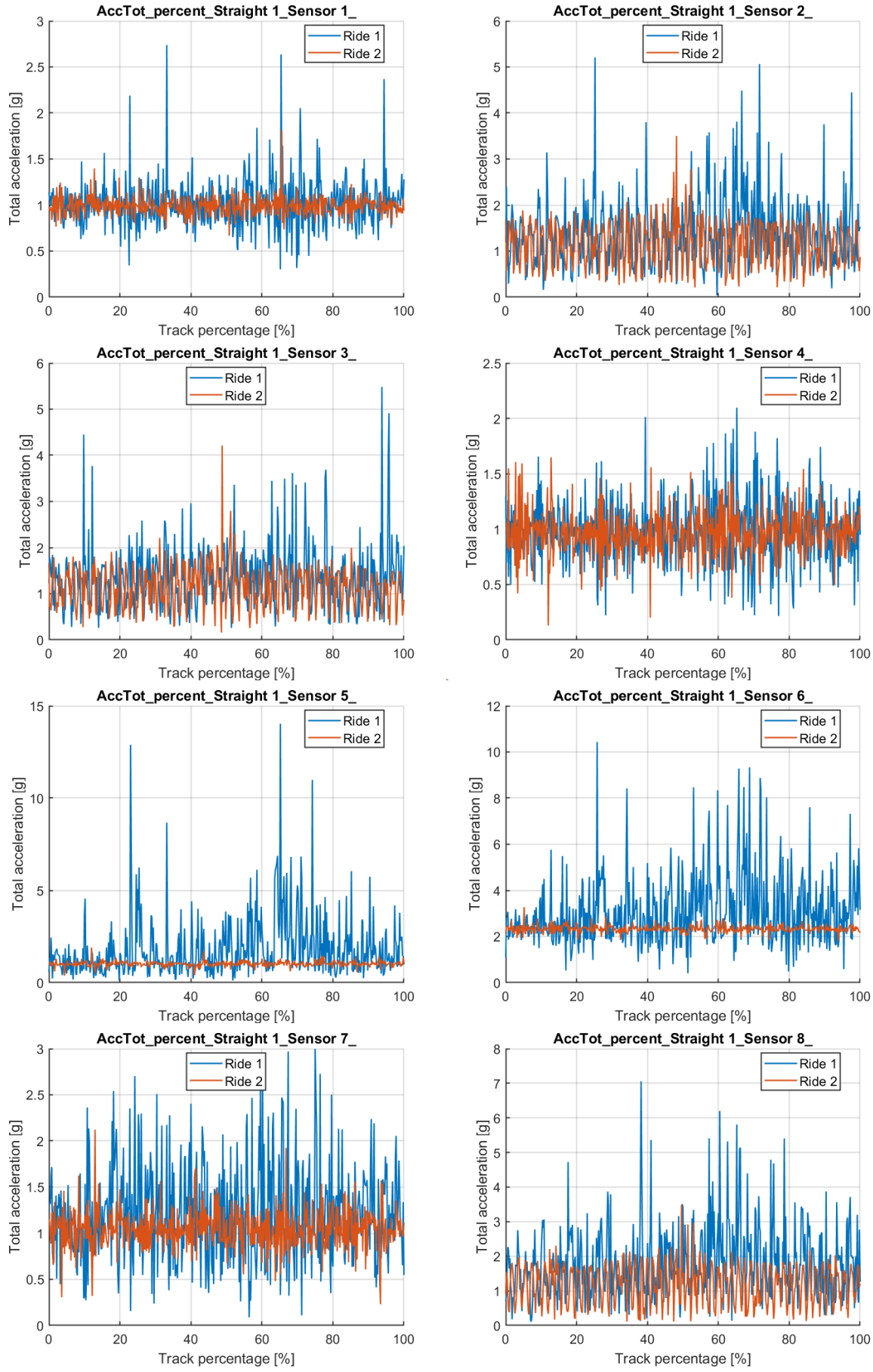

Fig. 5.8: *Percent-cycle traces of total acceleration (AccTot) for the Straight 1 segment across all sensors (Sensor 1–Sensor 8). Data are normalized to 0–100% of segment duration. Ride 1 (male, 32 y) is shown in blue; Ride 2 (female, 25 y) in red.*

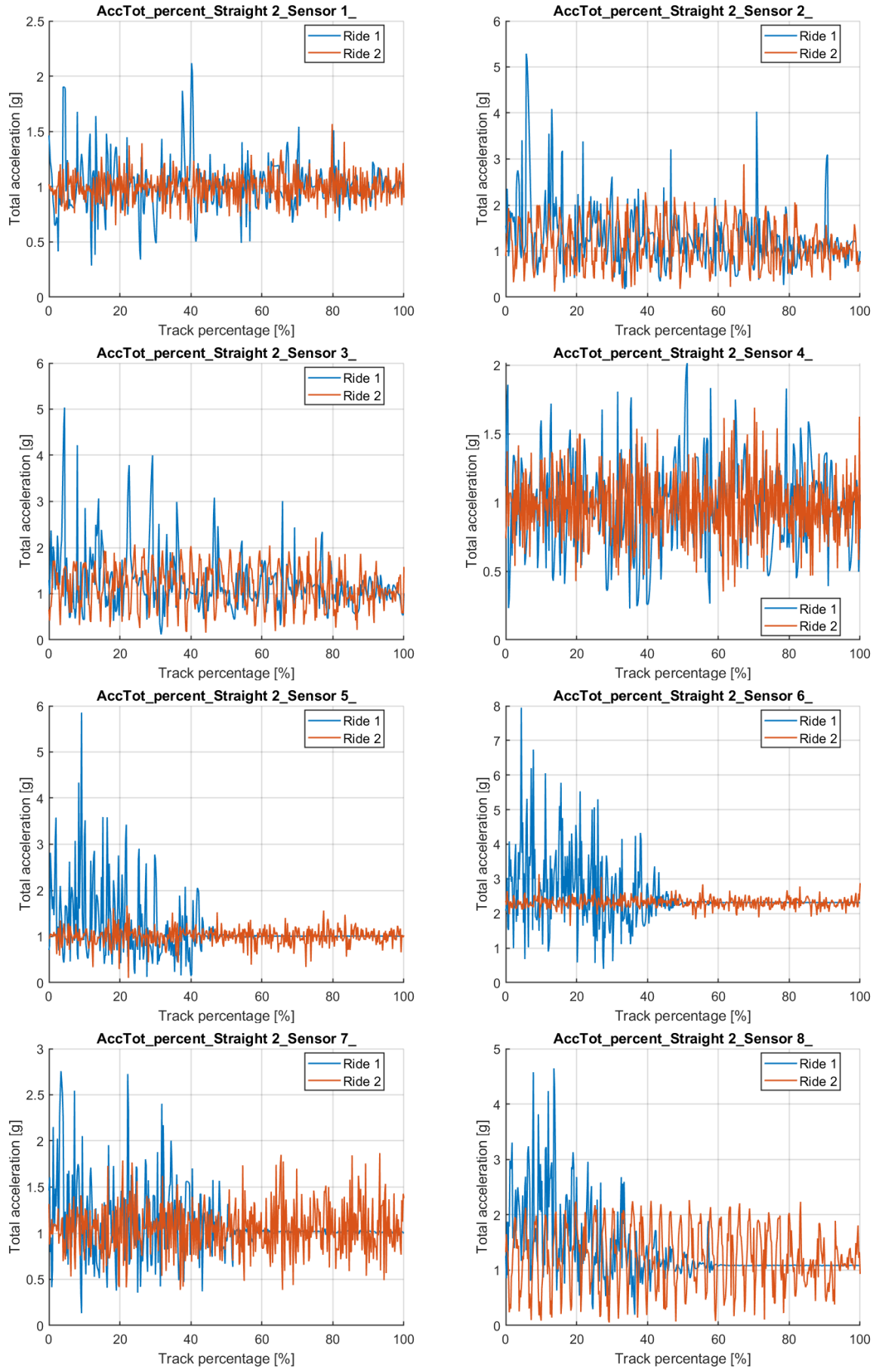

Fig. 5.10: *Percent-cycle traces of total acceleration (AccTot) for the Straight 2 segment across all sensors (Sensor 1–Sensor 8). Data are normalized to 0–100% of segment duration. Ride 1 (male, 32 y) is shown in blue; Ride 2 (female, 25 y) in red.*

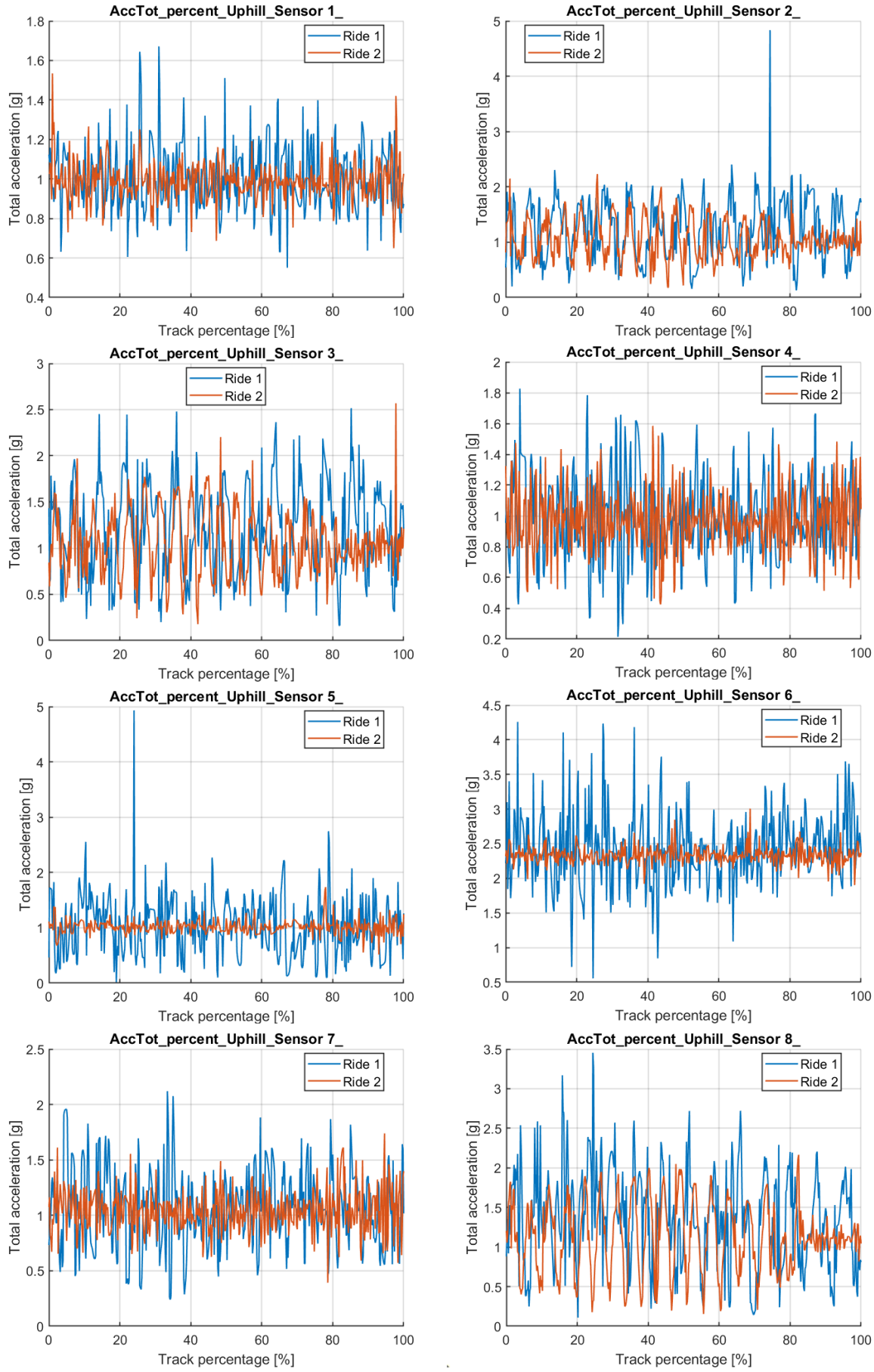

Fig. 5.12: *Percent-cycle traces of total acceleration (AccTot) for the Uphill segment across all sensors (Sensor 1–Sensor 8). Data are normalized to 0–100% of segment duration. Ride 1 (male, 32 y) is shown in blue; Ride 2 (female, 25 y) in red.*

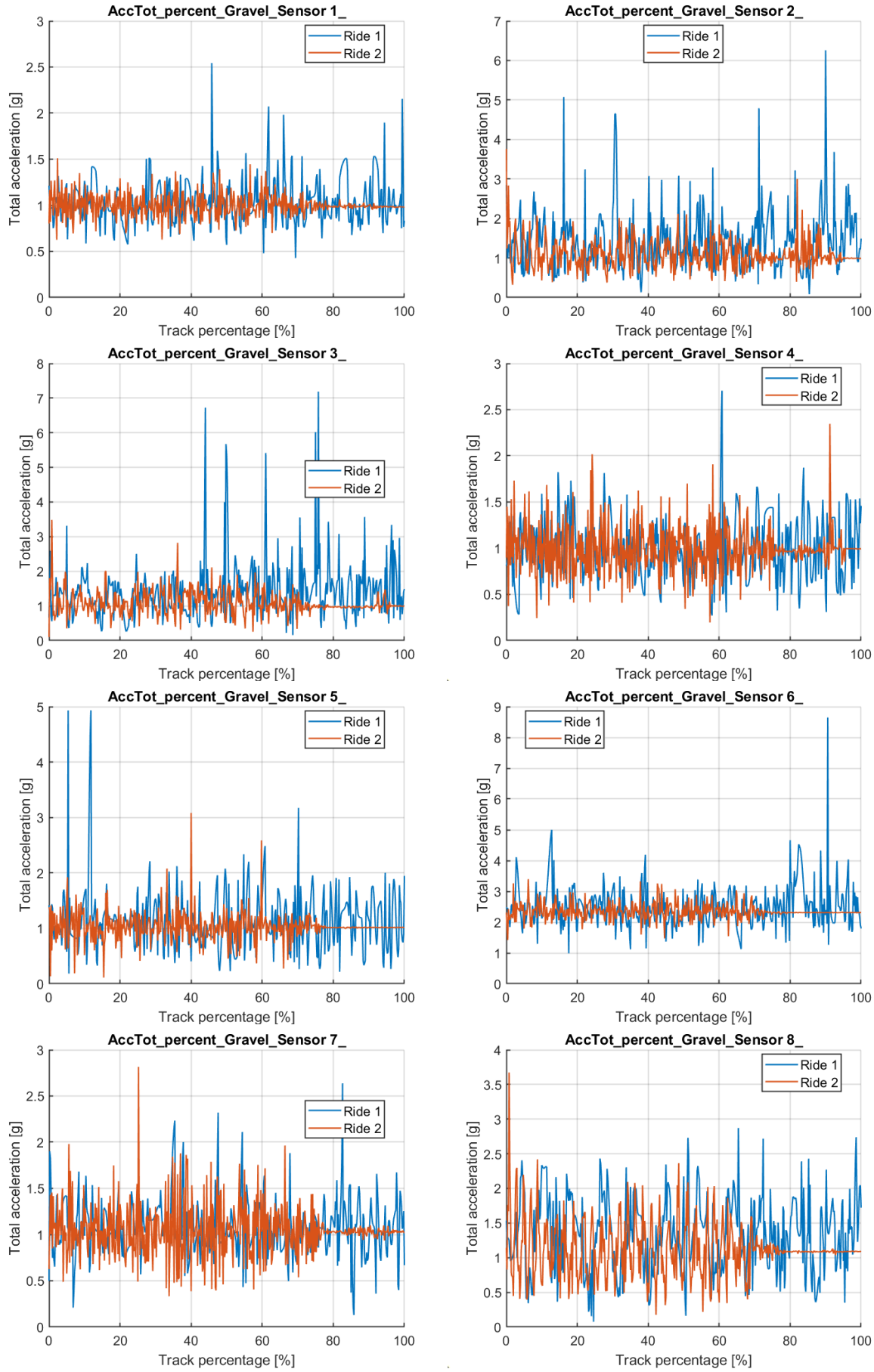

Fig. 5.14: *Percent-cycle traces of total acceleration (AccTot) for the Gravel segment across all sensors (Sensor 1–Sensor 8). Data are normalized to 0–100% of segment duration. Ride 1 (male, 32 y) is shown in blue; Ride 2 (female, 25 y) in red.*

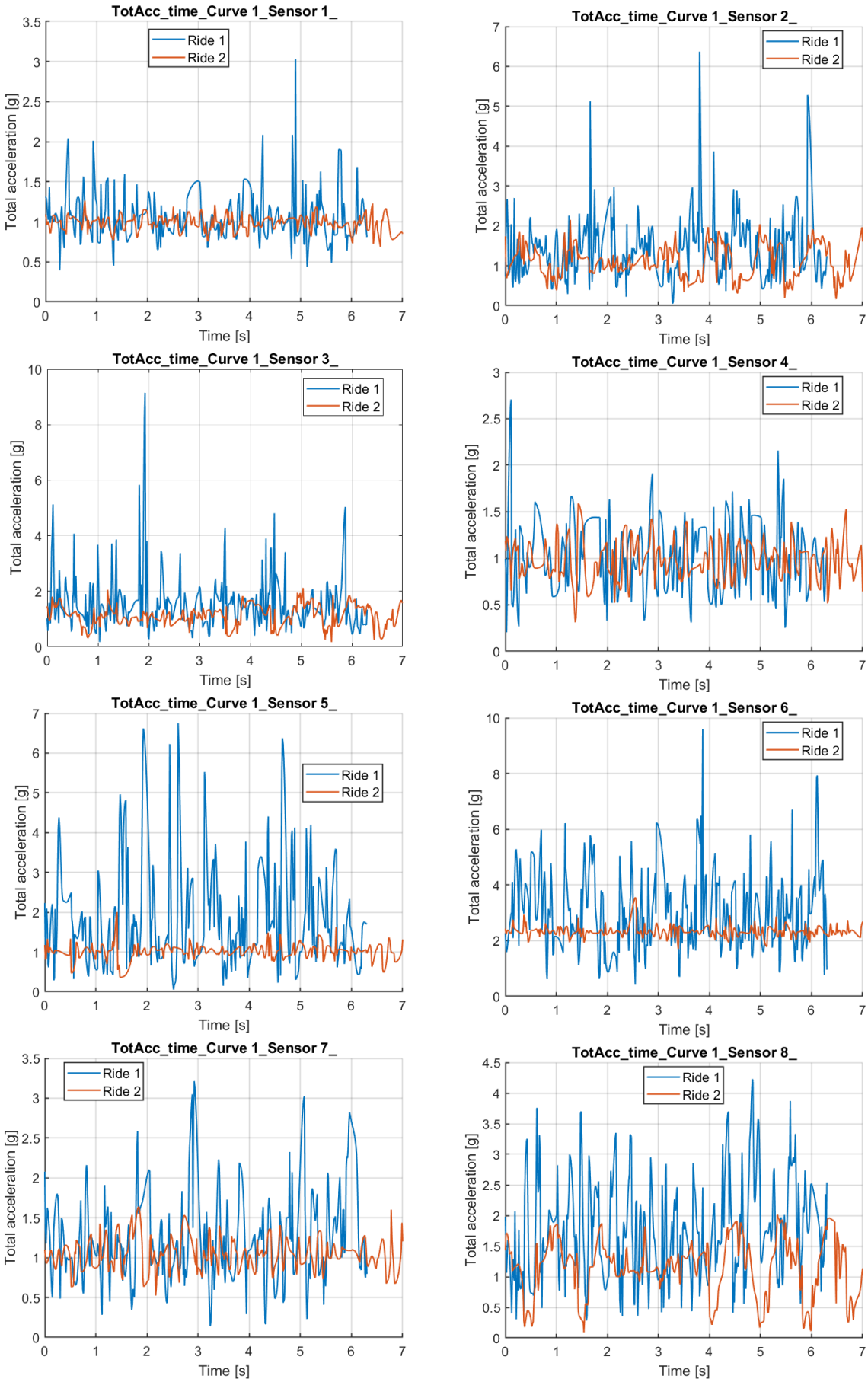

Fig. 5.15: *Curve 1 (time-aligned).* AccTot *time series for sensors S1–S8 with Ride 1 (blue) and Ride 2 (orange).*

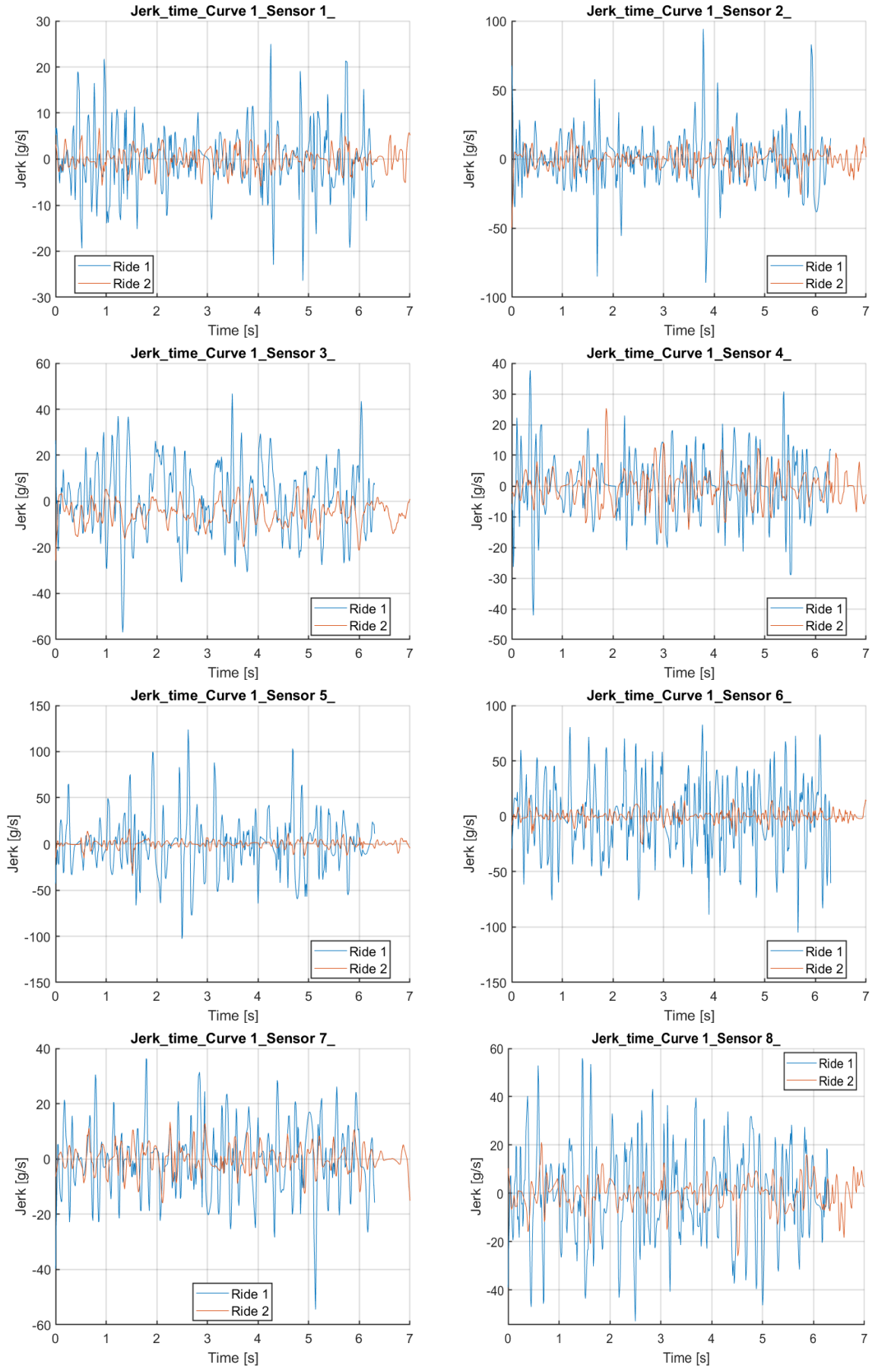

Fig. 5.16: *Curve 1 (time-aligned). Jerk time series (g/s). Ride 1 (blue) shows high-amplitude bursts vs. Ride 2 (orange).*

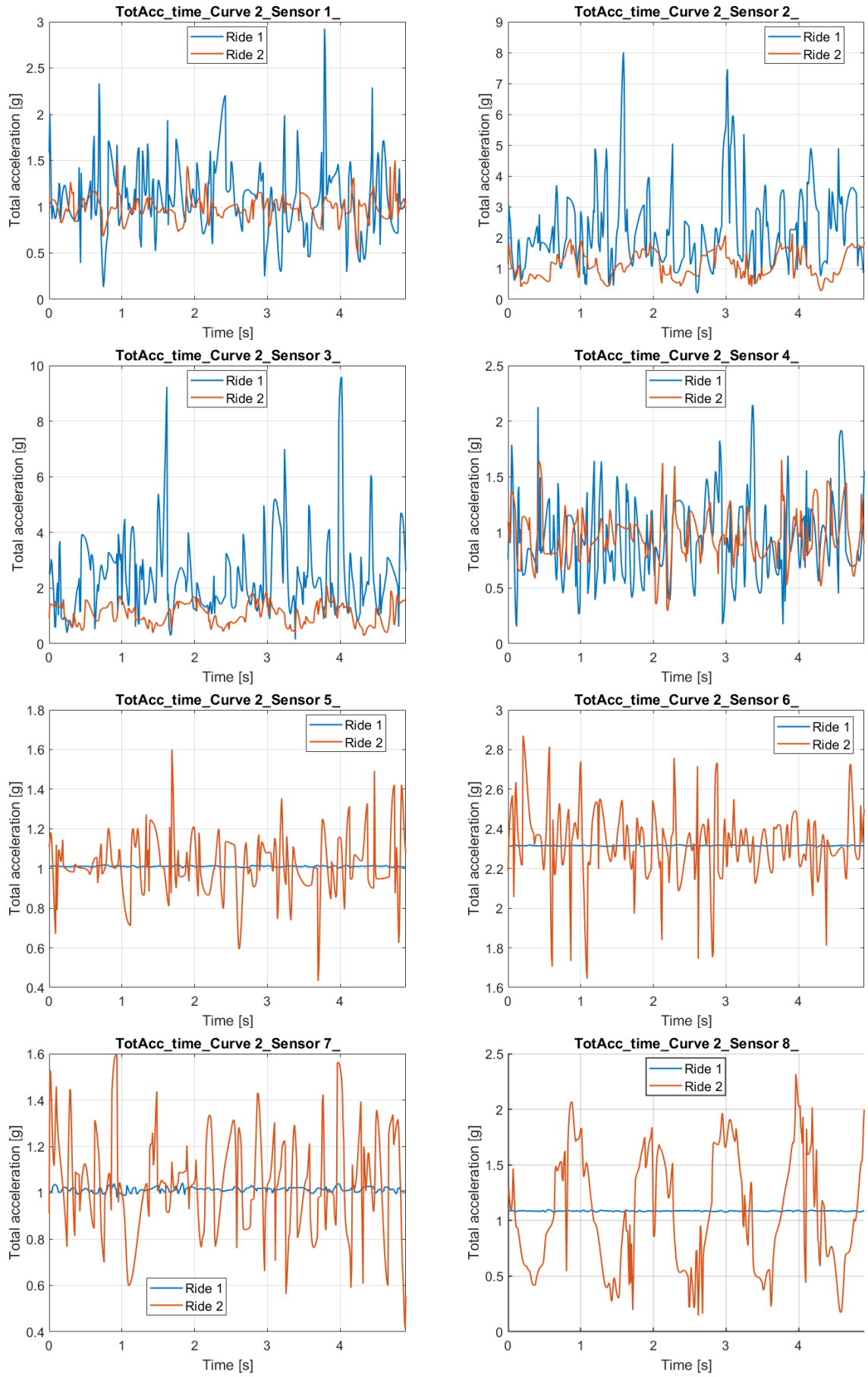

Fig. 5.17: *Curve 2 (time-aligned).* AccTot *time series for S1–S8 with Ride 1 (blue) and Ride 2 (orange).*

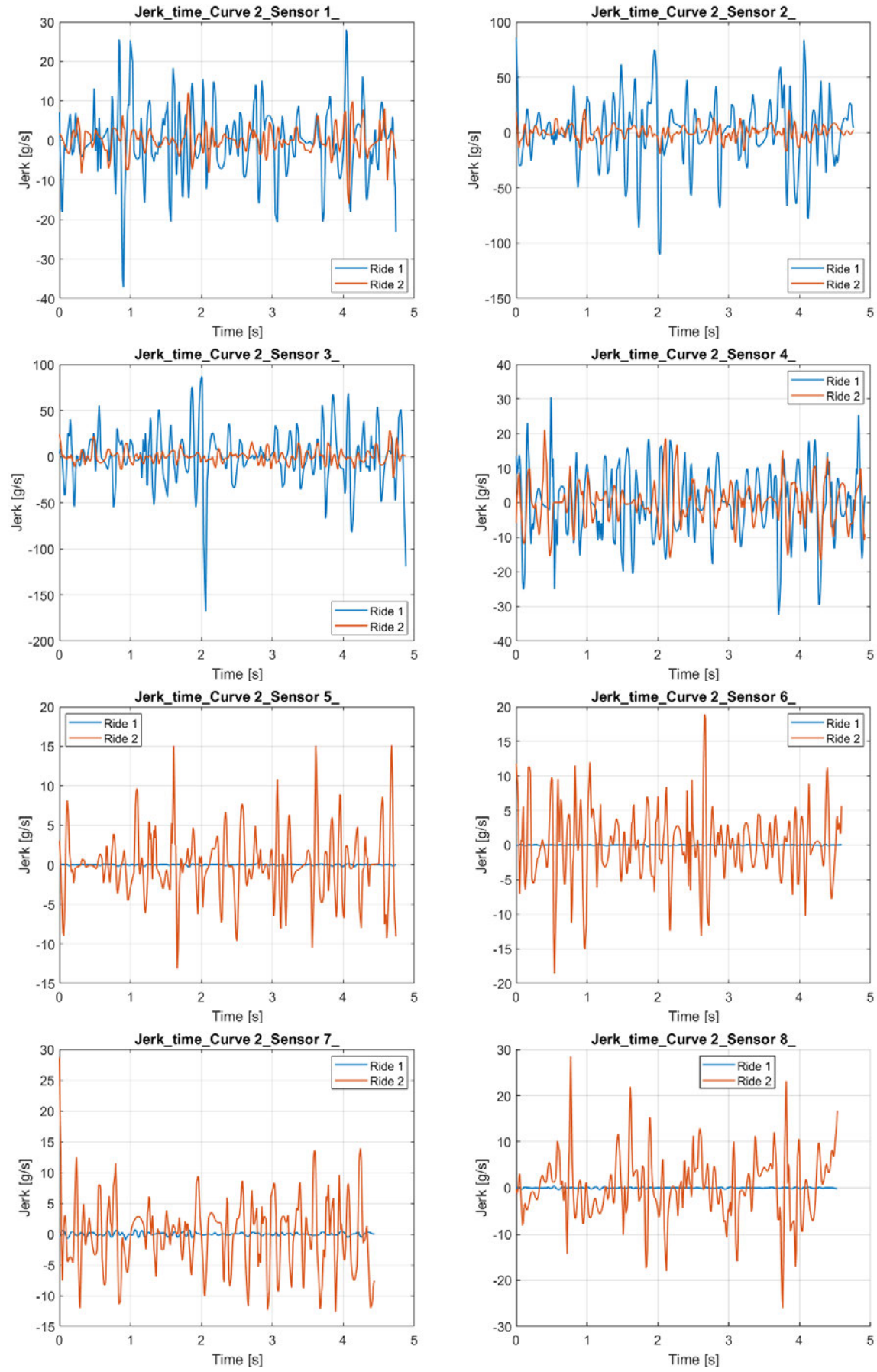

Fig. 5.18: *Curve 2 (time-aligned). Jerk time series (g/s). Extreme impulsivity at the wrists in Ride 1 is visible.*

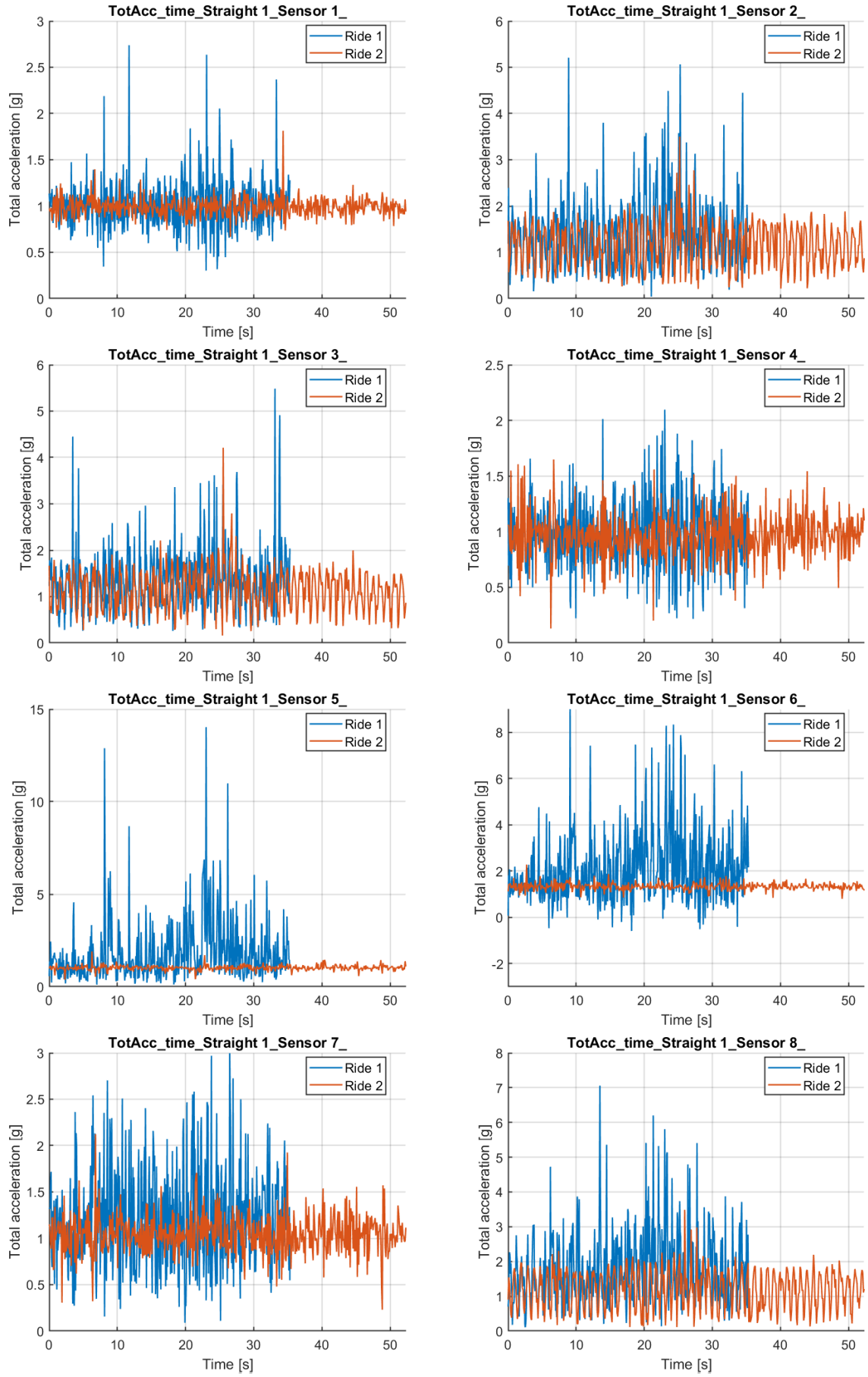

Fig. 5.19: *Straight 1 (time-aligned).* AccTot *time series for S1–S8 with Ride 1 (blue) and Ride 2 (orange).*

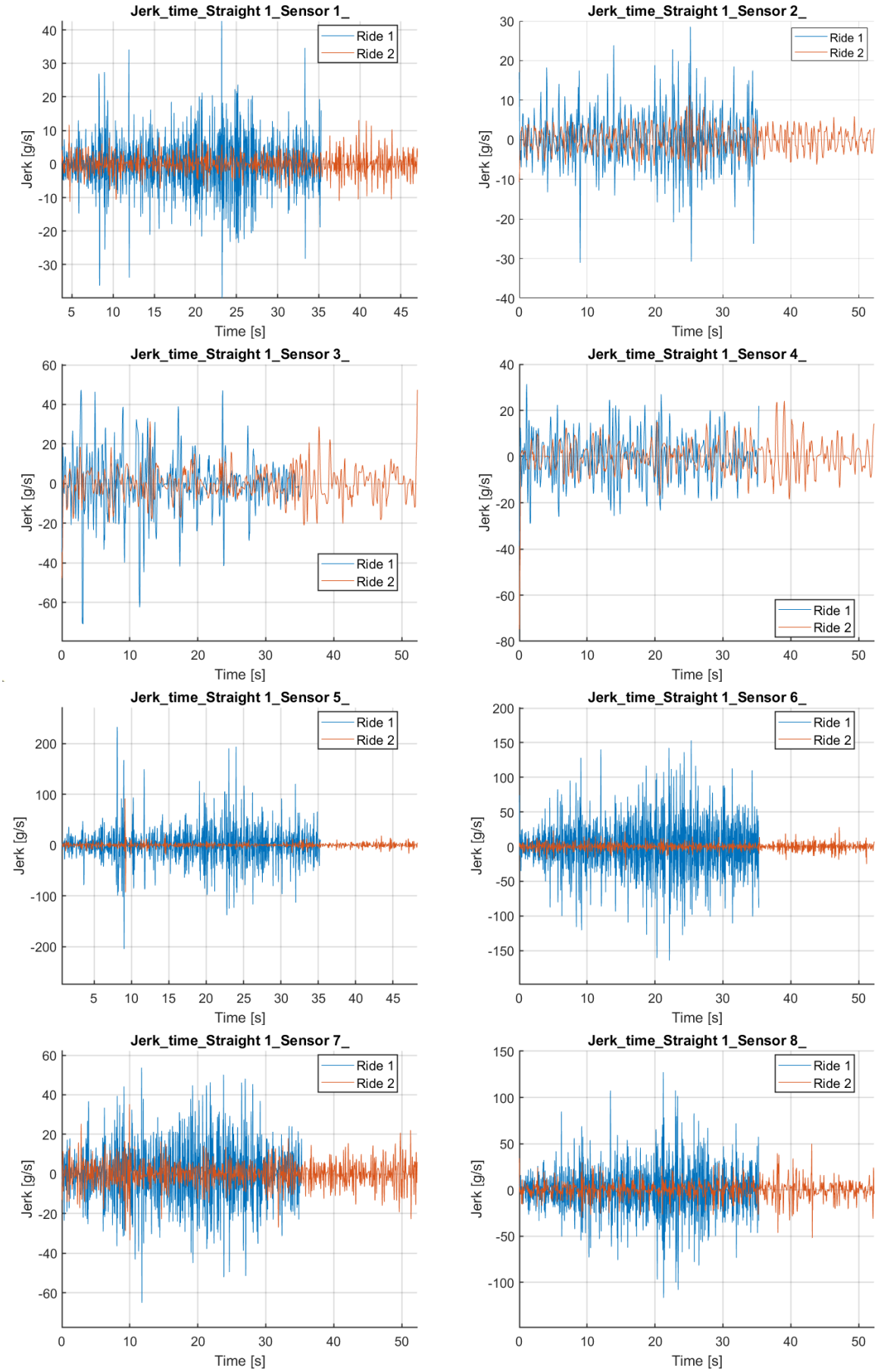

Fig. 5.20: *Straight 1 (time-aligned). Jerk time series (g/s). Ride 1 is characterized by high-amplitude, frequent bursts.*

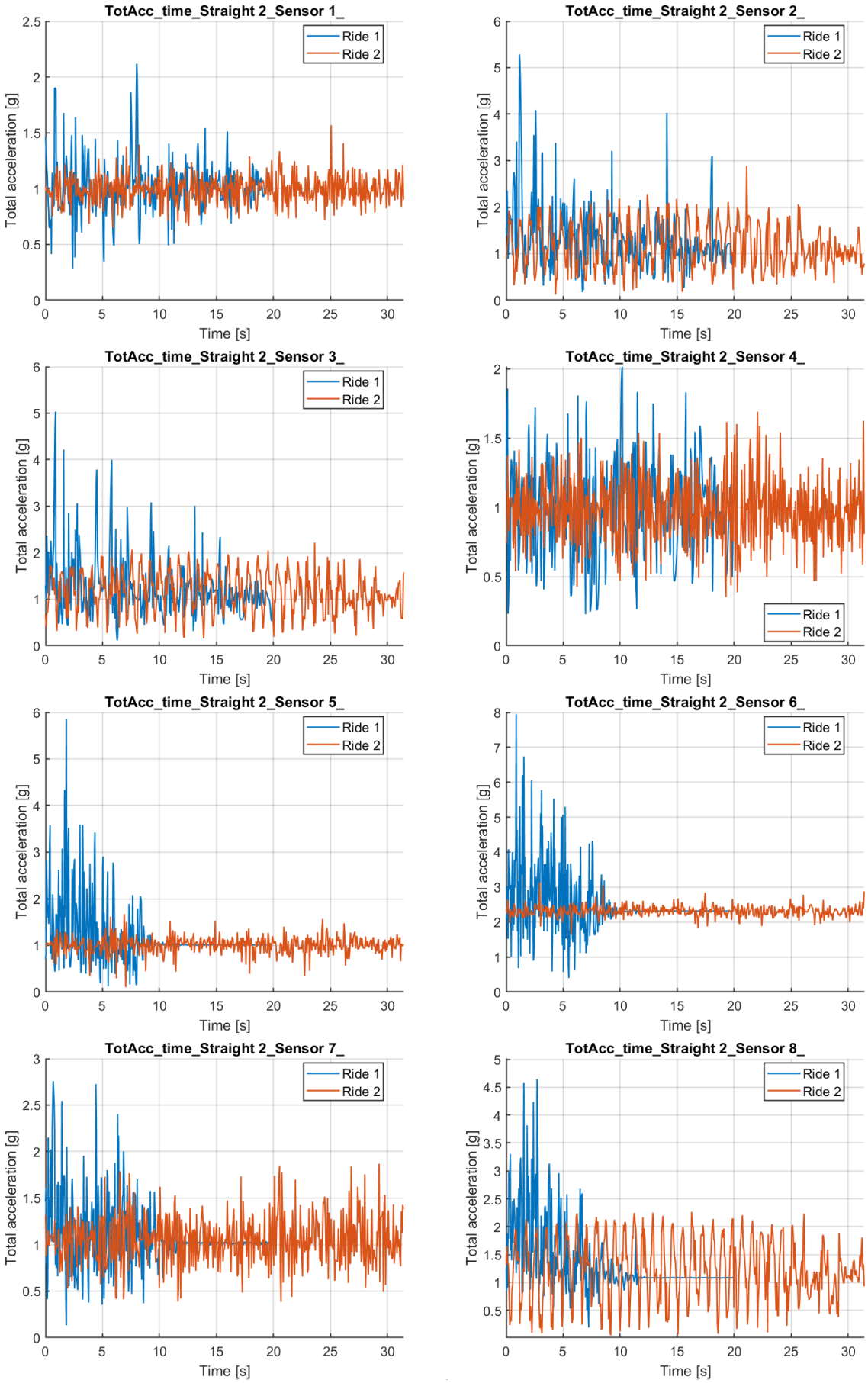

Fig. 5.21: *Straight 2 (time-aligned).* AccTot *time series for S1–S8 with Ride 1 (blue) and Ride 2 (orange).*

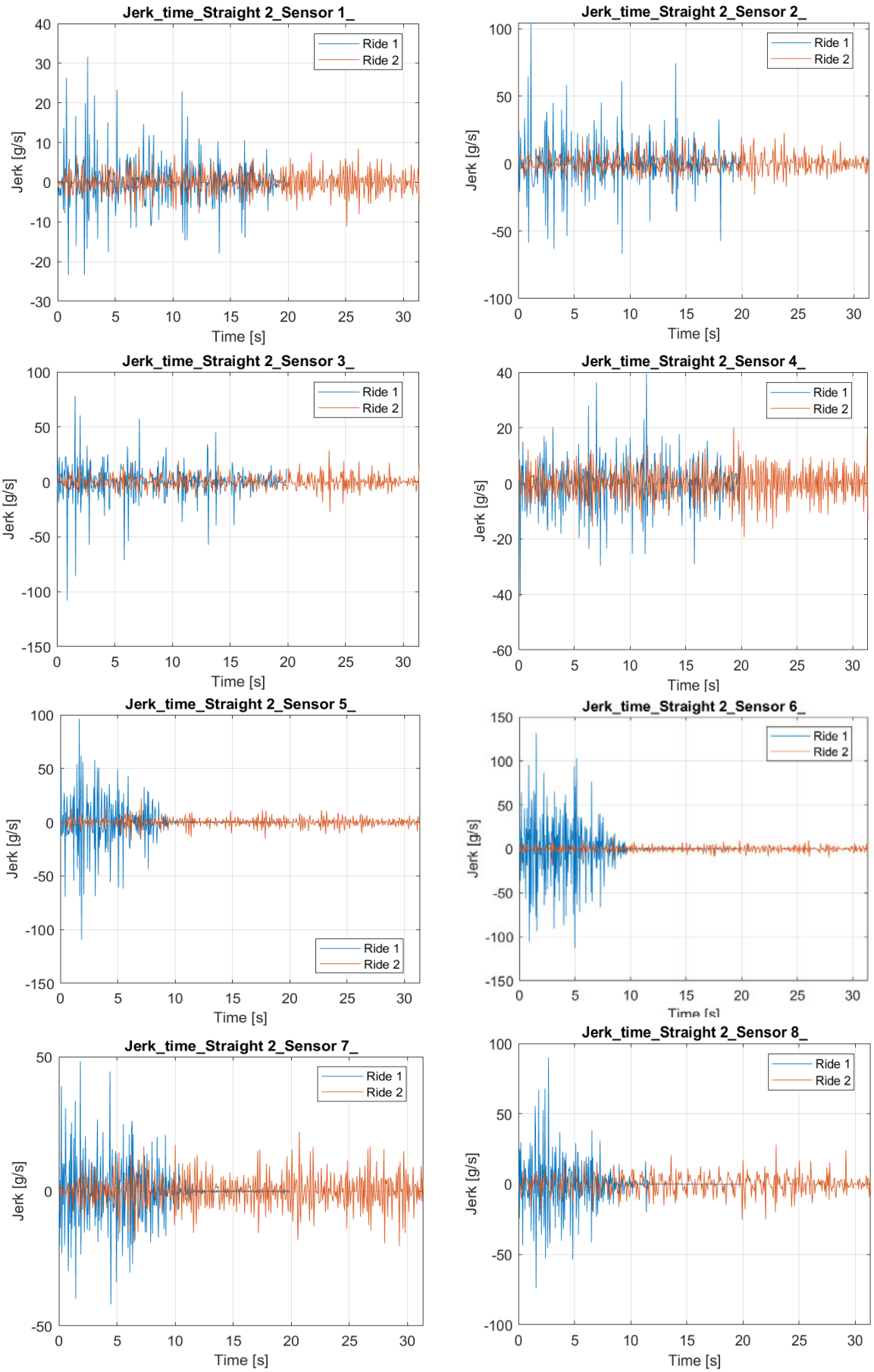

Fig. 5.22: *Straight 2 (time-aligned). Jerk time series (g/s) for S1–S8.*

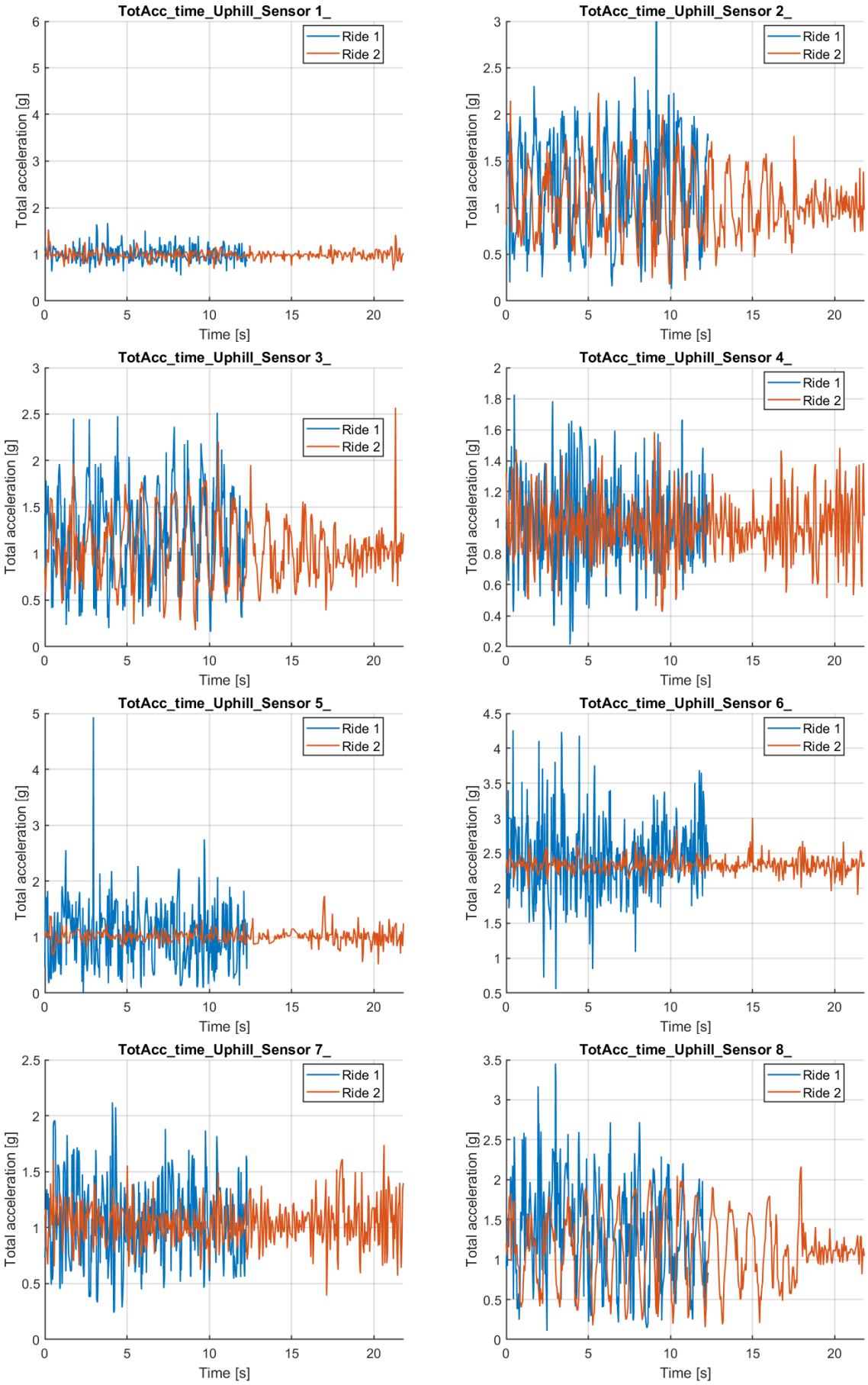

Fig. 5.23: *Uphill (time-aligned).* AccTot *time series for S1–S8 with Ride 1 (blue) and Ride 2 (orange).*

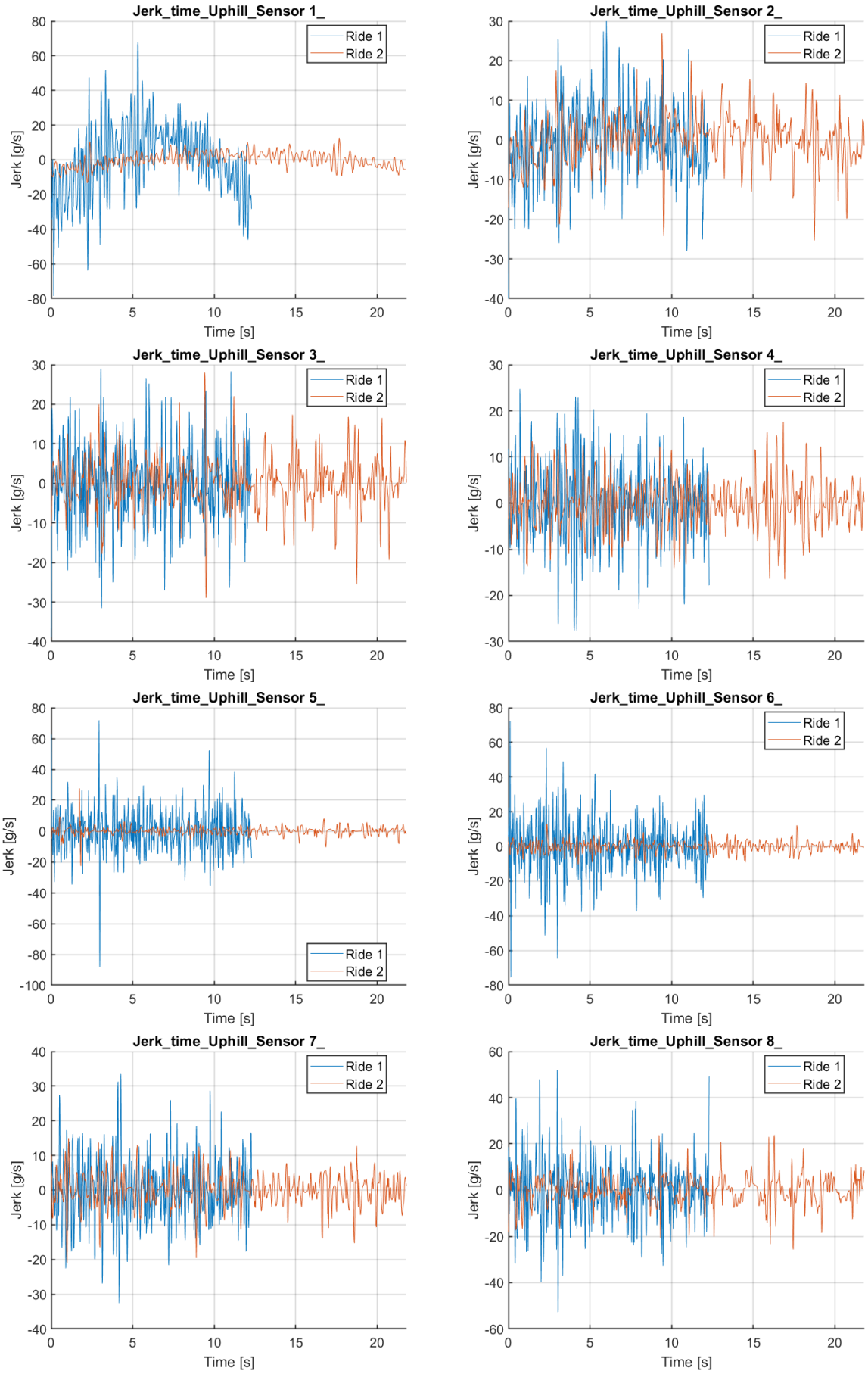

Fig. 5.24: *Uphill (time-aligned). Jerk time series (g/s) for S1–S8.*

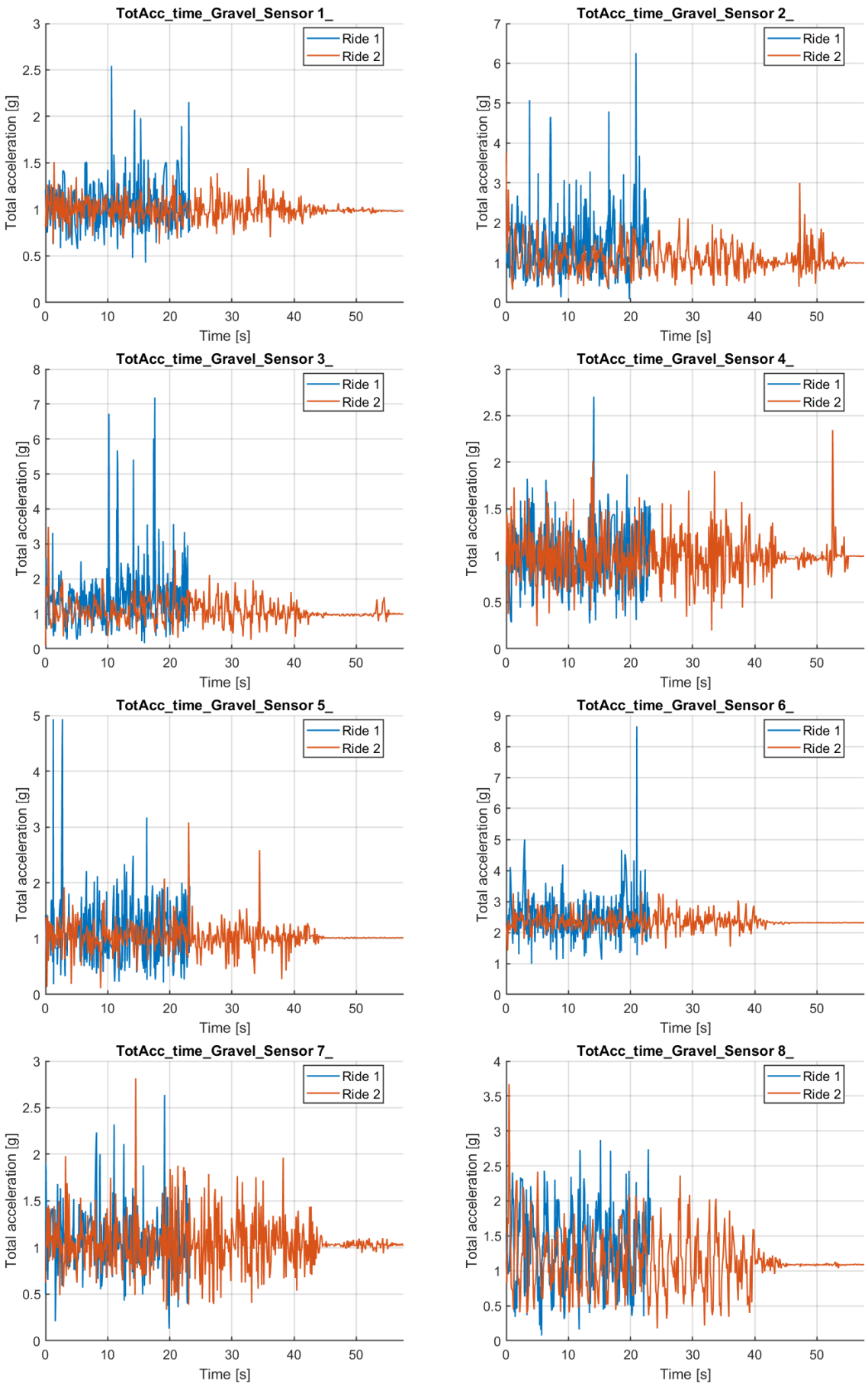

Fig. 5.25: *Gravel (time-aligned).* AccTot *time series for S1–S8 with Ride 1 (blue) and Ride 2 (orange).*

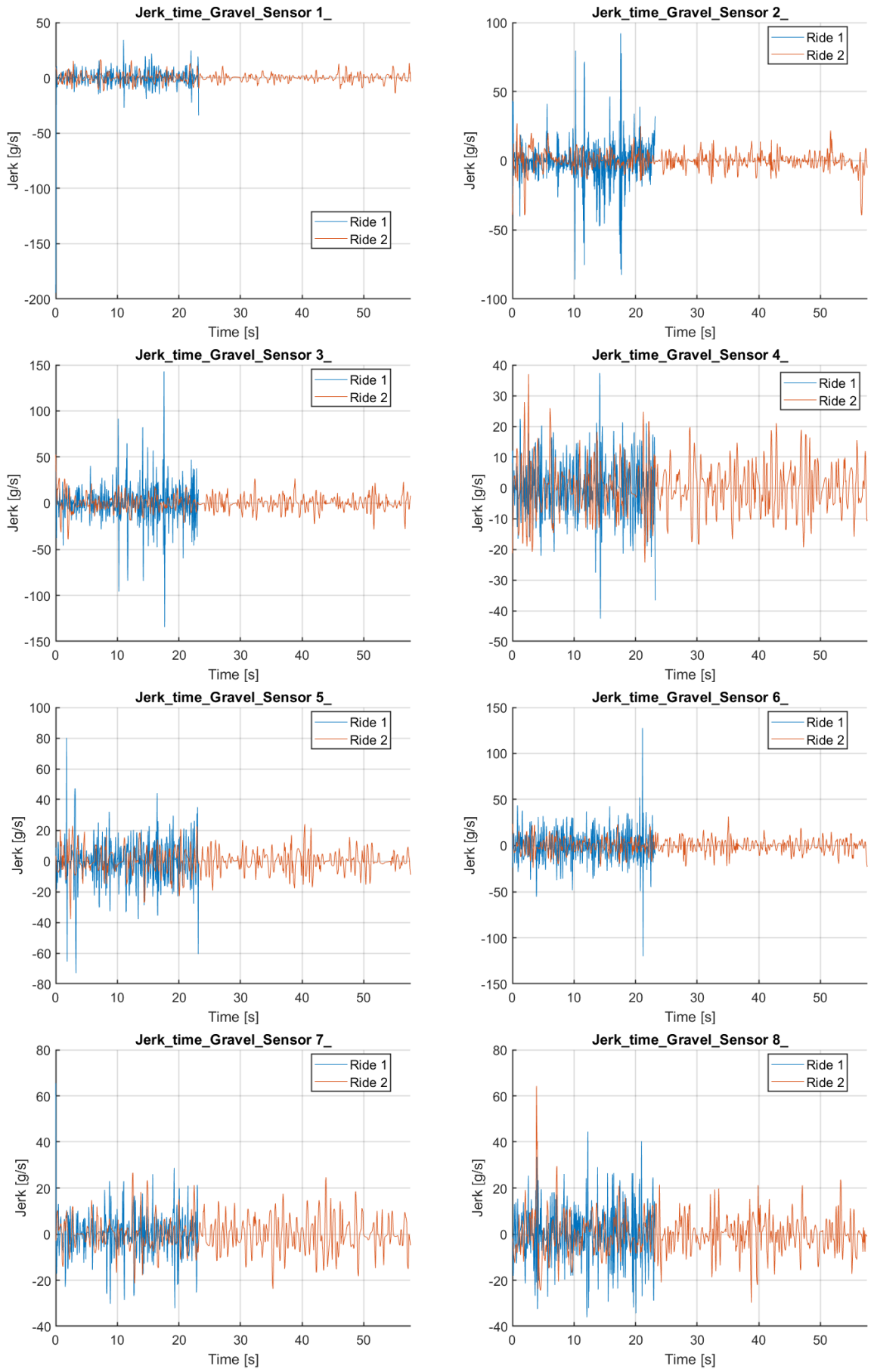

Fig. 5.26: *Gravel (time-aligned). Jerk time series (g/s) for S1–S8.*

Chapter 6

Discussion

The handbike, as an assistive, recreative and sporting device, stands at the intersection of engineering, health, and inclusivity [33, 9]. In this sense, quantitative analyses of vibration exposure and stability do not only address performance, but also contribute to broader goals of accessibility and safe mobility for people with disabilities, in line with international recommendations on inclusive transport and physical activity [34, 35].

This thesis contributes to bridging the gap between laboratory-based biomechanics and real-world performance evaluation [36, 25]. By validating the use of wearable sensors under field conditions, it demonstrates that quantitative vibration metrics, such as total acceleration and jerk, can serve as indicators of propulsion smoothness, mechanical stability, and comfort in outdoor handcycling. Moreover, the combination of distributed sensing and segment-wise analysis highlights that stability is not a single parameter but an emergent property of the whole rider-bike system, distributed along the input-transmission-control chain (wheel, backrest, upper limbs and steering) [16, 37].

From a broader perspective, the methodological principles established here are directly transferable to other domains such as wheelchair design [38], cycling ergonomics, and adaptive robotics. In rehabilitation, the same framework could support personalised feedback systems that encourage smoother, less fatiguing movement patterns, while in sports science it offers tools for monitoring performance evolution in field training [39, 40].

Building on the segment-wise percent-cycle results presented in subsection 5.4.2 and the time-aligned descriptors reported in subsection 5.4.3, the following subsections discuss the main findings, their relation to the vibrational model, and their methodological and practical implications.

6.1 Synthesis across the thesis

This thesis addressed handcycling comfort and performance through an integrated perspective combining (i) methodological validation of wearable sensing, (ii) simplified dynamic modeling for interpretability, and (iii) segment-wise field experimentation. The main contributions can be summarized as follows:

- **Measurement methodology:** a reproducible multi-IMU pipeline for outdoor hand-

cycling, including synchronization with GPS-based segmentation and the combined use of percent-cycle and time-aligned analyses.

- **Sensor placement implications:** empirical evidence that mounting conditions and local compliance (rigid structural nodes vs. soft-tissue interfaces) critically affect repeatability, informing both experimental protocols and future embedded monitoring solutions.
- **Interpretability via modeling:** a compact lumped-parameter model that supports a mechanistic reading of where vibration is generated, how it propagates, and which design parameters act as effective levers.
- **Field evidence:** segment-specific signatures of stability and harshness (variability and jerk) that distinguish straights, curves, uphill, and gravel, and localize the main control and transmission nodes along the rider–bike chain.

6.2 Design guidelines for handbike comfort, stability, and usability

Although the present work is exploratory, the combined evidence from bench validation, modeling, and field data suggests a set of practical guidelines that can support handbike design and setup when the goal is to reduce vibration exposure while preserving controllability:

1. **Treat the wheel–ground interface as the primary input node.** Tyre selection and pressure (and, where applicable, rim/tyre compliance) strongly shape the broadband content injected into the frame. Interventions at this interface are often the most effective way to reduce high-frequency excitation at the source.
2. **Control transmission at the seat/backrest interface.** The coupling between rider and frame governs whether road-induced motion is transmitted to the trunk or partially attenuated via compliant elements. Backrest/seat materials, geometry, and adjustability should be designed to balance isolation and control (excess compliance can increase relative motion and reduce perceived stability).
3. **Prioritize steering stability at the handle.** Distal interfaces (handle and wrists) are sensitive to micro-corrections. Design choices that reduce steering "chatter" (ergonomic grips, stiff/precise steering linkages, and vibration-aware handle interfaces) can reduce jerk bursts and vibrational exposure at the upper limbs.
4. **Design for posture-dependent damping.** Trunk stabilization strategies interact with mechanical transmission. Adjustable support that facilitates repeatable posture can reduce variability at the backrest and trunk sensors, particularly on technical or rough segments.

5. **Enable instrumented assessment.** From a measurement perspective, sensors mounted close to rigid structural anchors (wheel, frame, backrest) provide mechanically meaningful references; anatomical sensors remain valuable but require explicit acknowledgement of soft-tissue artefacts. These considerations support future smart-handbike concepts where vibration metrics can be monitored during training and rehabilitation.

6.3 Model-based interpretation of frequency-domain content

Within a simplified 3-DoF representation, the model provides a structured interpretation of the main frequency components observed in the measurements. In the low-frequency range, spectral content is expected to be dominated by the periodic propulsion and steering action. In the model, the prominence of these components at the rider coordinate x is primarily governed by the seat–rider coupling: increasing the interface stiffness k_s tends to enforce a tighter coupling between rider and frame, reducing the relative deformation at the interface, whereas a more compliant interface may attenuate part of the transmitted motion while allowing larger relative excursions.

At higher frequencies, broadband content is mainly influenced by tyre and frame-related properties. In particular, larger tyre stiffness values and lower tyre damping tend to increase the transmission of higher-frequency components from the road input to the frame coordinates. Conversely, increased dissipation (e.g., through c_1, c_2, and the interface term c_s) contributes to attenuating these components before they reach the rider coordinate. Overall, these trends are consistent with general principles of vibration transmissibility in seated human–vehicle systems and motivate the use of lumped-parameter models as interpretative tools.

From a methodological standpoint, the model acts as a bridge between the bench-based validation of sensor placement and the outdoor IMU analysis of Chapter 5. The AULM study showed that some sensor locations are intrinsically more repeatable than others; the vibrational model explains why certain locations, particularly those near structural anchors or rigid couplings, are also more predictable from a dynamic viewpoint. When both perspectives are combined, they support the design of sensor layouts that are not only repeatable but also mechanically meaningful.

The preliminary outdoor measurements used for nominal parameterization and qualitative comparison are necessarily limited in scope. They rely on a specific handbike model, a small number of riders, and a restricted set of surface conditions. Nevertheless, the fact that a simple 3-DoF model can reproduce the order of magnitude and qualitative structure of the main spectral features observed at the trunk and handle suggests that the dominant vibrational pathways in handcycling may be governed by relatively few parameters: tyre stiffness and damping, frame compliance, and the coupling between the seat and the rider. This has practical implications for both equipment design and training.

For designers, the model indicates that targeted modifications at the wheel and frame interface (e.g., tyre choice, rim design) and at the seat and backrest (e.g., materials, geometry, adjustability) can significantly alter the vibrational environment experienced by the rider, without necessarily changing global geometry. For coaches and clinicians, it suggests that posture adjustments and trunk stabilization strategies can be used as behavioural levers to modulate transmissibility, especially in rough or technical sections where comfort and stability are critical.

From a broader perspective, the model contributes to a shift from purely descriptive metrics (such as average accelerations) to a more structured understanding of how vibrations originate, propagate, and are perceived during handcycling. In combination with multi-IMU measurements and with the dual time and phase analysis adopted in Chapter 5, it supports the use of jerk and variability as interpretable indicators of control quality and mechanical stress.

6.4 Interpretation of field results (Chapter 5)

This section discusses the segment-wise field results of Chapter 5 in light of the methodological choices and of the simplified vibrational interpretation introduced above.

6.4.1 Interpretation of percent-cycle results

Percent-cycle normalization rescales each segment onto a common 0–100% progression axis, emphasizing the morphology of the acceleration field: the shape of the profiles, the relative timing of peaks and troughs, and the dispersion of the traces along the normalized segment progression. This view is particularly informative for identifying whether improvements reflect a more regular waveform morphology and smoother load distribution along the segment, or simply different pacing. [41].

Curves

In Curve 1, percent-cycle traces clearly distinguished the two control strategies. Ride 1 operated at higher mean total acceleration with substantially greater dispersion at nearly all instrumented sites, especially at the front wheel, backrest and wrists, where peaks frequently exceeded the 6-9 g range (Figure 5.4). Ride 2, by contrast, maintained lower means with markedly tighter envelopes across the cycle, with fewer sharp excursions and a more compact, quasi-periodic morphology (Figure 5.4). The observed reduction in variability along the normalized segment progression at mechanical and distal sites, combined with fewer impulsive transients, indicates a more economical and sustainable upper-limb locomotion.

Curve 2 isolates the upper-limb interface as the most stressed node of the system. In Ride 1 the wrists (S2, S3) recorded peak jerk values of 110 and 168 g/s respectively, the highest single-event impulsivity observed across the entire mixed-surface circuit, with standard deviations approximately five times higher than in Ride 2. The trunk (S1) and

the knee (S4) showed comparatively moderate increases (σ ratios of 2.7× and 1.7×), suggesting that the impulsive load is partially absorbed by the wrist–shoulder chain before propagating further along the kinematic chain. A transient acquisition malfunction on sensors S5–S8 during Ride 1 prevented the assessment of the rear and lower-limb chain in this segment; the available Ride 2 data on those sensors confirm a consistently low impulsive load (peaks below 30 g/s) and provide a baseline reference, but the asymmetry of the dataset on Curve 2 prevents a complete bilateral comparison for those channels.

Straights

Analysis of Straight 1 and Straight 2 reveals a shift from erratic to steady propulsion. During Ride 1, the data showed large fluctuations and sharp spikes at the front wheel and backrest, which also appeared to a lesser extent at the C7 vertebra and lower limbs. These irregular patterns suggest the rider was applying power unevenly and making frequent steering corrections. Ride 2 showed a much smoother pattern. The data profiles became narrower and more consistent, particularly at the bike's contact points, with fewer sharp peaks. At the wrists and handlebars, the readings remained within a tight band, indicating the rider applied constant force and kept the steering stable. Overall, this consistency suggests a more efficient riding style that places less stress on the body.

A more detailed inspection of Straight 2, in particular at the wrist-mounted sensors S2 and S3, suggested a possible functional asymmetry. Visual inspection of the percent-cycle traces (Figure 5.10) indicated that, for Rider 1, S2 displayed a more pronounced acceleration modulation in some portions of the segment, whereas S3 appeared comparatively steadier, despite similar summary statistics in Table 5.10. If confirmed by further analyses, this pattern would suggest that one hand acted as the primary driver of propulsion and speed modulation, while the contralateral hand mainly followed and stabilized the motion.

This asymmetry cannot be simply reduced to limb dominance. Straight 2 is gently curved to the right and the gear shifter is located on the right-hand side of the handbike, so steering corrections, chain-side loading, and local surface irregularities likely combine to allocate different roles to the two wrists. From a kinesiological perspective, such side- and segment-specific patterns underline the importance of going beyond global performance metrics and support the use of distributed IMUs to characterize how each upper limb contributes to propulsion and control in realistic conditions [11, 42].

Uphill

The uphill segment acted as a natural stress test for propulsion efficiency. Percent-cycle results confirmed that Uphill increased overall loads compared with the straights, but also magnified differences in control (Table 5.12). Ride 1 showed high mean and large dispersion at the front wheel and backrest, with irregular peaks spreading across the cycle and propagating to C7 and the wrists. Ride 2 reduced both the amplitude and dispersion of these normalized traces: the mechanical interfaces remained the most loaded sites, as expected on a climb, but their profiles were more compact and the number

of large excursions decreased (Figure 5.12). At anatomical sites, the narrowing of the envelopes indicated improved trunk stabilization and more consistent load transfer along the normalized segment progression, suggesting that coordinated trunk-backrest interaction can mitigate roughness exposure on inclines [43].

Gravel

On gravel, percent-cycle normalization showed the clearest contrast in morphology. Ride 1 displayed broad envelopes and frequent sharp excursions at the wheel, backrest, wrists and handle, consistent with unfiltered terrain-induced input superimposed on steering corrections (Table 5.14). Ride 2 drastically reduced dispersion at these sites: normalized traces converged around 1-2 g, with far fewer spikes, while proximal locations (C7, knee, leg) also narrowed (Figure 5.14). This global contraction of the normalized envelopes indicates that the female rider achieved both better line selection and improved damping along the mechanical chain, despite the inherently stochastic nature of the surface. The gravel segment therefore functions as a stringent test of the percent-cycle framework, confirming that morphology-based metrics can capture meaningful differences in stability under highly irregular excitation.

6.4.2 Interpretation of time-domain results

Percent cycle analysis focuses on the movement pattern itself, independent of duration. In contrast, the time-aligned approach maintains the original timing of the data. This allows us to detect speed changes, initial reactions when entering a section, and brief spikes that might be lost in a normalized view. Using both methods together ensures that we do not mistake slower riding or different starting speeds for actual improvements in technique.

Curves

For Curve 1, time-domain descriptors mirrored the percent-cycle results while adding crucial details on the magnitude of mechanical stress. Ride 1 exhibited an early burst followed by recurrent high-frequency surges throughout the arc; consequently, standard deviations at the wheel and backrest were over 500% higher than in Ride 2 (Table 5.15). The jerk analysis confirmed this harshness, with peak values exceeding 100 g/s at the mechanical interfaces. In contrast, Ride 2 showed a rapid stabilization after entry and maintained a steady state with significantly reduced impulsivity. This combination suggests that the strategy in Ride 2 not only smoothed the steering input but also effectively decoupled the frame from the road roughness, protecting the rider's hands from high-rate loading.

Curve 2 further highlighted the biomechanical implications of vibration management under lateral load. While mechanical sensor data for Ride 1 in this specific segment appeared attenuated (likely due to a logging anomaly, as confirmed by the near-zero standard deviations at S5–S8 in both the percent-cycle and time-aligned tables, Tables 5.6 and 5.17), the anatomical sensors provided unequivocal evidence of the stress experienced

by the rider. Ride 1 subjected the wrists (S2, S3) to extreme peak accelerations (> 8 g) and jerk values exceeding 90 g/s, indicative of a struggle to maintain control and stability. Ride 2, conversely, maintained wrist jerk below 25 g/s and reduced mean acceleration by over 50%. These differences persist even after accounting for pacing, supporting the interpretation that Ride 2 reflects a distinct, more stable control allocation rather than simple speed moderation.

Straights

Time-domain results for the straight sections emphasized the transition from a vibration-dominated to a steady propulsion regime. Straight 1 offered the starkest contrast: the front wheel sensor (S5) in Ride 1 registered a mean total acceleration of 1.81 gnearly double that of gravitywith impulsive peaks up to 14.0 g. This indicates a "rattling" regime where the wheel tracks the road profile with poor damping. Ride 2 successfully eliminated this vibrational offset, bringing the mean down to 1.02 g. Similarly, in Straight 2, the rear backrest (S6) exhibited a standard deviation approximately five times higher in Ride 1 compared to Ride 2. The reduction of jerk and impulsive content at these mechanical interfaces in Ride 2 is consistent with more continuous torque delivery and a stable chassis, implying a lower mechanical cost for the rider who does not need to dissipate this excess energy [44].

Uphill

Time-domain descriptors for the uphill segment confirmed that Ride 1 amplified impulsive behavior even under sustained, low-speed load. Although mean accelerations were comparable between laps (reflecting similar climbing speeds), the dispersion and jerk metrics revealed hidden instability. Ride 1 was characterized by sharp, high-frequency transients, with jerk peaks reaching 88 g/s at the wheel and 75 g/s at the backrest. Ride 2 smoothed these dynamics, keeping jerk peaks below 30 g/s. This shift towards a more stable, quasi-periodic propulsion pattern suggests that the more stable riding strategy facilitates smoother rolling and reinforced trunk stabilization, preventing the "micro-shocks" of the pedal stroke from destabilizing the bike's trajectory.

Gravel

The time-aligned analysis proved particularly revealing for the gravel section, serving as a stress test for transmissibility. Ride 1 exhibited frequent bursts at the wrists and backrest, with peak jerk values reaching 143 g/s at the right wrist (S3) and 128 g/s at the backrest (S6), consistent with poor isolation of the broadband stochastic input characteristic of loose surfaces. The backrest (S6) also showed a 170% increase in signal dispersion compared to Ride 2.

In contrast, Ride 2 markedly narrowed the amplitude envelope at most sites and showed fewer large jerk events at the main transmission nodes. Together, these findings indicate that Ride 2 provided better isolation on loose surfaces, limiting the propagation of wheel

input along the mechanical chain to the rider's spine and upper limbs. The main exception is the left handle (S8), where Ride 2 showed a higher isolated jerk peak than Ride 1, suggesting that local steering corrections may still occur even when the global vibration level is lower.

A technical caveat applies to the gravel segment analysis. In some trials, the time series indicated in orange (Ride 2) extends slightly beyond the phase of active movement, as the sensors recorded a few seconds of quasi-static posture before the acquisition was terminated. Although the segment limits were defined based on GPS coordinates to ensure geometric consistency, this inclusion effectively dilutes the relative weight of dynamic events in the time-aligned representation. However, the magnitude of the differences observedparticularly in peak jerk and standard deviationis too large to be an artifact of windowing alone, confirming the physical reality of the improved damping.

Interpreting time-domain descriptors across segments reveals a coherent picture. Rider 1 (Ride 1) achieved shorter lap times in some sections but incurred significantly higher peak accelerations and jerk values, particularly at the handle and backrest. In contrast, Rider 2 (Ride 2) exhibited moderate peaks and consistently lower jerk levels. From the perspective of energy and comfort, this trade-off supports the premise that the smoother profile of Ride 2 represents a more sustainable and mechanically efficient form of upper-limb propulsion, reducing the cumulative vibration dose absorbed by the athlete [2].

6.4.3 Linking vibrational modeling and experimental findings

The vibrational model developed in Chapter 4 was constructed as a reduced 3-DoF (Three degree of freedom) representation of the input, transmission, and control chain, explicitly distinguishing the wheel input, the backrest interface, and the steering and upper-limb node [16, 45]. Rather than reproducing the full complexity of the handbike, the goal was to capture the dominant modes of transmissibility and their frequency-dependent amplification or attenuation.

Experimental findings from the mixed-surface circuit confirm several qualitative predictions of this model. First, both model simulations and field data indicate that the front wheel and backrest act as primary concentrators of vertical vibration energy, with the steering and upper-limb node behaving as a partly damped continuation of this chain. In the model, changes in damping or stiffness at the backrest primarily affected mid-frequency transmissibility, while leaving low-frequency components linked to overall motion less altered. Experimentally, segments with improved trunk and backrest coupling (particularly Uphill and Gravel in Ride 2) showed reductions in dispersion and jerk at the backrest and handle, consistent with increased effective damping at that node [46, 47].

Second, the model suggested that small variations in posture or backrest angle could shift resonance peaks within the 5 to 15 Hz band, potentially moving them closer to or further from the main excitation frequencies associated with cadence and terrain irregularities. The time-domain results support this interpretation qualitatively: across segments, Ride 2 tended to exhibit more regular, quasi-periodic acceleration profiles with

reduced impulsive transients, while Ride 1 showed greater dispersion and more frequent high-amplitude bursts consistent with reduced effective damping and less controlled coupling.

Finally, the segment-wise comparison of curves, straights, uphill, and gravel illustrates how the simplified model can be used as a conceptual map for interpreting distributed IMU data. For the straight sections, the dominant pattern is consistent with predominantly vertical excitation and limited steering input, matching the model scenario of quasi-harmonic input at the wheel. During cornering and especially on gravel, additional lateral and torsional components are introduced, which in the experiments manifest as increased variability and roughness at the steering and upper-limb nodes. Although the model does not explicitly represent these degrees of freedom, the observed changes in vertical transmissibility at the three nodes follow the same qualitative trends predicted when additional input components or parameter changes are introduced in simulation [48]. In this sense, the model and the experimental data form a coherent picture: the former provides an interpretable framework for understanding how changes at one node propagate along the mechanical chain, while the latter validates that these mechanisms are observable under outdoor conditions.

6.4.4 Limitations and future perspectives

The interpretations presented in the preceding sections, regarding both percent-cycle and time-domain results as well as the link between modeling and experiments, must be considered in light of several limitations of the present work. However, these limitations also suggest meaningful avenues for future development.

Limitations of the literature review. The review of the state of the art was deliberately focused on vibration exposure, wheelchair and handbike dynamics, and IMU-based field assessment. As a consequence, other relevant strands of research, such as qualitative studies on user experience and the ergonomics of assistive devices in everyday mobility, represent valuable opportunities for future complementary investigations. In addition, the search strategy privileged peer-reviewed publications in English, which may have under-represented technical reports, institutional publications, and contributions from non-English-speaking communities. Future reviews could broaden the scope to include these sources and adopt more systematic search procedures, in order to provide a more comprehensive picture of how vibration, comfort, and accessibility are jointly addressed across disciplines.

Limitations of the vibrational model The mechanical-arm analysis, developed in Chapter 4, relied on a simplified vibrational representation with a reduced number of degrees of freedom and several linearity assumptions. While this choice allowed the main mechanisms of vertical transmissibility to be captured and related to measurable IMU quantities, it did not account for the full three-dimensional dynamics of the frame, the

nonlinear behaviour of tyres and soft tissues, or subject-specific variability in posture and muscle co-contraction. As a result, the model should be interpreted as a conceptual and exploratory tool rather than as a full predictive simulator of handbike dynamics. Future work could extend this representation by coupling it with finite-element or multibody models [49], and by calibrating the parameters against a larger set of experimental conditions, including different frames, backrest geometries, and surface types.

Limitations of the experimental handcycling study. The handcycling experiment presented in Chapter 5 involved two able-bodied participants with no prior handcycling experience (one male competitive cyclist, one female recreational cyclist), representing a specific user profile. Rather than providing definitive evidence for the broader handcycling community, this configuration should be regarded as a pilot study, primarily aimed at testing the feasibility of the current measurement protocol in mixed-surface outdoor conditions and at obtaining first estimates of variability and effect sizes. These estimates can in turn inform the calculation of an appropriate sample size for future, more extensive acquisition campaigns. The limited number and homogeneity of participants therefore constrain the generalisability of the present findings, and future studies should extend the protocol to larger cohorts, including athletes of different classes, levels of experience, and impairment profiles [50], to explore how anthropometry and functional ability influence vibration exposure and control strategies.

An additional, and partly unavoidable, source of variability in the present protocol is gear shifting. Riders were free to adjust the gear ratio within each segment according to perceived effort and comfort; consequently, cadence and effective mechanical load were not fully constrained and may have varied even within the same segment, especially on the climb and in the most technical portions of the track. From a methodological standpoint, reconstructing gear changes retrospectively from acceleration signals alone is not reliable, as it would require dedicated crank kinematics (e.g., continuous angular velocity at the cranks) or multi-step integration procedures that are prone to drift. For this reason, gear selection was not analysed explicitly and is instead acknowledged as a realistic but uncontrolled factor that may contribute to inter-rider and inter-segment differences. Future studies specifically targeting cadence or gearing effects should either fix the gear ratio for each segment or record gear changes synchronously with the IMU data [10, 51].

Certain practical issues also affected the raw signals. In isolated instances, indexing discrepancies, duplicated traces, or anomalously low-dispersion channels required additional data-quality checks. This was particularly relevant for the mechanical sensors in Curve 2 during Ride 1, where S5–S8 were interpreted as affected by a transient logging anomaly, and for selected jerk summaries in Straight 2, where some anatomical channels required cautious interpretation. These artifacts were either excluded from direct Ride 1/Ride 2 comparison or interpreted with appropriate caution, underscoring the importance of stringent quality control when managing multi-sensor outdoor datasets..

Finally, jerk metrics rely on derived quantities that are inherently sensitive to high-frequency noise. Although acceleration magnitude was low-pass filtered prior to numerical

differentiation, the selected cut-off represents a compromise between retaining task-relevant roughness-related components and attenuating spurious spikes. Different filter settings or alternative jerk formulations, such as those focusing solely on band-limited components, might alter absolute values, even if the relative trends between riders and segments remain stable. Furthermore, the present results derive from a single circuit of approximately 0.97 km, with moderate differences in mean speed between riders (about 12.5 and 14.8 km/h), which limits the immediate generalization of findings to other course typologies, speeds, or technical profiles.

Future perspectives: multi modal sensing and real-time feedback. While the present work relied exclusively on inertial data (accelerations, angular velocities, and derived quantities such as jerk), handcycling performance and comfort are inherently multidimensional phenomena. The integration of complementary physiological signals, such as electromyography [52] or cardiopulmonary measures [53], would provide a richer description of how mechanical and metabolic efficiency interact. This could help disentangle whether smoother propulsion is achieved primarily through mechanical optimization, neuromuscular adaptation, or energy redistribution between muscle groups. In particular, monitoring muscles directly involved in propulsion and stabilization (e.g., deltoids, pectoralis major, triceps, and trunk extensors) could reveal whether reductions in jerk and variability correspond to lower co-contraction demands or are achieved at the expense of higher stabilizing effort.

Another important direction lies in the evolution from post-processed analysis to real-time feedback. The methods and metrics developed throughout this thesis lend themselves to implementation in embedded systems or smart handbikes capable of monitoring vibration exposure during use. Transforming IMU data into immediate feedback (visual, auditory, or haptic) could support training, rehabilitation, and self-regulation, allowing users to perceive and correct instability as it occurs [54, 55]. Such systems are closely related to the logic of active-assistive rehabilitation devices, in which sensors and actuators are integrated into a closed-loop controller that continuously adapts the assistance level to the user's state [56].

Future perspectives: modelling and design implications. At the modeling level, the vibrational representation proposed in Chapter 4 can serve as a foundation for more advanced computational simulations. By coupling the simplified three-degree-of-freedom model with finite-element or multibody dynamic models, future research could investigate how specific frame geometries, damping materials, tyre characteristics, or posture adjustments modify transmissibility and comfort [57]. The combination of modeling and wearable data would enable a virtuous cycle of prediction, validation, and design refinement, with direct implications for the engineering of handbikes and related assistive devices.

Finally, the methodological principles and findings of this work can be extended beyond sport and rehabilitation. The same ideas of vibration attenuation, distributed sensing, and individualized feedback are relevant for urban mobility, adaptive cycling, and the

design of open-source monitoring platforms that democratize access to performance and comfort data [58]. In this broader perspective, the handbike becomes a case study for mobility systems that are both technically optimized and socially inclusive, in line with the Sustainable Development Goals on health and reduced inequalities (SDG 3 and SDG 10).

Chapter 7

Conclusions

Overview and Integration of Results

This doctoral thesis has explored the dynamics of handcycling from a multidisciplinary perspective that integrates biomechanics, vibration analysis, and wearable sensing. The overarching objective was to develop and validate a methodological and analytical framework capable of quantifying how vibrations and accelerations propagate through the handbikerider system, linking mechanical behavior to performance and comfort.

The research unfolded through a progressive sequence of studies, each addressing a specific layer of this complex system:

- **Chapter 2** provided a comprehensive overview of the scientific literature on handbikes, reviewing their main architectures, propulsion strategies, and actuation modes. This systematic analysis delineated the state of the art and revealed significant gaps in measurement standardization, vibration assessment, and in-field validity [9]. It also established the conceptual taxonomy of clinical, mechanical, and actuation domains that later guided data collection and interpretation [33].

- **Chapter 3** addressed the first methodological challenge: identifying reliable configurations for inertial measurement units (IMUs). Through controlled testing on an Artificial Upper Limb Mechanism (AULM), the study isolated the influence of sensor placement on signal repeatability, demonstrating that proximal sitessuch as the crank or trunkprovide more consistent readings than distal ones [25]. This validation phase laid the foundation for robust and reproducible acquisition in human experiments [12].

- **Chapter 4** advanced the analytical side of the work by introducing a simplified vibrational model of the handbikerider system. The model treated the frame, seat, and rider as coupled masses connected by elastic and damping elements, enabling a quantitative description of how surface-induced excitations propagate through the structure [16]. This representation provided the theoretical basis for interpreting IMU signals in terms of transmissibility, damping, and frequency-dependent vibration propagation [45].

- **Chapter 5** represented the culmination of the experimental effort. Using the validated IMU configuration, data were collected during two laps on a mixed-surface circuit and analyzed through a dual framework combining percent-cycle normalization and time-aligned comparison. The results revealed an overall reduction in variability, peak amplitude, and jerk in Ride 2 relative to Ride 1, especially at the main mechanical interfaces, suggesting smoother propulsion, reduced vibrational harshness, and more stable control. Segment-wise interpretation highlighted marked improvements on the straight and uphill sections, while corneringespecially Curve 2remained the most critical phase in terms of stability, steering corrections, and upper-limb impulsivity [59]. These findings confirmed the potential of distributed IMU sensing for field-based assessment of real-world handcycling.

Taken together, these four studies form a coherent trajectory: from a theoretical review, through methodological validation and modeling, to full-scale outdoor experimentation. Each phase informed the next, demonstrating that accurate vibration assessment in handcycling requires not only precise instrumentation but also a clear theoretical model and context-specific interpretation.

Scientific and Practical Contributions

The integrated outcomes of this research contribute to both the scientific understanding of handcycling and its practical applications:

1. **Methodological validation.** The thesis established a reproducible framework for IMU-based measurement in upper-limb propulsion tasks, identifying robust and mechanically meaningful sensor sites, synchronization protocols, and preprocessing steps [60]. These methods can be generalized to other assistive devices or adaptive sports.

2. **Analytical modeling.** The proposed vibrational model linked measurable accelerations to mechanical parameters, offering a bridge between field data and theoretical predictions [48]. It supports the interpretation of IMU signals in terms of transmissibility, damping, and mechanical coupling between the rider and the handbike.

3. **Design and rehabilitation implications.** The findings suggest that vibration attenuation at the backrest and handle interfaces, optimized seating geometry, and smoother propulsion strategies may help reduce mechanical stress and potentially limit fatigue-related demands [61, 62]. These insights can inform the design of future handbike frames, damping systems, and training protocols for users with spinal cord injuries [46].

Limitations and Future Directions

The scope and generalisability of the present findings are constrained by the small number of participants, the use of a single handbike model, and the reliance on inertial data alone. In addition, isolated data-quality issues, including transient logging anomalies and selected jerk summaries requiring cautious interpretation, further underline the need for stringent quality-control procedures in future multi-sensor field studies. These limitations, together with the perspectives opened by multimodal sensing, real-time feedback, and advanced modeling, are discussed in detail in Chapter 6.

A second limitation concerns the nature of the measured quantities. While the present work relied exclusively on inertial dataaccelerations, angular velocities, and derived quantities such as jerkhandcycling performance and comfort are inherently multi-dimensional phenomena. The integration of complementary physiological signals, such as electromyography or cardiopulmonary measures, would provide a richer description of how mechanical and metabolic efficiency interact [52, 63]. This multimodal approach could help identify whether smoother propulsion is achieved primarily through mechanical optimization, neuromuscular adaptation, or energy redistribution between muscle groups [64].

Another important direction lies in the evolution from post-processed analysis to real-time feedback. The methods and metrics developed throughout this thesis lend themselves to implementation in embedded systems or smart handbikes capable of monitoring vibration exposure during use. Transforming IMU data into immediate feedbackvisual, auditory, or hapticcould support training, rehabilitation, and self-regulation, allowing users to perceive and correct instability as it occurs [54, 65]. Such systems would embody the idea of closed-loop rehabilitation, where measurement and correction coexist seamlessly within the same device [56].

At the modeling level, the vibrational representation proposed in Chapter 4 can serve as a foundation for more advanced computational simulations. By coupling the simplified three-degree-of-freedom model with finite element or multibody dynamic models, future research could investigate how specific frame geometries, damping materials, or posture adjustments modify transmissibility and comfort [66, 67]. The combination of modeling and wearable data would enable a virtuous cycle of prediction, validation, and design refinement.

Finally, this work points toward a broader, societal perspective. The handbike, as an assistive and sporting device, stands at the intersection of engineering, health, and inclusivity [33]. The principles derived from this researchvibration attenuation, distributed sensing, and individualized feedbackcan contribute to the design of safer and more accessible mobility systems, in line with the Sustainable Development Goals (SDG 3 and SDG 10) [35]. Future developments may therefore extend beyond sport and rehabilitation, encompassing urban mobility, adaptive cycling, and open-source monitoring platforms that democratize access to performance data for all users.

Final Remarks

The research presented in this thesis demonstrates that the analysis of handcycling can no longer rely solely on controlled laboratory tests or descriptive observation. By combining validated sensing methods, analytical modeling, and real-world experimentation, it has been possible to capture the complex interaction between rider and handbike under realistic conditions. The methodological framework developed here provides a replicable pathway—from sensor placement to data interpretation—that can support both scientific inquiry and applied practice.

More broadly, the methodological principles established hereреliability of wearable data, transparency of preprocessing, and biomechanical interpretation of inertial metricsare directly transferable to domains such as wheelchair design, cycling ergonomics, and adaptive robotics. In rehabilitation, the same framework could support personalized feedback systems, while in sports science it offers tools for monitoring performance evolution under field conditions.

The handbike stands at the intersection of engineering, health, and inclusivity. By connecting biomechanics, design, and user-oriented performance through the lens of vibration and variability, this work opens the way to future applications in customized rehabilitation, adaptive coaching, and inclusive engineering—in line with the Sustainable Development Goals on health and reduced inequalities (SDG 3 and SDG 10).

In conclusion, this thesis builds a coherent bridge from theory to practice: from the taxonomy of handbike systems, through methodological and analytical development, to real-world application. It provides not only new insights into the dynamics of handcycling but also a solid foundation for a new generation of vibration-aware, data-driven approaches to adaptive mobility and sport.

Bibliography

[1] A. J. Dallmeijer et al. “Submaximal physical strain and peak performance in handcycling versus handrim wheelchair propulsion”. In: *Spinal Cord* 42.2 (Feb. 2004), pp. 91–98. ISSN: 13624393. DOI: 10.1038/sj.sc.3101566.

[2] U Arnet et al. “Shoulder load during handcycling at different incline and speed conditions”. English. In: (2012). ISSN: 02680033. DOI: 10.1016/j.clinbiomech.2011.07.002. URL: https://www.scopus.com/inward/record.uri?eid=2-s2.0-84655167549%7B%5C&%7Ddoi=10.1016%7B%5C%%7D2Fj.clinbiomech.2011.07.002%7B%5C&%7DpartnerID=40%7B%5C&%7Dmd5=dc7fc2d025b8c2ff56c6fb0fdaed1dfc.

[3] T. Abel et al. “Performance diagnostics in handbiking during competition”. In: *Spinal Cord* 44.4 (2006), pp. 211–216. ISSN: 14765624. DOI: 10.1038/sj.sc.3101845.

[4] I Rice. “Recent Salient Literature Pertaining to the Use of Technology in Wheelchair Sports”. English. In: (2016). ISSN: 21674833. DOI: 10.1007/s40141-016-0141-6. URL: https://www.scopus.com/inward/record.uri?eid=2-s2.0-85047817571%7B%5C&%7Ddoi=10.1007%7B%5C%%7D2Fs40141-016-0141-6%7B%5C&%7DpartnerID=40%7B%5C&%7Dmd5=0677ba6462033ccb58def8d382fbbd05.

[5] J L Flueck. “Nutritional considerations for para-cycling athletes: A narrative review”. English. In: (2021). ISSN: 20754663. DOI: 10.3390/sports9110154. URL: https://www.scopus.com/inward/record.uri?eid=2-s2.0-85120157413%7B%5C&%7Ddoi=10.3390%7B%5C%%7D2Fsports9110154%7B%5C&%7DpartnerID=40%7B%5C&%7Dmd5=2157aebf88ca72a81dc1d97974679392.

[6] G T Goodlin et al. “Adaptive Cycling: Classification, Adaptations, and Biomechanics”. English. In: (2022). ISSN: 10479651. DOI: 10.1016/j.pmr.2021.08.003. URL: https://www.scopus.com/inward/record.uri?eid=2-s2.0-85117382101%7B%5C&%7Ddoi=10.1016%7B%5C%%7D2Fj.pmr.2021.08.003%7B%5C&%7DpartnerID=40%7B%5C&%7Dmd5=da6a4b96d3ccfafe13df020bf7add3a4.

[7] L. H.V. Van Der Woude et al. “Active LifestyLe Rehabilitation Interventions in aging Spinal Cord injury (ALLRISC): A multicentre research program”. In: *Disabil. Rehabil.* 35.13 (2013), pp. 1097–1103. ISSN: 09638288. DOI: 10.3109/09638288.2012.718407.

[8] C F J Nooijen et al. “A behavioural intervention increases physical activity in people with subacute spinal cord injury: A randomised trial”. English. In: (2016). ISSN: 18369553. DOI: 10.1016/j.jphys.2015.11.003. URL: https://www.scopus.com/inward/record.uri?eid=2-s2.0-84950124442%7B%5C&%7Ddoi=10.1016%

7B%5C%%7D2Fj.jphys.2015.11.003%7B%5C&%7DpartnerID=40%7B%5C&%7Dmd5=43fee594fd948f61732504e8bec02893.

[9] Michele Sanguinetta et al. "Handbike for Daily Use, Sport, and Rehabilitation Purposes: A Literature Review of Actuation and Technical Characteristics". In: *Actuators* 13.2 (2024).

[10] Cassandra Kraaijenbrink et al. "Different cadences and resistances in submaximal synchronous handcycling in able-bodied men: Effects on efficiency and force application". In: *PLoS One* 12.8 (Aug. 2017). ISSN: 19326203. DOI: 10.1371/journal.pone.0183502.

[11] C Kraaijenbrink et al. "Steering Does Affect Biophysical Responses in Asynchronous, but Not Synchronous Submaximal Handcycle Ergometry in Able-Bodied Men". English. In: (2021). ISSN: 26249367. DOI: 10.3389/fspor.2021.741258. URL: https://www.scopus.com/inward/record.uri?eid=2-s2.0-85124505503%7B%5C&%7Ddoi=10.3389%7B%5C%%7D2Ffspor.2021.741258%7B%5C&%7DpartnerID=40%7B%5C&%7Dmd5=47ed5b5713d64ef3acdd55964f2ce319.

[12] Michele Sanguinetta, Giovanni Incerti, and Giovanni Legnani. "Handcycling Assessment Through a Bench Simulator: Preliminary Analysis of IMUs Positioning on an Artificial Upper Limb Mechanism (AULM)". In: *Mechanisms and Machine Science*. Vol. 164. 2024, pp. 538–545.

[13] M. J. Griffin. *Handbook of Human Vibration*. Academic Press, 1990.

[14] S. Kitazaki and M. J. Griffin. "A modal analysis of whole-body vertical vibration, using a finite element model of the human body". In: *Journal of Sound and Vibration* 200.1 (1997), pp. 83–103.

[15] S. Kitazaki and M. J. Griffin. "Resonance behaviour of the seated human body and effects of posture". In: *Journal of Biomechanics* 31 (1998), pp. 143–149.

[16] Michele M. Sanguinetta et al. "Handbike and Handcyclist: A Vibrational Model". In: *Mechanisms and Machine Science*. Vol. 179. nan. 2025, pp. 301–309.0. DOI: 10.1007/978-3-031-91151-4_34.

[17] T. P. Gunston, J. Rebelle, and M. J. Griffin. "A comparison of two methods of simulating seat suspension dynamic performance". In: *Journal of Sound and Vibration* 278 (2004), pp. 117–134.

[18] Gabrielle T. G.T. Goodlin et al. "Adaptive Cycling: Classification, Adaptations, and Biomechanics". In: *Physical Medicine and Rehabilitation Clinics of North America* 33.1 (2022), pp. 31–43.0. DOI: 10.1016/j.pmr.2021.08.003.

[19] Jonpaul J. Nevin et al. "The Science of Handcycling: A Narrative Review". In: *International Journal of Sports Physiology and Performance* 17.3 (2022), pp. 335–342.0. DOI: 10.1123/ijspp.2021-0458.

[20] Ben Thomas B.T. Stephenson et al. “Physiology of handcycling: A current sports perspective”. In: *Scandinavian Journal of Medicine and Science in Sports* 31.1 (2021), pp. 4–20.0. DOI: 10.1111/sms.13835.

[21] Cassandra C. Kraaijenbrink et al. “Biophysical aspects of handcycling performance in rehabilitation, daily life and recreational sports; a narrative review”. In: *Disability and Rehabilitation* 43.24 (2021), pp. 3461–3475.0. DOI: 10.1080/09638288.2020.1815872.

[22] Michele M. Sanguinetta et al. “Handbike for Daily Use, Sport, and Rehabilitation Purposes: A Literature Review of Actuation and Technical Characteristics”. In: *Actuators* 13.2 (2024). DOI: 10.3390/act13020050.

[23] Ulric Sena U.S. Abonie et al. “Effect of a 7-week low intensity synchronous handcycling training programme on physical capacity in abled-bodied women”. In: *Journal of Sports Sciences* 39.13 (2021), pp. 1472–1480.0. DOI: 10.1080/02640414.2021.1880171.

[24] Michael John M.J. Hutchinson et al. “Comparison of two Borg exertion scales for monitoring exercise intensity in able-bodied participants, and those with paraplegia and tetraplegia”. In: *Spinal Cord* 59.11 (2021), pp. 1162–1169.0. DOI: 10.1038/s41393-021-00642-4.

[25] Michele M. Sanguinetta, Giovanni G. Incerti, and Giovanni G. Legnani. “Handcycling Assessment Through a Bench Simulator: Preliminary Analysis of IMUs Positioning on an Artificial Upper Limb Mechanism (AULM)”. In: *Mechanisms and Machine Science*. Vol. 164 MMS. nan. 2024, pp. 538–545.0. DOI: 10.1007/978-3-031-64569-3_61.

[26] Thomas T. Abel et al. “Energy expenditure in wheelchair racing and handbiking - a basis for prevention of cardiovascular diseases in those with disabilities”. In: *European Journal of Preventive Cardiology* 10.5 (2003), pp. 371–376.0. DOI: 10.1097/01.hjr.0000096542.30533.59.

[27] Thomas T. Abel et al. “Performance diagnostics in handbiking during competition”. In: *Spinal Cord* 44.4 (2006), pp. 211–216.0. DOI: 10.1038/sj.sc.3101845.

[28] Thomas T. Abel et al. “The exercise profile of an ultra-long handcycling race: The Styrkeprøven experience”. In: *Spinal Cord* 48.12 (2010), pp. 894–898.0. DOI: 10.1038/sc.2010.40.

[29] Thomas T. Abel et al. “Effect of three different grip angles on physiological parameters during laboratory handcycling test in able-bodied participants”. In: *Frontiers in Physiology* 6.NOV (2015). DOI: 10.3389/fphys.2015.00331.

[30] Thomas T. Fuglsang et al. “Development and testing of a novel arm cranking-powered watercraft”. In: *Frontiers in Physiology* 8.AUG (2017). DOI: 10.3389/fphys.2017.00635.

[31] Lucas H.V. L.H. van der Woude et al. “Wheeled mobility: An ergonomics perspective”. In: *Assistive Technology Research Series*. Vol. 29. nan. 2011, pp. 728–736.0. DOI: 10.3233/978-1-60750-814-4-728.

[32] Giovanni G. Legnani et al. “An identification procedure for evaluating the dynamic parameters of the upper limbs during handcycling”. In: vol. 5A-2018. nan. 2018. DOI: 10.1115/DETC201885290.

[33] C Kraaijenbrink et al. “Biophysical aspects of handcycling performance in rehabilitation, daily life and recreational sports; a narrative review”. English. In: (2021). ISSN: 09638288. DOI: 10.1080/09638288.2020.1815872. URL: https://www.scopus.com/inward/record.uri?eid=2-s2.0-85090499868%7B%5C&%7Ddoi=10.1080%7B%5C%%7D2F09638288.2020.1815872%7B%5C&%7DpartnerID=40%7B%5C&%7Dmd5=c2b39fd6a229acaf93db3646b70f84f0.

[34] Fiona C. Bull et al. “World Health Organization 2020 guidelines on physical activity and sedentary behaviour”. In: *British Journal of Sports Medicine* 54.24 (2020), pp. 1451–1462.

[35] K Hickman. “Disabled cyclists in England: Imagery in policy and design”. English. In: (2016). ISSN: 17550793. DOI: 10.1680/udap.14.00048. URL: https://www.scopus.com/inward/record.uri?eid=2-s2.0-84967167596%7B%5C&%7Ddoi=10.1680%7B%5C%%7D2Fudap.14.00048%7B%5C&%7DpartnerID=40%7B%5C&%7Dmd5=4fd70f63e8cf3a9bd8193a583cdd83ac.

[36] B Stone et al. “Elite handcycling: a qualitative analysis of recumbent handbike configuration for optimal sports performance”. English. In: (2019). ISSN: 00140139. DOI: 10.1080/00140139.2018.1531149. URL: https://www.scopus.com/inward/record.uri?eid=2-s2.0-85059915804%7B%5C&%7Ddoi=10.1080%7B%5C%%7D2F00140139.2018.1531149%7B%5C&%7DpartnerID=40%7B%5C&%7Dmd5=90eb5573e95a8b65d9f3edb3daa81757.

[37] Ghazaleh G. Azizpour et al. “Dynamic analysis of handcycling: Mathematical modelling and experimental tests”. In: *Mechanisms and Machine Science*. Vol. 47. nan. 2017, pp. 33–40.0. DOI: 10.1007/978-3-319-48375-7_4.

[38] Rory A. R.A. Cooper, Rosemarie M. R.M. Cooper, and Adam James A.J. Susmarski. “Wheelchair sports technology and biomechanics”. In: vol. nan. nan. Springer International Publishing, 2024, pp. 23–34.0. DOI: 10.1007/978-3-031-44285-8_2.

[39] S Zeller, T Abel, and H K Strueder. “Monitoring training load in handcycling: A case study”. English. In: (2017). ISSN: 10648011. DOI: 10.1519/JSC.0000000000001786. URL: https://www.scopus.com/inward/record.uri?eid=2-s2.0-85044169446%7B%5C&%7Ddoi=10.1519%7B%5C%%7D2FJSC.0000000000001786%7B%5C&%7DpartnerID=40%7B%5C&%7Dmd5=b7855600bb6fbe36e9e7fb7e8f725859.

[40] J Nevin and P M Smith. "The anthropometric, physiological, and strength-related determinants of handcycling 15-km time-trial performance". English. In: (2021). ISSN: 15550265. DOI: 10.1123/IJSPP.2019-0861. URL: https://www.scopus.com/inward/record.uri?eid=2-s2.0-85101268174%7B%5C&%7Ddoi=10.1123%7B%5C%%7D2FIJSPP.2019-0861%7B%5C&%7DpartnerID=40%7B%5C&%7Dmd5=cf931737fec0c39216a2cdc5feaaea38.

[41] J Verellen et al. "Consistency of within-cycle torque distribution pattern in hand cycling". English. In: (2008). ISSN: 07487711. DOI: 10.1682/JRRD.2007.12.0205. URL: https://www.scopus.com/inward/record.uri?eid=2-s2.0-65949095880%7B%5C&%7Ddoi=10.1682%7B%5C%%7D2FJRRD.2007.12.0205%7B%5C&%7DpartnerID=40%7B%5C&%7Dmd5=0172f957482d9a96fe23924731a72923.

[42] P Meyns et al. "Coordinating arms and legs on a hybrid rehabilitation tricycle: The metabolic benefit of asymmetrical compared to symmetrical arm movements". English. In: (2014). ISSN: 14396319. DOI: 10.1007/s00421-013-2814-5. URL: https://www.scopus.com/inward/record.uri?eid=2-s2.0-84896491928%7B%5C&%7Ddoi=10.1007%7B%5C%%7D2Fs00421-013-2814-5%7B%5C&%7DpartnerID=40%7B%5C&%7Dmd5=8300250892cdb73f9b05880761011cce.

[43] R Muchaxo et al. "A Role for Trunk Function in Elite Recumbent Handcycling Performance?" English. In: (2021). ISSN: 02640414. DOI: 10.1080/02640414.2021.1930684. URL: https://www.scopus.com/inward/record.uri?eid=2-s2.0-85107508061%7B%5C&%7Ddoi=10.1080%7B%5C%%7D2F02640414.2021.1930684%7B%5C&%7DpartnerID=40%7B%5C&%7Dmd5=c3447cebd585d7538c2ef2ad1105a7e8.

[44] W G Groen, L H V Van Der Woude, and J J De Koning. "The power balance model: Useful in the study of elite handcycling performance". English. In: (2010). Ed. by Hettinga F J Hoekstra F Bijker K E Janssen T W J Houdijk J H P Dekker R van Aanholt P C T van der Woude L.H.V. de Groot S. ISSN: 1383813X. DOI: 10.3233/978-1-60750-080-3-85. URL: https://www.scopus.com/inward/record.uri?eid=2-s2.0-84865412295%7B%5C&%7Ddoi=10.3233%7B%5C%%7D2F978-1-60750-080-3-85%7B%5C&%7DpartnerID=40%7B%5C&%7Dmd5=c7f40beadc7a9fa5b55da4fa7a6117fb.

[45] G Azizpour et al. "Dynamic analysis of handcycling: Mathematical modelling and experimental tests". English. In: (2017). Ed. by Boschetti G Gasparetto A. ISSN: 22110984. DOI: 10.1007/978-3-319-48375-7_4. URL: https://www.scopus.com/inward/record.uri?eid=2-s2.0-84996931934%7B%5C&%7Ddoi=10.1007%7B%5C%%7D2F978-3-319-48375-7%7B%5C_%7D4%7B%5C&%7DpartnerID=40%7B%5C&%7Dmd5=5aecdc90d6580815474a7e9bccba8727.

[46] U. Arnet et al. "The effect of crank position and backrest inclination on shoulder load and mechanical efficiency during handcycling". In: *Scand. J. Med. Sci. Sport.* 24.2 (2014), pp. 386–394. ISSN: 16000838. DOI: 10.1111/j.1600-0838.2012.01524.x.

[47] S Litzenberger, F Mally, and A Sabo. "Biomechanics of elite recumbent handcycling: a case study: Influence of backrest position, crank length and crank height on muscular activity and upper body kinematics". English. In: (2016). ISSN: 13697072. DOI: 10.1007/s12283-016-0206-x. URL: https://www.scopus.com/inward/record.uri?eid=2-s2.0-84966549623%7B%5C&%7Ddoi=10.1007%7B%5C%%7D2Fs12283-016-0206-x%7B%5C&%7DpartnerID=40%7B%5C&%7Dmd5=42119a7bd96f65b367d986c121b4e5b7.

[48] G Legnani et al. "An identification procedure for evaluating the dynamic parameters of the upper limbs during handcycling". English. In: American Society of Mechanical Engineers (ASME), 2018. ISBN: 9780791851807. DOI: 10.1115/DETC201885290. URL: https://www.scopus.com/inward/record.uri?eid=2-s2.0-85057016977%7B%5C&%7Ddoi=10.1115%7B%5C%%7D2FDETC201885290%7B%5C&%7DpartnerID=40%7B%5C&%7Dmd5=1abd6f072d973fd6c0d1e57e5b20741c.

[49] E.-M. Felsner et al. "Musculoskeletal Modelling of Elite Handcycling Motion: Evaluation of Muscular On-and Offset". English. In: ed. by Jansen A.J. Elsevier Ltd, 2016. DOI: 10.1016/j.proeng.2016.06.208. URL: https://www.scopus.com/inward/record.uri?eid=2-s2.0-84983006922%7B%5C&%7Ddoi=10.1016%7B%5C%%7D2Fj.proeng.2016.06.208%7B%5C&%7DpartnerID=40%7B%5C&%7Dmd5=e2ea17cae81c1dd9eb6127f391fdc54d.

[50] B T Stephenson et al. "Physiology of handcycling: A current sports perspective". English. In: (2021). ISSN: 09057188. DOI: 10.1111/sms.13835. URL: https://www.scopus.com/inward/record.uri?eid=2-s2.0-85092096589%7B%5C&%7Ddoi=10.1111%7B%5C%%7D2Fsms.13835%7B%5C&%7DpartnerID=40%7B%5C&%7Dmd5=bec8f1ac07e03bb148db0a53f6f4721b.

[51] T Abel et al. "Effect of three different grip angles on physiological parameters during laboratory handcycling test in able-bodied participants". English. In: (2015). ISSN: 1664042X. DOI: 10.3389/fphys.2015.00331. URL: https://www.scopus.com/inward/record.uri?eid=2-s2.0-84949552896%7B%5C&%7Ddoi=10.3389%7B%5C%%7D2Ffphys.2015.00331%7B%5C&%7DpartnerID=40%7B%5C&%7Dmd5=b745100e8369576e55898f1bfc5fb1a3.

[52] O J Quittmann et al. "Reliability of muscular activation patterns and their alterations during incremental handcycling in able-bodied participants". English. In: (2021). ISSN: 14763141. DOI: 10.1080/14763141.2019.1593496. URL: https://www.scopus.com/inward/record.uri?eid=2-s2.0-85064701207%7B%5C&%7Ddoi=10.1080%7B%5C%%7D2F14763141.2019.1593496%7B%5C&%7DpartnerID=40%7B%5C&%7Dmd5=df78317c07441e1192905e3919989d9b.

[53] Michael J. Hutchinson et al. "Comparison of two Borg exertion scales for monitoring exercise intensity in able-bodied participants, and those with paraplegia and tetraplegia". In: *Spinal Cord* 59.11 (Nov. 2021), pp. 1162–1169. ISSN: 14765624. DOI: 10.1038/s41393-021-00642-4.

[54] Shivayogi V. Hiremath, Dan Ding, and Rory A. Cooper. "Development and evaluation of a gyroscopebased wheel rotation monitor for manual wheelchair users". In: *J. Spinal Cord Med.* 36.4 (2013), pp. 347–356. ISSN: 20457723. DOI: 10.1179/2045772313Y.0000000113.

[55] Maria Christina M.C. Maijers et al. "Is Fitbit Charge 2 a feasible instrument to monitor daily physical activity and handbike training in persons with spinal cord injury? A pilot study". In: *Spinal Cord Series and Cases* 4.1 (2018). DOI: 10.1038/s41394-018-0113-4.

[56] Sergio Andrés S.A. Ardila-Gomez et al. "Development of an electromechanical handbike prototype attachable to conventional wheelchairs". In: *Results in Engineering* 26.nan (2025). DOI: 10.1016/j.rineng.2025.105449.

[57] R A Himarosa and Sunardi. "Design, Frame Analysis and Manufacture of Handcycle Prototype". English. In: ed. by Rahim R Sesmiarni Z. Institute of Physics Publishing, 2020. DOI: 10.1088/1742-6596/1471/1/012058. URL: https://www.scopus.com/inward/record.uri?eid=2-s2.0-85082720643%7B%5C&%7Ddoi=10.1088%7B%5C%%7D2F1742-6596%7B%5C%%7D2F1471%7B%5C%%7D2F1%7B%5C%%7D2F012058%7B%5C&%7DpartnerID=40%7B%5C&%7Dmd5=0b54df67079f8403342400c893bd008c.

[58] A Cudicio et al. "Topographical and physiological data collection for urban handbike tracks design". English. In: ed. by Richiedei A Tira M. Pezzagno M. CRC Press/Balkema, 2019. ISBN: 9780367461713. URL: https://www.scopus.com/inward/record.uri?eid=2-s2.0-85117615192%7B%5C&%7DpartnerID=40%7B%5C&%7Dmd5=7d1ccc3af8b8b8d62eeefb3cf4ce6889.

[59] Alessandro Cudicio et al. "Topographical and physiological data collection for urban handbike tracks design". In: *Pedestrians, Urban Spaces and Health Proceedings of the 24th International Conference on Living and Walking in Cities*. 2019, pp. 225–229.

[60] Joseph A. J.A. Peters et al. "Validity and reliability of a single-unit inertial measurement unit: a real-time adapted sports assessment tool for handcycling-based activities". In: *Disability and Rehabilitation: Assistive Technology* nan.nan (2025). DOI: 10.1080/17483107.2025.2499186.

[61] Thom T. Snoek et al. "Sitting pressure during wheelchair propulsion and handcycling: effects of backrest angle, movement intensity and cushion type". In: *Disability and Rehabilitation: Assistive Technology* 20.4 (2025), pp. 1094–1103.0. DOI: 10.1080/17483107.2024.2434912.

[62] Sonja S. de Groot et al. "Handbike configurations and the prevalence of experienced sitting and riding-related problems in recreational handcyclists training for the HandbikeBattle". In: *Disability and Rehabilitation: Assistive Technology* 19.8 (2024), pp. 3172–3182.0. DOI: 10.1080/17483107.2024.2315466.

[63] Michael John M.J. Hutchinson et al. "Oxygen uptake and heart rate responses to 4 weeks of RPE-guided handcycle training". In: *European Journal of Applied Physiology* 123.9 (2023), pp. 1965–1973.0. DOI: 10.1007/s00421-023-05210-7.

[64] Paride P. Cavallone et al. “Electomyographic activities of shoulder muscles during Handwheelchair.Q vs pushrim wheelchair propulsion”. In: *Medical Engineering and Physics* 106.nan (2022). DOI: 10.1016/j.medengphy.2022.103833.

[65] Jordan Smith et al. “Peer-facilitated, progression-oriented handcycling training improves propulsion smoothness and adherence in individuals with spinal cord injury: A pilot study using wearable IMUs”. In: *Disability and Rehabilitation: Assistive Technology* 20.5 (2025), pp. 1322–1331. DOI: 10.1080/17483107.2025.2451760.

[66] Rela Adi R.A. Himarosa and undefined u. Sunardi. “Design, Frame Analysis and Manufacture of Handcycle Prototype”. In: *Journal of Physics: Conference Series*. Vol. 1471. 1. 2020. DOI: 10.1088/1742-6596/1471/1/012058.

[67] Eduard Max E.M. Felsner et al. “Musculoskeletal Modelling of Elite Handcycling Motion: Evaluation of Muscular On-and Offset”. In: *Procedia Engineering*. Vol. 147. nan. 2016, pp. 168–174.0. DOI: 10.1016/j.proeng.2016.06.208.